

# **Carbon Abatement Options for U.S. Transport and Industry**

by

Yongxian Zhu

A dissertation submitted in partial fulfillment  
of the requirements for the degree of  
Doctor of Philosophy  
(Mechanical Engineering)  
in the University of Michigan  
2021

## Doctoral Committee:

Assistant Professor Daniel R. Cooper, Chair  
Associate Professor Neil Dasgupta  
Professor Steven J. Skerlos  
Professor Ming Xu

Yongxian Zhu

yxzhu@umich.edu

ORCID iD: 0000-0002-0257-5014

© Yongxian Zhu 2021

## **Dedication**

This dissertation is dedicated to my family and friends who have supported me throughout my education.

## **Acknowledgments**

I would like to thank my advisor, Dr. Daniel R. Cooper, without whose advice and support this thesis would not have been possible.

I would like to thank Dr. Steven J. Skerlos, Dr. Ming Xu, and Dr. Neil Dasgupta, who provided great help and advice in the U.S. light-duty vehicle emissions analysis.

I would like to thank Kyle Syndergaard, who helped with the collection of extensive amounts of steel industry data for the steel material flow analysis.

I would like to thank Laurent B. Chappuis from Light Metal Consultants, Robert De Kleine, Hyung Chul Kim, Timothy J. Wallington, and George Luckey from Ford Motor Company for the extremely useful help on the automotive aluminum recycling project.

I would also like to thank the various funders that made this work possible: the National Science Foundation, Ford Motor Company, the University of Michigan Mcubed program, and the Michigan-Cambridge Research Initiative.

## Table of Contents

<b>Dedication</b> . . . . .	<b>ii</b>
<b>Acknowledgments</b> . . . . .	<b>iii</b>
<b>List of Figures</b> . . . . .	<b>vi</b>
<b>List of Tables</b> . . . . .	<b>xi</b>
<b>List of Appendices</b> . . . . .	<b>xiv</b>
<b>Abstract</b> . . . . .	<b>xv</b>
<b>Chapter</b>	
<b>1 Introduction</b> . . . . .	<b>1</b>
1.1 The Contribution of U.S. Emissions to Climate Change . . . . .	1
1.2 Emissions from U.S. Transport . . . . .	3
1.2.1 Opportunities to Reduce U.S. LDV Emissions . . . . .	4
1.3 Emissions from U.S. Industry . . . . .	5
1.3.1 Emissions from the Steel and Aluminum industry . . . . .	6
1.3.2 Opportunities to Reduce U.S. Steel and Aluminum Emissions . . . . .	7
1.4 Thesis structure . . . . .	9
<b>2 Reducing Greenhouse Gas Emissions from US Light-Duty Transport in Line with the 2 °C Target</b> . . . . .	<b>11</b>
2.1 Chapter Background . . . . .	12
2.1.1 Scope of This Chapter . . . . .	16
2.2 Chapter Methods . . . . .	16
2.2.1 Calculating U.S. LDV Emissions and Targets . . . . .	16
2.2.2 Annual Vehicle Production, Fleet Size, and EOL Flows (see section A3 of the Appendix A for more details) . . . . .	17
2.2.3 Life Cycle Emissions Released per Vehicle (A4 in Appendix A) . . . . .	21
2.3 Chapter Results and Discussion . . . . .	25
2.3.1 How the U.S. LDV Sector Can Meet the Emissions Target . . . . .	27
2.3.2 The Role of Fleet Electrification . . . . .	30
2.3.3 The Role of LDV Transport Demand . . . . .	31
2.3.4 The Role of Production Emissions . . . . .	31
2.3.5 Chapter Conclusions and Limitations . . . . .	33

<b>3 Mapping the Annual Flow of Steel in the United States</b>	<b>34</b>
3.1 Chapter Background	35
3.1.1 Previous Steel Maps and Production Statistics	35
3.1.2 Scope of this Chapter	37
3.2 Chapter Methodology	37
3.2.1 Data Records on the U.S. Steel /industry (Nodes: 1-23)	38
3.2.2 Data Records on U.S. Manufacturing and End-Use Products (Nodes: 24-47)	40
3.2.3 Data Records on International Trade (Nodes 48 and 49)	41
3.2.4 Data Reconciliation (B1)	42
3.3 Chapter Results	47
3.4 Chapter Discussion	49
3.4.1 Completing the Picture: In-Use Stocks and Scrap Flows	49
3.4.2 Reducing U.S. Demand for New Steel	50
3.4.3 Global Lessons for the Circular Economy	51
3.5 Chapter Conclusions and Limitations	54
<b>4 An Optimal Reverse Material Supply Chain for U.S. Aluminum Scrap</b>	<b>55</b>
4.1 Current U.S. EOL Aluminum Recycling	57
4.1.1 Section Background	57
4.1.2 Section Methodology	58
4.1.3 Section Results and Discussion	65
4.1.4 Section Conclusion	69
4.2 The Coming Wave of Aluminum Sheet Scrap from Vehicle Recycling in the U.S.	69
4.2.1 Section Background	69
4.2.2 Section Methodology	73
4.2.3 Section Results (C4 in Appendix C)	80
4.2.4 Section Discussion	84
4.3 Emerging Aluminum Separation and Refining Technologies	89
4.3.1 Summary of the Aluminum Separation and Refining Technology Catalog	90
4.3.2 Applying Emerging Recycling Technologies to Upcoming U.S. ABS Scrap for Closed-Loop Recycling	102
<b>5 Conclusion and Future Work</b>	<b>115</b>
5.1 Contributions of this Thesis	115
5.2 Future Work	116
5.2.1 Updating the GREET Life Cycle Analysis Data for Transport Research	116
5.2.2 Data Reconciliation for MFA Analysis: Uncertainties and New Methods	119
5.2.3 Design for Recycling of Aluminum Autobody Sheet	121
<b>Appendices</b>	<b>123</b>
<b>Bibliography</b>	<b>266</b>

## List of Figures

### FIGURE

1.1	Annual U.S. GHG emissions by economic sectors in 2015 (U.S. EPA, 2021) . . . . .	2
1.2	Annual global GHG emissions and U.S. transport attributable (production, use, and disposal) GHG emissions in 2015. Prod stands for production emissions. F&E stands for fuel and electricity production emissions. HDVs: heavy duty vehicles. LDVs: light duty vehicles. See Appendix A for data and derivations . . . . .	3
1.3	Annual U.S. industry GHG emissions including direct and indirect emissions (U.S. EPA, 2021) . . . . .	6
1.4	Direct and indirect GHG emissions intensity of steel and aluminum production derived from International Energy Agency (2007); International Aluminum Institute (2007) and Milford et al. (2011) . . . . .	7
2.1	Global GHG emissions (left), U.S. transport GHG emissions (middle) and U.S. transport GHG emissions splitting domestic and import(right) in 2015 . . . . .	13
2.2	Cumulative CO <sub>2</sub> <sub>eq.</sub> emissions for the powertrain sales share simulations. The circular data points show the emissions when all other parameters and scenarios are base cases. The error bars show the range of cumulative emissions achieved by varying the other vehicle life cycle parameters and the electricity decarbonization and fuel economy scenarios. Table A14 describes the pathways corresponding to the error bar limits for each sales share simulation. . . . .	25
2.3	The percentage of pathways that stay within the cumulative emissions limit (i.e., ‘successful’ pathways) for changing vehicle life cycle parameters (top and bottom-left), vehicle technology scenarios (bottom-center), and electricity emissions scenarios (bottom-right). . . . .	26
2.4	Cumulative CO <sub>2</sub> <sub>eq.</sub> emissions attributable to U.S. LDVs. The cumulative emissions limit compatible with the 2 °C target is 23.1 Gt CO <sub>2</sub> <sub>eq.</sub> , 38% lower than the BAU emissions. An equivalent figure showing global temperature increases is presented in Figure A23 in Appendix A. . . . .	28
2.5	Cumulative CO <sub>2</sub> -equivalent U.S. LDV emissions and attributable global warming. Decarbonization strategies correspond to the numbered arrows in Fig 3b. . . . .	29
3.1	The coordinate system used to define the steel flow and catalogue data records. See B1.2 for complete details of the cataloguing method . . . . .	38
3.2	The multi-dimensional matrix-based cataloging system used for setting up the reconciliation . . . . .	44

3.3	A flow chart showing the tasks a practitioner must follow in order to produce a material map using the cataloging structure shown in Figure 3.2 . . . . .	45
3.4	Formally reconciled U.S. flow of iron and steel (including embedded alloying elements) in 2014. Drawn using eSankey software. Note: The iron ore flow represents the iron embedded within the ore and excludes the mass of oxygen and gangue. . . . .	48
3.5	Low resolution U.S. steel map for 2014. U.S. population in 2014: 318.6 million. . . .	50
4.1	(a) Demand estimate; (b) Scrap discard estimate with actual collection rate shown (Bertram et al., 2017; Hatayama et al., 2009) . . . . .	60
4.2	Scrap and new alloy mid-range compositions for seven U.S. product categories . . . .	62
4.3	2017 simulation A results ( $\alpha = 0.5$ ). Virgin metal and scrap sources used to meet U.S. aluminum demand in 2017 . . . . .	66
4.4	2017 Simulation A-G results showing sensitivity to economic furnace constraint parameter ( $\alpha$ ) . . . . .	67
4.5	2050 Simulation A-G results showing sensitivity to economic furnace constraint parameter ( $\alpha$ ) . . . . .	68
4.6	Brands share of aluminum ABS contributions to the U.S. fleet in 2018 (aluminum ABS embedded in sales). Derived from Chappuis (2018) with data provided on the condition of brand anonymity. . . . .	72
4.7	Methodology used to estimate the on-road aluminum ABS stock and future availability of aluminum ABS scrap from discarded vehicles . . . . .	73
4.8	Vehicle survival rates based on U.S. vehicle registrations (some deregistered vehicles are exported) . . . . .	80
4.9	Vehicle survival rates based on U.S. vehicle registrations (some deregistered vehicles are exported) . . . . .	81
4.10	Vehicle and alloy annual sales, stock level, and de-registrations from the U.S. fleet. The grey areas correspond to vehicles already sold in 2015-2020. F-Series is composed of F-150 and Super Duty. . . . .	82
4.11	Markov chain transition diagram of an aluminum intensive vehicle (left); Sankey diagram representation of vehicle lifespan and destinations (indexed to 100 vehicles) derived from baseline F-150 data shown in Table 4.5. . . . .	83
4.12	Summary of 2035 (baseline scenario) aluminum ABS compositional limits and estimated mixed scrap and new alloy compositions and quantities for the four vehicles in this study. The blue x-axis represents different scrap mixtures and the blue ring-shaped radar plots represent the lower and upper bound composition for five key alloying elements. The green y-axis represents new aluminum ABS alloy demand and the green ring-shaped radar plots represent the lower and upper compositional limit for the same five key alloying elements. . . . .	86
4.13	Flowchart of the aluminum recycling process . . . . .	91
4.14	Illustration of the Ford vehicle structure (figure constructed from SAE, 2015 and Darby, 2015) . . . . .	104
4.15	Illustration of design variable setup . . . . .	106
5.1	vehicle production GHG emissions before and after updating the steel and aluminum fabrication yield . . . . .	118



5.2	The material flows during product life, adapted from Ashby (2013) and Hammond and Jones (2011)	119
5.3	Level of conflict in the data records (darker grey means more conflicting data records and lightest grey means lacking data)	120
5.4	Coordinating between vehicle design, vehicle manufacturing, and vehicle recycling is needed to increase recycling	122
A.1	Global GHG emissions by economic sectors in 2015	123
A.2	U.S. GHG emissions by economic sectors in 2015	124
A.3	Global GHG emissions (left), U.S. transport GHG emissions (middle) and U.S. transport GHG emissions splitting domestic and import(right) in 2015	125
A.4	Figure A.4 Temperature response due to 1-kg pulse emissions of greenhouse gases with a range of lifetimes (given in parentheses). Calculated with a temperature impulse response function taken from Boucher and Reddy (2008) which has a climate sensitivity of 1.06 K	127
A.5	Emission budget to achieve 70% reduction by 2050 from 2010 level in line with the 2°C target	129
A.6	Global mean surface temperature rises according to IPCC (2018)	130
A.7	Historical vehicle ratio of sales by powertrains	133
A.8	Estimated historical vehicle fleet age distribution.	136
A.9	Future aggregate vehicle travel demand	137
A.10	Ratio of annual km traveled per vehicle with respect to vehicle age a.	137
A.11	Estimated future vehicle production for U.S. sales.	138
A.12	Base case sales share of alternative fuel vehicles	140
A.18	Vehicle sales share of alternative fuel vehicles	141
A.19	System boundary of the product-level LCA study	143
A.21	passenger car material composition	145
A.23	SUV material composition	146
A.25	Light truck material composition	147
A.26	FASTSim UI	153
A.36	fuel economy improvement estimations of passenger car, SUVs and light trucks by powertrains	156
A.37	Life cycle GHG emissions for passenger car simulated using base case vehicle lifespans and electricity GHG intensities that are constant throughout the life cycle. The hatched area represents the emissions that could theoretically be reduced if the recycled contents of all vehicle materials increase to 90%.s	163
A.38	Life cycle GHG emissions for SUV simulated using base case vehicle lifespans and electricity GHG intensities that are constant throughout the life cycle. The hatched area represents the emissions that could theoretically be reduced if the recycled contents of all vehicle materials increase to 90%.	164
A.39	Life cycle GHG emissions for light truck simulated using base case vehicle lifespans and electricity GHG intensities that are constant throughout the life cycle. The hatched area represents the emissions that could theoretically be reduced if the recycled contents of all vehicle materials increase to 90%.	165

A.40	(Left) Annual U.S. LDV emissions for the BAU pathway. (Middle) Annual U.S. LDV emissions for the moderate (fuel economy improvement) vehicle technology scenario (all other scenarios and parameter value being base case). (Right) Annual U.S. LDV emissions for the high (fuel economy improvement) vehicle technology scenario (all other scenarios and parameter values being base case) . . . . .	167
A.41	The lower bound, base case and upper bound set of scenarios shown in Figure 1 of the main manuscript. . . . .	168
A.43	Cumulative emissions and temperature rises corresponds to Figure 4 in the main manuscript. . . . .	171
A.42	Global temperature rises for varying vehicle life cycle parameters, vehicle technology scenarios. and electricity emissions scenarios. The higher dashed horizontal lines refer to BAU temperature rises. BC-RR: base case recycling rates. 90% RR: 90% recycling rates. The numbered arrows correspond to the cumulative emissions wedge plot shown in Figure 4. . . . .	172
A.44	Cumulative production emissions before and after recycling . . . . .	173
B.1	The multi-dimensional matrix-based cataloging system used for setting up the reconciliation . . . . .	190
B.2	A flow chart showing the tasks a practitioner must follow in order to produce a material map using the cataloguing structure shown in Figure B.1 . . . . .	191
B.3	Objective function value and maximum constraint violation versus the number of iterations . . . . .	198
B.4	Greatest differences between the informally (manually) reconciled steel map, the initial values used in the formal reconciliation, and the final formal reconciliation map shown in Figure 2 of the main article . . . . .	198
B.5	Size of residuals in initial variable set, final optimized variable set, and informally (manually) reconciled variable set . . . . .	200
B.6	Intermediate products to end-use goods based on Cullen . . . . .	207
B.7	U.S. imports and exports of 29 product categories in 2014 . . . . .	220
B.8	Network of nodes and flows represented in matrix form . . . . .	221
B.9	Network of nodes and flows represented in matrix form . . . . .	221
B.10	Historical and future U.S. steel scrap arising aggregated over the end-use sectors . . . . .	223
B.11	Absolute steel stocks in the construction sector . . . . .	223
B.12	Absolute steel stocks in the transport sector . . . . .	224
B.13	Absolute steel stocks in the machinery sector . . . . .	224
B.14	Absolute steel stocks in the metal goods (products) sector . . . . .	225
B.15	Absolute material footprint versus prosperity for different countries in 2008 . . . . .	227
B.16	Relative material footprint versus prosperity for different countries in 2008 . . . . .	227
C.1	Share of overall claim count by vehicle age (CCC, 2015) . . . . .	235
C.2	Vehicle survival rates based on the avoidance of vehicle totaling loss . . . . .	236
C.3	Vehicle survival rates by generations (starting with 6th generation for F-150 and Super Duty and 1st generation for Expedition and Navigator) . . . . .	237
C.4	Vehicle survival rates by scenarios . . . . .	239

C.5	Lifespan distributions for (a) F-150, (b) Super Duty trucks, (c) expedition, and (d) navigator . . . . .	240
C.6	Historical and predicted future annual sales of the four types of vehicle . . . . .	241
C.7	Definition of the stage in the Markov chain study . . . . .	244
C.8	Annual sales, stock level and de-registered from fleet according to types of vehicle (left) and alloy families (right) under baseline survival rate and reference sales growth rate . . . . .	246
C.9	Annual sales, stock level and de-registered from fleet according to types of vehicle (left) and alloy families (right) under baseline survival rate and low sales growth rate .	247
C.10	Annual sales, stock level and de-registered from fleet according to types of vehicle (left) and alloy families (right) under baseline survival rate and high sales growth rate .	248
C.11	Annual sales, stock level and de-registered from fleet according to types of vehicle (left) and alloy families (right) under pessimistic survival rate and reference sales growth rate	249
C.12	Annual sales, stock level and de-registered from fleet according to types of vehicle (left) and alloy families (right) under pessimistic survival rate and low sales growth rate	250
C.13	Annual sales, stock level and de-registered from fleet according to types of vehicle (left) and alloy families (right) under pessimistic survival rate and high sales growth rate	251
C.14	Annual sales, stock level and de-registered from fleet according to types of vehicle (left) and alloy families (right) under optimistic survival rate and reference sales growth rate . . . . .	252
C.15	Annual sales, stock level and de-registered from fleet according to types of vehicle (left) and alloy families (right) under optimistic survival rate and low sales growth rate	253
C.16	Price profiles for primary aluminum versus post-consumer aluminum scrap grades. Graph constructed from London Metals Exchange data (LME, 2020), Taylor(2013), and Schlesinger (2014). . . . .	254

## List of Tables

### TABLE

3.1	Methodology for assigning confidence scores to data records . . . . .	46
3.2	Strategies to reduce per capita steel stocks . . . . .	52
4.1	Nomenclature . . . . .	59
4.2	Common alloying and tramp elements in aluminum scraps (Davis, 2001; Gaustad, Olivetti, and Kirchain, 2012). . . . .	61
4.3	Example of new alloy compositional constraints . . . . .	63
4.4	Average aluminum ABS content in the F-150, Super Duty, Navigator, and Expedition . . . . .	75
4.5	Transition probability values for the Markov chain transition diagram (Figure 4.11) assuming mean characteristics for baseline, pessimistic (short), and optimistic (long) vehicle lifespan scenarios. . . . .	83
4.6	data confidence level measuring rubric . . . . .	95
4.7	2050 recycling rate (RR) and recycled content (RC) of six major aluminum alloys and scraps without contamination . . . . .	109
4.8	2050 recycling rate (RR) and recycled content (RC) of six major aluminum alloys and scraps with 1% Fe contamination . . . . .	110
4.9	2050 recycling rate (RR) and recycled content (RC) of six major aluminum alloys and scraps with 1% Cu contamination . . . . .	111
4.10	2050 recycling rate (RR) and recycled content (RC) of six major aluminum alloys and scraps with 1% Fe and 1% Cu contamination . . . . .	112
A.1	GWP and AGTP of CO <sub>2</sub> , CH <sub>4</sub> , and N <sub>2</sub> O . . . . .	128
A.2	Historical U.S. LDV production (EPA, 2020) . . . . .	131
A.3	LDV lifespan distribution parameters . . . . .	133
A.4	2020 Recycled content and EOL closed loop recycling rates . . . . .	142
A.5	2020 vehicle battery configurations summary . . . . .	150
A.6	Fuel economy scenarios and associated technical parameters . . . . .	152
A.8	Summary of pathway vehicle life cycle parameters, vehicle technology scenario and electricity emissions scenarios (continued) . . . . .	152
A.7	vehicle technical parameters in 2020 and 2050 . . . . .	153
A.10	Fuel emissions intensities . . . . .	157
A.9	comparison between FASTSim and Physical based model fuel economy prediction . . . . .	157
A.11	Electricity emissions intensity changes . . . . .	158
A.12	Primary material emission factor related to electricity . . . . .	159

A.13	Primary material emission factor not related to electricity . . . . .	160
A.14	Secondary material emission factor related to electricity . . . . .	161
A.15	Secondary material emission factor not related to electricity . . . . .	161
A.16	Battery emission factor separated by non-electricity and electricity related based on current electricity intensity. . . . .	162
A.17	Summary of vehicle life cycle parameters, vehicle technology scenarios and electricity emissions scenarios in the stimulated pathways . . . . .	166
A.18	Summary of pathway vehicle life cycle parameters, vehicle technology scenario and electricity emissions scenarios . . . . .	169
A.19	Summary of pathway vehicle life cycle parameters, vehicle technology scenario and electricity emissions scenarios (continued) . . . . .	170
A.20	Cumulative emissions equivalent breakdown . . . . .	171
B.1	Type of MFA Variables . . . . .	192
B.2	Summary of Variables . . . . .	196
B.3	Summary of Constraints . . . . .	197
B.4	Summary of Data Sources . . . . .	197
B.5	Summary of residuals . . . . .	199
B.6	Steelmaking and fabrication process yields . . . . .	201
B.7	Categorization of intermediate products by continuous cast product (USGS, 2016a) . . . . .	202
B.8	AISI Profile steel intermediate use by end-use sector . . . . .	205
B.9	Breakdown of intermediate products in construction applications from Moynihan et al. (2012) . . . . .	209
B.10	Breakdown of intermediate products in construction applications from Cooper et al. (2012) . . . . .	209
B.11	Intermediate product use in U.S. construction according to product breakdowns from Moynihan et al. (2012) and Cooper et al. (2012) . . . . .	210
B.12	U.S. Production of Vehicles 2014 . . . . .	212
B.13	Intermediate products embedded in vehicles in 2014 . . . . .	213
B.14	Composition of machinery and equipment steel mass by intermediate product as described by Daehn et al. (2017) . . . . .	214
B.15	Bottom-up estimates of intermediate products used in machinery and equipment manufacturing . . . . .	214
B.16	Total steel mass of appliances sold in the U.S. in 2014 . . . . .	215
B.17	End-use categories for part and final product entries from Table B.22 . . . . .	217
B.18	Degree of fabrication & assembly (high=1; low=0) . . . . .	218
B.19	Presence of energy transformation system (no=0; yes=1) . . . . .	219
B.20	The quantity and copper tolerance of steel product imports in 2014. Blue: tolerance $\leq$ 0.2wt.%Cu; Green: tolerance $\geq$ 0.2wt.%Cu . . . . .	226
C.1	Vehicle generation by model years . . . . .	234
C.2	Mean vehicle lifespan by vehicle generation (starting with 6th generation for F-150 and Super Duty and 1st generation for Expedition and Navigator) . . . . .	238
C.3	Mean vehicle lifespan by scenarios . . . . .	238
C.4	Parameters of survival rate models by scenarios . . . . .	239

C.5	Number of the four types of vehicle and (column 1) share of the four types of vehicle in all used vehicles to be exported (column 2) and age distribution (column 3-5) . . . .	243
C.6	Annual used vehicle export estimation between 2014 and 2018 . . . . .	243
C.7	Mean vehicle deregistered by age groups and share of vehicle exported comparing to overall deregistration . . . . .	244

## **List of Appendices**

<b>A Reducing greenhouse gas emissions from U.S. light-duty transport in line with the 2 degrees Celsius target . . . . .</b>	<b>123</b>
<b>B Mapping the annual flow of steel in the United States . . . . .</b>	<b>187</b>
<b>C The coming wave of aluminum sheet scrap from vehicle recycling in the U.S. . . . .</b>	<b>232</b>
<b>D Recycling technology catalog . . . . .</b>	<b>261</b>

## Abstract

Annual anthropogenic greenhouse gas emissions must be cut by 40-70% by 2050 to limit global warming this century to 2 °C above the pre-industrial temperature and avoid the worst consequences of climate change. This cut in global emissions is likely infeasible without U.S. decarbonization efforts equaling the global target. The transport and industry sectors account for 57% of U.S. GHG emissions. These two sectors must decarbonize and match the target if the U.S. is to achieve the necessary cut in emissions.

Emissions from U.S. transport and industry are coupled with advanced transport technologies (e.g., electric vehicles with Li-ion batteries) typically requiring emissions-intensive manufacturing. Previous studies have largely ignored the transport-industry emissions nexus. Instead, this thesis presents a parametric fleet-scale production-use-disposal model that combines life cycle assessment with macro-level demand parameters to calculate consumption based cumulative emissions and global temperature changes attributable to U.S. light duty vehicles (LDVs). Future pathways account for emerging powertrain technologies, electricity decarbonization, transport demand, recycling rates, and vehicle lifespans. Only 3% of the 1,512 modeled pathways meet the emissions target. Without aggressive actions, U.S. LDVs will likely exceed the cumulative emissions budget by 2039. Cumulative emissions are most sensitive to transport demand, the speed of fleet electrification and electricity decarbonization. Increasing the production of battery electric vehicles (BEVs) to 100% of sales by 2040 (at the latest) is necessary, and early retirement of internal combustion engine vehicles is beneficial. Rapid electricity decarbonization minimizes emissions from BEV use and increasingly energy-intensive vehicle production. Deploying high fuel economy vehicles can increase emissions from the production of BEVs and lightweight materials. Increased recycling has only a small effect on these emissions because over the time period there are few batteries and lightweight materials available for recycling.

A quarter of U.S. industry emissions are from the steel and aluminum sectors. Previous studies have shown that there are limited opportunities for further energy efficiency improvements in these upstream industries; however, increased material efficiency might prove fruitful, where services are delivered using less emissions-intensive materials produced from natural resources. Detailed material flow analyses (MFAs) are needed to identify the opportunities for material efficiency and to model the supply chain emissions. MFA construction is time-consuming and fraught with



missing and contradictory data. This thesis presents an easily updatable nonlinear least-squares data reconciliation framework for MFA that is then applied to the annual U.S. steel flow. The MFA reveals key opportunities for U.S. steel material efficiency: increased manufacturing process yields and domestic recycling of landfilled and exported scraps.

To understand the barriers to increased recycling, an optimal reverse supply chain model is derived using linear programming (LP). It shows that U.S. domestic steel and aluminum recycling is already constrained by compositional mismatches between the scrap streams and industry demand. The LP model is coupled with a dynamic material flow analysis to show that the increasing volumes of high-quality wrought aluminum being used in U.S. vehicles are likely to be downcycled or landfilled at vehicle end-of-life. The LP model is revised to show the potential for using emerging scrap separation and refining technologies to increase closed-loop recycling rates to over 90%.

The technical assessments presented in this thesis highlight the scope for change. In future work, socioeconomic analyses could be coupled with these models to further assess the viability of the material efficiency strategies highlighted throughout.

# Chapter 1

## Introduction

Since the industrial revolution, human activities (e.g., burning of fossil fuels and agriculture development) have had an increasing impact on the climate at a global scale. Many extreme climate events have been observed especially after 1950 (IPCC, 2014). Examples include shrinking glaciers, rising sea levels, shifting plant and animal ranges, and more frequent occurrences of extreme weather (IPCC, 2014). The emissions of greenhouse gases (GHGs) from human activity have substantially enhanced the greenhouse effect and caused the increasing global mean temperature (IPCC, 2014). It is unequivocal that anthropogenic GHG emissions have been the dominant cause of global warming and climate change related events since the mid-20th century (IPCC, 2014). Climate scientists have high confidence that the global mean temperature will continue to rise and, in a business-as-usual scenario that does not limit global anthropogenic GHG emissions, the global mean surface temperature is likely to increase from the pre-industrial levels by 2.6 °C to 4.8 °C by the end of the 21st century (IPCC, 2014).

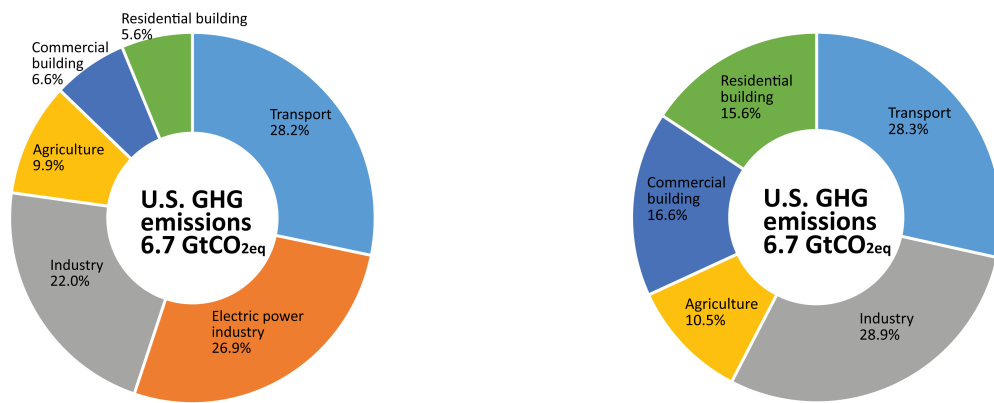
To avoid the worst consequences of climate change, the Intergovernmental Panel on Climate Change (IPCC) recommends that we limit the global mean temperature rise to a less than 2 °C rise above the pre-industrial revolution temperature by reducing GHG emissions (IPCC, 2014). To achieve the 2 °C target, the most recent (5th) IPCC report (2014, by the time of this research was conducted and dissertation were written) recommends a 40-70% reduction in global annual anthropogenic GHG emissions by 2050 compared to the 2010 level and that anthropogenic emissions reach net zero or below by 2100 (IPCC, 2014).

### 1.1 The Contribution of U.S. Emissions to Climate Change

To understand a country's contribution to the climate change problem, it is important to look at not only the current and future GHG emissions but cumulative historical emissions because climate change is largely a result of cumulative emissions and because cumulative national levels are an approximate indicator of a country's development and cumulative wealth (Baumert et al., 2005; IPCC, 2014). Cumulatively, the U.S. has emitted more GHG emissions than any other country

(Gütschow et al., 2021; Damassa, 2014). Data on country-level GHG emissions shows that the U.S. has emitted around 20% of the global cumulative GHG emissions since 1850 (Gütschow et al., 2021; Damassa, 2014).

Until 2005, the U.S. was still the world’s greatest annual GHG emitter (Gütschow et al., 2021; Damassa, 2014). In 2018, the U.S. emitted 15% of global annual CO<sub>2eq</sub> emissions (Gütschow et al., 2021; Damassa, 2014), second only to China but where a significant chunk of Chinese industrial GHGs have in recent years been emitted during the production of goods for export to the U.S. (Yang et al., 2020). On a per-capita basis, the U.S. ranks 4th highest among all the countries and nations in 2020 at 16.56 t CO<sub>2eq</sub>/capita annually which is 2.34 times that of Chinese per capita CO<sub>2eq</sub> emissions (UCUSA, 2019).



(a) Electric power industry as a separate sector.

(b) Electric power emissions allocated.

Figure 1.1: Annual U.S. GHG emissions by economic sectors in 2015 (U.S. EPA, 2021)

According to the U.S. Environmental Protection Agency (U.S. EPA, 2021) transport, electric power and industry are the top three economic sectors that dominate U.S. annual direct GHG emissions. Direct GHG emissions (also called scope 1 emissions) are emissions from sources that are owned or controlled by the reporting entity; e.g., on-site fossil fuel combustion emissions and tailpipe emissions (U.S. EPA, 2021). Direct transport sector emissions account for around 28.6% of the U.S. GHG emissions and rank the highest among all the economic sectors. Direct emissions from the industry sector account for 22.9% of overall emissions and are only lower than the transport and electric power sector. If the electricity-related emissions are allocated to the corresponding economic sector in which the electricity is used, then industry and transport sector emissions rise to 29.7% and 28.7% respectively. **The U.S. transport and industry sectors, therefore, dominate U.S. GHG emissions (see Figure 1b). Any decarbonization strategy for the U.S. must address these two sectors.**

## 1.2 Emissions from U.S. Transport

U.S. transport sector direct emissions (Figure 1.2) account for around 4% of global anthropogenic GHG emissions. If emissions from the vehicle, fuel, and electricity production are allocated to the U.S. transport sector, the overall U.S. transport emissions rise to 5.5% of global anthropogenic GHG emissions ((Figure 1.2)). The enormous emissions from the U.S. transport sector are because of the much higher travel demand in the U.S. than in many other countries. The U.S. has one of the highest demands for per-capita light-duty vehicle (LDV) travel in the world (U.S. average: 23,000 vehicle km/year-capita vs. European average: 10,800 vehicle km/year-capita (FHWA, 2020)) and this demand is projected to increase by 0.9%/year between 2018 and 2048 (FHWA, 2020). LDVs encompass passenger cars, SUVs, and light trucks. Among all the categories in the transport sector, LDV emissions account for almost 60% of U.S. transport emissions. Reducing LDV emissions is a priority for the decarbonization of U.S. transport.

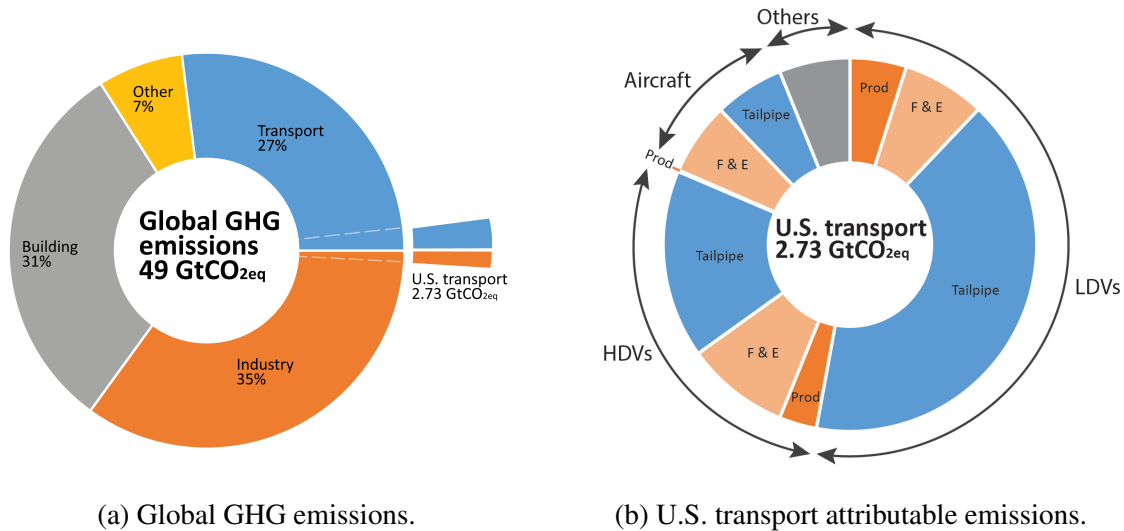


Figure 1.2: Annual global GHG emissions and U.S. transport attributable (production, use, and disposal) GHG emissions in 2015. Prod stands for production emissions. F&E stands for fuel and electricity production emissions. HDVs: heavy duty vehicles. LDVs: light duty vehicles. See Appendix A for data and derivations

Looking beyond the direct transport GHG emissions from vehicle tailpipes, fulfilling LDV travel demand also requires the production of fuels, vehicles, and infrastructure which induce “indirect” emissions (emissions that result from the generation of electricity, heat, or steam purchased by the agency from a utility provider (U.S. EPA, 2021)). EPA’s emission accounting method (used to generate Figure 1.1) only attributes the direct tailpipe GHG emissions to the transport sector while attributing the fuel and vehicle production emissions to industry. Estimation of 2015 U.S. vehicle production and use shows that the fuel and vehicle production emissions can contribute a

significant portion of LDV emissions – equivalent to 30% of direct use-phase tailpipe emissions (see Appendix A). As travel demand increases, more vehicles will be needed to satisfy the demand which will further increase the material and vehicle production emissions. Furthermore, alternative fuel vehicles (e.g., battery electric vehicles), which are likely to be needed for decarbonization, have higher absolute and relative (to use-phase) production emissions (Elgowainy et al., 2018; Ellingsen et al., 2016; Hawkins et al., 2013).

### **1.2.1 Opportunities to Reduce U.S. LDV Emissions**

Strategies to reduce LDV emissions can be classified as use-phase oriented or production-phase oriented. U.S. regulations (the CAFE standard) and previous analyses in the literature (Greene and DeCicco, 2000; Kim et al., 2010; Luk et al., 2017; Ward et al., 2019) typically focus on reducing use-phase emissions by improving the vehicle fuel efficiency. The use-phase has likely been the focus of previous studies because previous single-vehicle life cycle assessments (LCAs) have shown that the use-phase accounts for over 90% of a typical internal combustion engine vehicle (ICEV)'s life cycle GHG emissions (Bauer et al., 2015; Hawkins et al., 2013; Ma et al., 2012). Examples of use-phase strategies are vehicle lightweighting, engine efficiency improvement, tire friction reduction, vehicle electrification, and substituting LDV travel with more public transportation and active traveling (exercise), etc. (Greene and DeCicco, 2000; Kim et al., 2010; Luk et al., 2017; Ward et al., 2019). However, many of the use-phase strategies reduce use-phase emissions while shifting the emission burden from the transport sector to the industry and electric power sectors. For example, vehicle electrification requires mass production of traction batteries which significantly increases the vehicle production emissions for the automotive battery industry (Elgowainy et al., 2018; Ellingsen et al., 2016; Hawkins et al., 2013; Karabasoglu and Michalek, 2013; Lewis et al., 2014; Majeau-Bettez et al., 2011).

Previous studies have looked at how the use-phase emissions from the U.S. LDV sector could be reduced in line with the 2 degree C target targets (Yang et al., 2009; Greene et al., 2010; Bastani et al., 2012; Supekar and Skerlos, 2017). McCollum and Yang (2009) calculate that 2050 U.S. LDV fleets consisting of either 100% biofuel-powered vehicles or a combination of hydrogen fuel cell vehicles (FCVs), battery electric vehicles (BEVs), and ICEVs would result in 2050 GHG emissions being 80-90% lower than in 1990. Later, Greene et al. (2011) and Bastani et al. (2012) estimate that a 50-65% emissions reduction by 2050 (from 2010) is possible if biofuels, FCVs, and BEVs comprise 40-65% of the 2050 fleet and vehicle mileage is reduced by 0-20%. Replogle and Fulton (2014) estimate that if 50% of urban U.S. LDV mileage (equaling 30-35% of total U.S. LDV mileage) could be replaced by 2050 with public transportation, cycling, and walking (replicating average EU urban transport patterns), it would reduce urban U.S. LDV use-phase emissions by 60% compared to 2010 (Replogle and Fulton, 2014). Elsewhere, Supekar and Skerlos (2017) analyze

how the U.S. automotive and electricity sector can collectively meet a 70% reduction in use-phase GHG emissions by 2050 (from 2010) using a least-cost approach. They find that climate action must begin by 2023-2026 if the target is to remain feasible and that any delay only increases costs. Supekar and Skerlos exclude emissions from vehicle production and power plant construction. However, without considering the vehicle production and disposal, the climate mitigation actions could lead to spillover of the GHG emissions from the transport sector to industry and power sectors.

No regulations in the U.S. have attempted to reduce vehicle production emissions. Several studies, though, have investigated vehicle production emission reduction through material efficiency strategies such as recycling and vehicle downsizing (Wolfram et al., 2021; Milovanoff et al., 2019, 2020; Serrenho et al., 2017). However, these studies are either not U.S. centered or did not investigate how the LDV production and use-phase together could reduce their emissions in line with the 2 °C target. Therefore, a holistic study that investigates how the LDV production, use, and disposal emissions could be limited to meet the IPCC recommended climate change target is needed.

### **1.3 Emissions from U.S. Industry**

The U.S. industry sector emits 29% of U.S. GHG emissions (Figure 1.2b) and this does not account for the emissions associated with many imported raw materials, semifinished products, and finished goods (U.S. EPA, 2021). Although domestic industrial emissions have declined significantly since 1990, largely due to production shifting to other countries, the GHG emissions attributable to U.S. industry product consumption continue to increase (U.S. EPA, 2021). Figure 1.2a shows the breakdown of U.S. industrial processes and product GHG emissions. Industrial GHG emissions come from both the burning of fuels to produce energy (e.g., natural gas-fired heat treatment furnaces) and as a byproduct of the chemical and physical transformations needed in material production (e.g., reduction of iron ore using coke results in liquid iron and carbon dioxide waste gases) (U.S. EPA, 2021). These chemical and physical transformations can result in the release of GHGs such as carbon dioxide (CO<sub>2</sub>), methane (CH<sub>4</sub>), nitrous oxide (N<sub>2</sub>O), and fluorinated greenhouse gases (e.g., HFC-23). The GHG byproduct generating processes include iron and steel production, metallurgical coke production, cement production, petrochemical production, lime production, etc. (U.S. EPA, 2021).

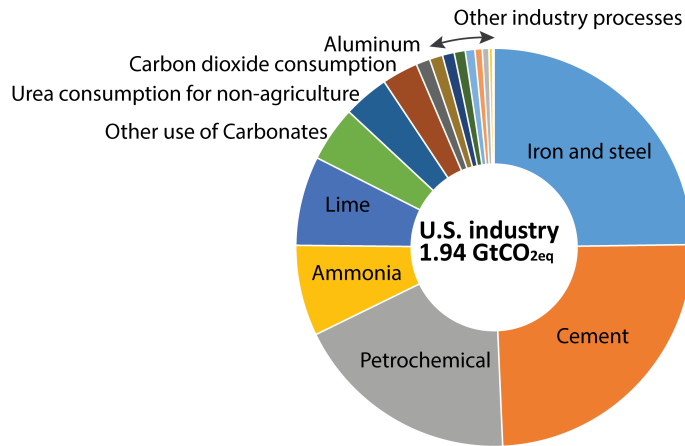


Figure 1.3: Annual U.S. industry GHG emissions including direct and indirect emissions (U.S. EPA, 2021)

### 1.3.1 Emissions from the Steel and Aluminum industry

Among all the industrial processes, material production dominates industry emissions; e.g., iron and steel production contributes to around 24% of U.S. industry GHG emissions. Aluminum production, as the second-largest metal industry GHG emitter, accounts for around 1% of U.S. industry GHG emissions (Figure 1.3). The GHG intensity of primary aluminum production is 8.6 t CO<sub>2eq.</sub> eq./t, more than five times the GHG intensity of primary steel production (Milford et al., 2011). These steel and aluminum products are consumed across transport, construction (buildings and infrastructure), energy, consumer goods, and other sectors. More than 82 Million tons (Mt) of finished steel products (USGS, 2021b) and 2.87 Mt of finished aluminum products (USGS, 2021a) were consumed by the U.S. in 2020. Although consumption declined in 2020 due to supply chain interruptions because of the COVID-19 pandemic, U.S. steel and aluminum demand is expected to recover (Holcomb, 2021; Egan, 2021) and the aluminum demand is predicted to increase continuously, driven by the expanded production of lightweight vehicles (Egan, 2021).

The emissions from the transport and industry sector are highly linked. Among all the end-use sectors, 26% of steel products (Zhu et al., 2019) and 44% of aluminum products (Zhu and Cooper, 2019) are produced for use by the transport sector. This is because around 60% of vehicle components (by weight) are steel and 10% are aluminum (Argonne, 2020). As U.S. LDV travel demand continues to increase (FHWA, 2020), more materials need to be produced for use in new vehicles to supply the transport need. This increased vehicle production and vehicle lightweight design using high-strength steel and aluminum (Kim et al., 2010; Milovanoff et al., 2019) will likely drive the demand and emission increase from the automotive steel and aluminum industry.

### 1.3.2 Opportunities to Reduce U.S. Steel and Aluminum Emissions

To reduce the steel and aluminum sector emissions, energy efficiency strategies have been proposed (Tanaka, 2011; Worrell et al., 2009). Energy efficiency strategies include implementing the best available technologies or innovative technologies at steel and aluminum production facilities. For example, Worrell et al. (2007) indicate that coke substitution in primary steel production and more efficient electrolysis in primary aluminum production could improve the energy consumption and emission performance at current steel and aluminum production facilities. Allwood et al. (2012) and Ryan et al. (2020) looked at adopting innovative technologies, e.g., smelt reduction and electrolysis for steel and inert anodes in aluminum production. However, even with the most innovative technologies implemented, Allwood et al. (2010) estimate the energy efficiency strategies can only achieve a 34% reduction of global steel production emissions and a 23% reduction of aluminum production emissions because the current practice of steel and aluminum making are approaching the practical thermodynamic limit (Gutowski et al., 2013). It is impossible to achieve the required 70% emission reduction target suggested by IPCC with energy efficiency strategies only. Therefore, Allwood et al. (2010) indicate that material efficiency strategies are needed for the industry to meet its emission reduction obligations. Material efficiency means delivering services with smaller amounts of materials (Cooper, 2014). Examples of material efficiency strategies include improving fabrication process yield and increased recycling (Allwood et al., 2010).

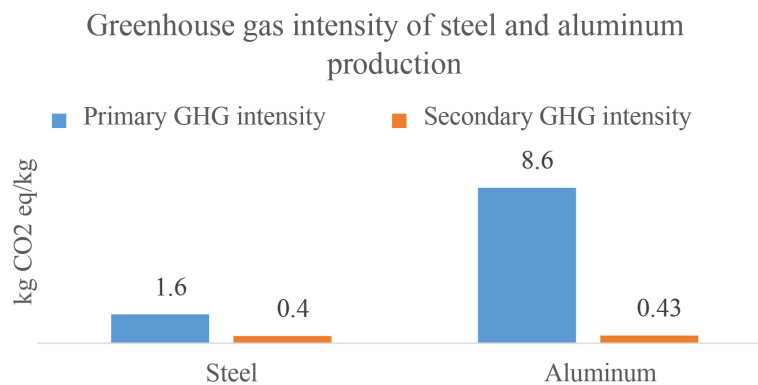


Figure 1.4: Direct and indirect GHG emissions intensity of steel and aluminum production derived from International Energy Agency (2007); International Aluminum Institute (2007) and Milford et al. (2011)

To identify where in the metal supply chain system material efficiency strategies could be applied, a detailed understanding of the material flow and thus loss and scrap generation is needed. Material flow analysis (MFA) is often used to quantify the stocks and flows of materials in defined temporal and economic or geographic boundaries, and a detailed MFA gives insight into the chemical composition of flows and the difficulties of recycling (e.g., copper wiring contamination in steel



scrap). Although numerous detailed steel MFA studies have been conducted for the UK (Michaelis and Jackson, 2000a,b) and globally (Cullen et al., 2012), no such MFA exists for the U.S. steel industry.

Constructing a high-quality MFA often requires a large amount of information which leads to the common problem of data scarcity and inconsistency (Brunner and Rechberger, 2017; Kopec et al., 2016). Current MFA studies are heavily dependent on expert knowledge and the data are often manually manipulated to satisfy the mass balance and other constraints of the network (Brunner and Rechberger, 2017; Cullen et al., 2012). The resulting MFA networks are thus susceptible to personal bias during the data reconciliation process and lack the updatability and flexibility to accommodate new data or a change in network structures (e.g., new exports and consumption of U.S. produced direct reduced iron (DRI) resulting in a change to the upstream material flows). Given the data availability and inconsistency issues in MFA, at least three formal data reconciliation methods have been proposed: nonlinear least-square optimization (Kopec et al., 2016), Bayesian updating (Lupton and Allwood, 2018), and the RAS input-output matrix method (Ploeg, 1988) to solve the problem. However, the previous data reconciliation research often only focuses on the theoretical applicability aspect with a problem-dependent set up to address the specific data reconciliation issue. A general framework to produce MFA networks in a fast, flexible, and updateable manner is needed in order to evaluate the potential for increased material efficiency in materials systems such as the U.S. steel sector.

Unlike the status of steel MFA studies, several detailed MFA studies have been conducted for the U.S. aluminum industry (Hatayama et al., 2010; Chen and Graedel, 2012; Bertram et al., 2017). Reviewing the aluminum MFA studies reveals that currently, the U.S. end-of-life (EOL) aluminum recycling rate is between 34-63% (Hatayama et al., 2010; Chen and Graedel, 2012; Bertram et al., 2017) which is much lower than the 90% recycling rate suggested by previous studies to meet the 2 °C target (Allwood et al., 2010). Part of the collected scraps is exported and recycled overseas which further contributes to the material loss in the U.S. (USGS, 2021c). Compared to primary production, secondary steel and aluminum production reduces the GHG emissions by 75% and 95% respectively (Figure 1.4). In order to improve the recycling rate, studies have looked at the reasons for the low EOL aluminum recycling rate in the U.S. (Atherton, 2007; McMillan et al., 2010; Hatayama et al., 2012). They point out that the scrap collection, scrap contamination, scrap mixing, and new alloy chemical composition requirement potentially cause the low current aluminum recycling rates in the U.S. while the quantitative impact of each potential reason is unclear. Among all the aluminum end-use sectors, the automotive wrought aluminum sector is driving U.S. aluminum demand while the closed-loop recycling rate of current automotive wrought aluminum is close to zero. Research is needed to analyze this emerging market to prepare manufacturers and recyclers for future aluminum wastes.

Laboratory scale scrap separation and refining technologies have been proposed to remove the tramp elements in contaminated and mixed scraps so that they can be used to produce products that meet the new alloy demand (Gaustad et al., 2012; DeYoung et al., 2011; Ambrose et al., 1983; Gesing et al., 2010; F. and V., 2017). Many of these technologies are still in their infancy, require long R&D times, huge investment, and the potential impact/benefits in the supply chain system remain unclear. Therefore, a holistic model is needed to quantitatively understand the problems that constrain the recycling rates and the potential of emerging recycling technologies to overcome the barriers to increase recycling .

## **1.4 Thesis structure**

In light of the review presented in Sections 1.1-1.3, this thesis presents research on how to reduce U.S. LDV sector emissions and U.S. steel and aluminum industry emissions.

The objectives of Chapter 2 are to answer the following research questions:

- What is the effect of increasing deployment of U.S. alternative fueled vehicles on cumulative emissions and the global mean temperature between now and 2050?
- How can the U.S. LDV sector meet a 70% cut in attributable emissions (production, use and disposal) by 2050?

The objectives of Chapter 3 are to answer the following research questions:

- How to record and reconcile inconsistent MFA input data and produce an easily updateable and internally consistent material flow network?
- How does U.S. steel flow from iron ore through steel processing and fabrication to end-use consumption as products?
- Where are the key opportunities for the U.S. steel industry to become more materially efficient?

The objectives of Chapter 4 are to answer the following research questions:

- How does scrap collection and the chemical compositional mismatch between the available scrap streams and demand for metal affect U.S. EOL aluminum recycling rates?
- How are the composition and scale of demand and scrap availability going to change in the key aluminum demand driver, the U.S. automotive aluminum sheet market?

- What is the performance (efficacy, energy, cost, yield, and environmental impact) of key existing and emerging aluminum recycling technologies and how could they be used to increase the recycling rate of U.S. EOL autobody aluminum sheet scrap?

A summary of the contributions is presented in Chapter 5, along with potential future research that could be conducted in these three research areas.

## Chapter 2

### Reducing Greenhouse Gas Emissions from US Light-Duty Transport in Line with the 2 °C Target

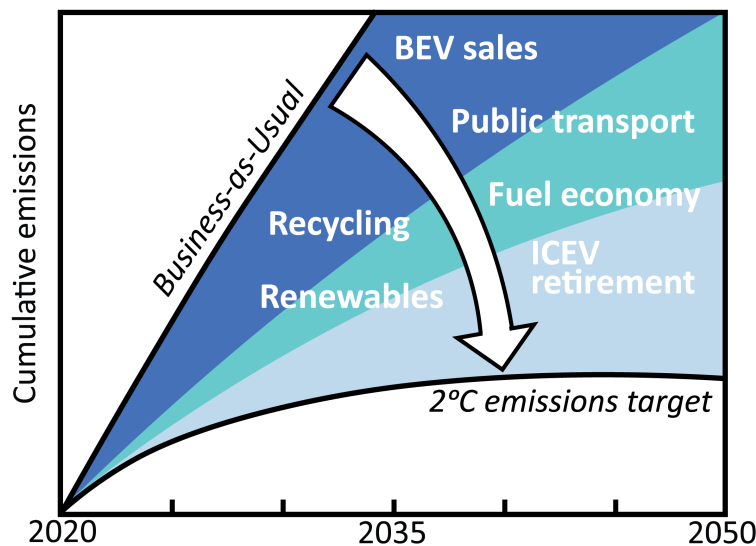
Publication related to this work:

Conference articles:

- Zhu, Y., Skerlos, S.J., Xu, M. and Cooper, D.R., 2020. System level impediments to achieving absolute sustainability using LCA. *Procedia CIRP*, 90, pp.399-404.

Journal articles:

- Zhu, Y., Skerlos, S.J., Xu, M. and Cooper, D.R., 2021. Reducing Greenhouse Gas Emissions from US Light-Duty Transport in Line with the 2 °C Target. *Environmental Science & Technology*, 55 (13), pp.9326-9338.



Making, driving, and disposing of U.S. light-duty vehicles (LDVs) accounts for 3% of global greenhouse gas emissions related to energy and processing. This chapter calculates future emissions and global temperature rises attributable to U.S. LDVs. We examine how 2021-2050 U.S. LDV

cumulative emissions can be limited to 23.1 Gt CO<sub>2</sub><sub>eq.</sub>, helping to limit global warming to less than 2 °C. We vary four vehicle life cycle parameters (transport demand, sales share of alternative fuel vehicles, vehicle material recycling rates, and vehicle lifespans) in a dynamic fleet analysis to determine annual LDV sales, scrappage, and fleet compositions. We combine these data with vehicle technology and electricity emissions scenarios to calculate annual production, use, and disposal emissions attributable to U.S. LDVs.

Only 3% of the 1512 modeled pathways stay within the emission limit. Cumulative emissions are most sensitive to transport demand, and the speed of fleet electrification and electricity decarbonization. Increasing production of battery electric vehicles (BEVs) to 100% of sales by 2040 (at the latest) is necessary, and early retirement of internal combustion engine vehicles is beneficial. Rapid electricity decarbonization minimizes emissions from BEV use and increasingly energy-intensive vehicle production. Deploying high fuel economy vehicles can increase emissions from the production of BEV batteries and lightweight materials. Increased recycling has a small effect on these emissions because over the time period there are few postconsumer batteries and lightweight materials available for recycling. Without aggressive actions, U.S. LDVs will likely exceed the cumulative emissions budget by 2039 and contribute a further 0.02 °C to global warming by 2050, 2.7% of the remaining global 2 °C budget.

## **2.1 Chapter Background**

The Intergovernmental Panel on Climate Change (IPCC) recommends that humanity cuts global annual anthropogenic greenhouse gas (GHG) emissions by 41-72% by 2050 from the 2010 level to avoid the worst consequences of climate change and to prevent global warming this century of more than 2 °C above the pre-industrial temperature (IPCC, 2014). Over three-quarters of anthropogenic GHG emissions are from the use of energy and industrial processes (Masson-Delmotte et al., 2018). Almost 3% of these emissions (Figure 2.1) are attributable to U.S. light-duty vehicles (LDVs), which comprises passenger cars (sedans/wagons), SUVs (car SUVs and truck SUVs), and light trucks (minivans/vans and pickups). Attributable emissions include production emissions at the start of a vehicle's life cycle (material production and manufacturing processes), use phase emissions released throughout the vehicle lifespan as a consequence of driving the vehicle, and disposal emissions from end-of-life (EOL) processing.

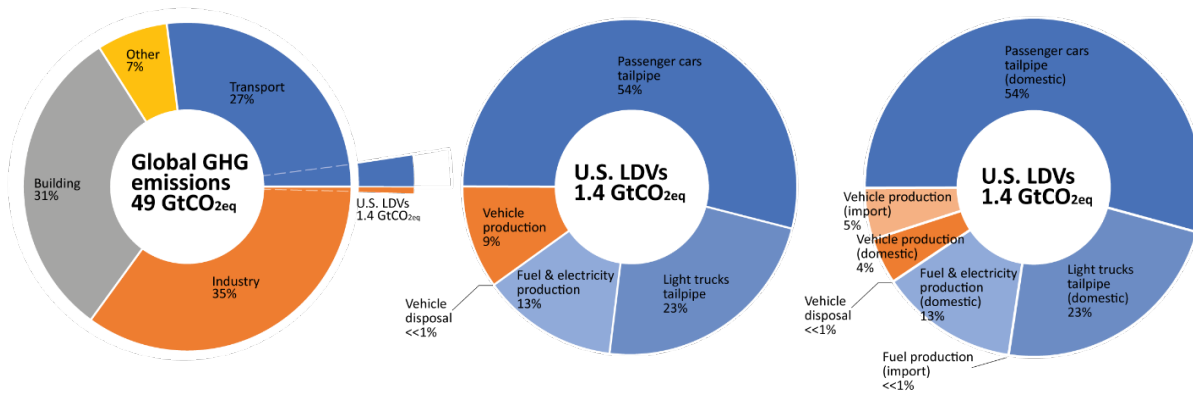


Figure 2.1: Global GHG emissions (left), U.S. transport GHG emissions (middle) and U.S. transport GHG emissions splitting domestic and import(right) in 2015

Most previous LDV emissions research and all current U.S. legislation focus on use phase emissions, which are released from tailpipes, fuel production, and electricity generation (for vehicle charging). Life cycle assessments (LCAs) of internal combustion engine vehicles (ICEVs) show that the use phase accounts for over 90% of a single vehicle's life cycle emissions (Hawkins et al., 2013; Bauer et al., 2015; Messagie et al., 2014; Ma et al., 2012; U.S. EPA and NHTSA, 2016). Options explored in the literature and by industry to reduce use phase emissions include improved air-conditioning systems (Farrington and Rugh, 2000), lightweighting through material substitution and/or downsizing (Wolfram et al., 2021; Heywood et al., 2015; Kim et al., 2011; Luk et al., 2017), more intensive use (Wolfram et al., 2021), exhaust after-treatment devices (Black et al., 1980), improved engine and transmission efficiencies (Greene and DeCicco, 2000), and alternative-fueled vehicles such as battery electric vehicles (BEVs) (Javid and Nejat, 2017; Mayyas et al., 2017; Miotti et al., 2016). U.S. legislative efforts to curb use phase emissions include the federal Corporate Average Fuel Economy (CAFE) standard (U.S. EPA and NHTSA, 2016), which regulates new vehicle use phase fuel economy and GHG emissions. In 2020, the Safer Affordable Fuel-Efficient (SAFE) Vehicles Rule was issued that eases the previous CAFE standard from a 4% annual fleet average fuel economy increase to 1.5% (U.S. EPA and NHTSA, 2016). In addition, the California Air Resources Board sets its own Advanced Clean Cars Program (Board, 2020) which has been (partially) adopted by at least 11 other states to promote the deployment of vehicles with zero tailpipe GHG emissions. No U.S. legislation to date aims to curb GHG emissions from vehicle production or disposal.

Several studies have analyzed how U.S. LDV use phase emissions can be cut in line with IPCC targets (Yang et al., 2009; Greene et al., 2014; Bastani et al., 2012; Replogle and Fulton, 2014; Supekar and Skerlos, 2017). McCollum and Yang (2009) calculate that 2050 U.S. LDV fleets consisting of either 100% biofuel-powered vehicles or a combination of hydrogen fuel cell vehicles

(FCVs), battery electric vehicles (BEVs), and ICEVs would result in 2050 GHG emissions being 80-90% lower than in 1990. Later, Greene et al. (2011) and Bastani et al. (2012) estimate that a 50-65% emissions reduction by 2050 (from 2010) is possible if biofuels, FCVs, and BEVs comprise 40-65% of the 2050 fleet and vehicle mileage is reduced by 0-20%. Replogle and Fulton (2014) estimate that if 50% of urban U.S. LDV mileage (equaling 30-35% of total U.S. LDV mileage) could be replaced by 2050 with public transportation, cycling, and walking (replicating average EU urban transport patterns), it would reduce urban U.S. LDV use phase emissions by 60% compared to 2010. Elsewhere, Supekar and Skerlos (2017) analyze how the U.S. automotive and electricity sector can collectively meet a 70% reduction in use phase GHG emissions by 2050 (from 2010) using a least-cost approach. They find that climate action must begin by 2023-2026 if the target is to remain feasible and that any delay only increases costs. Supekar and Skerlos exclude emissions from vehicle production and power plant construction.

Despite the dominance of use phase emissions in most LCAs, there are at least three reasons why production and disposal emissions are important to consider in analyses of future LDV emissions:

- Vehicle production emissions are increasing both in absolute terms and relative to life cycle emissions. Lightweight structural materials (e.g., aluminum and composites) are increasingly used in vehicle construction but are more emissions-intensive to produce than traditional steel vehicle structures (Zhu et al., 2020). The shift in powertrains is also increasing production emissions with recent LCAs finding that production accounts for 40-70% of BEV life cycle GHG emissions depending on the battery size (Hawkins et al., 2013; Kelly et al., 2015; Elgowainy et al., 2018; Ellingsen et al., 2016; Karabasoglu and Michalek, 2013; Lewis et al., 2014; Majeau-Bettez et al., 2011). Dai et al. (2019) estimate that 70% of Li-ion battery production emissions are from battery cell manufacturing where half of those emissions are from mining and refining the electrode materials (e.g.,  $\text{Li}_2\text{CO}_3$  and  $\text{CoSO}_4$ ) (Dai et al., 2019). Increased EOL recycling could reduce production emissions (Harper et al., 2019). Ciez and Whitacre (2019) and Dai et al. (2019) claim that direct physical recycling of battery cathode materials could reduce battery production emissions by 15-20% (Harper et al., 2019; Ciez and Whitacre, 2019).
- “Fleet effects” amplify production emissions (Field et al., 2000; Kim et al., 2010). Growing production rates, with a greater number of new (production) emissions-intensive LDVs produced each year, means that the annual fraction of emissions attributable to production is greater than in single vehicle LCAs (Zhu et al., 2020; Sutherland et al., 2020). Zhu et al. (2020) showed that this effect can delay the benefit of reduced cumulative emissions when switching to vehicles with lower life cycle (but higher production) emissions (Zhu et al., 2020).

- The effect of LDVs on the global temperature may depend on the timing and species of GHGs released. The global temperature response to an impulse of emitted GHG depends on both the time that has elapsed since the release of the emissions and the GHG species; e.g., the temperature impulse responses to CH<sub>4</sub> and N<sub>2</sub>O peak after 10 and 30 years, respectively (Stern and Johansson, 2017; IPCC, 2014). The release of production emissions early in the vehicle life cycle will increase global temperatures. Over time, the share of different GHG species will also likely vary between production and use. For example, analysis of GREET model (Argonne, 2020) emissions factors indicates that a greater proportion of CH<sub>4</sub> is released in coal and natural gas production (and therefore current electricity generation and subsequent vehicle production) than in gasoline production.

Few studies consider production as well as use phase emissions attributable to future U.S. LDVs. Exceptions are Onat et al. (2016) and Milovanoff et al. (2019, 2020). Onat et al. consider four vehicle deployment scenarios (ICEV dominant, HEV dominant, PHEV dominant, and BEV dominant) and find that 100% BEV new vehicle sales in 2050 can reduce annual emissions by 30% compared to 2010. Milovanoff et al. (2019) calculate a maximum reduction in annual emissions of 25% when combining lightweighting (by material substitution) and electrification scenarios. Milovanoff et al. (2020) calculate that electrification can reduce 2015-2050 cumulative CO<sub>2</sub> emissions (excluding other GHGs) in line with the 2 °C target if BEVs reach 60% of sales by 2040 combined with 100% renewable electricity and increasingly efficient and lightweight ICEVs. However, their CO<sub>2</sub> budget (Milovanoff et al., 2020), based on an extrapolation from GCAM data, is less stringent (>25% higher) than those used in comparable studies (McCollum and Yang, 2009; Greene et al., 2014; Bastani et al., 2012; Replogle and Fulton, 2014; Supekar and Skerlos, 2017). Relaxing the emissions budget for any of the major emitting sectors is likely to render the targets in the remaining sectors infeasible (Allwood et al., 2010). As part of a sensitivity analysis, Milovanoff et al.'s model finds no solution for meeting a lower emissions budget as used in the majority of studies (including the present article); however, they assume a negligible improvement in future BEV fuel economies and model neither decarbonization of the electricity used in vehicle production (other than aluminum production) nor policies that increase public transport or accelerate the turnover/decarbonization of the existing fleet. Studies that are not focused on the U.S. include Modaresi et al. (2014). They estimate that lightweighting through greater use of high-strength steel (HSS) or aluminum could reduce cumulative global passenger car emissions (2010-2050) by 4-8% with a further 2-3% reduction possible through closed-loop recycling of the lightweight materials (Modaresi et al., 2014). Elsewhere, in an analysis of Great Britain's passenger car emissions, Serrenho et al. (2017) find that a combination of lightweighting, increasing vehicle intensity of use, and increasing BEV and PHEV sales (60% by 2030 and 100% by 2050) could reduce cumulative emissions (2015-2050) by 21% (Serrenho et al., 2017). In both these studies, emissions-intensive light trucks account for a



negligible fraction of vehicle sales; whereas, light truck (truck SUV, minivan, and pickup) sales have accounted for around 42% of all LDV sales in the U.S. over the last decade (U.S. EPA, 2020).

### 2.1.1 Scope of This Chapter

This chapter seeks to understand the physical basis for how the U.S. LDV sector can cut annual fleet life cycle GHG emissions (the sum of vehicle production, use phase including fuel cycle, and disposal emissions in a single year) by 70% by 2050 from the 2010 level, which is close to the maximum reduction recommended by the IPCC for meeting the 2 °C target (IPCC, 2014). We model the annual life cycle GHG emissions and the global temperature rise attributable to the U.S. LDVs between 2021 and 2050 under a variety of pathways informed by the literature reviewed above and existing policies elsewhere in the world. We attribute to U.S. LDVs any emissions released outside of the U.S. in making or disposing of vehicles and fuels used in the U.S. A business-as-usual (BAU) pathway is defined as the base case set of vehicle life cycle parameters combined with the base case vehicle technology and electricity emissions scenarios (see Section 2.2 Methods).

## 2.2 Chapter Methods

### 2.2.1 Calculating U.S. LDV Emissions and Targets

The basis of the analysis is summarized in Eqns 2.1 and 2.2:

$$\begin{aligned}
 \text{Annual emissions}[kgCO_2/CH_4/N_2O] = & \sum_{P.T.} (EI_{P.T.}^{prod} \times Prod_{P.T.} \\
 & + EI_{P.T.}^{use} \times Fleet\ size_{P.T.} \\
 & + EI_{P.T.}^{disposal} \times Vehicle\ scrapped_{P.T.})
 \end{aligned} \tag{2.1}$$

$$\begin{aligned}
 \text{Global mean temperature rise}_{2050}[^{\circ}C] = & \sum_i \int_0^{t=2051-2021} (Annual\ emissions_i(s) \\
 & \cdot AGTP_i(t-s))ds
 \end{aligned} \tag{2.2}$$

The GHG attributable to U.S. LDVs is the sum of emissions from vehicle production, use, and disposal. For each year of the analysis (2021-2050), we calculate the number of vehicles produced (both domestically and internationally) for U.S. consumption ( $Prod$  in Equation 2.1), the fleet size, and the number of vehicles scrapped. Then, we calculate the emissions of the major GHG species (CO<sub>2</sub>, CH<sub>4</sub>, and N<sub>2</sub>O (IPCC, 2014)) released per vehicle in each year of the vehicle life cycle (emissions intensity, EI). For each year of the analysis, these emissions species are agglomerated in

CO<sub>2</sub> equivalents using the characterization factor (global warming potential (GWP) with a 100-year time horizon). Equation 2.1 is used to calculate a cumulative emissions budget (2021-2050) of 23.1 Gt CO<sub>2</sub> eq. (Appendix A), which corresponds to a 70% reduction in annual emissions (at a constant annual rate) by 2050 from 2010. This budget is similar to previous estimates assuming an equal proportional emissions reduction across all end-use sectors (Yang et al., 2009; Greene et al., 2010; Bastani et al., 2012; Replogle and Fulton, 2014; Supekar and Skerlos, 2017).

The world's remaining temperature budget between 2021 and 2050 if the globe is not to exceed the 2 °C target is 0.87 °C (Appendix A, medium IPCC scenario (Masson-Delmotte et al., 2018)). The annual release of individual emissions species calculated using Equation 2.1 is used in Equation 2.2 to determine the future contribution of U.S. LDVs to the global mean surface temperature rise. Equation 2.2 uses the convolution integral over time of the annual emissions of each GHG species (*i*) and the Absolute Global Temperature Change Potential (*AGTP*) (i.e., global temperature impulse response) of the different GHG species (Appendix A). The global mean temperature rise metric is further down the cause-effect chain from emissions to climate change impacts than the GWP. It may be more relevant for determining the environmental consequences of emissions; however, the calculation is also far more uncertain (Levasseur et al., 2016). It is important to determine whether the temperature rise closely correlates with cumulative CO<sub>2</sub> eq. and therefore whether the conclusions of an emissions analysis are robust across these different climate metric approaches (Levasseur et al., 2016). A gross decoupling of results determined using the two metrics may indicate that over the time period of interest GWP alone is an insufficient metric on which to base mitigation and adaptation policies (Levasseur et al., 2016).

We analyze ten types of powertrains (P.T.) for passenger cars and light trucks: gasoline ICEVs (which can be retrofitted to use bioethanol gasoline (Fuel Flex kit, 2021)), 100-mile BEVs, 200-mile BEVs, 300-mile BEVs, 10-mile all-electric range gasoline plug-in hybrid electric vehicles (PHEVs), 40-mile all-electric gasoline PHEVs, hybrid electric vehicles (HEVs), FCVs, compressed natural gas vehicles (CNGVs) and diesel ICEVs. All these powertrains are included in the U.S Energy Information Administration's (EIA) prediction of powertrains sold into the U.S. LDV fleet between 2020 and 2050 (U.S. EIA, 2020). We model vehicle size class at the resolution of passenger cars, SUVs, and light trucks due to LCA data limitations.

## **2.2.2 Annual Vehicle Production, Fleet Size, and EOL Flows (see section A3 of the Appendix A for more details)**

The future number of passenger cars, SUVs, and light trucks produced, used, scrapped, and recycled each year containing each type of powertrain (needed in Equation 2.1) depends on the size, age, and powertrain composition of the current LDV fleet and the vehicle life cycle parameters: the aggregate LDV vehicle travel demand (measured in kilometers) needed to provide transport

services, the percentage sales of alternative fuel vehicles that determines the addition of different car, SUV and light truck powertrains to the fleet, the vehicle lifespan that determines how often vehicles need to be replaced, and the recycling rate that helps to determine production emissions. These four parameters were selected so that the vehicle and material flow occurring at each stage of the life cycle could be adjusted: production, use, and disposal. The selection was informed by a mechanistic understanding of what drives LDV production (provision of transport services not satisfied by public transport), the fuel requirements of the fleet (the fleet size, age, and powertrain composition), and LDV disposal (vehicle lifespans).

The current age and composition of the U.S LDV fleet (Equation 2.3) were determined using a flow-driven dynamic material flow analysis (DMFA) approach, using LDV production data (1975-2018) from EPA (2020), and vehicle lifespan probability mass functions for passenger cars, and light trucks produced between 1975 and 2020 from Liao et al. (2021) (Liao et al., 2021). In the absence of other data, the vehicle lifespan for SUVs is assumed to be the average of passenger cars and light trucks.

$$Fleet\ size_t = \sum_{t_0=1975}^t (Prod_{t_0} \times (1 - F_{t_0,t-t_0+1})) \quad (2.3)$$

where  $F(t_0, t - t_0 + 1)$  is the cumulative distribution function of the vehicle lifespans (Liao et al., 2021). Future vehicle flows are calculated using a fleet-driven (stock-driven) DMFA where for a given year (t) the number of vehicles scrapped of each powertrain, size, and age (a) is given by Equation 2.4. The production of new LDVs of different powertrains for U.S. consumption is given by Equation 2.5, and the aggregate fleet size is given by Equation 2.6.

$$Vehicle\ scrapped_{t,a} = Prod_{t-a} \times F_{t-a} \quad (2.4)$$

$$Prod_t = (aggregate\ LDV\ travel\ demand_t - \sum_{a=1}^{a_{max}-1} ((Fleet\ size_{t-1,a} - Vehicle\ scrapped_{t,a+1}) \times km\ traveled\ per\ vehicle_{t,a+1})) / (km\ traveled\ per\ vehicle_{t,a=1}) \quad (2.5)$$

$$Fleet\ size_t = Prod_t + \sum_{a=1}^{a_{max}} Fleet\ size_{t-1,a} - \sum_{a=1}^{a_{max}} Vehicle\ scrapped_{t,a} \quad (2.6)$$

To determine the inputs to the fleet-driven DMFA, three life cycle parameters are needed: the

vehicle travel demand, the percentage sales of alternative fuel vehicles, and the vehicle lifespan. The vehicle material recycling rate is then applied to the vehicle DMFA results to determine the recycled content of vehicle materials that will affect vehicle production emissions.

#### **2.2.2.1 Vehicle Life Cycle Parameter Values Simulated**

The future LDV fleet size depends on the aggregate LDV vehicle travel demand (in vehicle km/year) and the average km traveled per vehicle of age  $a$  (in vehicle km/vehicle-year which is a function of both year and vehicle age). We define four values of vehicle travel demand: three extrapolations of the historical U.S. travel trend (base case, low growth, and high growth vehicle travel demand), and a demand substitution case that models increased public transportation, walking, and cycling. The base case aggregate LDV vehicle travel demand is informed by the Federal Highway Administration's report of 1969-2019 LDV travel trends (4.63 trillion LDV km in 2019) (FHWA). (2021) and a prediction that this aggregate demand is likely to increase at an average rate of 0.7% annually (FHWA, 2020), which is consistent with EIA (2020)'s reference case prediction. Sensitivity analyses are included equal to 0.1% and 1.0% annual growth in aggregate demand, corresponding to the EIA (2020)'s low and high economic growth case predictions respectively (see A3 in Appendix A). In any year, the annual km traveled per vehicle of age  $a$  years is a fraction (less than 1) of the kilometers travelled by the vehicle at age 1 year. The decline in the annual km travelled for older vehicles (Appendix A) is derived from U.S. EPA and NHTSA (2016). The annual km traveled per vehicle of age 1 year (new vehicles) is assumed to increase at a constant annual rate of 0.2% between 2021 and 2050 calculated from EIA (2020)'s reference case prediction (A3 in Appendix A). The demand substitution case builds on the analysis of Replogle and Fulton (2014): a transition to European urban transportation patterns that will see increased personal exercise, a doubling in public transport, and both the aggregate and per vehicle U.S. LDV travel demand decrease by 30% at a constant rate from 2023 to 2050 (A4 in Appendix A). When modeling replacement of personal LDV travel with public transportation, we include the additional emissions from vehicle production for public transport (e.g., busses, trains etc.) calculated from Chester and Cano (2016) and Chan et al. (2013) and the use-phase emissions of the new public transport vehicles calculated from Replogle and Fulton (2014) and Logan et al. (2020). However, we do not model the embodied emissions of new public transport infrastructure (e.g., constructing new urban rapid transit systems), which is a limitation of this chapter.

This chapter does not include autonomous vehicle (AV) deployment scenarios because the effect on emissions of level 5 AVs, if and when they became commonplace, is very unclear. Some researchers have suggested that AVs will lower emissions by reducing congestion, parking infrastructure, and leading to lighter vehicles and platooning (Greenblatt and Saxena, 2015; Kopelias et al., 2020). However, others indicate that emissions could rise as AVs lead to increased vehicle

speeds, commuting distances, and unoccupied travel (Fagnant and Kockelman, 2014; Harper et al., 2016; Miller and Heard, 2016; Taiebat et al., 2018).

While the aggregate LDV vehicle travel demand determines the fleet size, the sales share of alternative fuel vehicles determines the powertrain composition of the new LDVs produced and the fleet. We model 7 sales share cases for alternative fuel vehicles. The base case equals the EIA (2020) prediction of future vehicle sales that includes sales of all 10 powertrains and an increasing sales shares for alternative fuel vehicles from 6% in 2020 to 16% of new LDV sales by 2050 (Figure A3 in Appendix A). All other cases simulate a constant increase in the sales share of a single powertrain from the 2020 value. Four cases simulate a 100% sales share by 2050 for HEVs, PHEV40s (already proven and popular technologies (at Argonne National Laboratory, 2020)), biofuel fuel flex vehicles (a 100% biofuel share is deemed feasible by McCollum and Yang (McCollum and Yang, 2009)), and BEV300s (BEV300 2050) respectively. Our LCAs (Figure A20 in Appendix A) and cumulative emissions results (Figure 2.2) showed that BEVs have the greatest potential to lower life cycle emissions. Therefore, we conducted two further sets of simulations of accelerated BEV300 sales: 100% BEV300 sales by 2040 (BEV300 2040) and 2030 (BEV300 2030). BEV300 vehicles (which have a comparable range to top-selling U.S. ICEVs (Van Haaren, 2011)) are assumed to dominate BEV sales due to range anxiety, as indicated by existing consumer preferences recorded by Accenture (Accenture, 2011). The accelerated BEV sales share simulations are informed by EV deployment plans elsewhere in the world; e.g., the BEV300 2030 case is comparable to the California (Office of Governor Gavin Newsom, 2020), Norway (Norwegian E.V. policy., 2021) and UK's (Twidale, 2020) EV deployment plan. The BEV300 2040 case is comparable to BloombergNEF's prediction of China and Europe EV sales (BloombergNEF, 2020) and the BEV300 2050 case is comparable to BloombergNEF's prediction of the U.S. EV sales shares (BloombergNEF, 2020). FCVs, CNGVs and diesels have the lowest current sales of all the LDV powertrains considered (each <1% in 2019 (U.S. EIA, 2020)). Although emissions attributable to these vehicles are modeled in the base case sales share, we do not simulate FCV dominant, CNGV dominant and diesel-dominant pathways.

Three vehicle lifespans (base case, ICEV early retirement at 20 years, and ICEV early retirement at 10 years) are modeled to determine when a vehicle is likely to be disposed of once it enters the LDV fleet. The base case vehicle lifespan is equal to Liao et al.'s prediction, which models current and future lifespan probability mass functions for U.S. passenger cars, SUVs and light trucks with respect to the year of production. The ICEV early retirement simulations are motivated by our LCAs (section 2.2.3), which show ICEVs have the highest life cycle (and use phase) emissions of all the powertrains analyzed, and the precedent set by the 2009 U.S. "Cash-for-Clunkers" program (Morrison et al., 2010). In the early retirement simulations, ICEV vehicles that have survived to 10 or 20 years old (depending on the simulation) are then scrapped. The scrappage of the old ICEV

vehicles is phased in over a ten-year period (2023-2033) to prevent a large and temporary spike in demand for new vehicles that could not be met by industry. So, in 2023, ICEVs that are 10 years older than the target retirement age (e.g., 20 years old for the case of ICEV early retirement at 10 years) are scrapped. In 2024, ICEVs 9 years older than the target retirement age are scrapped, and so on until all ICEV vehicles reaching the target retirement age are scrapped by 2033 and thereafter. The 10 and 20-year lifespans are selected because they roughly correspond to the range of minimum vehicle ages used to qualify for a subsidy in previous vehicle early retirement programs such as “Cash-for-Clunkers” (Morrison et al., 2010).

Two sets of vehicle material EOL recycling rates are simulated to determine the availability of 13 secondary material feedstocks for new vehicle production. The base case assumes that the recycling rates from 2020 remain constant (A3, Table A4 in Appendix A). The 90% recycling rate case models a constant rate increase in the recycling rate for each material (including those where significant challenges to economic recycling remain; e.g., composites) from the current value to 90% in 2050 starting from 2023. Simulating this high recycling rate case is motivated by the potential for emissions savings from increased recycling (Milford et al., 2011) and the scope for improvement between current closed-loop recycling rates (e.g., 12% for wrought aluminum) and the 90% suggested as a practical maximum by previous researchers (Allwood et al., 2010; RU., 1999).

### **2.2.3 Life Cycle Emissions Released per Vehicle (A4 in Appendix A)**

The emissions released in the production, use, and disposal phases of the vehicle (the EIs in Equation 2.1) are dependent on the energy requirements in each phase and the emissions intensity of the supplied energy. We first define vehicle technology scenarios which are then translated into production, use-phase and disposal energy requirements. Throughout, the split between electrical and non-electrical fuel energy is tracked and, for production, material production vs. manufacturing and assembly energy requirements are disaggregated in order to determine the effect of increased material recycling. The life cycle energy requirements are then translated into life cycle emissions per vehicle using fuel emissions intensities, and electricity emissions scenarios. Figures A20 in Appendix A summarize the calculated life cycle emissions per vehicle for all the powertrains in this analysis.

#### **2.2.3.1 Vehicle Technology Scenarios**

For each combination of powertrain and vehicle size (car, SUV, and light truck), vehicle technology scenarios were defined by reviewing 12 vehicle technology forecasts extracted from the academic (Hawkins et al., 2013; Supekar and Skerlos, 2017; Kim et al., 2010; Milovanoff et al., 2019; Ahmadi et al., 2018; Grunditz, 2016; Shabbir and Evangelou, 2014; Thomas, 2014; Philips

and Megli, 2017; Ambrose et al., 2020) and grey literature (U.S. EPA and NHTSA, 2016; U.S. Department of Energy (DOE), 2015; Moawad et al., 2016). The three vehicle technology scenarios (base case, moderate and high fuel economy improvement scenarios, see Table A6 in Appendix A) are based on increasingly aggressive improvements to the following vehicle characteristics: powertrain efficiency, aerodynamics, rolling resistance, accessory power load (e.g., safety features, air conditioning, and other comfort features), and vehicle lightweighting (through material substitution and battery weight reduction). Full details are in A4 in Appendix A.

The current (2021) powertrain efficiency, aerodynamic drag, rolling resistance, and accessory load for each combination of powertrain and vehicle size are extracted from U.S. EPA and NHTSA (2016). Future powertrain efficiency improvements are informed for: gasoline and diesel ICEVs, and CNGVs by Thomas (2014), Philips and Megli (2017) and Moawad et al. (2016) ; for BEVs by Ahmadi et al. (2018), Ahmadi et al. (2018), Grunditz (2016), and Moawad et al. (2016); and, for FCVs, PHEVs and HEVs by Moawad et al. (2016). For all vehicles, we apply the range of potential improvements to aerodynamic drag, rolling resistance, and accessory load described by Moawad et al. (2016).

The current (2021) material compositions for all combinations of powertrain and vehicle size are extracted from GREET (Argonne, 2020). The GREET material data is chosen because of its U.S. centered production assumptions, comprehensiveness, transparency, widespread use, and public accessibility. Regarding vehicle weight, the base case, moderate and high fuel economy improvement scenarios correspond to vehicle weights in 2050 that are respectively 10%, 20%, and 30% lighter than in 2020. In the base case, it is assumed that HSS will continue replacing mild steel (mass substitution factor of 0.67) until 50% of the mild steel in current vehicles is replaced by 2050. In the moderate fuel economy improvement scenario, 80% of the mild steel in current vehicles is replaced by 2050 with wrought aluminum (mass substitution factor of 0.55). These lightweighting scenarios are defined by calculating the average vehicle lightweighting potential of HSS and aluminum from Kim et al. (2010), Kelly et al. (2015), and Milovanoff et al. (2019). In the high fuel economy improvement scenario, 80% of the mild steel and all of the aluminum in a current vehicle is replaced by 2050 with carbon-fiber-reinforced plastic (CFRP) (CFRP for mild steel: mass substitution factor of 0.50; CFRP for aluminum: mass substitution factor of 0.93). This high fuel economy improvement scenario is informed by the vehicle lightweighting potential of CFRP described by Kelly et al. (2015) and U.S. Department of Energy (DOE) (2015). For PHEVs and BEVs, the weight of the NMC (Ni, Mn, and Co cathode) Li-ion battery is simulated to be 36% lighter by 2025 and constant thereafter across all fuel economy improvement scenarios. Li-ion battery lightweighting is likely as carmakers transition from using the current NMC622 (60% Ni, 20% Mn, 20% Co) traction batteries (Schmuck et al., 2018) of around 150 Wh/kg system level energy density to cheaper and higher energy density NMC 811 batteries. New Li-ion batteries are

assumed to reach a system level (i.e., battery level) energy density of 235 Wh/kg by 2025 equal to the goal set for commercialization batteries set by USABC (USABC, 2020). It has also been widely recognized that reaching a system level energy density of 235 Wh/kg is necessary if the cost and weight of long range electric vehicles is to be similar to ICEVs (Schmuck et al., 2018). We assume that the Li-ion battery capacity, chemistry, and energy density remain unchanged between 2025 and 2050 to avoid modeling the high uncertainties in future battery chemistry choices and associated life cycle impact estimations. The energy density of lead-acid batteries for ICEVs and nickel metal hydride (NiMH) traction batteries (for HEVs and FCVs) are assumed constant (Xu et al., 2017; Ding et al., 2019).

### **2.2.3.2 Use Phase Fuel Economy**

The vehicle technology scenarios define the vehicle characteristics for new vehicles produced in each year of the analysis and for each combination of powertrain and vehicle size. The vehicle characteristics are used in the FASTSim vehicle simulation tool<sup>88</sup> with the Federal Test Procedure (FTP/EPA75) drive cycle (Brooker et al., 2015) to estimate the fuel economy of new vehicles over time (see Fig. A10 in Appendix A for simulated fuel economies); thus, for each type of vehicle the three vehicle technology scenarios correspond to three different projections of new use phase fuel economy over time. The FASTSim vehicle simulator is chosen among many vehicle simulation tools (e.g., ADVISOR, AVL CRUISE, IGNITE by Ricardo) because it is open source (vehicle technology scenarios can be easily edited), computationally fast, and has 90-95% simulation accuracy compared to real-world fuel economy (Brooker et al., 2015). The simulated annual fuel economy improvements lie between the minimum annual improvement rate (1.5%/year) in the recent SAFE standard and the maximum annual improvement rate (5%/year) specified under the previous CAFE standard.

### **2.2.3.3 Production and Disposal Energy (A4 in Appendix A)**

Production energy is the sum of material production, assembly, and finishing (e.g., painting) energy requirements. The vehicle technology scenarios specify vehicle material compositions. These material compositions are converted to material production energy requirements via the energy intensity of primary and secondary production for each material (Table A11 in Appendix A) and each material's recycled content is calculated from the DMFA results and recycling rate parameter (Table A4 in Appendix A)). Energy requirements per vehicle for vehicle assembly and vehicle painting are assumed constant and independent of the vehicle technology scenario and powertrain. For the vehicle disposal phase, we account for the energy needed to disassemble the vehicle, i.e., 1.1 MJ/kg of vehicle mass for disassembly (Argonne, 2020).



### 2.2.3.4 Converting Energy to Emissions

The emissions intensities (EIs) of the fuel and electricity used in each stage of the vehicle life cycle are needed in order to convert the fuel economy, production energy, and disposal energy to GHG emissions. The current (2020) EI of biofuel (production and combustion) is extracted from the EPA report on biofuel life cycle emissions (U.S. EPA , 2020) and the EIs of all other fuels are extracted from GREET. The average proportion of fuel ethanol in typical U.S. gasoline (a blend of gasoline and ethanol) is modeled to increase from 10% in 2021 to 15% by 2050 based on EPA's analysis (U.S. EPA , 2019). For all fuels other than biofuel, the EIs are assumed to be constant over the modeling time period because combustion emissions are dominant and stoichiometrically determined. For biofuels (i.e., fuel ethanol), production emissions are dominant and could decrease significantly with changes to the feedstock and production technologies. 96% of current fuel ethanol is produced from corn starch through conventional dry milling (Garside, 2020) and their EI is averaged around 80% of gasoline (U.S. EPA , 2020). Cellulosic ethanol production, e.g., from switchgrass, has an average EI of 30% that of gasoline (U.S. EPA , 2020) and currently accounts for <1% of fuel ethanol production (Garside, 2020). The Energy Independence and Security Act of 2007 set the goal of 16 billion gallons of cellulosic ethanol production by 2022 but this is not happening yet (Garside, 2020; U.S. EPA , 2007; U.S. Department of Energy , 2016). In this analysis, cellulosic ethanol production is modeled to account for 10%, 50%, and 80% of all biofuel production in 2050, corresponding to the base case, moderate and high fuel economy improvement scenario respectively.

Approximately 17% of current (2021) U.S. electricity is generated from renewable sources (U.S. EIA, 2020), corresponding to an average U.S. EI of 421 g CO<sub>2 eq.</sub>/kWh delivered. Various U.S. electric companies (e.g., Pacific Gas and Electric (2017)) have plans for low carbon grids by 2050, and numerous researchers have shown that 80-100% renewable grids are feasible (Pacific Gas and Electric, 2017; Cochran et al., 2015; Heard et al., 2017; Pleßmann et al., 2014; Connolly et al., 2011). In this analysis, we, therefore, define three electricity emissions scenarios (Table A10 in Appendix A) corresponding to increasingly aggressive, but feasible, grid decarbonization: (1) A base case 30% electricity EI reduction following EIA's reference scenario prediction in the Annual Energy Outlook 2021 (from 421 g CO<sub>2 eq.</sub>/kWh in 2021 to 295 g CO<sub>2 eq.</sub>/kWh in 2050 with rapid decline before 2035), (2) An electricity EI decreasing by 50% at a constant rate from 421 g CO<sub>2 eq.</sub>/kWh in 2021 to 211 g CO<sub>2 eq.</sub>/kWh in 2050, and (3) An electricity EI decreasing by 80% at a constant rate from 421 g CO<sub>2 eq.</sub>/kWh in 2021 to 84 g CO<sub>2 eq.</sub>/kWh in 2050.

## 2.3 Chapter Results and Discussion

In this analysis, we simulated 1,512 future pathways for the U.S. LDV sector: 4 LDV transport demands, 7 different deployments of alternative fuel vehicles, 2 recycling rates, 3 vehicle lifespans, 3 vehicle technology scenarios, and 3 electricity emissions scenarios (Table A13 in Appendix A). The BAU pathway results in 34.8 Gt.CO<sub>2</sub><sub>eq.</sub> of cumulative emissions (2021-2050): 51% above the cumulative emissions limit compatible with 2 °C of global warming (23.1 Gt.CO<sub>2</sub><sub>eq.</sub>). Across all simulation pathways, the dominant GHG is CO<sub>2</sub>, accounting for 91-95% of carbon dioxide equivalent cumulative emissions. Use phase emissions account for the majority of the cumulative emissions under all simulated pathways. Disposal emissions are negligible (<1%) and production emissions vary from 7% to 35% of cumulative emissions.

Only 3% of the simulated pathways stay within the emissions limit. Figure 2.2 shows the sensitivity of the cumulative emissions to the simulated powertrain sales share parameter. Even with a 100% sales share of alternative fuel vehicles by 2050, none of the pathways meet the cumulative emissions limit. A BEV300 2050 pathway comes close but only when combined with the most favorable set of vehicle life cycle parameters and electricity and fuel economy scenarios.

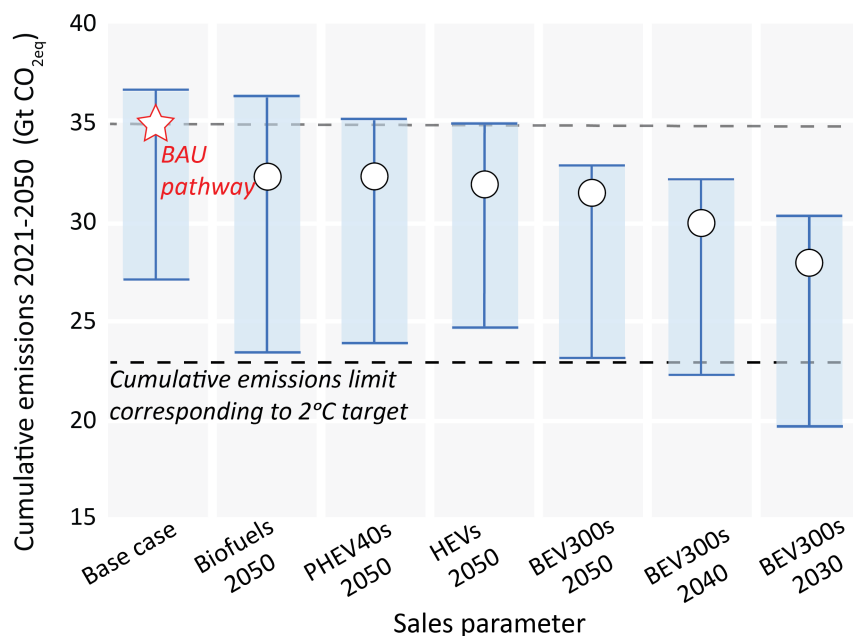


Figure 2.2: Cumulative CO<sub>2</sub><sub>eq.</sub> emissions for the powertrain sales share simulations. The circular data points show the emissions when all other parameters and scenarios are base cases. The error bars show the range of cumulative emissions achieved by varying the other vehicle life cycle parameters and the electricity decarbonization and fuel economy scenarios. Table A14 describes the pathways corresponding to the error bar limits for each sales share simulation.

Figure 2.2 shows that accelerating BEV deployment to 100% of sales before 2050 might enable the emissions target to be met. Hydrogen FCV dominant, CNGV dominant, and diesel dominant pathways were not simulated and are not included in Figure 2.2. These powertrains each account for <1% of current U.S. vehicle sales. Vehicle level LCAs (Figure A20 in Appendix A) also show that these powertrains are unlikely to deliver the same emission savings as BEVs, PHEVs, or HEVs. For example, hydrogen FCVs use more electricity than equivalent BEVs because of energy losses from converting electricity to hydrogen and then back to electricity as well as potential hydrogen losses in storage (Bauer et al., 2015; Shinnar, 2003).

Figure 2.3 presents how the percentage of simulated pathways (not to be interpreted as probabilities) that stay within the cumulative emissions limit changes with the modeled vehicle life cycle parameters, vehicle technology scenarios, and electricity emissions scenarios. Figure 2.3 shows that the cumulative emissions are most sensitive to the speed of fleet electrification: the sales share of BEVs, the electricity EI, ICEV lifespans, and the demand for LDV transport. Cumulative emissions are relatively insensitive to increases in the EOL recycling rate and the fuel economy of individual powertrains.

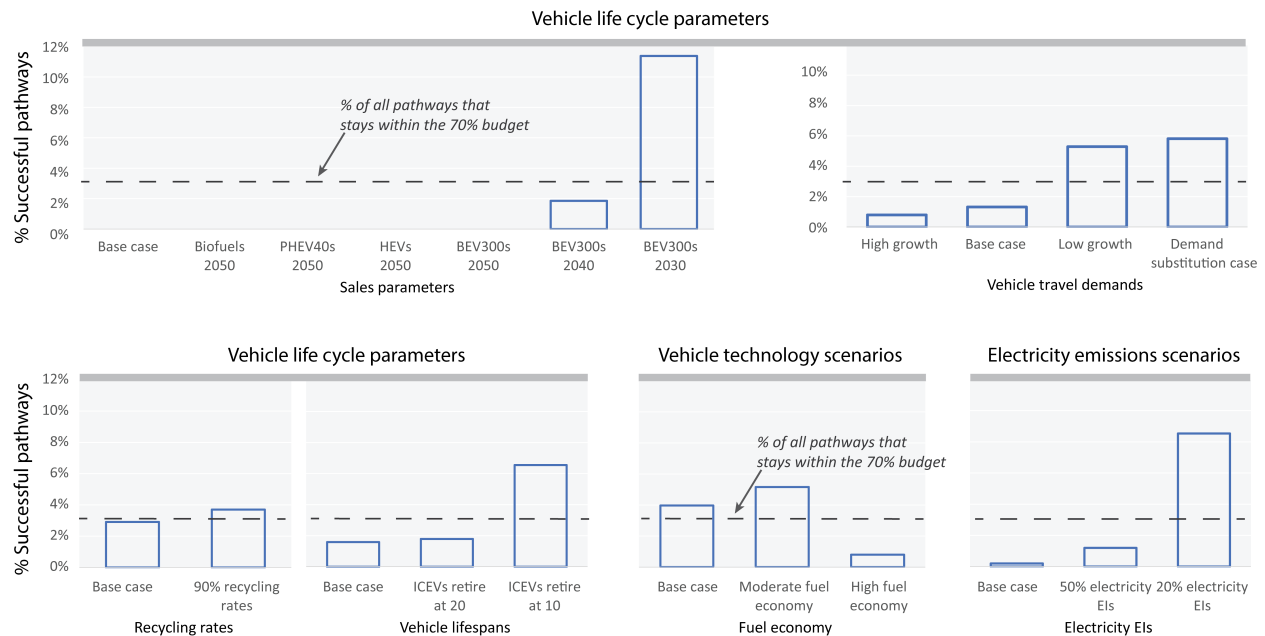
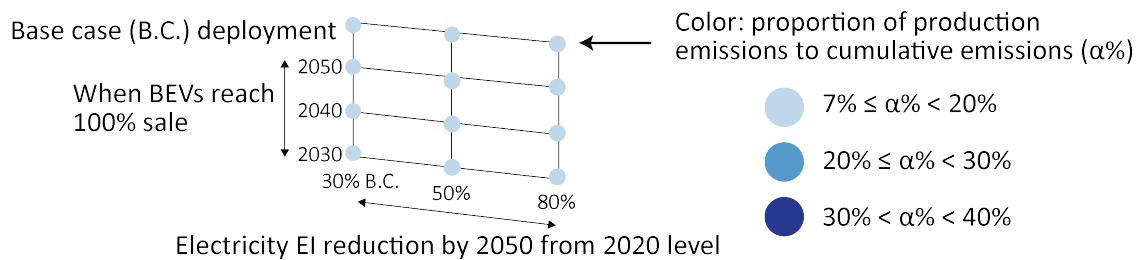


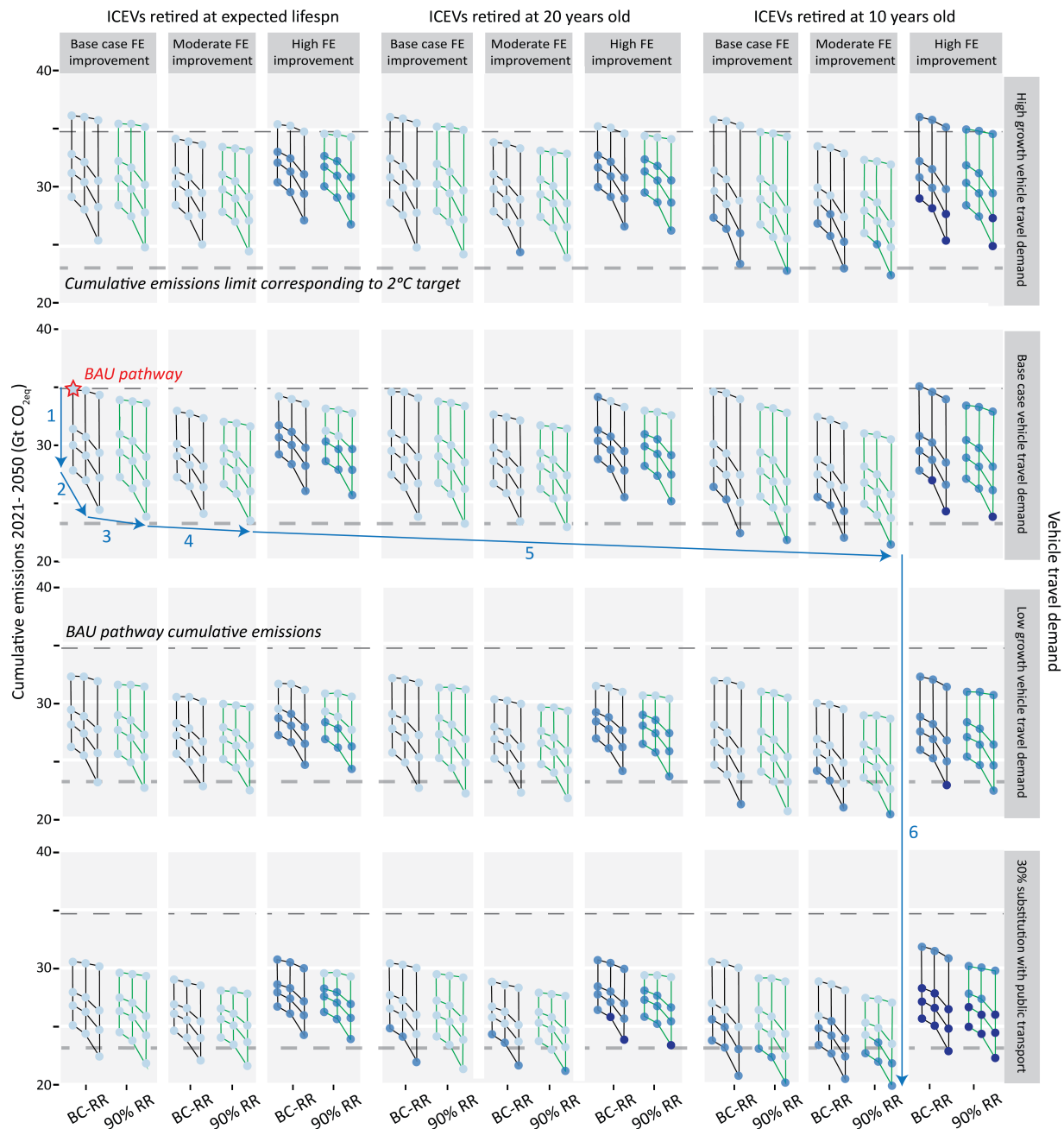
Figure 2.3: The percentage of pathways that stay within the cumulative emissions limit (i.e., ‘successful’ pathways) for changing vehicle life cycle parameters (top and bottom-left), vehicle technology scenarios (bottom-center), and electricity emissions scenarios (bottom-right).

### 2.3.1 How the U.S. LDV Sector Can Meet the Emissions Target

Figure 2.4 focuses on the base case and BEV dominant pathways. It presents how the parameters and scenarios combine to determine the cumulative emissions for each pathway, the fraction of those emissions attributable to vehicle production, and which combinations stay within the cumulative emissions limit. We focus on BEVs because both our LCAs (section 2.2.3 2.3 and A4.4 in Appendix A) and system-level results (Figure 2.2) showed that deploying BEVs has the greatest potential to lower life cycle emissions. The results shown in Figure 2.4 are likely to be indicative of similar interactions (e.g., the variation in cumulative emissions attributable to changing fuel economies) for other powertrain deployments.



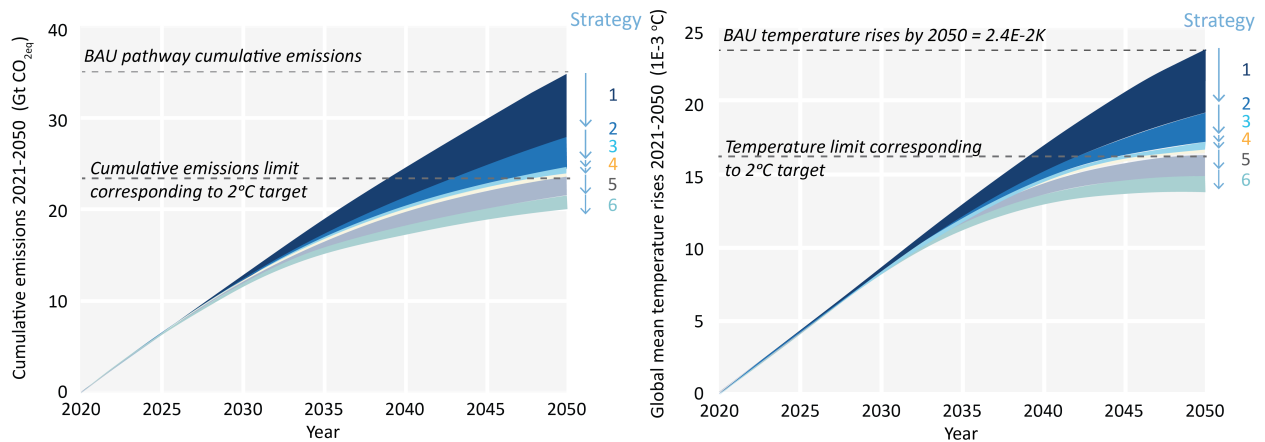
(a) The horizontal position of a node on a flag corresponds to the Electricity emissions scenario and the vertical position of the node corresponds to the Sales share of alternative fuel vehicles.



(b) Cumulative emissions for varying vehicle life cycle parameters, vehicle technology scenarios, and electricity emissions scenarios. The higher dashed horizontal lines refer to BAU pathway emissions and the lower dashed lines refer to the cumulative emissions limit. FE: fuel economy. BC-RR: base case recycling rates. 90% RR: 90% recycling rates. The numbered arrows correspond to the cumulative emissions wedge plot shown in Figure 2.5

Figure 2.4: Cumulative  $\text{CO}_2_{\text{eq}}$  emissions attributable to U.S. LDVs. The cumulative emissions limit compatible with the  $2^\circ\text{C}$  target is  $23.1 \text{ Gt CO}_2_{\text{eq}}$ , 38% lower than the BAU emissions. An equivalent figure showing global temperature increases is presented in Figure A23 in Appendix A.

All pathways in Figure 2.4 that stay within the cumulative emissions limit represent a significant departure from BAU. No single strategy represents a ‘silver bullet’. Immediate actions are needed to accelerate fleet electrification and electricity decarbonization (section 3.2), limit transport demand (section 3.3), and limit the growth of production emissions (section 3.4). Figure 2.5 shows that without intervention (BAU pathway), the U.S. LDV sector is likely to exceed its cumulative emissions budget by 2039 and cause  $2.7E-3$  °C of global warming by 2050, 2.71% of humanity’s remaining 2 °C budget. Figure 2.5 also shows one pathway for how multiple strategies may be combined to satisfy the emissions limit and reduce the contribution to global warming to 1.59% of the remaining 2 °C budget.



	U.S. LDV GHG Mitigation Strategies	% reduction from BAU cumulative emissions	% reduction from BAU temperature rises	Contribution to remaining 2°C budget
	BAU pathway	0%	0%	2.71%
Strategy 1	+BEV300s reach 100% sales by 2030	-20%	-19%	2.21%
Strategy 2	+80% Grid GHG intensity reduction	-10%	-9%	1.97%
Strategy 3	+90% EOL closed loop vehicle and battery recycling by 2050	-2%	-2%	1.93%
Strategy 4	+20% vehicle lightweight by 2050 for moderate fuel efficiency improvement	-1%	-1%	1.90%
Strategy 5	+Retire ICEVs older than 10 years starting 2020	-6%	-7%	1.72%
Strategy 6	+Absolute reduction of 30% LDV travel	-4%	-5%	1.59%

Figure 2.5: Cumulative CO<sub>2</sub>-equivalent U.S. LDV emissions and attributable global warming. Decarbonization strategies correspond to the numbered arrows in Fig 3b.

Figure 2.5 shows the close correlation between LDV cumulative carbon dioxide equivalent emissions and the attributable global temperature increase; thus, the conclusions of this chapter are robust across these two climate metrics. This close correlation is likely because CO<sub>2</sub> dominates annual GHG emissions (91%-95%) in all the simulated pathways and has a relatively constant temperature response. We would expect less correlation in a system (e.g., a natural gas power plant) with greater emissions of GHGs (e.g., CH<sub>4</sub>) that exhibit a clearer time-varying temperature impulse

response (Edwards and Trancik, 2014).

### 2.3.2 The Role of Fleet Electrification

All successful pathways require quicker BEV deployment than in the BAU pathway (12% sales share in 2050). 100% BEV sales before 2050 is a necessary condition of meeting the target (Figure 2.3) and 100% BEV sales by 2030 is likely to be required unless transport demand plummets (Figure 2.3)). This rapid increase in sales will likely require a U.S. government BEV deployment plan similar to that in the UK (reaching 100% alternative fueled vehicles by 2030 (Twidale, 2020)) or California (reaching 100% alternative fueled vehicles by 2035 (Office of Governor Gavin Newsom, 2020)). Switching from the BAU pathway to 100% BEV300 sales by 2030 reduces cumulative emissions by 20% but still exceeds the limit (Fig. 2.4). Combining 100% BEV300 sales by 2030 with an 80% reduction in the electricity EI by 2050 further reduces cumulative emissions but is still insufficient to meet the emissions limit. Early retirement of ICEVs is likely to be needed to accelerate the conversion of the LDV fleet to BEVs.

The quickest conversion of the fleet to BEVs simulated in this analysis (100% BEV300 sales by 2030 with retirement of ICEVs older than 10 years phased in between 2023 and 2033) sees a BEV only fleet by 2040 which, when combined with an 80% decrease in electricity EI, reduces cumulative emissions from the BAU by 36% to 22.4 Gt CO<sub>2</sub> eq., successfully satisfying the emissions limit (see Figure 2.4)). A decades-long retirement plan requires U.S. government support and would be expensive: the 2-month U.S. “cash-for-clunkers” program in 2009 increased annual sales by 3-5% but cost \$3 billion (Mian and Sufi, 2012). As a cheaper alternative to early retirement, we also simulate converting all ICEVs older than 10 years from 2023 onwards to run on 85% (low emission cellulosic) ethanol-gasoline by retrofitting them with ethanol fuel flex engine injector kits (\$300-500/vehicle (Fuel Flex kit, 2021)). Combined with 100% BEV300 sales by 2030 and an 80% decrease in electricity EI, this retrofitting strategy reduces cumulative emissions from the BAU pathway by 36% in the base case transport demand (just below the emissions limit) and assumes that the challenges associated with the rapid increase of cellulosic ethanol production are overcome.

The annual electricity demand for LDVs increases under all simulated pathways. Decarbonized electricity not only benefits new vehicle production and BEV operation but also reduces the use phase emissions of BEVs and PHEVs (but not HEVs) already on the road. In 2021, 78 TWh of electricity (the equivalent of 2% of 2020 U.S. delivered electricity, 3,754 TWh) was used to make, use, and dispose of U.S. LDVs. Under the BAU pathway, electricity demand will increase by 170% to 210 TWh in 2050. Annual electricity demand is even higher in 2050 under the successful pathways: an average of 1,380 TWh (9% production, 91% use phase, <1% disposal) and equivalent to 37% of 2020 U.S. delivered electricity. Supekar and Skerlos (2017) calculate that high adoption of wind and solar power combined with the early retirement of coal/petroleum power plants is

needed between 2030 and 2050 to ensure that at least 50% of this increased electricity demand is generated from renewables by 2035. Without grid decarbonization, the benefits of BEVs are significantly diminished as can be seen in Figure A20 in Appendix A (vehicle LCAs as a function of electricity grid EI) and by the stretching of each individual flag plot in Figure 2.4 towards the bottom-right. In addition to the potential GHG emissions benefits, converting the fleet to BEVs also reduces emissions of air pollutants such as volatile organic compounds, NO<sub>x</sub>, SO<sub>2</sub> and PM2.5 (Ke et al., 2017).

### **2.3.3 The Role of LDV Transport Demand**

The results show the importance of driving less in being able to meet the emissions target. Cumulative emissions are sensitive to even the modest variation in transport demand predicted by the EIA (Figure 2.3). The 30% reduced LDV demand case (accompanied by increased urban public transport and exercise) further reduces cumulative emissions and makes it possible to observe the emissions limit without early retirement of ICEVs (Figure 2.4). Increasing low-carbon public transportation is a priority of the new Biden administration (Biden, 2021); however, delivering European style urban transport systems will require \$trillion-level investments in efficient and widespread public transport as well as safe and attractive conditions for walking and cycling (Replogle and Fulton, 2014). Previous studies have found that these changes may be difficult in the U.S. due to the population density, historical transport policies, and cultural attitudes (Sager et al., 2011; Buehler, 2011; Ercan et al., 2016). Another barrier to reducing transport demand while also improving fuel economies (and a limitation of this chapter) is the potential for rebound effects. For example, Craglia and Cullen (2020) found that improving vehicle efficiency has resulted in increased travel in the U.K. with a rebound effect of around 5%. EPA and NHTSA (2016) assumed a rebound effect of 10% in the technical assessment report for CAFE standard based on another U.K. study by Sorrell and Dimitropoulos (2008) while the California Air Resources Board used a rebound effect of 3% when setting the Advanced Clean Cars Program. Some of the pressure to reduce LDV mileage through increased public transport may be relieved through increased remote work: 30% of U.S. LDV transport vehicle mile demand is for commuting to work (NHTSA, 2017). Recent U.S. worker surveys reveal that 24-35% of U.S. workers are able to work remotely (Duffin, 2020; Statista, 2021).

### **2.3.4 The Role of Production Emissions**

Production emissions will account for an increasing share of LDV emissions in the coming decades. In the successful pathways, the average share of annual emissions attributable to production is 38% in 2050. This compares to 10% of annual emissions in 2021. The share of production



emissions is increased by the shift towards BEVs, the use of lightweight structural materials, the early retirement of ICEVs, and the rapid production of new public transport vehicles (Figure 2.3).

Figure 2.4 shows that in the high fuel economy improvement scenario (where CFRP is used to extensively replace mild steel and aluminum), cumulative emissions are typically higher than in the moderate fuel economy improvement scenario and can even exceed the cumulative emissions in the base case fuel economy improvement scenario if early retirement takes place. This increase in cumulative emissions is caused by an increase in annual production emissions under the high fuel economy improvement scenario (all over scenarios and parameters being equal to their base case values) of 108% by 2050 and despite a decrease in annual use phase emissions of 47% (Figure A21 in Appendix A).

Increasing the EOL recycling rate for vehicle materials to 90% by 2050 decreases cumulative emissions by only 1-5% (Figure 2.4). Approximately a third of these savings are from EV battery recycling and two thirds are from increased recycling of structural materials. The savings are small because either recycling rates are already high (for traditional vehicle materials) or it will be decades before scrap volumes rival new material demand (for EV batteries and emerging structural materials such as aluminum sheet and composites, Figure A25 in Appendix A). Similarly, BEV battery recycling will not be able to supply a significant share of the critical materials (cobalt, lithium, manganese) needed for lithium-ion battery production.

Electricity currently accounts for approximately 30% of vehicle production energy and will increase to an average of 39% in the successful pathways because of electricity-intensive NMC Li-ion battery production. Therefore, the electricity EI has a significant effect on the production as well as use phase emissions (Figure A20 in Appendix A). The EI of upstream production (e.g., aluminum-making) might be reduced through sourcing more material from smelters using renewable hydro energy rather than coal-heavy grids (Cooper et al., 2017). In downstream manufacturing, there is the potential to reduce material demand by increasing process material utilization (Cooper et al., 2017; Allwood et al., 2010) and to build “passive” factories powered by on-site renewable energy generation (Raykar, 2015). Otherwise, vehicle downsizing (without extensive material substitution) could reduce production (as well as use phase and disposal) emissions but is in conflict with current U.S. customer preferences for larger vehicles (U.S. Department of Commerce, 2018). Customer preferences could change, and sales of smaller vehicles could be incentivized by the government. The potential emissions savings are significant. For example, if all SUV and light truck sales from 2023 onwards were instead purchases for passenger cars, then that alone would reduce cumulative emissions from the BAU pathway by 10-18%.

### 2.3.5 Chapter Conclusions and Limitations

This chapter has laid out the scale and urgency of the transformation needed for emissions from U.S. LDVs to reduce in line with the 2 °C target. New policies are needed to address key challenges including rapid BEV deployment and electricity decarbonization, supplying cellulosic biofuels at scale, financing public transport systems and “cash-for-clunkers” programs to accelerate BEV penetration, and changes to behavior/work to reduce transport demand. This analysis has highlighted the need for low carbon vehicle production because of the shift towards transport production emissions. This effect is likely to be repeated, at least in the short term, in the power sector as new renewable power and BEV infrastructure is built; therefore, an increasing focus is needed on low carbon production as well as on reducing use phase emissions.

Several limitations have been discussed in the analysis. The environmental impacts associated with the public transportation infrastructure and charging infrastructure are not considered in this analysis due to modeling complexity. A direction for future research would be a comprehensive analysis of transport sector, industry sector, building and construction sector to avoid the danger of shifting the environmental burden from the transport sector to the other sectors. The option of autonomous vehicles is not considered in this analysis due to high uncertainties associated with L-5 autonomous driving. In addition, there are uncertainties with the future LDV travel demand predictions due to possible rebound effects with autonomous vehicles, fuel efficient vehicles or electric vehicles. This rebound effects will likely increase emissions from vehicles and make it even harder for the U.S. LDV sector to meet the 2 °C target.

Chapter reprinted with permission from Zhu, Y., Skerlos, S.J., Xu, M. and Cooper, D.R., 2021. Reducing Greenhouse Gas Emissions from US Light-Duty Transport in Line with the 2 °C Target. *Environmental Science & Technology*, 55 (13), pp.9326-9338.. Copyright 2021 American Chemical Society.

## Chapter 3

### Mapping the Annual Flow of Steel in the United States

Publication related to this work:

Journal articles:

- Zhu, Y., Syndergaard, K. and Cooper, D.R., 2019. Mapping the annual flow of steel in the United States. *Environmental science & technology*, 53(19), pp.11260-11268.
- Cooper, D.R., Ryan, N.A., Syndergaard, K. and Zhu, Y., 2020. The potential for material circularity and independence in the US steel sector. *Journal of Industrial Ecology*, 24(4), pp.748-762 .



A detailed understanding of material flows is needed to target increased material efficiency and the circular economy. In this chapter, the U.S. steel flow is modeled as a series of nodes representing

processes and products. An easily updatable nonlinear least squares optimization is used to reconcile the inconsistencies across 293 collated data records on flows through and between the nodes. The data come from an integrated analysis that includes top-down estimates of steel flow from trade bodies and government statistical agencies, bottom-up estimates of the steel embedded in products based on production statistics and bills of materials, and the mass of imports and exports based on international money flows. A weighting methodology is used to consistently assign confidence scores to the data and the optimization is used to achieve mass balance and minimize the sum of the squares of the weighted residuals. The results indicate that yield improvement efforts should focus on sheet metal forming in the car industry, which accounts for nearly half of all generated fabrication scrap. The quantity of end-of-life scrap exported and landfilled is greater than the quantity of steel products imported. Increased domestic recycling of end-of-life scrap might displace around a third of these imports.

### **3.1 Chapter Background**

The steel industry accounts for 30% of global industrial greenhouse gas emissions (GHG) (International Energy Agency, 2008). The Intergovernmental Panel on Climate Change (IPCC) recommends an overall 40% to 70% reduction in GHG emissions from 2010 levels by 2050 (IPCC, 2014). However, with current best steelmaking practices already approaching thermodynamic limits, even deployment of cutting-edge production technologies will not be enough for the steel industry to meet the IPCC's emissions targets (Allwood et al., 2010; Gutowski et al., 2013).

The realization that steel production must decrease if emissions targets are to be achieved has helped lead to new research areas under the banners of 'material efficiency' (Allwood et al., 2010) and the 'circular economy' (Ellen MacArthur Foundation, 2013), both aimed at reducing emissions-intensive material production. Researchers in these new areas require a detailed material map in order to identify opportunities.

Unlike in the developing world, U.S. per capita steel stocks plateaued around 1980. The stock saturation level has been estimated at 9.1-14.3 t/capita (Hatayama et al., 2010; Muller et al., 2006; Pauliuk et al., 2013). Per capita stocks are expected to saturate in much of the developing world to a level similar to those in the U.S. by the late 21st century (Pauliuk et al., 2013; Milford et al., 2013). Therefore, the derived U.S. consumption pattern may represent a population-scaled surrogate model of the future global state.

#### **3.1.1 Previous Steel Maps and Production Statistics**

A detailed snapshot of global production and consumption in 2008 is provided by Cullen et al. (2012), and Pauliuk et al. (2013) estimate the in-use iron stocks for 200 countries for the same year.

Wang et al. (2007) construct global and country level iron cycles for the year 2000. Other global flows focus on the production of crude steel without analyzing the flow of intermediate products (Hatayama et al., 2010; Hernandez et al., 2018; Yellishetty et al., 2010).

There have been numerous studies on steel use in regions and states, including for the U.K. (Michaelis and Jackson, 2000a,b), Japan and Asia (Igarashi et al., 2007; Nakajima et al., 2005), the U.S. (Hatayama et al., 2010; Muller et al., 2006; Pauliuk et al., 2013; Muller et al., 2011), and North America (Pauliuk et al., 2013). However, these studies either present steel flow data at such a low resolution as to make it difficult to glean detailed recommendations or are mainly concerned with steel stock levels and scrap discards, which are only a portion of the overall steel flow.

U.S. focused studies that provide a one year snapshot of the steel flow include Andersen and Hyman, who create calibrated energy and material flow models for the steel industry in 1994 based on publicly available data and starting with raw materials and proceeding through to semi-finished products (Andersen and Hyman, 2001). Müller et al. constructed a flow diagram for steel in 2000 including imports and exports, but only showing aggregated flows of products (e.g., “construction”) (Muller et al., 2006).

The World Steel Association (WSA) releases a yearly dataset showing production, consumption, and trade data for over 80 countries (WorldSteel, 2017). High resolution domestic production data are presented for intermediate products such as hot rolled coil or construction reinforcement bar (rebar). The WSA also publishes international trade data as mass flows but aggregates direct trade (imports and exports of steelmaking raw materials such as iron ore and steel mill products such as cold rolled coil) into broad categories such as “flat products,” and only provide an overall indirect trade mass flow. Indirect trade is of finished products (e.g., automobiles) that contain steel. The WSA provides no information on finished goods fabrication or scrap generation and trade.

The United States Geological Survey (USGS), using data largely derived from the trade body American Iron and Steel Institute (AISI, 2015), presents more specifics on the U.S. steel industry than the WSA. A yearly “Minerals Yearbook” has sections on iron and steel (United States Geological Survey, 2016b), iron and steel scrap (United States Geological Survey, 2016c), and iron ore (United States Geological Survey, 2016d). Unlike the WSA, USGS reports granular data on the intermediate product (direct) imports and exports, and scrap consumption. Neither USGS nor the WSA publishes statistics with standard deviation errors; however, errors are clearly present that manifest themselves as discrepancies both within and across the data sources. One source of error is the process of collecting and aggregating the data through regular surveys of steel companies. For example, the Iron and Steel Scrap section of the 2015 USGS Minerals Yearbook (United States Geological Survey, 2016c) notes that data are derived from voluntary monthly or annual surveys, and that about 68% of known pig iron and raw steel producers responded that year, representing only 32% of the total scrap consumed that year. USGS reports data for the most recent year and several previous years.

Numbers for previous years have often been revised as the result of continuing industry survey returns. There is therefore a tradeoff between the pertinence and the reliability of the data when using the comprehensive USGS datasets to help examine steel flows.

### 3.1.2 Scope of this Chapter

A detailed U.S. steel material flow analysis (MFA) is needed to determine the production (and hence emissions) attributable to U.S. consumption and to identify the most effective strategies to reduce steel demand. This chapter focuses on 2014 as the most recent year for which detailed and reliable production and intermediate product data are available from USGS and the WSA.

The MFA is tabulated in the Supporting Information (Table B2 in Appendix B) and is presented as a Sankey diagram, which is a common form of depicting energy and mass flows (Schmidt, 2008a,b). The flow from U.S. mining and scrap purchases to final U.S. consumption (flow of steel into use) is shown sequentially from the left side of the diagram to the right. The width of the lines on the diagram are proportional to the size of the mass flows.

## 3.2 Chapter Methodology

Several methods exist which could generate a U.S. steel map. Economic data could be used to assign steel flows to monetary flows based on commerce reporting. However, formal input-output tables only provide sectoral level resolution (e.g., construction) and the conversion from money flows to steel flows varies widely among products. Otherwise, top-down data on steel production (e.g., the WSA Statistical Yearbook) can be used to estimate low resolution steel flows to the level of intermediate products (e.g., wire rod) and in some cases low resolution sectors (e.g., transport). The opposite approach of using bottom-up data is based on combining sales data for specific classes of products with average bills of materials.

An integrated analysis is used in this chapter that leverages the knowledge embedded in all the above techniques. Data from trade organizations (e.g., the WSA), governmental scientific agencies (e.g., USGS), and academic literature (e.g., Wang et al. (2007)) is combined with monetary trade statistics (e.g., Comtrade data on imports and exports (UN, 2020)), and bottom-up estimates derived by the authors (see **Data Records on U.S. Manufacturing** . . .). The steel flow is modeled as a series of connected nodes representing major steel processing technologies (e.g., the blast furnace) and major products used and created by industry (e.g., iron ore or passenger cars). Data records from the integrated analysis are cataloged (B3 in Appendix B) under the corresponding flow coordinate shown in Figure 3.1. For example, USGS (United States Geological Survey, 2016d) states that 26.8 Mt of iron (contained within iron ore) enters the blast furnace (BF). This datum is cataloged under the coordinate (1,2). Multiple, potentially conflicting data records may be cataloged under the

same coordinate; e.g., data sources report that domestically produced pig iron exports in 2014 were equal to 6.77 kt (United States Geological Survey, 2016b), 7 kt (United States Geological Survey, 2016a), and 52 kt (WorldSteel, 2017). All these records are cataloged under the coordinate (2,49). Unconventional data referring to multiple flows are cataloged as well. For example, United States Geological Survey (2016b) does not record the production of continuously cast billets, blooms, and slabs separately (each is a “node” in the steel map) but does record the sum of the three. This datum is recorded under coordinate (8,55).

Inconsistencies between the collated and derived data records are reconciled using a least squares optimization model (see **Data Reconciliation**). The next three sections describe the modeled steel flow and the origin of key data records used to generate the steel map. All data records used in this analysis can be found in the Appendix B.

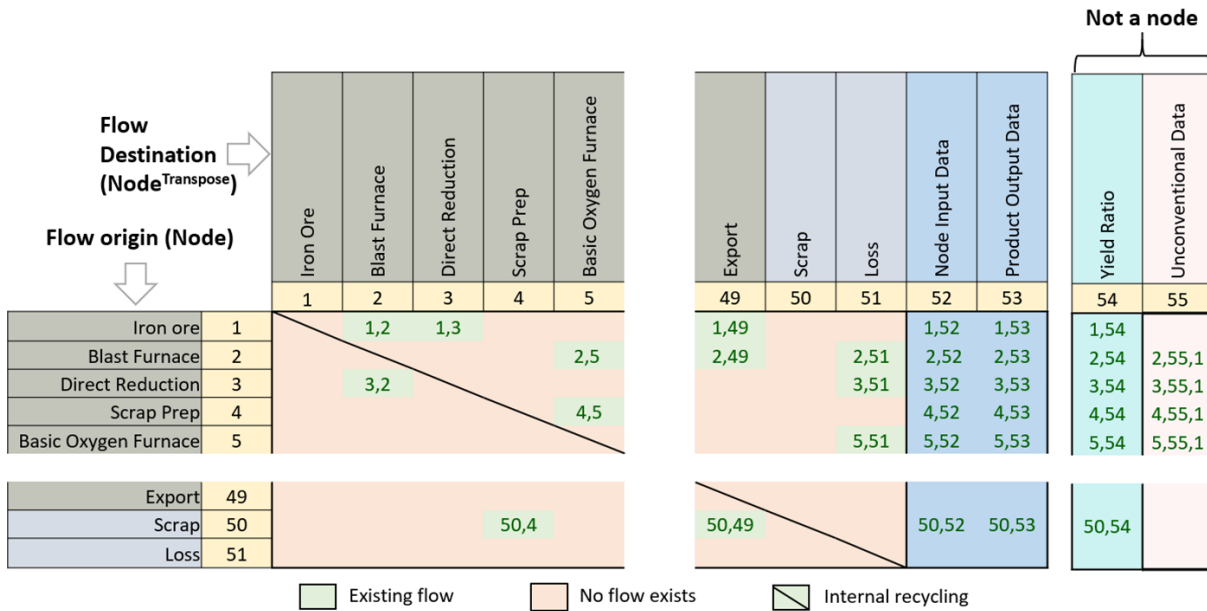


Figure 3.1: The coordinate system used to define the steel flow and catalogue data records. See B1.2 for complete details of the cataloguing method

### 3.2.1 Data Records on the U.S. Steel /industry (Nodes: 1-23)

Steel “flows” from liquid steel production through casting, intermediate product manufacturing, fabrication of end-use goods, use, and finally end-of-life (EOL) processing. There are additional flows into and out of these categories in the form of imports, metal losses, scrap generation, and exports.

### **3.2.1.1 Liquid Metal Production**

In primary steelmaking, iron ore is first converted to pig iron in a blast furnace (BF) and then to steel in a basic oxygen furnace (BOF). Small amounts of scrap, DRI, and other iron inputs are consumed alongside iron ore in the BF. The quantities of each input are reported by United States Geological Survey (2016b). Iron ore production, import, and export are reported in the USGS Minerals Yearbook in both the Iron and Steel section and the Iron Ore section. Iron ore is also used to produce direct reduced iron (DRI), which is another raw material used in steelmaking. The production, import, and export of DRI are reported in the (WorldSteel, 2017) and by Midrex (Midrex Technologies, Inc., 2014).

Liquid high-carbon-content pig iron is typically sent straight from the BF to the BOF, where it is combined with scrap that helps to cool the melt (Yellishetty et al., 2010). However, the pig iron may instead be cast into ingots that are later used for iron castings, scrap contaminant dilution in EAFs, or in BOFs not situated near the BF. The WSA reports the production, import, and export of pig iron in the U.S. (United States Geological Survey, 2016b).

In secondary steelmaking, scrap metal is melted in electric arc furnaces (EAFs) (United States Geological Survey, 2016b). EOL and manufacturing scrap consumption is reported in the USGS Minerals Yearbook in the Iron and Steel Scrap section 25. Some pig iron and DRI, up to 50% of the melt (OICA, 2016), are also used in the EAF to control the concentration of steel scrap impurities.

A small percentage (<1%) of U.S. liquid steel production uses coke-fired cupola furnaces, which use scrap and pig iron as metal inputs (United States Geological Survey, 2016b). The quantities of pig iron, steel scrap, and DRI consumed separately in the BOF, EAF, and cupola furnace are reported in the Iron and Steel Scrap section of the USGS Minerals Yearbook.

### **3.2.1.2 Continuous Casting of Semi-Finished Products**

Liquid steel is refined in a secondary metallurgy process, which happens either in the BOF, EAF or in holding furnaces prior to casting (Pretorius, 2018). The output from the secondary metallurgy process is reported by furnace type in the WSA Yearbook (WorldSteel, 2017). The refined liquid steel is either continuously cast into “semi-finished” shapes (i.e. billets, blooms, and slabs) or cast into ingots, which require additional processing before forming in the “primary mill.” The WSA reports that 98.5% of all steel in the U.S. was continuously cast in 2014 (WorldSteel, 2017). Billets, blooms, slabs, and ingots are rolled into intermediate steel products such as rods, bars, sheets, and plates. Steelmaking, continuous casting, and intermediate product forming frequently occur in the same facility 24, called an integrated mill, reducing the need for reheating between the steps.

No statistics exist on U.S. production of the separate billet, bloom, and slab categories; however, these semi-finished products are used separately to make different types of intermediate good (e.g.,



billets are used to make rod and bar while blooms are used to make sections) and the quantity of each can therefore be inferred by examining the quantity of different intermediate goods produced (B2.2 in Appendix B). The liquid steel flow is simplified by assuming that all steel made in the BOF, which has a low tramp element concentration (e.g., pig iron contains less than 0.01 wt.% copper (Cu) (Company, 2018)) is destined for flat (slab) products, which have a low contamination tolerance; e.g., less than 0.06 wt.% Cu for drawing steels (Daehn et al., 2017). Steel from the EAF supplies the balance of demand for flat products and all demand for billet and bloom products.

### **3.2.1.3 Producing Intermediate Products**

Steel mills sell intermediate steel products and the quantities shipped are reported by USGS at a fine resolution: production, import, and export data are shown for 13 flat product categories, 8 tubing and pipe categories, 6 rod and bar categories, 2 section categories, and 3 cast product categories (United States Geological Survey, 2016d). The WSA also reports domestic production statistics at a similar resolution (B2.3 in Appendix B).

## **3.2.2 Data Records on U.S. Manufacturing and End-Use Products (Nodes: 24-47)**

U.S. manufacturers convert cast and intermediate products into finished components and assembled products. For the steel map, it is necessary to estimate the quantity of different intermediate products used to make different end-use goods, the manufacturing scrap generated by this conversion, and the steel embedded in the end-use products.

Top-down data on the steel flow from intermediate to end-use products are sparse. AISI (2018) estimates the fraction of intermediate steel used to make products belonging to different end-use sectors (B2.4 in Appendix B); e.g., they estimate that 40% of all intermediate products (by mass) are used to make construction products (United States Geological Survey, 2016c). The AISI breakdown reveals neither the types of intermediate products used during manufacturing different end-use products, the quantity of scrap generated during manufacturing, nor the quantity of steel embedded in the final product. United States Geological Survey (2016a) records some data on the annual generation of manufacturing scrap belonging to categories such as turnings and borings. These scrap types can be linked to manufacturing processes (e.g., turnings are created by machining). The scrap quantities recorded by USGS are used in this analysis as lower bounds on the scrap generated from different manufacturing processes and EOL scrap discards.

The above top-down data are supplemented with higher resolution estimates provided by bottom-up analyses conducted by the authors (B2.6 in Appendix B). First, the steel embedded in the different end-use products is estimated by multiplying production numbers with typical product masses and the steel fraction. For example, OICA reports that 4,253,098 passenger cars were produced in the

U.S. in 2014 (OICA, 2016). These cars had an average empty mass of 1,614 kg (U. S. EPA, 2018), of which 65% was steel (13,35,38); therefore, 4.4 Mt of steel was embedded in finished passenger cars produced in the U.S. in 2014. The type as well as quantity of embedded steel is needed to estimate the flow from the various intermediate product nodes to the end-use product nodes. The quantity of an intermediate product category embedded in an end-use product ( $Int.product_{embedded}$ ) is estimated through literature reviews on bills on materials. For example, Schnatterly states that 16.3% of the mass of North American passenger cars is galvanized cold rolled coil (CRC galv.) (Schnatterly, 2010). Therefore, a bottom-up estimate used in the catalogue is that 717 kt of CRC galv. is embedded in U.S. produced passenger cars.

The quantity of intermediate product used to manufacture an end-use product ( $Int.product_{manf}$ ) is equal to the ( $Int.product_{embedded}$ ) divided by the process yield ( $\gamma$ ). The difference between ( $Int.product_{manf}$ ) and ( $Int.product_{embedded}$ ) is equal to the quantity of manufacturing scrap generated when fabricating the end-use product. The process yield  $\gamma = (0, 1)$  is equal to the mass of useful outputs (product or component) from a process divided by the mass of the steel inputs. The process yield depends on both the intermediate product being processed and the final geometry produced; e.g., the process yield when making an irregular sheet metal car side body panel (38%, (Omar, 2011)) is lower than when making rectangular sheet metal domestic appliance panels (80%). Process yields for intermediate product to end-use product flows are extracted from the literature, e.g., Milford et al. (2011) and Horton and Allwood (2017) for stamping) and used as data points in the reconciliation (see Section **Data Reconciliation**).

### 3.2.3 Data Records on International Trade (Nodes 48 and 49)

The mass flows associated with international trade of steel mill products (direct imports and exports) are reported by United States Geological Survey (2016a,b,c,d), U.S. Census Bureau (2015), and the U.S. International Trade Commission (2018). The WSA also reports an aggregated annual estimate of the steel mass flow associated with the international trade of steel-containing finished goods (indirect imports and exports) (United States Geological Survey, 2016b). In this work, finer resolution estimates of indirect steel trade are derived using the U.N. Comtrade Database (UN, 2020). The trade of 29 steel intensive products—as defined by Wang et al. (2007)—is extracted from the database. The traded product mass, when reported by Comtrade, is converted into the traded steel mass by multiplying by steel content factors for each product taken from Wang et al. (2007). The steel traded within the other product categories (for whom Comtrade has only reported a monetary value associated with the trade) is estimated by deriving an empirical relationship between steel intensity (kg.steel per USD of trade) and different product attributes; e.g., end-use sector and fractional iron content (B2.7 in Appendix B).

### 3.2.4 Data Reconciliation (B1)

The integrated analysis inevitably introduces data contradictions and inconsistencies. One method of reconciling incompatible mass flows is to combine the law of mass conservation with expert industry knowledge and judgments on the reliability of the collected data; thus, the practitioner uses her discretion to adjust mass flows while satisfying mass conservation constraints. Such an informal reconciliation was used in Cullen et al.'s seminal work on global steel and aluminum flows (Cullen et al., 2012; Cullen and Allwood, 2013); however, this approach will typically result in a material map that is a suboptimal fit to the available data. This is because, even in the event of a data fit metric being calculated (e.g., sum of the square residuals), it is unlikely that a practitioner can achieve a significant improvement in fit without employing mathematical optimization techniques. Updates to and adaptations of an MFA are time-consuming and require significant industry expertise. This is because, using the informal reconciliation method, the practitioner must manually evaluate the repercussions of any new or deleted flows on the whole network. In this chapter, a formal reconciliation method is used instead to generate the steel map (Figure 3.4).

An informally reconciled steel map is still derived manually in order to compare the methods (B1.5 in Appendix B).

#### 3.2.4.1 Formal Reconciliation Options

At least three formal MFA data reconciliation methods have been identified in the literature (B1.1 in Appendix B): nonlinear least-square optimization (Kopec et al., 2016), Bayesian updating (Lupton and Allwood, 2018), and the RAS input-output matrix method (Ploeg, 1988). This chapter implements a generalized nonlinear least squares optimization method because of its ability to handle a plethora of data types (e.g., pig iron mass flows from BF to BOF, stamping process material yields, and the sum of welded and seamless tube products) and its effectiveness even when few data sources exist per flow variable (Kopec et al., 2016). The STAN software package is the most widely used method of performing a nonlinear reconciliation MFA (Cencic, 2016). STAN is not used in this study because it neither allows multiple data records to be directly considered for an individual flow variable, nor does it include data quality measures.

A generalized least squares method was introduced by Kopec et al. (2016) to revise Cullen et al.'s global steel flow (Cullen et al., 2012). Kopec et al. achieved a significant reduction in the sum of square residuals (between the final MFA variables and data sources) but they did not present a revised steel map. To the authors' knowledge, this chapter will be the first time that a generalized nonlinear least squares data reconciliation method has been used to derive a new material flow map. In addition, a new weighting methodology is presented with which to assign consistent confidence scores to the data sources, and a matrix-based cataloging structure is introduced (Figure 3.4) that

makes it easy for a practitioner to update and adapt the steel map.

### 3.2.4.2 Formulation

Figure 3.1 sets up a basic template for systematic data recording based on the MFA network structure. The matrix template is repeated many times in the code used to define the reconciliation and run the optimization. The different copies of the matrix are used to define different parameters of the steel flow (e.g., the existence or not of a flow between two nodes or the upper bound on a flow) and to enter the data records. Figure 3.2 shows how the matrix in Figure 3.1 is repeated to become a multi-dimensional matrix used to define the flow and catalog the data records. Alongside the schematic in Figure 3.2, are definitions and examples.

Once the matrix is set up for an MFA study, MFA practitioners could follow the procedures listed in Figure 3.3 to perform the formal data reconciliation. The objective function (Equation 3.1) minimizes the sum of weighted normalized square residuals  $r_{i,j}$  between final assigned MFA variables  $x_i$  (where  $i$  is the variable index) and up to  $J_i$  empirical values  $\hat{x}_i$  for the same MFA variables recorded from the integrated analysis ( $\hat{x}_i$  values are recorded in B3.2 in Appendix B).  $x_i$  may refer to any relevant steel flow data; e.g., flows into and out of nodes, between nodes, yield ratios, sums of flows through nodes, etc. A confidence score  $\Phi_{i,j}$  is assigned to each residual-squared to decrease the chance of distorted MFA results due to the inclusion of erroneous data sources. The confidence score corresponding to each empirical data source (see B3.2 in Appendix B) is calculated as the weighted sum across three quality criteria (see Table 1): (1) industry coverage of the data source; (2) recording frequency of the data source; and (3) the spatial coverage, geographically and/or across different manufacturing processes. The criteria were defined by examining common characteristics of widely cited and trusted data sources (e.g., USGS). This methodology helps to ensure a consistent evaluation of data quality.

$$\text{Minimize} : \sum_{i=1}^I \sum_{j=1}^{J_i} \Phi_{i,j} \cdot r_{i,j}^2 / J_i \quad (3.1)$$

Where  $r_{i,j} = (x_i - \hat{x}_{i,j}) / \hat{x}_{i,j}$  are the residuals (normalized to the corresponding data record) and  $J_i$  is the total number of empirical data records for each MFA variable  $x_i$ .

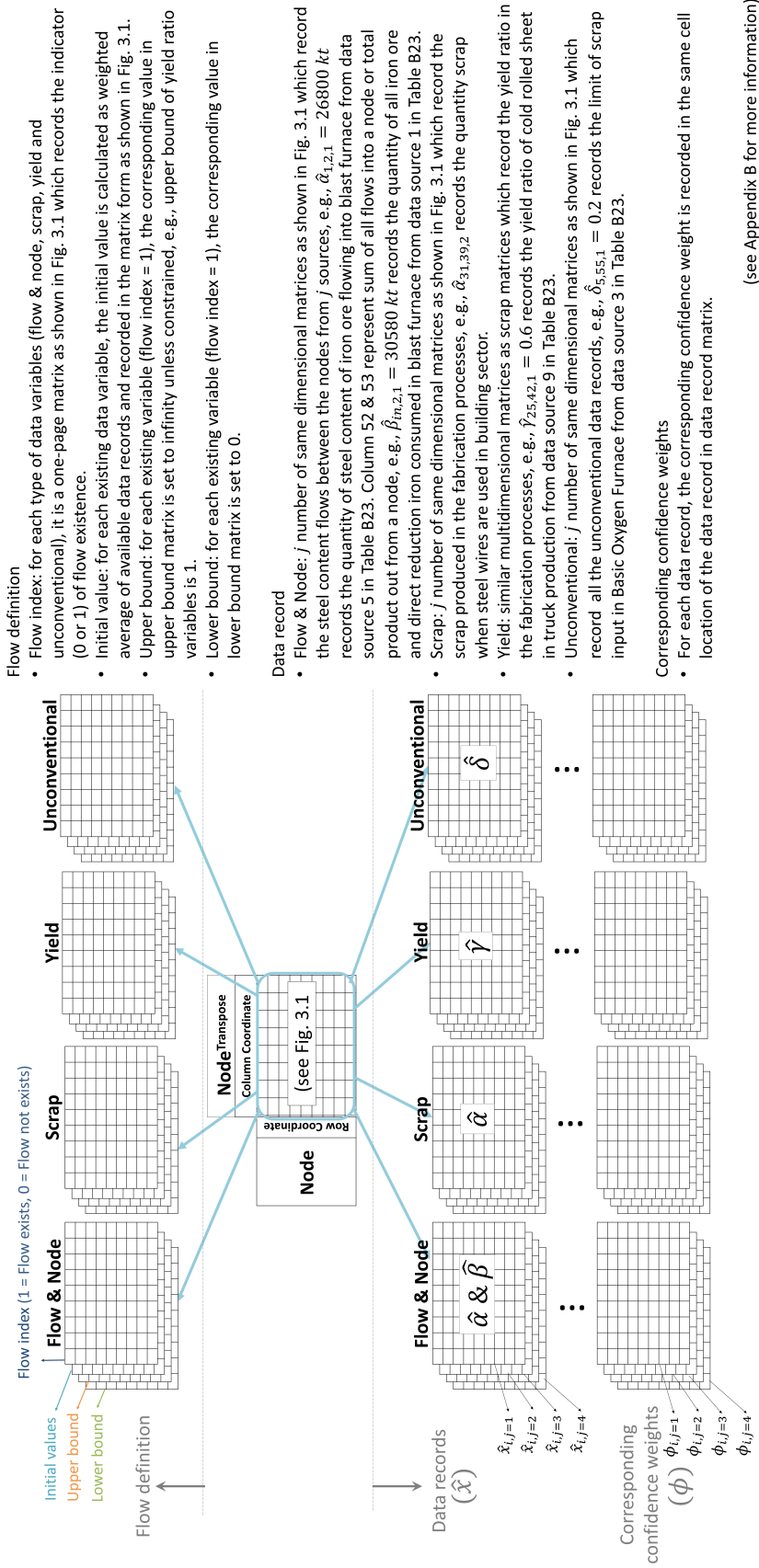


Figure 3.2: The multi-dimensional matrix-based cataloging system used for setting up the reconciliation

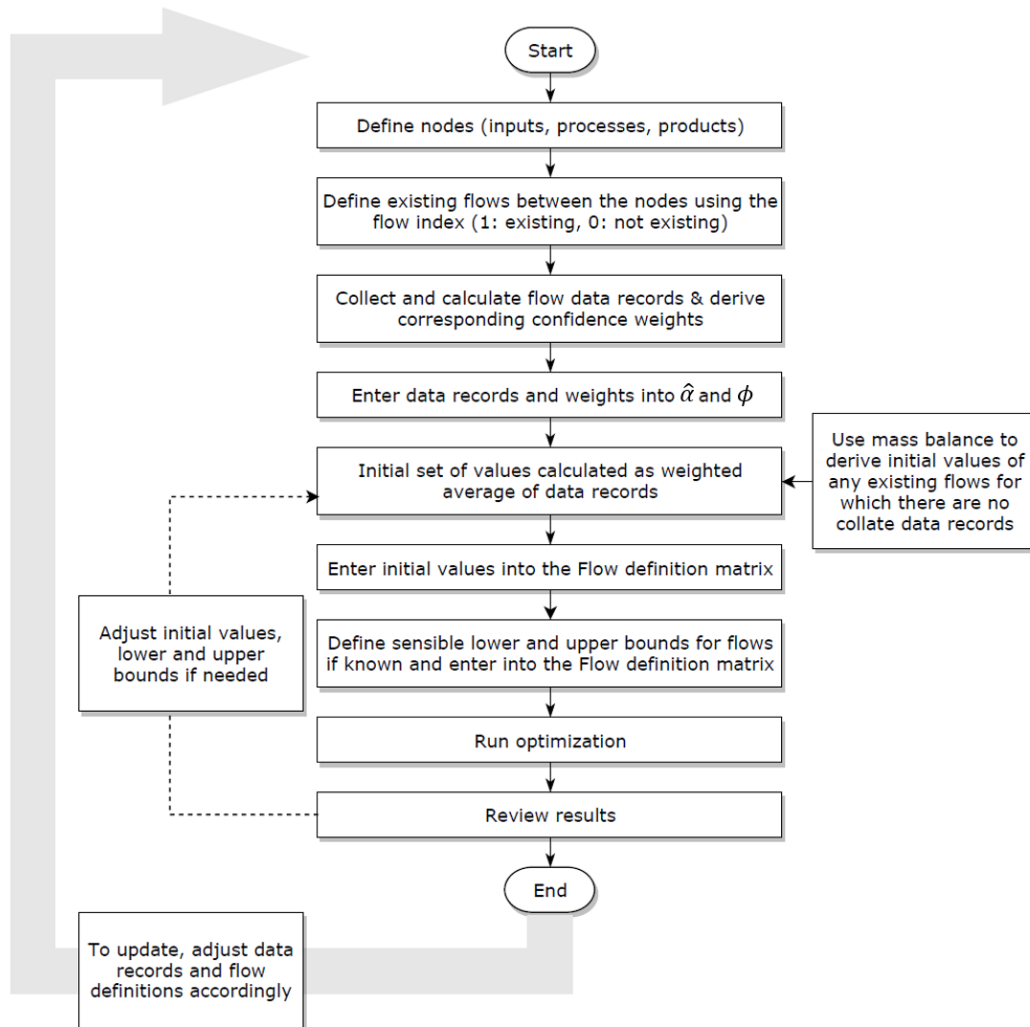


Figure 3.3: A flow chart showing the tasks a practitioner must follow in order to produce a material map using the cataloging structure shown in Figure 3.2

The steel flow contains 464 non-zero variables (Table B3 in Appendix B), comprised of 270 variables representing flows between nodes, 83 variables representing process yield ratios, 78 variables representing total steel flows into and out of nodes, and 33 unconventional variables representing, for example, the sum of all intermediate goods used to make construction products. The optimization is subject to mass conservation constraints (Table B4 in Appendix B): the sum of all flows into a node is equal to the sum of all flows leaving a node. The flow variables were reconciled around 293 empirical data records (elements of  $\hat{x}$ , Table B5 in Appendix B), collated and derived using the integrated analysis described in Section Data records on the U.S. steel industry, Data records on U.S. manufacturing. . . and Data records on international trade.

A sensible initial set of flow variables is derived (B1.4 in Appendix B) to increase the likelihood

Data quality criteria	Score range (1-4)	Weight	Data record (example)	
			WSA	U.S. Dept of Commerce
Coverage	4: 50% of industry 3: 50% of industry 2: Clusters of case studies 1: Single case study	33%	4	3
Frequency	4: Monthly 3: Annually 2: Infrequent 1: Lone data point	33%	3	2
Spatial boundary	4: U.S. only / Same process 3: U.S. Canada/ Parent process group 2: Other industrialized country/Similar process 1: Global Scaling from elsewhere in industry	33%	4	4
Weighted total score			3.67	3
Confidence score ( $\Phi_{i,j}$ :0-1)			0.92	0.75

Table 3.1: Methodology for assigning confidence scores to data records

of the optimization converging to a near global optimum solution. Where available, the initial set uses the weighted mean of all recorded data points for each variable. If no recorded data are available, initial values are calculated using a simple mass balance (B1.3 in Appendix B). The optimization was implemented with Matlab's `fmincon` algorithm using the 'interior-point' method (Byrd et al., 1999; `fmincon` Nonlinear, 2013). It took 450 iterations for the objective function to converge (Figure B3 in Appendix B): 30 hours using an Intel(R) Core™ i7-6600U CPU, 2.81 GHz, with 16 GB of RAM. The optimization achieved mass balance after an initial maximum constraint violation of 10.9 Mt (corresponding to a discrepancy between reported ferrous flows into and out of the EAF: Table B23 in Appendix B) and reduced the objective function by 74% from a maximum of 57.5 during mass balancing to 14.7 at convergence (Figure B3 in Appendix B). Meanwhile, the informally reconciled steel map (B1.5 in Appendix B) has an equivalent objective function value of 19.6.

When new data records are collected, the MFA practitioners could easily add them to the data record matrix shown in Figure 3.2. If the MFA network structure is changed (e.g., if technology advance enables direct reduction iron to be used in the basic oxygen furnace), new MFA variable needs to be added by switching the corresponding flow index from 0 to 1. No other changes to the optimization algorithm will be needed and the MFA practitioners only need to re-run the optimization to generate the new internal consistent material flow network. To reduce the time needed for optimization, previous optimization results could be used as the initial guess for the new optimization.

### 3.3 Chapter Results

The estimated 2014 U.S. steel flow is shown in Figure 3.4 and Table B2 in Appendix B. In Figure 3.4, light grey lines represent scrap flows and black lines represent system losses (e.g., oxidation losses from the EAF). Nearly two-thirds (63%) of U.S. steel production is from EAFs. The recycled content of the inputs to the U.S. steel industry (BOF, and EAF) is 63% but the EOL scrap recycled content is only 40%. Approximately 112 Mt of new steel products entered U.S. service in 2014, requiring the domestic production of 88 Mt of liquid steel and the net import of a further 43 Mt in the form of semi-finished, intermediate, and finished products.

Using E-Sankey software, we create live links between the data reconciliation optimization results file and an automatically updated Sankey diagram (Figure 3.4). The live link files allow the users to regenerate annual U.S. steel maps that require less than an hour to revise the results format, and which could be further automated. This matrix method proves the feasibility of a universal structure for resource flow studies. The quick and updateable feature of the method can greatly reduce the effort required for resource flow research.



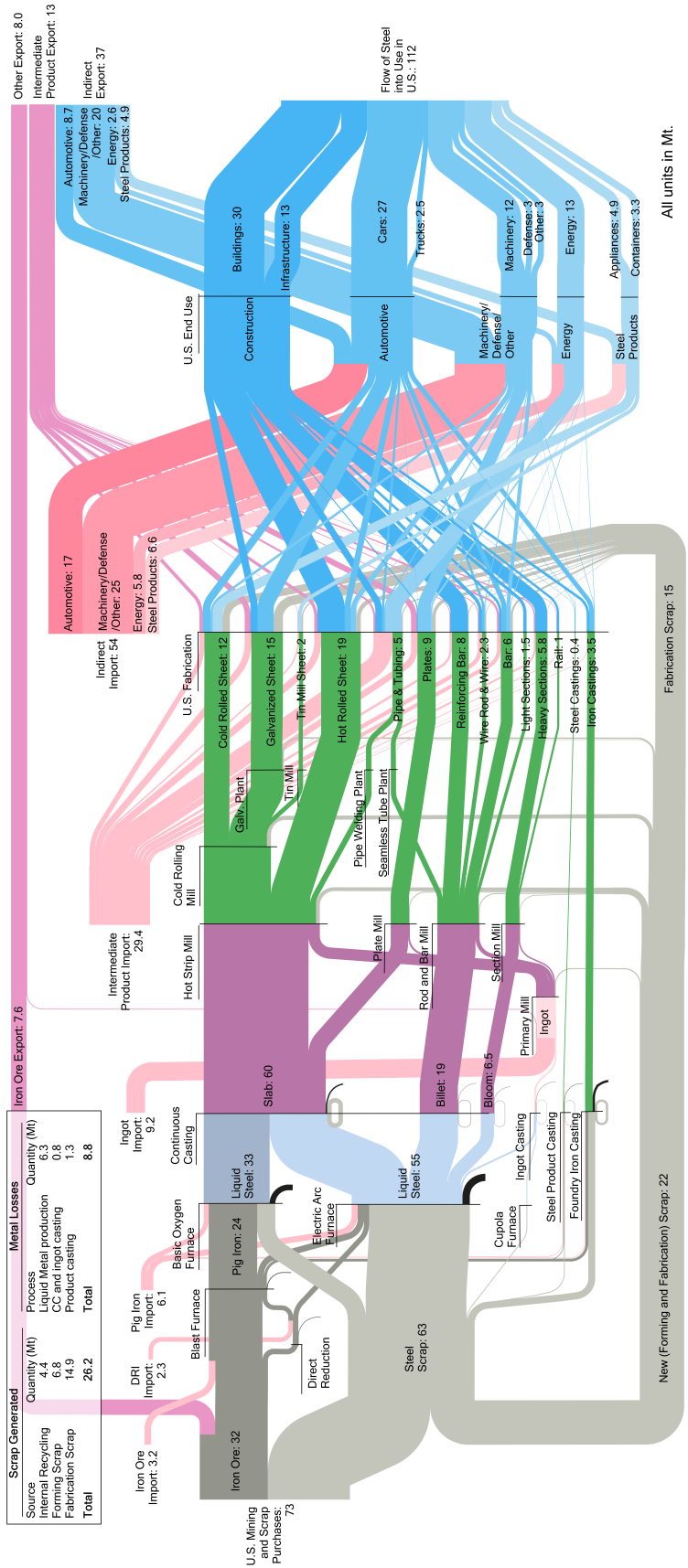


Figure 3.4: Formally reconciled U.S. flow of iron and steel (including embedded alloying elements) in 2014. Drawn using eSankey software. Note: The iron ore flow represents the iron embedded within the ore and excludes the mass of oxygen and gangue.

### 3.4 Chapter Discussion

The steel flow was calculated by first implementing an integrated analysis that leverages the great quantity of data available on U.S. steel flows. This was followed by a nonlinear least squares data reconciliation that ensures conservation of mass and minimizes the deviations of the final flow from recorded data. Distortion of the final result due to the inclusion of erroneous data records was minimized by using a new, structured, weighting methodology to assign confidence scores to the data sources. The optimization reduces the objective function by decreasing the quantity and size of large residuals (Figure B5 in Appendix B). For example, the flow from iron casting to machinery equals 434 kt in the informally reconciled map (weighted normalized residual: 3.11) compared to 267 kt in the formally reconciled map (weighted normalized residual: 0.99). Other differences include less domestically recycled scrap in the formally reconciled steel map (62.1 Mt) than in the informally reconciled map (69.2 Mt) (Figure B4 in Appendix B). This is because the creator of the informally reconciled map, increased the domestic scrap flow to account for an apparent shortfall in ferrous inputs to the BOF and EAF. In contrast, the formal method smoothed the reconciliation of mass imbalances across the network.

#### 3.4.1 Completing the Picture: In-Use Stocks and Scrap Flows

A low-resolution steel map for 2014 (Figure 3.5) is produced by combining the results in Figure 3.4 with EOL steel scrap data (United States Geological Survey, 2016c) and Cooper et al.'s calculated U.S. in-use steel stocks and scrap availability (B4 in Appendix B). The process yields in the Rest of the World (RoW) steel flow are calculated from Cullen et al.'s global map (Cullen et al., 2012). American industry and consumers drove 203 Mt of liquid steel production in 2014, 55% of which took place overseas. Per capita U.S. steel consumption (351 kg/person/year) is double the global average (162 kg/person/year (Cullen et al., 2012)).

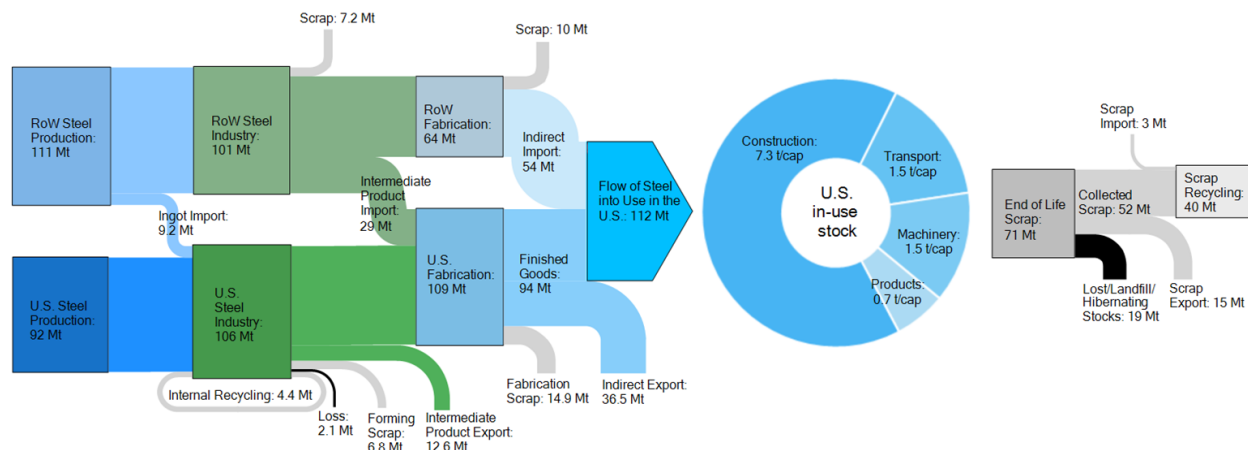


Figure 3.5: Low resolution U.S. steel map for 2014. U.S. population in 2014: 318.6 million.

### 3.4.2 Reducing U.S. Demand for New Steel

There are opportunities to decrease new steel demand by reducing new scrap generated by industry (22 Mt: Figure 3.4). New scrap is not directly lost from the steel cycle, but the energy invested in forming and heat treating the steel has been wasted and additional energy must be invested to recycle the scrap, where mass losses amount to 13% of the scrap inputs. The steel map shows that nearly half (46%) of fabrication scrap is generated from manufacturing sheet metal into automobile parts. This 6.8 Mt scrap flow is double the relative size of the global sheet metal scrap flow, which accounts for only 25% of global fabrication scrap. U.S. industry yield improvements efforts should therefore focus on the automotive industry. Horton and Allwood (2017) find no correlation between stamping process yield and the size of vehicle, production volumes, or the number of sheet metal components. However, scrap quantities may be reduced through stamping innovations. For example, novel technologies could be developed that reduce or replace the gripping area around the periphery of the part during forming. The gripping area is sacrificial material currently necessary to prevent wrinkling and springback of the part. Alternatively, technologies may be developed that allow high-density nesting of otherwise poorly tessellating blank shapes (Carruth and Allwood, 2013). Morgan and Liker show that greater emphasis on minimizing process scrap during new vehicle product and process development could deliver 10% improvements to material utilization without capital investments (Morgan and Liker, 2018). For example, they recommend inserting utilization checks into the design and manufacturing process and making both designers and stamping engineers jointly responsible for achieving utilization targets. Policymakers could encourage greater material efficiency in the car industry by funding metal forming research into reduced scrap generation and by incorporating embodied energy and material utilization metrics into vehicle environmental standards (e.g., CAFE).

U.S. scrap sent to landfill and export (34 Mt) exceeds carbon-intensive pig iron production (24 Mt) and intermediate steel product imports (29 Mt). On the face of it, increased domestic recycling could help to displace these carbon-intensive steel sources. However, a technical barrier to realizing this opportunity is contamination of EOL scrap with tramp elements, of which copper is the primary concern (Material Economics, 2018). Daehn et al. showed that copper contamination does not currently constrain global recycling rates. Their study highlighted that the construction products, in particular rebars ( $\leq 0.4\text{wt.}\% \text{Cu}$ ), act as impurity sinks. In contrast, the cold rolled sheet used mainly in transport applications has the strictest impurity requirements ( $\leq 0.06 \text{ wt.}\% \text{ Cu}$ ). The U.S. has a relatively large end-use transport sector 26% of final consumption in the U.S. (Figure 3.4) versus 13% globally (Cullen et al., 2012) and a small construction sector (38% vs. 55% globally (Cullen et al., 2012)). Moreover, the new steel map shows that just 21% of U.S. construction demand is for impurity-tolerant rebar, compared to 28% globally (Cullen et al., 2012). A smaller construction sector with less rebar means a smaller sink for scrap contaminants.

EOL scrap contains 0.18-0.4wt.%Cu Daehn et al. (2017). With modest additions of pig iron and DRI to the EAF (see Section Recycling contaminated scrap), it is assumed that EOL scrap currently exported and landfilled could be domestically recycled into intermediate products that have a copper tolerance above 0.2wt.%Cu. Therefore, increased domestic recycling might displace around 8.4 Mt (29%) of direct steel imports (B5), including all imports of rebar and sections, but excluding pipe and tubing ( $\leq 0.15\text{wt.}\% \text{Cu}$ ). Further displacement would require either significant dilution with primary iron or an aggressive increase in product design for recycling approaches that reduce EOL scrap contamination; e.g., designing easily detachable copper wiring harnesses for vehicles (Economics, 2018).

### 3.4.3 Global Lessons for the Circular Economy

A circular economy is hindered both in the U.S. and globally by the continuing increase in absolute material stocks and by the imperfect recycling of (often contaminated) EOL scrap. Haas et al. estimate that two-thirds of current global metal production is used to add to, rather than replace, stocks (Haas et al., 2015). For steel specifically, Allwood et al. report that 60% of global production was added to stock in 2006. The American experience analyzed in this study (Figure 3.3) shows that even modest population growth ( $\approx 1\%/ \text{year}$ ) can drive significant new production: despite saturated per capita stocks, 35% of U.S. steel consumption is added to absolute stocks, providing services to new American consumers. A circular U.S. economy could therefore only be realized by a reduction in per capita U.S. stocks, facilitating a proportionate increase in population with no new material being required (if existing material could be perfectly reused or recycled). Strategies to decrease per capita stocks (without a loss in material services) are shown in Table 3.2 alongside design principles, U.S. opportunities, and policy suggestions.

Table 3.2: Strategies to reduce per capita steel stocks

Principles	Opportunities (U.S. examples)	Policy suggestions
Topology optimization.	The American preference for structural steel means that there is relatively high demand for sections: 22% of building demand in U.S. vs. 15% globally. There are opportunities to roll and fabricate optimized steel beam cross-sections that are 25% lighter than prismatic alternatives.	Sustainable building schemes (e.g., LEED) could specify minimum beam utilization rates as a percentage of beam capacity; or, for a given application, a maximum steel structure weight per unit of floor area.
Material selection using "Ashby" principles.		
Part consolidation (e.g., using 3d printing).		
Identify underutilization of loading during use and/or of frequency of use.	The U.S. transport sector is double the size of the global transport sector (26% of final consumption in U.S. vs. 13% globally). Average U.S. car occupancy rates continue to fall (now averaging 1.4 passengers). Increasing transport occupancy rates should be a priority and encouraged through public transport and carpooling schemes.	Flexible public transport systems, and expansion of high vehicle occupancy lanes.  Financial incentives (tax-breaks, interest free loans) for shared services such as laundrettes and multi-use building spaces.
Using smart telecommunications to coordinate simultaneous loading (e.g., uber pool) and/or continual use (e.g., zip car).		
Increase IoT <sup>a</sup>		
Increase IoT <sup>b</sup>		

<sup>a</sup>Reduce product capacity to match required loading.

<sup>b</sup>Increase intensity of use: increase product loading and frequency of use to match capacity.

Note: Prescriptive, product specific (command and control) based policies may be justified because labor taxes neuter incentive based Pigouvan taxes such as a carbon or material tax.

### 3.4.3.1 Recycling contaminated scrap

A small construction sector with relatively little use of rebar means that the U.S. has a small sink for scrap contaminants. The U.S. has partly responded by exporting 29% of the steel scrap it does collect to developing markets with high demand for impurity tolerant construction materials (Pauliuk et al., 2012). The U.S. has also improved the quality of its recycled steel. Globally, high quality flat steel products are overwhelmingly produced using BOF primary metal; no flow from the EAF to flat products is shown in Cullen et al.'s global map. In contrast, Figure 3.4 shows that 28 Mt of U.S. EAF steel is made (mainly by Nucor) into flat products, such as class A car panels. Nucor's strategies include dilution of scrap impurities with virgin metal (pig iron and DRI), the proximity of their mills to generators of clean industry scrap (e.g., car stamping factories), shorter oxidation times, and chemical composition adjustments during remelting (Rod et al., 2006).

Global data on material footprint versus GDP shows a trend of decreasing construction consumption (as a ratio of the total) with increasing prosperity (B6 in Appendix B). Therefore, the relative size of the global contaminant sink (construction) is likely to decrease in the decades ahead while, concurrently, global production shifts towards more recycling (Pauliuk et al., 2013). Nucor's approach should then be implemented globally to help promote the production of high-quality recycled material that can displace primary production.

### 3.4.3.2 A Surrogate Model for Future Global Consumption

Per capita U.S. steel stocks saturated around 1980 (Muller et al., 2006). Steel flow analyses of other countries suggest that saturation is a feature of postindustrial societies (Muller et al., 2011). The authors believe the U.S. steel flow can therefore be used to help identify broad global trends that are likely to manifest as developing countries industrialize. These trends, reflected by comparing the current global (Cullen et al., 2012) and U.S. flows (Figure 3.4), are likely to include reduced demand for construction products and increased demand for transport products relative to total end-use consumption. Also, new scrap flows will be increasingly dominated by transport sheet metal scrap and, as the global percentage of consumption "added to stock" decreases, new scrap generation will decrease relative to end-of-life scrap flows.

A country's per capita saturation level will still depend on its development path. For example, both the U.K. and France have saturated per capita stocks that are around 2 t/cap lower than in the U.S. (Muller et al., 2011). Caution must also be exercised when extrapolating granular U.S. flows to the global level. Some features in Figure 3.4 are due to short-term factors. For example, the high (import) demand for pipe and tubing is probably due to the U.S. shale gas energy revolution. This led to a peak in demand for oil country tubular goods from which domestic producers were unable to fully respond (Preckel and Vivian, 2018; Nemeč, 2018). Elsewhere, the breakdown of

intermediate products entering construction is as dependent on national preferences for different building materials as it is on economic maturity: reinforced concrete frames are preferred in France, China, and India; while, structural steel frames are preferred in the U.S., U.K. and Japan (Moynihan and Allwood, 2012). At this granular level, the U.S. provides just one sensible scenario of what future global steel flows may look like.

### **3.5 Chapter Conclusions and Limitations**

This chapter presents a novel matrix cataloging system that provides an easy data recording and reconciliation framework for material flow analysis. Using the framework, we evaluated the U.S. steel flow network and identified material efficiency opportunities in the U.S. steel industry and supply chain. However, there are uncertainties in the developed steel flow network related to data sources as well as the network structure. We use the data quality weighting system with weighted least square optimization method to minimize result uncertainties due to low quality data. To study the structural uncertainties related to existence of nodes or flows in the steel flow network, future research is needed on new methods such as Bayesian updating.

Chapter reprinted with permission from Zhu, Y., Syndergaard, K. and Cooper, D.R., 2019. Mapping the annual flow of steel in the United States. *Environmental science & technology*, 53(19), pp.11260-11268.. Copyright 2021 American Chemical Society.

## Chapter 4

### An Optimal Reverse Material Supply Chain for U.S. Aluminum Scrap

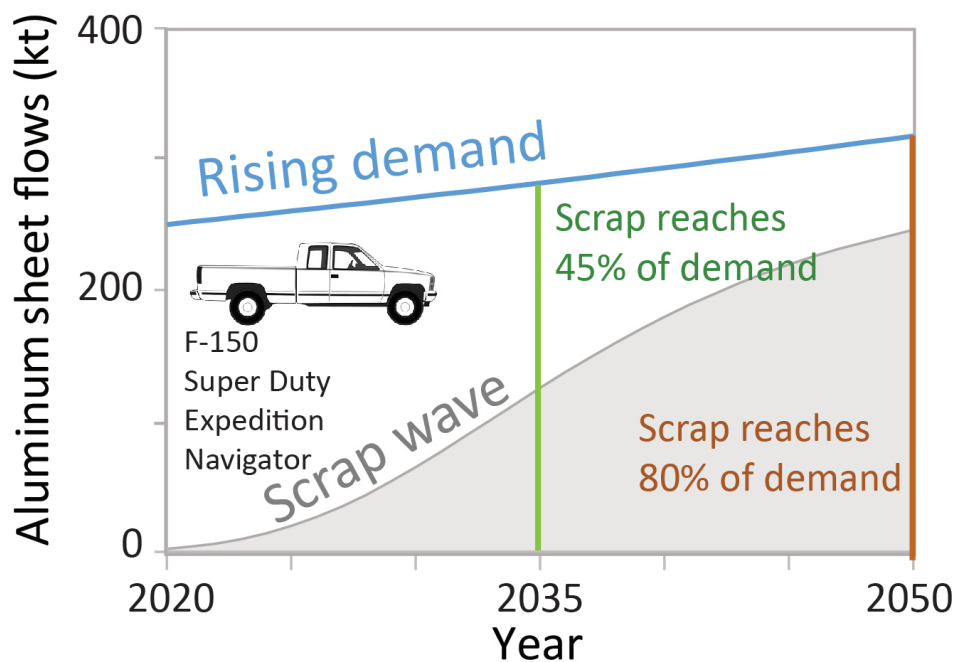
Publication related to this work:

Conference articles:

- Zhu, Y. and Cooper, D.R., 2019. An optimal reverse material supply chain for US aluminum scrap. *Procedia CIRP*, 80, pp.677-682.

Journal articles:

- Zhu, Y., Chappuis, L.B., De Kleine, R., Kim, H.C., Wallington, T.J., Luckey, G. and Cooper, D.R., 2021. The coming wave of aluminum sheet scrap from vehicle recycling in the United States. *Resources, Conservation and Recycling*, 164, p.105208.



Increased recycling is one of the most promising material efficiency strategies to reduce aluminum industry GHG emissions (Allwood et al., 2010; Gutowski, 2013). However, current U.S. EOL



aluminum recycling rates (34-63% (Chen and Graedel, 2012; Kelly and Matos, 2006; Gaustad et al., 2010)) are well below the level necessary (90% by 2050) to meet the IPCC's climate mitigation target as suggested by previous studies (Allwood et al., 2010; Gutowski et al., 2013). In order to improve the U.S. EOL aluminum recycling rate and intelligently target research efforts, it is important to know the technical barriers behind current low recycling rates. Potential technical underlying barriers to greater recycling identified in the literature include low scrap collection rates (Atherton, 2007) and, what we term, the chemistry mismatch between collected scrap streams and the alloys demanded by the industry. The compositional mismatch means that scrap must be "sweetened" during recycling with virgin metals (primary unalloyed aluminum and alloying elements) to satisfy the chemistry constraints of the new alloys. We identify the origins of this chemistry mismatch including scrap mixing (Lovik et al., 2014; Hatayama et al., 2008) (e.g., wrought aluminum scrap mixed with cast aluminum scrap), scrap contamination (McMillan et al., 2012; Lovik et al., 2014; Gaustad et al., 2010) (e.g., automotive aluminum scrap contaminated by steel rivets), and current industry demanding alloy compositions that are different from in previous years when the material that is now entering the scrap stream was first produced (Bertram et al., 2017; Lovik et al., 2014; Gaustad et al., 2010) (e.g., vehicle electrification leads to decreasing cast aluminum demand for engine components). Due to this compositional mismatch, the majority of aluminum scraps are not recycled into the original alloys. Instead, aluminum alloy scrap is downcycled into lower purity and lower value alloys (Lovik et al., 2014) (e.g., 1xxx alloys from electrical power cables recycled into 6xxx extrusion alloys or cast alloys for transmission housing (Lovik et al., 2014)). If the mismatch is too great, then recycling becomes unviable.

In this section, we answer the following questions:

- **How does scrap collection and the compositional mismatch between the available scrap streams and demand for metal affect U.S. EOL aluminum recycling rates?** Section 4.1 uses a linear optimization model to quantitatively show that increasing the collection rate alone can only lead to a limited increase in the domestic recycling rate and it is the compositional mismatch between scrap and new alloys that ultimately determines the technical limit to recycling.
- **How are the composition and scale of demand and scrap availability going to change in the key U.S. aluminum market, the U.S. automotive aluminum sheet?** Section 4.2 uses a dynamic material flow analysis (DMFA) and chemical composition analysis of four leading U.S. aluminum-bodied vehicles to show that scrap separation and refining technologies are needed to increase recycling of the incoming wave of aluminum autobody sheet (ABS) scraps.
- **What is the performance (efficacy, energy, cost, yield, and environmental impact) of key existing and emerging aluminum recycling technologies and how could they be used to**

**increase the recycling rate of U.S. EOL autobody aluminum sheet scrap?** Section 4.3 presents an overview of 11 aluminum recycling technologies and apply a modified version of the linear optimization model from Section 4.1 to the U.S. ABS DMFA results from Section 4.2 to show how representative scrap separation and refining technology could be used to increase EOL aluminum ABS scrap recycling rates to 100%.

## **4.1 Current U.S. EOL Aluminum Recycling**

Only around half of U.S. end-of-life (EOL) aluminum scrap is recycled. We investigate the extent to which the EOL recycling rate is constrained by the ability to collect EOL scrap versus the ability to recycle scrap into new alloys given the compositional mismatch between available scrap and the new alloys demanded by the industry. The compositional mismatch means that scrap must be “sweetened” during recycling with virgin metals (primary unalloyed aluminum and alloying elements) to satisfy the chemistry constraints of the new alloys. If the mismatch is too great, then recycling becomes unviable.

We first review the reasons for the compositional mismatch by examining its three causes: contamination with tramp elements; mixing of different aluminum scraps during recycling; and shifting demand for new alloys. A linear optimization model is then used to analyze the current and potential domestic U.S. recycling rate at different levels of collection from end-use scrap categories such as buildings. The model determines the minimum quantity of virgin metal needed to satisfy new alloy demand if different metal sources (including scrap and virgin metal) can be combined to make the new alloys just like they are in the recycling industry. Optimization constraints include not exceeding the use of available scrap, satisfying the demand for new alloys, meeting the chemical composition limits of the new alloys, and an economic furnace constraint that limits the weight fraction of virgin metals used in a recycling furnace. The results show that even if all EOL aluminum scrap could be collected in the U.S. then, because of the compositional mismatch between scrap and new alloys, only around 70% could be recycled domestically.

### **4.1.1 Section Background**

The quantity of greenhouse gas (GHG) emissions released from aluminum recycling ( $0.43 \text{ t CO}_{2\text{eq}}/\text{t metal}$ ) is just 5% of that released from primary aluminum production (Allwood et al., 2010). Previous researchers (Allwood et al., 2010; Bauer, 2012; Milford et al., 2013; Pauliuk et al., 2013) have found that 90% end of life (EOL) metal recycling rates are necessary for meeting the Intergovernmental Panel on Climate Change’s (IPCC) 2 °C target (IPCC, 2014). Despite the need for 90% recycling rates, estimates of the U.S. EOL aluminum scrap recycling rate range from 34% to 63% (Chen and Graedel, 2012). It is necessary to explore the main factors that limit the current

EOL aluminum scrap recycling rate in order to inform policy making on how to motivate higher recycling rates.

Beyond the environmental benefits, a higher U.S. recycling rate could help meet the rising U.S. demand for aluminum using domestic resources without importing expensive, new aluminum from other countries. This is an important consideration given the U.S. tariffs imposed in 2018 to cut aluminum imports (U.S. Department of Commerce, 2018).

Previous research includes case studies on the current and optimal EOL strategy for specific product categories such as vehicles, mobile phones, and other electronic devices (Gesing and Wolanski, 2001; Jang and Kim, 2010; Jofre and Morioka, 2005; Modaresi and Muller, 2012). Few studies attempt to find the underlying reasons for the low recycling rate. Atherton (2007) pointed out that the industry has limited ability to collect EOL scrap because of metal loss during use, dispersion as hibernating stocks, and difficulties in separating components (Atherton, 2007). Later research by McMillan et al. (2012) suggests that more limiting on the recycling rate than the collection rate per se could be the contamination of the EOL scrap coupled with the new alloys' compositional constraints (McMillan et al., 2012). Hatayama et al. (2009) determine the maximum aluminum recycling potential in select countries by applying a multi-material pinch analysis to data on the quantity and composition of Japanese scrap discards and new alloy demand (Hatayama et al., 2009). They assume that all EOL aluminum scrap is available for recycling and that all scraps from the same product category (e.g., building and construction) have homogeneous compositions. In reality, within a scrap category, the purest/highest value scrap will be recycled first. Across scrap categories though, mixing with other materials in the waste stream means that some of the purest aluminum alloys (e.g., foil) are those least likely to be collected for recycling.

This section is a U.S. specific study that recognizes the reality of imperfect collection rates, the heterogeneity of scrap compositions within as well as across scrap categories, and the compositional mismatch between collected scraps and new metal alloys. We examine how simulated changes to the EOL scrap collection rate and the purity of the collected scrap effects the modeled maximum domestic recycling rate. All analysis is for 2017 and neither scrap exports nor recycling melt losses are included in this study. Both will be included in future work.

#### **4.1.2 Section Methodology**

In order to evaluate the influence of the scrap collection rate and scrap chemical composition on the recycling rate, we need to determine the quantity and chemistry of the collected scrap and the quantity and chemistry constraints of the new alloy demand. Section 2.1 describes how we estimated the quantity of different alloys needed to produce new products in 2017, and how we estimated the quantity of different types of aluminum scrap that were discarded that year. Section 2.2 first describes the different reasons for the compositional mismatch between the available scrap

and the new alloys demanded by the industry. It then describes how we estimated the chemical composition of scrap collected from different product categories as well as the new alloys' chemistry constraints. In Section 2.3, a minimum virgin metal optimization model is formulated as a linear blending problem using the data generated in Section 2.1 and 2.2. Table 4.1 lists the nomenclatures used in the section.

Table 4.1: Nomenclature

$d$	A metal alloy demanded by industry; e.g., AA6063.
$D$	Total number of new metal alloys. $D=18$ .
$s$	A metal source; e.g., unalloyed primary aluminium.
	Unalloyed primary aluminium: $s=1$ .
	Six alloying elements: $s=2:7$ (see Figure 4.2).
	Eight scrap categories: $s=8:15$ (see Figure 4.1).
$S$	All types of metal sources. $S = 15$ .
$k$	An alloying or tramp element; e.g., copper.
$K$	All alloying or tramp elements. $K = 7$ (see Table 4.1.2.2).
$\theta_{d,s}$	Quantity of metal source $s$ used to produce new alloy $d$ [Mt].
$Alloy\_demand_d$	Demand for new metal alloy $d$ [Mt].
$Metal\_source_{s=8:15}$	Availability of scrap source $s = 8:15$ [Mt].
$c\_source_{s,k}$	Concentration of element $k$ in metal source $s$ [%].
$c\_alloy_{lb,d,k}$	Lower bound concentration of element $k$ in new alloy $d$ [%].
$c\_alloy_{ub,d,k}$	Upper bound concentration of element $k$ in new alloy $d$ [%].
$c\_alloy_{mrd,k}$	Midrange concentration of element $k$ in new alloy $d$ [%].

#### 4.1.2.1 New Alloy Demand and Scrap Availability

Material flow analysis (MFA) is a method for quantifying the stocks and flows of metals in a defined temporal and economic or geographic boundary. It can be dynamic, which assesses the stocks and flows of material in a system over time, or static, which is a snapshot of the system usually for a single year (McMillan et al., 2010). In this work, we use Hatayama et al.'s (2008) U.S. dynamic MFA results (2003-2050) to estimate U.S. aluminum demand and scrap discards from seven product categories in 2017: consumer durables, container and packaging, machinery and equipment, electrical, transportation (which can be further split into wrought and cast products), building and construction, and an "other" sector (Hatayama et al., 2009). Figure 4.1 shows the estimated aluminum demand for these product categories and the estimated scrap arising from these product categories in 2017. The quantity of collected scrap, which includes scrap that is recycled

both domestically and overseas, is estimated by the International Aluminum Institute (IAI) and is shaded in Figure 4.1b with the collection rate labeled above the columns (Bertram et al., 2017). The overall collection rate is estimated to be 63% (Bertram et al., 2017).

The demand for 18 metal alloys used in the product categories is determined from the product-to-alloy breakdown shown in Hatayama et al. (2007) for wrought alloys and Carruth and Allwood (2013) for cast alloys.

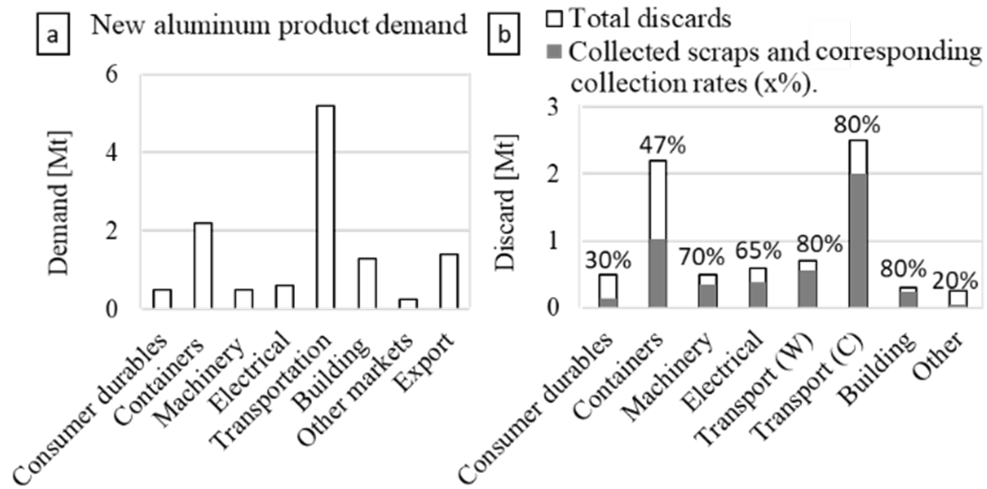


Figure 4.1: (a) Demand estimate; (b) Scrap discard estimate with actual collection rate shown (Bertram et al., 2017; Hatayama et al., 2009)

#### 4.1.2.2 Composition of Collected Scrap and New Alloys

A compositional mismatch often exists between the collected scrap and the new alloys demanded by industry because of scrap contamination with tramp elements, shifting new alloy demand, and mixing of different scrap types. Common non-metals in aluminum scrap piles such as rubber, plastic, and foam are removed by hand sorting and air suction (Gaustad et al., 2012). Industry uses magnetic and eddy current separation as well as salt fluxing during the remelt to minimize the contamination of the scrap with foreign tramp elements such as iron, copper, and silicon. However, it is often commercially infeasible to reduce the concentration of impurities to sufficiently low levels to prevent problems in subsequent forming processes. Table 4.1.2.2 summarizes the source and impact of common alloying or tramp elements in aluminum.

Table 4.2: Common alloying and tramp elements in aluminum scraps (Davis, 2001; Gaustad, Olivetti, and Kirchain, 2012).

Element	Source	Advantage	Disadvantage
Iron	Mixed iron scraps (rivets) or die-casted molds.	Increases strength at elevated temperature.	Reduces ductility and toughness. Causes corrosion.
Silicon	Cast aluminum.	Reduces melting temperature for casting.	Reduces ductility and toughness.
Copper	Mixed copper wires and motors or copper alloyed aluminum.	Basis of heat treatable alloys containing copper.	High copper content reduces ductility.
Manganese	3xxx series wrought aluminum.	Increases alloy stability in the presence of magnesium.	Reduces ductility. High manganese content leads to cracking in hot rolling.
Magnesium	5xxx & 6xxx series wrought and 3xx.x & 5xx.x series cast aluminum.	Increases corrosion resistance and weldability.	Reduces ductility. High magnesium content leads to cracking in hot rolling.

Shifting demand for new alloys is another reason for the compositional mismatch. Metal scrap is collected from discarded products often many years after the products were made. Over the intervening years, the quantity and composition of new products may have changed significantly. For example, demand for aluminum alloys for car production has increased significantly since the early 1990s due to the focus on reducing component weights. In the future, demand for cast aluminum alloys (having higher silicon content compared to wrought alloys) for the car industry may reduce because emerging electric vehicles do not require a cast engine block.

In this study, we estimate the composition of scrap from a product category (e.g., machinery) as the weighted sum of the compositions of the alloys used in that product category (using midrange element concentrations,  $c_{\text{alloy}_{mrd,k}}$ ). As described in section 4.1.2.1, the breakdown of alloys used in each product category is determined from Hatayama et al. and Cullen et al. The calculated composition of each of the eight scrap categories is shown in Figure 4.2 within the orange boxes on the left-hand side. This estimation of scrap composition assumes that the scrap only contains alloying and tramp elements existing in the original products. Future work will relax this assumption.

The elemental composition constraints of the new alloys determine the degree of sweetening needed to recycle the scrap, and were determined from ANSI/ISO standards (Hatayama et al., 2006; ISO 7376:2009, 2008; Schlesinger, 2014; The Aluminum Association Inc., 2006). The concentration range (from lower to upper bound) of seven key elements in eighteen alloys was included in the model. An example of the elemental concentration range is shown in Table 4.3 for



Figure 4.2: Scrap and new alloy mid-range compositions for seven U.S. product categories

Al 3003. The mid-range elemental concentration for all studied alloys is shown in Figure 4.2.

Table 4.3: Example of new alloy compositional constraints

Alloy	Elemental composition (weight %)						
	Si	Fe	Cu	Mn	Mg	Al	Other
Al 3003	0-0.6	0-0.7	0.05-0.20	1.0-1.5	0-0.05	96.7-99	0-0.25

#### 4.1.2.3 Optimization Model for Minimizing Virgin Metal Demand

In the model, different metal sources are mixed together to satisfy the demand for new metal alloys while simultaneously minimizing the demand for virgin metals (the sum of unalloyed primary aluminum and alloying elements). There are  $D$  types of new metal alloy demand and  $S$  metal sources (including unalloyed primary aluminum, alloying elements, and EOL scraps). Elements in matrix  $\theta_{d,s}$  represent the quantity (in mass units) of metal source  $s$  used to produce metal alloy  $d$ .

Linear optimization is used in this study to increase computational speed and to avoid the complication of multiple local minima. The decision parameters are physically independent; however, it is recognized that weak coupling may exist through socio-economic effects (e.g., scrap price elasticity of the collection rate). Linear optimization blending problems are a well-studied topic in mathematical programming and operations research (Diwekar, 2003; Williams, 2013). Previous studies include those focused on waste stream treatment and food production; e.g., minimizing the cost of producing sausages from a mixture of meat and ingredient while meeting nutrition requirements such as minimum protein content and maximum sodium content (Steuer, 1984). We adopt the blending problem setup to investigate how new metal alloy demand can be met with a minimum quantity of virgin metal production; thus, maximizing the recycling rate. The main model assumptions are that there is unlimited availability of virgin metal and no melt losses during recycling. The model only includes domestic new metal alloy demand, predicting a maximum domestic recycling rate. Scrap collected in the U.S. but recycled overseas is not considered.

The objective function is shown in Equation 4.1, subject to the inequality constraints shown in Equation 4.1-4.6. Note that  $s=1$  represents unalloyed primary aluminum and  $s=2:7$  represents the six alloying elements shown in Table 4.1.2.2.

$$\text{Minimize : } \sum_{d=1}^D \sum_{s=1}^{s=7} \theta_{d,s} \quad (4.1)$$

$$\text{Subject to : } \sum_{s=1}^S \theta_{d,s} \geq \text{Alloy\_demand}_d \quad (4.2)$$



$$\sum_{d=1}^D \theta_{d,s=8:15} \leq Metal\_source_{s=8:15} \quad (4.3)$$

$$\frac{\sum_{s=1}^S (\theta_{d,s} \cdot c\_source_{s,k})}{\sum_{s=1}^S \theta_{d,s}} \geq c\_alloy\_lb_{d,k} \quad (4.4)$$

$$\frac{\sum_{s=1}^S (\theta_{d,s} \cdot c\_source_{s,k})}{\sum_{s=1}^S \theta_{d,s}} \leq c\_alloy\_ub_{d,k} \quad (4.5)$$

$$\alpha \cdot \left( \frac{\sum_{s=1}^S \theta_{d,s} \cdot c\_source_{s,k}}{c\_alloy\_mr_{d,k}} \right) \leq \sum_{s=8}^{s=15} \theta_{d,s=8:15} \quad (4.6)$$

There are four groups of inequality constraints: alloy demand constraints; scrap supply constraints; alloy chemistry constraints; and economic furnace constraints. The 18 ( $D = 18$ ) alloy demand constraints (Equation 4. 2) ensure that the production of each new metal alloy,  $d$ , is greater than or equal to alloy demand ( $Alloy\_demand_d$ ). The 8 ( $s = 8 : 15$ ) scrap supply constraints (Equation 4. 3) ensure that the quantity of a used scrap source does not exceed the amount available ( $Metal\_source_{s=8:15}$ ). The 252 ( $D \times K \times 2 = 18 \times 7 \times 2$ ) alloy chemistry constraints ensure that the elemental composition of the new metal alloys falls between the lower bound (Equation 4. 4) and upper bound (Equation 4. 5) of that specified by ANSI/ISO standards (Hatayama et al., 2006; ISO 7376:2009, 2008; Schlesinger, 2014; The Aluminum Association Inc., 2006). The 126 ( $D \times K = 18 \times 7$ ) economic furnace constraints (Equation 4. 6) ensure that the scrap content in a recycling furnace is no less than the required weight fraction  $\alpha$ .

#### 4.1.2.4 Simulations

Two sets of twenty-one simulations are conducted in order to explore the effect of changing collection rates and scrap purity on the U.S. domestic recycling rate in 2017 and 2050, respectively. The first set of twenty-one simulations are based on 2017 U.S. demand for new alloys (quantity and chemical constraints) and the second set of twenty-one simulations are based on the 2050 U.S. demand for new alloys (quantity and chemical constraints) derived from Hatayama et al. (2009).

In the first set of simulations, simulation A models the actual collection rate in 2017, when 4.77 Mt of scrap (63% of all discarded aluminum) was collected (see shaded bars in Figure 4.1b). Simulation B models a theoretical 100% collection rate scenario (7.55 Mt of available scrap (Hatayama et al., 2009): see full bars in Figure 4.1b) where the composition of the new scrap available in the model (but that was landfilled in reality and implicitly in Simulation A) is assumed to be identical to the rest of the scrap from that product category. Additional simulations then model this additionally available scrap at decreasing levels of aluminum purity. Simulation C corresponds

to a 1% decrease in aluminum concentration for previously landfilled scrap, Simulation D models a 2% decrease, and so on until Simulation G which models a 5% reduction in aluminum concentration for previously landfilled scrap. Note that Simulation G corresponds to a 2% reduction in the mean aluminum content of all scraps (90% to 88%, see Figure 4.4).

The second set of simulations model scrap availability and alloy demand in 2050 according to Hatayama et al. (2009), when 12.92 Mt scraps are discarded and 15.48 Mt alloys are needed. Simulation A models the collection rate in 2050 when 8.64 Mt of scrap (67% of all discarded aluminum in 2050) was collected. Simulation B - G model the theoretical 100% collection rate scenarios while the level of aluminum purity decrease from B to G as in 2017 simulation.

A realistic value for the economic furnace constraints parameter ( $\alpha$ ) was determined through site visits to aluminum recyclers and interviews with industry experts, suggesting  $\alpha = 0.5$  reflects a typical operation limit for rotary and reverberatory furnaces (the most common aluminum recycling furnaces). A sensitivity study reveals the effect of reducing  $\alpha$  on the modeled recycling rate (see Figure 4.4).

The optimizations were run using MATLAB's linprog solver (Zhang, 1998) and an Intel(R) Core™ i7-6600U CPU, 2.81 GHz, with 16 GB of RAM. Convergence times were less than 10 seconds.

### 4.1.3 Section Results and Discussion

Figure 4.3 presents the simulation A results in 2017, modeling the actual collection rate. The 2017 simulation A results show the use of different metal sources, their destination in different new alloys, and the recycling rate in different scrap categories. The reliability of the model is assessed by comparing the simulation results shown in Figure 4.3 to what actually happened in 2017, as estimated in Figure 4.1. The simulated and actual recycling rates are within  $\pm 0.5\%$  in all but one category (cast transport scrap), where the collection rate in Figure 4.1 is 80% but the simulated domestic recycling rate in Figure 4.3 is 26%. The explanation for this difference is that our recycling rate prediction only considers domestically recycled scrap while IAI's (Bertram et al., 2017) value includes a portion of scrap that is exported and recycled overseas. Significant quantities of low-grade, silicon-rich scrap are exported from the U.S. to meet developing world demand for lower grade material (Cooper, 2018). The scrap destination as predicted by our model is further checked against the common industrial practice; e.g., in reality, the majority of recycled container and packaging scrap is used to make beverage cans (closed loop recycling) and, consistently, the Simulation A results show the production of new 3004 and other 3xxx series alloys (used in beverage can bodies) from the container scrap.

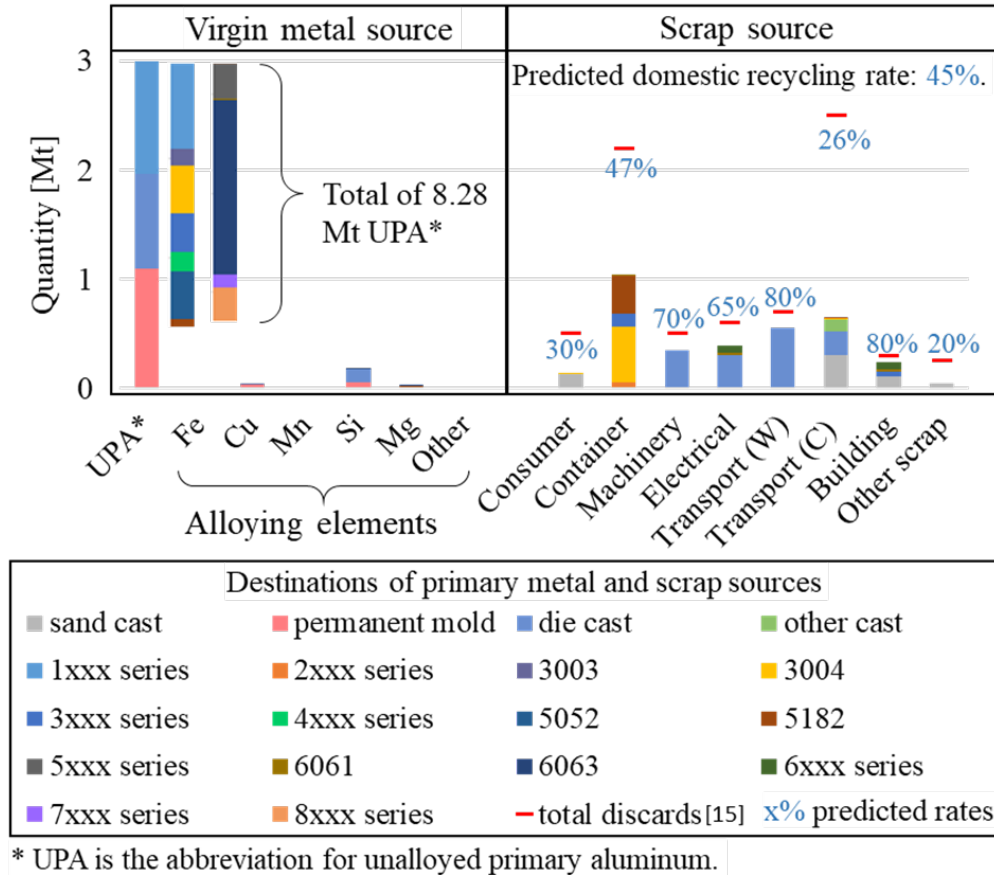


Figure 4.3: 2017 simulation A results ( $\alpha = 0.5$ ). Virgin metal and scrap sources used to meet U.S. aluminum demand in 2017

#### 4.1.3.1 Effect of Collection Rate and Scrap Purity on the Modeled Recycling Rate

The Simulation A result suggests that the optimization model is giving representative results of the current recycling reality. The results of Simulations B-G are shown in Figure 4.4 and are used in this section to evaluate the potential impact on the maximum recycling rate of changes to the collection rate and scrap purity.

The points labeled "A" in Figure 4.4 show the potential domestic recycling rate if only scrap that is currently collected is assumed available. Blue point A in Figure 4.4 corresponds to the results shown in Figure 4.3. The orange and yellow As show the recycling rates under relaxed furnace constraints. It is found that relaxing the furnace constraint (from  $\alpha = 0.5$  to  $\alpha = 0$ ) increases the simulated domestic recycling rate (based on current collection rates) to a maximum of 62%, which would also allow some of the dirty aluminum scrap that is currently exported to be recycled domestically. However, this situation would require recyclers to use much more virgin metal which seems unlikely in the short term for cost reasons. For example, if a scrap contains 98% AA3005

alloy and 2% iron contaminant then it would require around 600% dilution with primary unalloyed aluminum to make a new AA3005 ingot (containing less than 0.3% iron). This is possible, but if such dilutions became typical then the predominant throughput of a recycling facility would be virgin metal, not scrap.

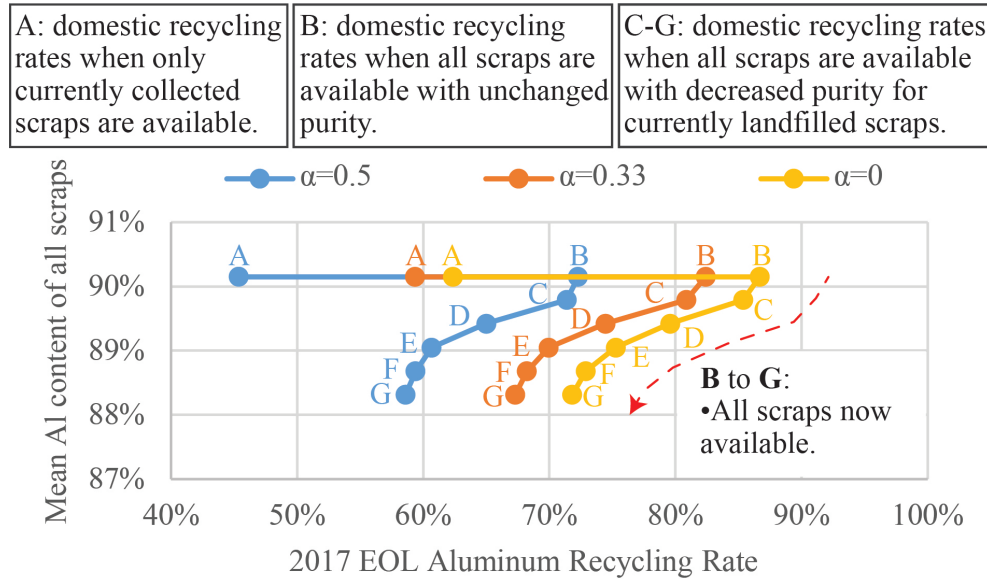


Figure 4.4: 2017 Simulation A-G results showing sensitivity to economic furnace constraint parameter ( $\alpha$ )

The points labeled "B" in Figure 4.4 assume a 100% collection rate and that all scrap belonging to the same product category (the columns in Figure 4.1b) have the same composition. Figure 4.4 shows that even if the collection rate is increased to 100% with no furnace constraint in the extreme case (yellow point B) then still less than 90% of all scrap discards get recycled.

It is likely that in reality, the scrap that is currently not collected is, overall, less pure than the scrap that is collected. To reflect this likelihood, the model is run where the additional scrap made available by increasing the collection rate from 63% to 100% is less pure than the scrap that is already collected. The results of these analyses are shown by the lines from the Bs to the Gs in Figure 4.4. As expected, more contaminated/lower quality scrap lowers the potential recycling rate even further.

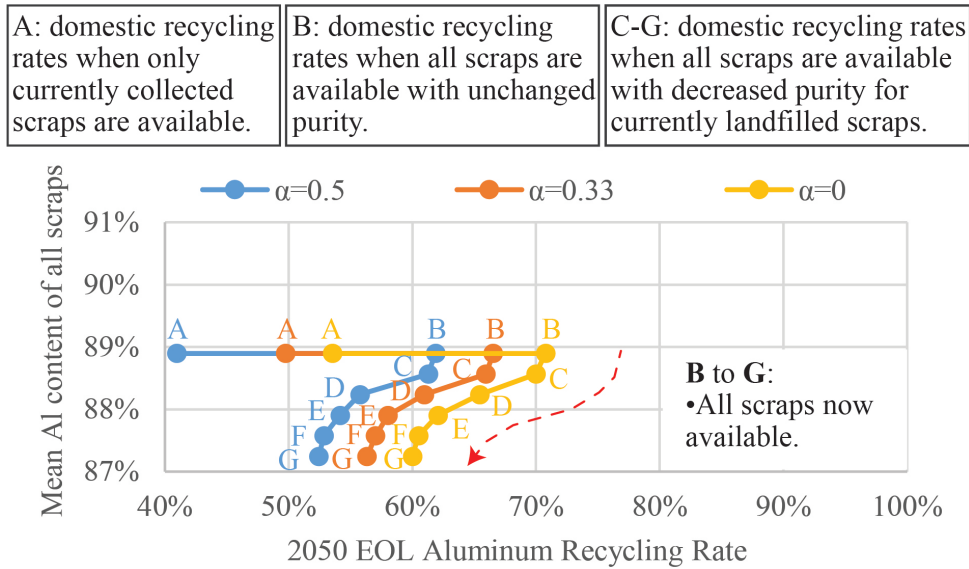


Figure 4.5: 2050 Simulation A-G results showing sensitivity to economic furnace constraint parameter ( $\alpha$ )

Figure 4.5 presents the analysis results of U.S. recycling rates in 2050 under varying scrap collection and contamination assumptions. In figure 4.5, points "A" assumes 67% scrap collection rate and the scrap recycling rate drops to 40% due to lower demand to scrap ratio and lower scrap quality. The scrap quality is estimated from the weighted average of the compositions of discarded scraps according to Hatayama et al. (2009)'s prediction. Lower demand to scrap ratio and lower scrap quality indicate fewer dilution opportunities and aggressive compositional mismatch problems between the scrap and new alloy demand.

In short, this investigation indicates that increasing the collection rate alone (even to 100%) can only lead to a limited increase in the domestic recycling rate and it is the compositional mismatch between scrap and new alloys that ultimately determines if and how the scrap is recycled.

#### 4.1.3.2 Policy Implications

The results show that in order to achieve a higher recycling rate, more effort should be put into reducing the compositional mismatch between scraps and alloy products. Suggestions include developing advanced separation technologies to acquire cleaner scraps (e.g., continued commercialization of LIBs (Wyss and Schultz, 1999)) and updating alloy composition requirements to be more tolerant of impurities (Gaustad, Olivetti, and Kirchain, 2010). Moreover, emerging refining technologies, such as fractional crystallization (Muñiz-Lerma et al., 2017) and hot crush techniques (Ambrose et al., 1983) should be evaluated using the proposed optimization method to determine their potential impact on recycling rate and thus the appropriate level of investment and government support through tax-breaks, etc.

#### **4.1.4 Section Conclusion**

This study suggests that even if all U.S. EOL aluminum scrap could be collected then only around 70% could be recycled domestically (up from around 45% today). Without the deployment of advanced scrap separation and refining technologies then the compositional mismatch will prevent recycling rates in excess of 90%, which are necessary if the industry is to achieve the IPCC's recommended emissions cuts.

### **4.2 The Coming Wave of Aluminum Sheet Scrap from Vehicle Recycling in the U.S.**

The emergence of mass-produced aluminum sheet-intensive vehicles presents an opportunity for recyclers to shift towards high value recycling into wrought alloys. We use dynamic material flow analyses (2015-2050) to estimate the timing, scale, and composition of U.S. aluminum automotive body sheet (ABS) scrap generated from the aluminum ABS intensive vehicles with the highest U.S. sales: Ford F-150, Super Duty, Expedition, and Lincoln Navigator. Lifespan distribution models are derived for each vehicle, and 5xxx and 6xxx series sheet alloys are aggregated according to their copper and magnesium content. A Markov chain model is used to estimate the fraction of deregistered vehicles scrapped domestically versus exported.

It is found that the above four vehicles account for around 1,200 kt of aluminum ABS embedded within the 2020 U.S. fleet. The aluminum ABS intensive construction of these vehicles presents a unique opportunity to U.S. recyclers. If production continues at the current volumes, aluminum ABS scrap from these vehicles will increase to approximately 121 kt/year in 2035 and 239 kt/year in 2050. The majority of this scrap will be available for U.S. processing with  $\ll 10\%$  of deregistered vehicles exported or achieving vintage status. For comparison, only 121 kt of aluminum auto shred (containing negligible aluminum ABS) was domestically consumed in the U.S. in 2017. We analyze the composition of the future potential scrap streams, revealing the need for alloy separation and tramp element removal if closed loop aluminum ABS recycling is to be achieved.

#### **4.2.1 Section Background**

Aluminum has long been recognized as a lightweight alternative to steel that can deliver significant transport fuel savings depending on the degree of material substitution and the subsequent reduction in vehicle weight (Kim and Wallington, 2013). The downside is that primary aluminum production is energy-intensive (9 times greater than primary steelmaking according to Milford et al., (2011)); however, Modaresi et al. (2014) point out that in the future there will be greater opportunities to use aluminum vehicle scrap to increase the recycled content and lower the energy-intensity of aluminum in vehicles. Closed loop recycling will be required to realize this opportunity (Modaresi et al., 2014; Milovanoff, et al., 2019).

Aluminum automotive body sheet (ABS) first appeared on vehicle hoods in the late 1970s and its use in bolt-on body components on U.S. vehicles has increased significantly since then. Aluminum body vehicle structures included the 1991 Acura NSX, 1994 Audi A8, 2001 Honda Insight, 2012 Tesla Models S, and 2012 Land Rover (Chappuis and Sanders, 2019); however, these vehicles represent a negligible portion of overall U.S. vehicle registrations. In the 2015 model year, Ford Motor Company introduced the mass produced aluminum-bodied F-150 pickup truck, which makes extensive use of aluminum ABS (Arowosola and Gaustad, 2019; Chappuis, 2015). Ford introduced aluminum-bodied Super-Duty trucks in 2017, and the Expedition and Navigator full-size SUV in 2018. This growing use of aluminum ABS means that there will be a wave of aluminum ABS scrap becoming available for recycling as the first mass produced aluminum intensive vehicles reach end-of-life/end-of-service (EOS).

Recycling aluminum sheet intensive vehicles presents an opportunity for recyclers to enter higher value markets (i.e., selling wrought rather than casting alloys) and an opportunity for automotive manufacturers to close the loop and use recycled aluminum for sheet components; thus, reducing the *embodied impacts* of the vehicle, which refers to the environmental impacts caused by material extraction and vehicle production. However, closed loop wrought scrap to wrought alloy recycling poses a technical challenge due to the stringent compositional requirements of aluminum ABS. Auto makers and recyclers need to have estimates of when significant quantities of aluminum ABS scrap from U.S. vehicles will become available for domestic manufacturing so that they can then plan by implementing design for recycling paradigms to vehicle production and/or by developing scrap separation and refining technologies. We provide the first analysis of the scale and timing of the future opportunity to recycle high quality aluminum ABS from U.S. vehicles.

#### **4.2.1.1 Current Recycling of Aluminum from Vehicles**

The materials in a discarded vehicle go through multiple processes before entering a recycling furnace (Kelly and Apelian, 2016). First, scrap dealers drain all fluids from the vehicle and remove the reusable and hazardous components such as the filters, brake calipers, water pumps, starters, alternators, and batteries (Kelly and Apelian, 2016). The remaining vehicle is crushed and shredded at auto-shredding plants. Common separation techniques such as magnetic separation and air separation are then used to separate the shredded scraps into a ferrous scrap stream and a non-ferrous light metal scrap stream. The latter, also named "Zorba", typically contains at least 65% aluminum by weight with possible contaminants including magnesium, zinc, iron, and copper. From Zorba, aluminum alloy scraps are extracted using processes such as hand sorting, eddy-current separation, and air separation. The extracted aluminum scraps contain 90-98% aluminum alloy by weight and are named Twitch or Tweak depending on the separation method used. These scraps are usually mixed together with other scrap sources such as aluminum wheel scraps, aluminum

bumper scraps, and aluminum turning scraps to produce secondary aluminum alloys. In the recycling furnace, scraps are melted and processed by fluxing, degassing, and filtering to remove contaminants and impurities such as alkali elements, moisture, and oxides. However, these basic refining processes are not able to reduce excess alloy concentrations of, for example, iron, silicon, magnesium, or copper. The molten scrap is cast into ingots (<25 kg), T-bars, or sows (<500 kg) for sale or shipped to nearby casting shops using over-the-road crucibles for further shape casting (Schlesinger, 2018).

The ability to recycle aluminum scrap in a closed loop fashion is determined by the quality (compositional homogeneity) of the scrap stream. Mixed aluminum alloy scrap streams and contamination with non-aluminum tramp elements can result in a scrap stream composition that reduces the quality of the recycled aluminum. For example, excessive quantities of iron contamination (e.g., from rivets) or copper contamination (e.g., from wiring or 2xxx series aluminum ABS alloys used in the early aluminum hoods, rotors, wheel spokes, and structural components (Arowosola and Gaustad, 2019; Kumar et al., 2015)) can reduce the ductility of the recycled aluminum. Insufficient alloying element concentrations can be remedied by adding alloying elements to the recycled metal; however, excess alloy and tramp element concentrations are a greater problem and require dilution of the recycled metal with energy-intensive primary aluminum and/or down cycling.

Traditionally, recyclers have typically processed both cast and wrought aluminum scrap into casting alloys (e.g., A356). This is because casting alloys are tolerant of mixed alloy compositions (e.g., mixed wrought and cast scrap) and tramp element contamination. Also, until recently, the demand for castings (e.g., for engine blocks, wheels, and suspension frames etc.) has been sufficient to provide a market for the aluminum scrap recycled into casting alloys. However, there is now strong evidence that U.S. domestic recycling of aluminum is being limited by the inability to maintain the value of wrought alloys during recycling. Bertram et al. (2017) showed using a material flow analysis (MFA) that U.S. casting demand is smaller than U.S. scrap arisings, and Zhu and Cooper (2019) showed using an MFA coupled to a linear programming model that only around 70% of domestically available aluminum scrap in 2017 could have been recycled domestically due to compositional constraints. Exports of aluminum scrap (particularly to China) helped to mask the U.S. recycling issue until recently. In 2017, 1,570 kt of U.S. aluminum scrap was exported (USGS, 2017). The majority of this exported scrap was auto shred scrap (Southwood, 2019) with only 121 kt of aluminum auto shred scrap domestically consumed in the U.S. that year (USGS, 2017). In 2018, China tightened restrictions on metal scrap imports (Reuters, 2019; Aluminium Insider, 2019) and, in 2019, aluminum scrap was accumulating in U.S. scrap yards (Tita, 2019; Desai, 2019) waiting for either alternative foreign buyers to be found or new recycling strategies to be employed. These difficulties in recycling U.S. aluminum scrap might be further exacerbated by a shift towards electric vehicles (Hatayama et al., 2012), which could decrease casting demand as cast aluminum engine blocks and transmission casings are eliminated (Løvik et al., 2014; Modaresi and Müller,



2012).

#### 4.2.1.2 Scope of the Section

Dynamic material flow analyses (DMFAs) are developed for four aluminum ABS intensive vehicle models: Ford F-150, Super Duty, Expedition, and Lincoln Navigator. We focus on these vehicles because they dominate U.S. sales of aluminum ABS intensive vehicles, accounting for around 65% of all the aluminum ABS embedded in the U.S. light-duty vehicle fleet and around 61% of the aluminum ABS added to the U.S. fleet each year (see Figure 4.6) (Chappuis, 2018). The four vehicle models share structural commonalities (e.g., body-on-frame designs with vehicle bodies containing similar 9 to 1 ratio of aluminum sheets to extrusions) that provide a common basis on which to evaluate recycling options. Figure 4.6 shows that the other contributions to the U.S. stock of aluminum ABS are thinly spread across 15 brands. These contributions are even more diffuse at the level of individual vehicle models. Limited alloy, production, and vehicle lifespan data availability prevent rigorous DMFAs on all these diffuse uses of aluminum ABS and are beyond the scope of the present paper.

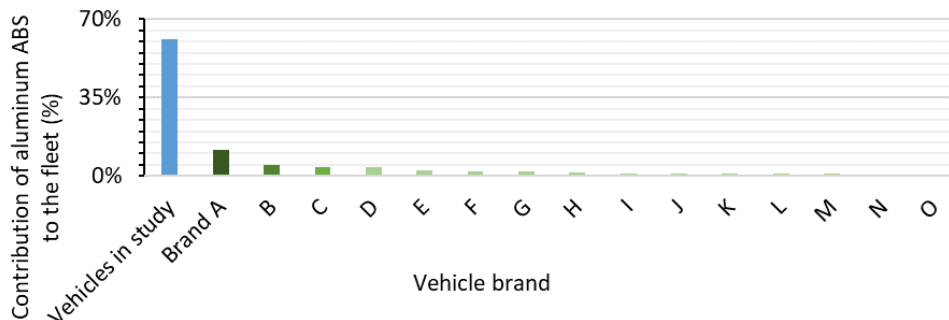


Figure 4.6: Brands share of aluminum ABS contributions to the U.S. fleet in 2018 (aluminum ABS embedded in sales). Derived from Chappuis (2018) with data provided on the condition of brand anonymity.

The vehicle DMFAs presented in this study are used to estimate the aluminum ABS (rolling) stock embedded in the U.S. vehicle fleet and the future availability of aluminum ABS scrap from deregistered U.S. vehicles. An analysis of the fate of deregistered vehicles is used to find the probability that the aluminum ABS embedded in deregistered vehicles will become available for U.S. scrap processing versus either being exported as part of a used vehicle or reaching hibernating status embedded within a vintage vehicle. The results are used to discuss the opportunities and barriers to future aluminum recycling.

## 4.2.2 Section Methodology

The DMFAs require estimates of material composition, lifespan, and annual production for each type of vehicle. Figure 4.7 shows a schematic of the methodology.

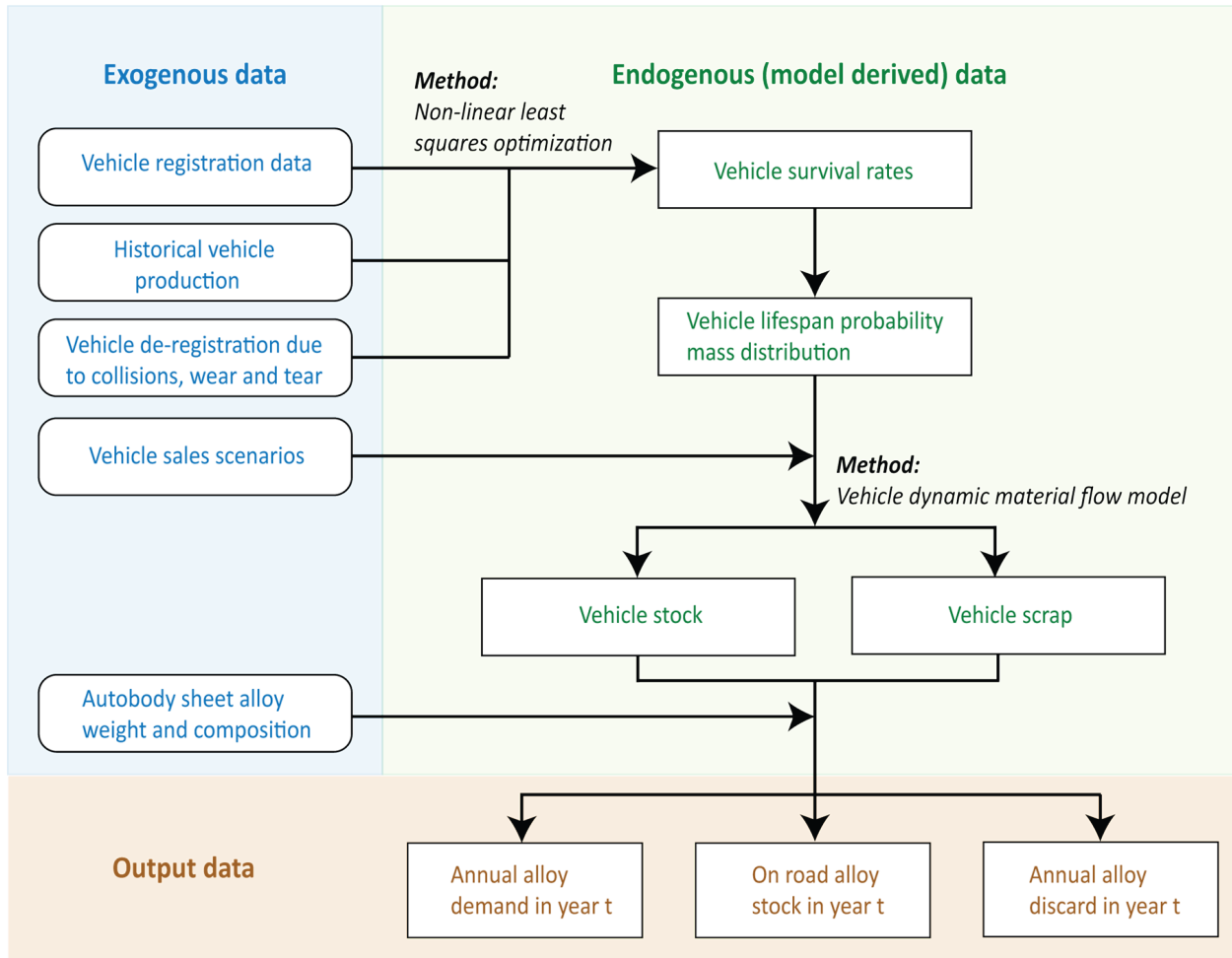


Figure 4.7: Methodology used to estimate the on-road aluminum ABS stock and future availability of aluminum ABS scrap from discarded vehicles

Section 4.2.2.1 describes the quantity and alloy specification of the aluminum ABS in each of the four types of vehicles studied in this analysis. Section 4.2.2.2 describes how survival rate curves are derived for each type of vehicle by comparing historical production, vehicle registration, and accident totaling loss data. Section 4.2.2.3 then describes how the survival rate curves are combined with the composition data and estimates of future annual production in a flow driven DMFA. Some of the deregistered vehicles in the U.S. are not sent for domestic scrap processing but are instead exported for use as second-hand vehicles in mainly developing countries. Section 4.2.2.4 describes the modeling and export data used to estimate the impact of used vehicle exports on the availability of automotive aluminum scrap for domestic U.S. recycling.

#### 4.2.2.1 Vehicles Analyzed

We focus on the top four selling aluminum intensive vehicles in the U.S.: Ford's 2015 F-150 (production began in 2014), 2017 Super Duty (production began in 2016), 2018 Expedition (production began in 2017), and 2018 Lincoln Navigator (production began in 2017). For example, in 2019, 14,100 Tesla Model S vehicles (another aluminum bodied vehicle) were sold in the U.S. (CSB, 2020) compared to 1,011,604 aluminum intensive Ford vehicles (Ford, 2020). Other U.S. automotive companies, such as light truck manufacturers Ram and Chevrolet, are focusing on the use of high-strength steels for lightweight vehicle design (WAS, 2020; White and Carey, 2018), and General Motors is developing composite solutions such as the carbon-fiber pickup box (WardsAuto, 2019).

The aluminum ABS content of the four aluminum intensive vehicles is shown in Table 4.4. The alloys are grouped according to the two major alloying elements, copper, and magnesium. The alloy specifications are published by Ford to inform sheet aluminum suppliers (Ford, 2014 and 2020). Ford specifies the acceptable composition window for eight elements for each aluminum ABS alloy. These elements (silicon, iron, copper, manganese, magnesium, chromium, zinc, and titanium) help determine the mechanical property of the alloys. The upper and lower elemental limits of Ford's aluminum 5xxx and 6xxx series aluminum ABS alloys are closer together than those recorded for the alloys in the Aluminum Association's "Teal Sheet" standards (Aluminum Association, 2009). These narrower compositional limits allow greater control of the mechanical properties and enable efficient closed-loop prompt scrap recycling by sheet metal suppliers.

Table 4.4: Average aluminum ABS content in the F-150, Super Duty, Navigator, and Expedition

Sheet alloy grouping	Compositional tolerance	Included alloys	Mass in each vehicle (kg)		
			F-150	Super Duty	SUVs (Navigator and Lincoln Expedition)
Low Cu	≤0.20 wt.% copper 0.50-1.00 wt.% silicon ≤0.30 wt.% iron ≤0.15 wt.% manganese 0.40-0.80 wt.% magnesium ≤0.10 wt.% chromium ≤0.10 wt.% zinc ≤0.10 wt.% titanium	6xxx series (skins)	92.6	102.6	65.3
High Cu	0.5-0.8 wt.% copper 0.55-0.95 wt.% silicon ≤0.30 wt.% iron ≤0.30 wt.% manganese 0.55-0.95 wt.% magnesium ≤0.10 wt.% chromium ≤0.10 wt.% zinc ≤0.10 wt.% titanium	6xxx series (high strength structural)	95.2	92.0	142.8
Low Mg	2.9-3.5 wt.% magnesium ≤0.25 wt.% silicon ≤0.35 wt.% iron ≤0.10 wt.% copper ≤0.50 wt.% manganese ≤0.10 wt.% chromium ≤0.10 wt.% zinc ≤0.10 wt.% titanium	5xxx series (non-heat treatable)	31.4	27.5	41.8
High Mg	4.2-5.0 wt.% magnesium ≤0.20 wt.% silicon ≤0.35 wt.% iron ≤0.10 wt.% copper 0.20-0.50 wt.% manganese ≤0.10 wt.% chromium ≤0.10 wt.% zinc ≤0.10 wt.% titanium	5xxx series (high formability, non-heat treatable)	19.7	18.0	27.1

#### 4.2.2.2 Vehicle Longevity (C1 section of Appendix C)

Estimates of vehicle longevity are needed to determine fleet turnover periods and therefore the length of time between an aluminum alloy entering the fleet and its emergence as aluminum scrap in a discarded vehicle. Vehicle survival rate studies have used historical vehicle registration data (EPA and NHTSA, 2012; Fridstrøm et al., 2016; Greenspan and Cohen, 1999; NHTSA, 2006; NHTSA and EPA, 2018); however, previous research was focused on national level fleet average survival rates for passenger cars and light trucks rather than specific vehicle types.

The aluminum ABS intensive vehicles in our study are no more than five years old; therefore, very few of these vehicles have been scrapped and there is little data with which to directly understand their lifespans. However, traditional steel intensive versions of each of the four types of vehicles have been produced for far longer and can be used to make sensible estimates of the longevity of the new aluminum intensive versions. In this study, survival rate curves and lifespan probability mass functions were developed for all four vehicles of interest using historical annual production data (Gunnell, 2003), registration data (IHS Markit, 2019), and collision totaling rates (CCC, 2015; Hartwig and Weisbart, 2016). As such, vehicle lifespan here refers to the time between production and deregistration of the vehicle. The final destination of these deregistered vehicles (e.g., the scrap yard versus used car exports) is investigated in Section 2.4. A detailed explanation of how each longevity model was derived (alongside the graphical result) is given in the Appendix C with a summary given below.

A survival rate curve shows the fraction of vehicles produced in model year  $t_0$  that are in the fleet at age  $a$  in year  $t$ , where  $t = t_0 + a + 1$ . Vehicle model year is used to describe the version of the vehicle. Production of vehicles in a new model year typically starts in August to September before the corresponding calendar year. However, there is usually a delay between when the vehicles are produced and when all the vehicles of the model year are sold. For example, a 1990 model year vehicle is likely to be sold by 1991 and turns into a one-year-old vehicle in 1992. Survival rate curves for different model years were determined for each of the four types of vehicles using Equation 4. 7.

$$\text{Survival rate}(a, t) = \frac{\text{Fleet size}(a, t)}{\text{Vehicle production volume}(t_0)} \quad (4.7)$$

Where  $t_0 = t - a - 1$ . For all four types of vehicles, the age ( $a$ ) distribution of the vehicles within the vehicle fleet in year  $t$ , was determined for each year between 2000 and 2008 using U.S. vehicle registration data available from IHS Markit (2019). This date range was used due to a lack of available data before 2000 and a change in IHS Markit data collection methodology in 2009 that makes the more recent data incompatible with the 2000-2008 dataset (NHTSA, 2018; EPA, 2018). For the F-150 and Super Duty vehicles, survival rate curves for each model year were derived by

comparing the fleet age distribution between 2000 and 2008 with the annual production volumes between 1966 and 1994 taken from Gunnell (2003). No production data were available for model years 1994-2000. For the Expedition and Navigator SUVs, the survival rates for vehicles between 1 and 7 years old were determined using the 2000-2008 fleet age distribution dataset by assuming that the vehicle fleet size in year  $t_0 + 1$  is approximately equal to the production volume (IHS Markit, 2019). Estimated survival rates for older SUVs (8-17 years old) had to be estimated using the fleet age distribution from 2000 to 2008 for the Ford Explorer as a proxy. This was because the first production year of the Expedition and Navigator was 1997 and 1998 respectively, whereas, the Explorer has been produced since 1990. For each type of vehicle, survival rate data at different ages is grouped according to the vehicle generation (Figure C3), which refers to a number of consecutive production years in which the vehicle went without a major redesign (Table C1).

An inherent problem in using registration data in the survival rate calculations is the double counting of vehicles that are registered in two or more U.S. states within the same calendar year. In the years immediately after production (when few vehicles have been scrapped), this inflated number of registered vehicles can rise above the original production volume, resulting in erroneous negative survival rates being calculated. To avoid this problem, the survival rate data calculated from the registration and production data are combined with data on "totaling" of vehicles. *Vehicle totaling* is a term used by insurance companies to describe when a vehicle needs to be scrapped because it is not economically advantageous to repair it due to severe damage from an accident. A vehicle declared "total loss" is usually sold for part dismantling; however, it is noted that some of the totaled vehicles may be re-registered after repair (see Appendix C1.1). For vehicles less than ten years old, the survival rate is largely determined by the totaling rate (Figure C1). Hartwig and Weisbart (2016) report the likelihood of vehicles of different ages being involved in a collision that results in an insurance claim being made. CCC (2015) reports the percentage of insurance claims for vehicles of different ages that are flagged as a "total loss". The totaling data from Hartwig and Weisbart (2016) and CCC (2015) are combined to calculate a mean vehicle survival rate just based on the avoidance of totaling the vehicle (Figure C2). For each type of vehicle and each vehicle generation, a nonlinear least-squares optimization is then conducted (using Matlab's `fmincon` function) to fit the NHTSA (2006) survival rate functional form (shown in Equation 4. 8) to the survival rate data extracted from the registration data/production volume comparison with an inequality constraint applied that the survival rate of all types of vehicle and vehicle generations for the first 9 years of vehicle life is within a  $\pm 5\%$  band of the mean survival rate calculated from the totaling data. This  $\pm 5\%$  band is slightly greater than the uncertainty suggested by the error bars provided in the analyses by CCC (2015) and Hartwig and Weisbart (2016).

$$Survival\ rate(a, g) = 1 - \exp(-\exp(c_1 + (c_2 \times a))) \quad (4.8)$$

Where  $a$  is the age of vehicles from model generation,  $g$ , and  $c_1$  and  $c_2$  are fitted constants that define the shape of the survival rate curve.

$$Lifespan\ pmf(a, g) = survival\ rate(a - 1) - survival\ rate(a) \quad (4.9)$$

The methodology described above generates survival rate curves for multiple generations (defined in Table C1 in Appendix C) of each of the four types of the vehicle of interest. These survival rates are converted to lifespan distributions using Equation 4.9. The lifespan distribution is expressed as a probability mass function (pmf) because the original data sources are in reference to discrete years or ages.

For each type of vehicle, the generational lifespan distribution with the highest mean lifespan is designated the baseline lifespan scenario used in the DMFAs because it corresponds to the most recent vehicle generation (see Table C2 in Appendix C). For each type of vehicle, the generational lifespan distribution with the lowest mean lifespan is designated as the pessimistic lifespan scenario used in the DMFAs. An optimistic lifespan scenario is then defined for each type of vehicle by assuming that the percentage improvement in average vehicle lifespan between the pessimistic and baseline scenario can be replicated again between the baseline and optimistic scenario. Moving from pessimistic, baseline, to optimistic lifespan distributions captures the trend of increasing vehicle longevity over time, which is consistent with the findings of the NHTSA and EPA (NHTSA, 2006; NHTSA and EPA, 2018). Comparing historical and current U.S. light-duty vehicle survival rates show that in general new vehicles are lasting longer and showing a higher survival rate early in their lives (NHTSA, 2006; NHTSA and EPA, 2018).

#### 4.2.2.3 Dynamic Material Flow Analysis (C2 in Appendix C)

A flow-driven DMFA is used to estimate the annual aluminum ABS stock and scrap availability in the U.S. between 2015 and 2050. A flow-driven DMFA is used because light duty vehicle sales growth predictions are available from the U.S. Energy Information Administration (EIA, 2019) and a stock-based DMFA is not practical when analyzing individual vehicle models that are far from saturation (see Appendix C2 for more details). Historical annual U.S. sales data for the four aluminum ABS intensive vehicles (2015-2020) are collated from Ford financial reports (Ford, 2020). Future annual vehicle sales are used as exogenous variables and are simulated for a range of scenarios including a cessation of aluminum ABS intensive vehicle production in 2021, and also continued annual vehicle sales growth of 0.8% (the baseline scenario), -0.1% and 1%. These growth figures correspond to the U.S. Energy Information Administration's prediction of light duty vehicle sales under expected, low, and high economic growth scenarios (EIA, 2019). Figure C6 presents all historical and prospective annual sales profiles used in this analysis.

For each type of vehicle, the annual aluminum ABS scrap arising from discarded vehicles is calculated using Equation 4.10. The stock of aluminum ABS embedded in the vehicle fleet for each type of vehicle in year  $t$  is calculated using Equation 4.11. The maximum age,  $a_{max}$ , equals the age of the oldest vehicle model produced since 2015 for F-150, 2017 for F-50s, and 2018 for the Navigator and Expedition.

$$Scrap(t) = \sum_{a=1}^{a_{max}} (Sales_{U.S.}(t-a-1) \times pmf(a)) \quad (4.10)$$

$$Stock(t) = Stock(t-1) + Sales_{U.S.}(t) - Scrap(t) \quad (4.11)$$

#### 4.2.2.4 Exported and Vintage Vehicles (C3 in Appendix C)

The DMFAs are used to estimate the annual number of vehicles, and the corresponding quantity of aluminum ABS, reaching EOS in future years. However, these DMFA results are driven by lifespan predictions based on vehicle registrations. When a vehicle ceases to be registered, it is either scrapped, exported for secondhand use abroad, or "hibernated" in the form of a vintage vehicle. It is noted that some U.S. states do however require vintage vehicles to be registered under a special category (Fridstrøm et al., 2016). Araghi et al. (2017) report an increasing fleet of U.S. vintage vehicles since the 1990s (Araghi et al., 2017). Regarding export, Davis, and Kahn (2010) report that the U.S. exported 2.45 million used vehicles to Mexico alone between August 2005 and July 2008. Coffin et al. (2016) estimate that used vehicle exports accounted for 14% of U.S. vehicle exports in 2014. Exported and vintage vehicles will not enter the U.S. scrap processing supply chain and therefore cannot be treated as a valuable source of aluminum for U.S. recyclers.

In this section, estimates are made of the fraction of deregistered vehicles that are either exported or "hibernated" in vintage vehicles. A simple absorbing Markov chain of vehicle states is developed for each type of vehicle to show the probability that, at a given age, a vehicle will transition to one of the three absorbing states: scrapped, exported, or hibernated as a vintage vehicle. The transition matrix is estimated by combining fleet export data from the U.S. International Trade Commission (2019) with specific export data (trade volumes and vehicle ages) for the four types of vehicle in this study, derived using data collated from Car Export America (2019), and a study of vintage vehicles by Araghi et al. (2017). A detailed explanation of how the transition probabilities were derived is given in the SI with a summary given below.

The U.S. International Trade Commission (2019) provides annual statistics on used vehicle exports: an average of approximately 700,000 used vehicles was exported every year between 2014 and 2018. Among all the exported vehicles, the share of the four types of the vehicle of interest in this study was estimated by analyzing the sales data on Car Export America (2019), which as of



September 2019 listed 63,266 used U.S. vehicles for export. The four Ford vehicles accounted for 2.5% of export sales with the majority being the F-150 or Super Duty. For each vehicle in this study, the probability of a vehicle at a given age either being exported or remaining as a U.S. registered vehicle was estimated by comparing the export sales with the fleet registration data (IHS Markit, 2019). The probability that a vehicle older than 30 years transitions to vintage status is estimated such that 1% of all vehicle types end up as a vintage vehicle, per Araghi et al. (2017). The final destination of different types of vehicles into each of the absorbing states (scrapped, exported, or hibernated as a vintage vehicle) was determined by calculating the limiting matrix of the Markov chain model.

### 4.2.3 Section Results (C4 in Appendix C)

Figures 4.8 and 4.9 show the modeled vehicle survival rate and corresponding lifespan distribution models, respectively. In the baseline scenario, the Super Duty has the highest mean lifespan (21 years), followed by the F-150 (19 years), and then the Expedition and Navigator (17 years). The trend that light trucks last longer than SUVs (and passenger cars) aligns with previous analysis (NHTSA, 2006; NHTSA and EPA, 2018). This could be related to the durability requirement for light trucks and the higher average cost of light trucks compared to SUVs or passenger cars.

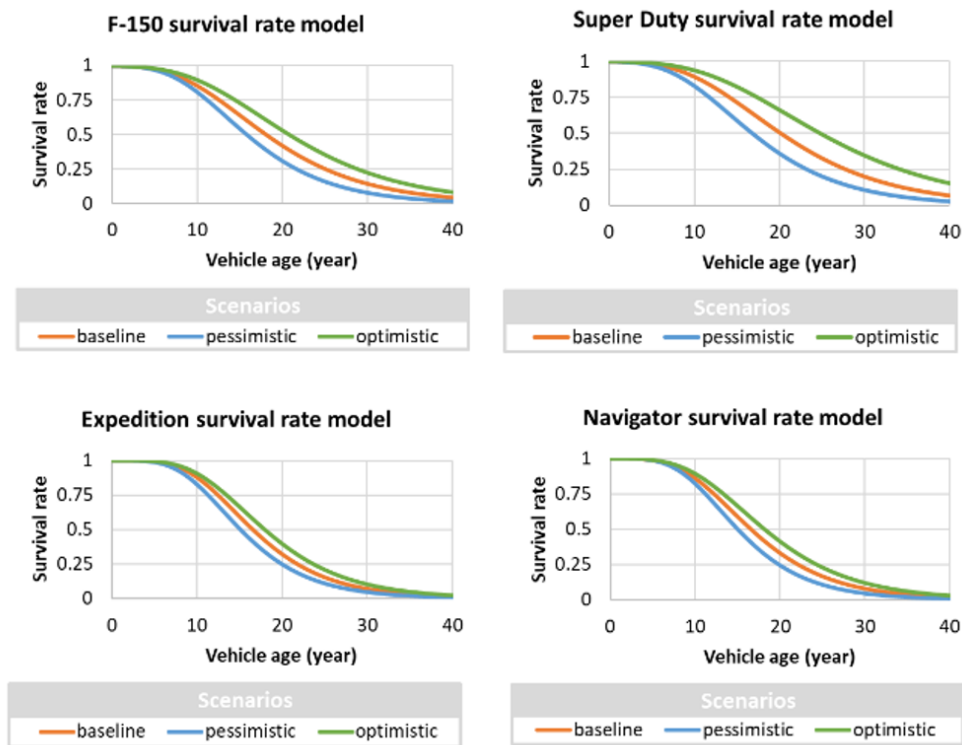


Figure 4.8: Vehicle survival rates based on U.S. vehicle registrations (some deregistered vehicles are exported)

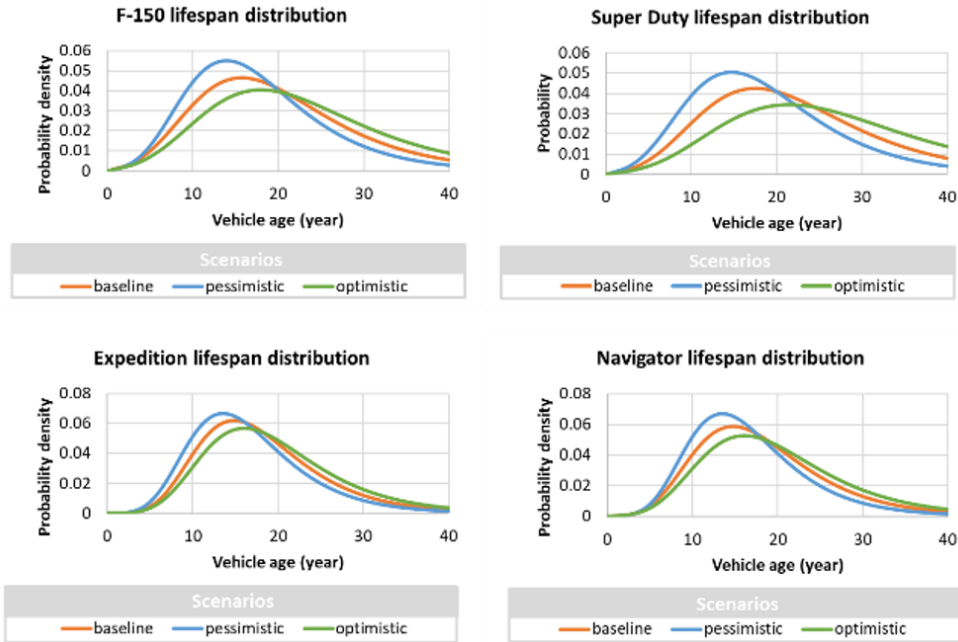
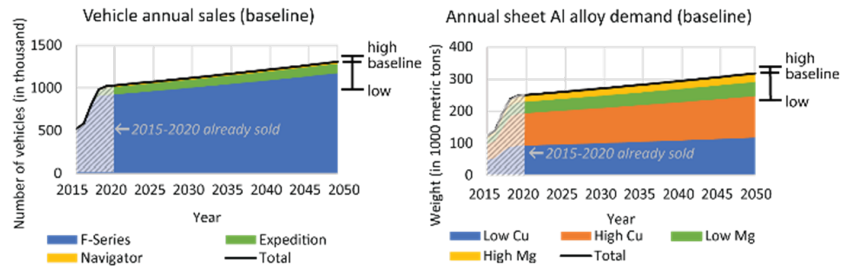
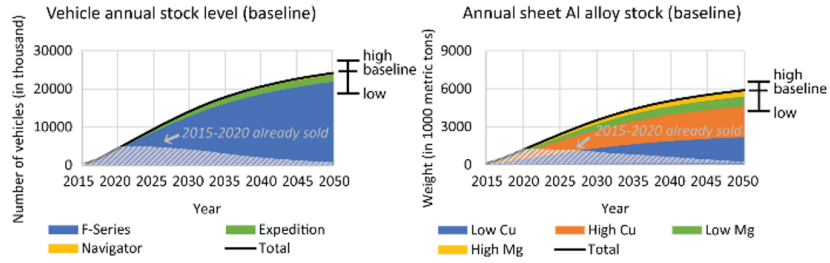


Figure 4.9: Vehicle survival rates based on U.S. vehicle registrations (some deregistered vehicles are exported)

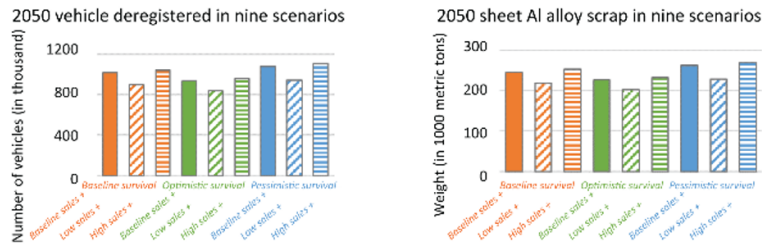
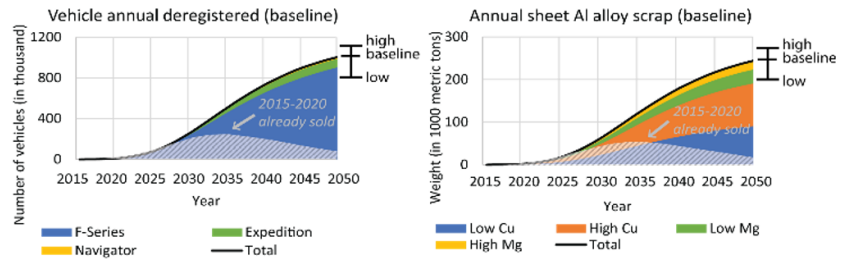
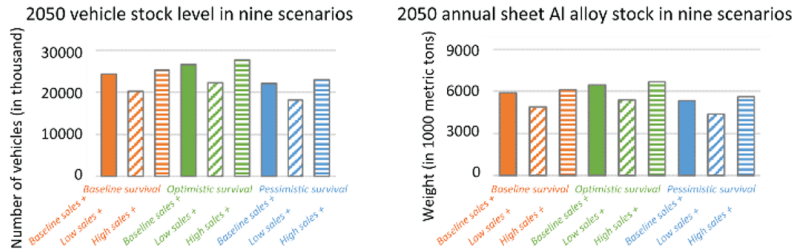
The left-hand side of Figure 4.10 shows the estimated number of vehicles sold, vehicles present in the U.S. fleet, and vehicles deregistered in each year between 2015 and 2050. The right-hand side of Figure 4.10 shows the estimated mass of aluminum ABS in these vehicles. The grey shaded pattern in Figure 4.10 corresponds to the vehicles that have already been sold (before 2021). Across all simulated scenarios, the aluminum ABS alloys associated with deregistered vehicles arising in 2050 was smallest under the optimistic lifespan and low sales growth scenario at 203kt/year, and largest under the pessimistic lifespan and high sales growth scenario at 269 kt/year (Figure 4.10c (right)), compared to the baseline scenario of 246 kt/year (Figure 4.10c (right)).



(a) Vehicle (left) and alloy (right) sales from 2015 to 2050.



(b) Vehicle (left) and alloy (right) stock from 2015 to 2050.



(c) Vehicles deregistered (left) and alloy scrap arising (right) from 2015 to 2050.

Figure 4.10: Vehicle and alloy annual sales, stock level, and de-registrations from the U.S. fleet. The grey areas correspond to vehicles already sold in 2015-2020. F-Series is composed of F-150 and Super Duty.

Figure 4.11 and Table 4.5 shows the absorbing Markov chain of vehicle states for the four vehicle models. Across the four vehicle models, between 1% and 7% of deregistered vehicles are exported. A small percentage (1%) achieve vintage/hibernating status, and the remainder will enter the scrap processing system in the U.S.

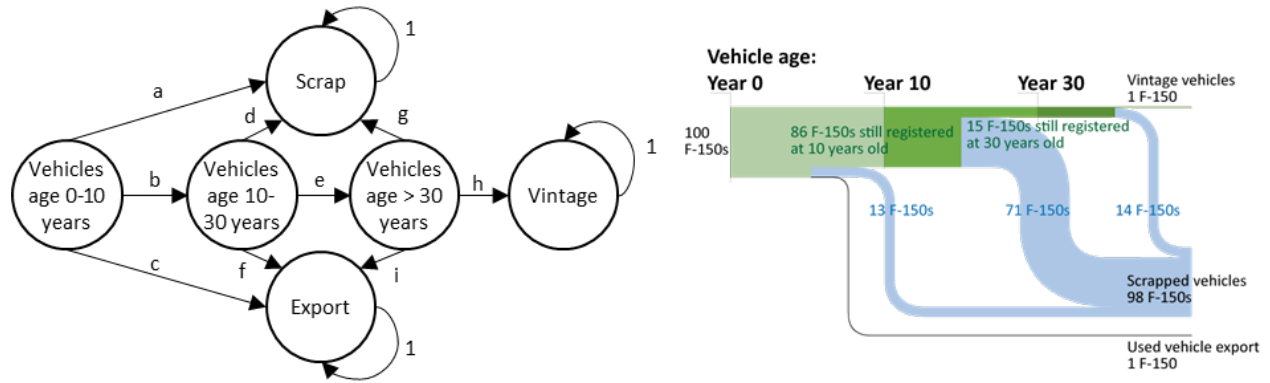


Figure 4.11: Markov chain transition diagram of an aluminum intensive vehicle (left); Sankey diagram representation of vehicle lifespan and destinations (indexed to 100 vehicles) derived from baseline F-150 data shown in Table 4.5.

Table 4.5: Transition probability values for the Markov chain transition diagram (Figure 4.11) assuming mean characteristics for baseline, pessimistic (short), and optimistic (long) vehicle lifespan scenarios.

	Transition probabilities									Fraction of vehicles in the absorbing state		
	a	b	c	d	e	f	g	h	i	scrap	export	vintage
Lifespan scenario	Navigator											
baseline	0.10	0.86	0.04	0.89	0.09	0.02	0.87	0.13	0.00	0.93	0.06	0.01
pessimistic	0.13	0.82	0.05	0.92	0.05	0.02	0.77	0.23	0.00	0.92	0.07	0.01
optimistic	0.08	0.89	0.03	0.85	0.13	0.02	0.92	0.08	0.00	0.94	0.05	0.01
	Expedition											
baseline	0.09	0.88	0.03	0.91	0.08	0.01	0.85	0.15	0.00	0.95	0.04	0.01
pessimistic	0.13	0.82	0.04	0.93	0.05	0.02	0.78	0.22	0.00	0.94	0.05	0.01
optimistic	0.07	0.90	0.02	0.87	0.11	0.01	0.90	0.10	0.00	0.95	0.04	0.01
	Super Duty											
baseline	0.10	0.89	0.00	0.76	0.22	0.02	0.94	0.05	0.01	0.97	0.02	0.01
pessimistic	0.17	0.83	0.01	0.85	0.13	0.02	0.90	0.09	0.01	0.97	0.02	0.01
optimistic	0.06	0.94	0.00	0.61	0.37	0.02	0.96	0.03	0.01	0.97	0.02	0.01
	F-150											
baseline	0.14	0.86	0.01	0.83	0.17	0.00	0.93	0.07	0.00	0.98	0.01	0.01
pessimistic	0.18	0.81	0.01	0.90	0.10	0.00	0.87	0.13	0.00	0.98	0.01	0.01
optimistic	0.10	0.90	0.00	0.75	0.25	0.00	0.95	0.05	0.00	0.98	0.01	0.01

## 4.2.4 Section Discussion

### 4.2.4.1 Scale of the Opportunity

The DMFAs (Figure 4.10 and Section C4) show that the U.S. aluminum intensive vehicle fleet size is growing rapidly and that the fleet of four vehicles studied in this analysis is projected to reach  $23 \pm 5$  18-28 million vehicles by 2050. The Markov chain model (Figure 4.11) suggests that 92-98% of the four vehicles are likely to be scrapped in the U.S., and therefore they present a potentially valuable resource to the domestic recycling industry so long as they are not shredded and then exported. In the baseline scenario, the aluminum ABS scrap generated in 2035 from discarding the four vehicle types studied in this analysis is 121 kt (this number excludes any aluminum ABS embedded in vehicles that are exported or achieve vintage status) which is nearly half of the projected new sales that year (282 kt). Even if production of these four aluminum vehicles were to cease today, aging of the existing stock of 4 million vehicles (around 1,180 kt of embedded aluminum ABS) would result in the scrap availability peaking at 54 kt/year in 2035 (excluding aluminum ABS in exported and vintage vehicles). These aluminum ABS scrap volumes represent a potential doubling of the U.S. automotive aluminum scrap consumption in a little over ten years; U.S. aluminum auto-shred scrap consumption (which presently contains negligible aluminum ABS) is currently around 121 kt/year according to the latest USGS Aluminum Minerals Yearbook (USGS, 2017). Further into the future, domestic aluminum ABS scrap availability from the four vehicle types is expected to reach 239 kt/year by 2050 and continue rising.

Recycling of aluminum ABS presents both environmental and economic benefits. The energy requirements and greenhouse gas emissions associated with recycling aluminum are only around 5% of those associated with primary aluminum production (Milford et al., 2011). Automotive manufacturers could therefore decrease the embodied impacts of vehicle production if they are able to source aluminum ABS made from aluminum ABS scrap. The price gap between these post-consumer scraps and primary aluminum represents the maximum profit opportunity attainable from closed loop recycling or reuse of old sheet into high quality wrought alloys (Allwood et al., 2010; Cooper and Allwood, 2012), and may be sufficient to prompt investment into advanced recycling technologies (see Section 4.3). Figure C18 in the SI shows the price profile for two grades of post-consumer automotive scrap (Twitch and Taint) alongside the primary aluminum price. The price of Twitch and Taint in the U.S. in 2012 was around 41% and 21% of the primary aluminum price, respectively (Schlesinger, 2014).

### 4.2.4.2 Recycling Aluminum Automotive Body Sheet Scrap (C5)

This subsection presents a high-level analysis of the opportunities and barriers to the recycling of aluminum ABS scraps. The recycling of aluminum ABS first requires the removal of non-aluminum

contaminants. As introduced in Section 4.2.1, current vehicle aluminum recycling already involves multiple stages to separate the aluminum from fluids, ferrous metals, plastics, etc. However, due to the inefficacy of the separation processes, tramp element contaminants are often present in the segregated aluminum scrap stream. For example, the ferrous rivets used to assemble aluminum ABS panels are difficult to remove completely during scrap processing. The iron level in EOS automotive aluminum scraps such as Twitch or Tweak can be as high as 1-1.5 wt.% (Kelly and Apelian, 2016), which is significantly higher than the iron tolerance of the aluminum ABS alloys (<0.3-0.35 wt.%). Opportunities to reduce tramp element contamination include higher density shredding of the scraps to improve the efficacy of conventional separation processes such as magnetic separation (Sekulic et al., 2017). Electrolytic and fractional crystallization-based refining technologies are available but remain niche and expensive processes at present (Gaustad et al., 2012; Zhu and Cooper, 2021). In addition to separation and refining, another strategy for reducing iron contamination is to eliminate steel rivets in car body constructions. However, alternative joining technologies (e.g., resistance spot welding or laser welding) cannot fully replace riveting at present due to their low production rate, high capital, and energy costs, and the limited mechanical performance of the resulting joints.

There are three main categories of aluminum vehicle components: sheet components, extrusions, and castings. For closed loop recycling of aluminum ABS scrap into new aluminum ABS sheet (maximum silicon limit of 0.2-1 wt.%, Table 4.1), then the aluminum ABS scrap must be separated not only from non-aluminum contaminants but also from the scrap aluminum castings (silicon compositional range of 7 – 10 wt.%). If the whole vehicle is shredded, then a potential method for segregating wrought and cast alloys is to use a separation technology such as the laser-induced breakdown spectroscopy (LIBS) process (Gaustad et al., 2012; Zhu and Cooper, 2021). However, each of the four vehicles examined in this study has a body-on-frame design where the aluminum castings are located in the vehicle frame. The sheet-intensive vehicle bodies could therefore be isolated from the cast components by separating (unbolting) the body from the frame. For all four vehicles, the aluminum in the vehicle body is approximately 90% sheet and 10% extrusions. Aluminum ABS scrap contamination with extrusion scrap ( $\approx$ AA6082) is unlikely to be a great hurdle to closed loop aluminum ABS recycling because the copper content of the extrusions (<0.1 wt.%) is lower than the copper content of all the aluminum ABS sheet alloys: both high and low magnesium aluminum ABS alloys have <0.1 wt.% copper; low copper aluminum ABS alloys have <0.2 wt.% copper; and, high copper ABS alloys have 0.5-0.8 wt.% copper. The magnesium content of the extrusions ( $\approx$ 0.6-1.2 wt.%) is also lower than the magnesium content of the high and low magnesium aluminum ABS alloys ( $\approx$ 2.9-5.0 wt.%) and is similar to the magnesium content of the high and low copper aluminum ABS alloys ( $\approx$ 0.4-0.95 wt.%). Alloying elements (e.g., copper and magnesium) can be added to the recycled aluminum to correct the composition.

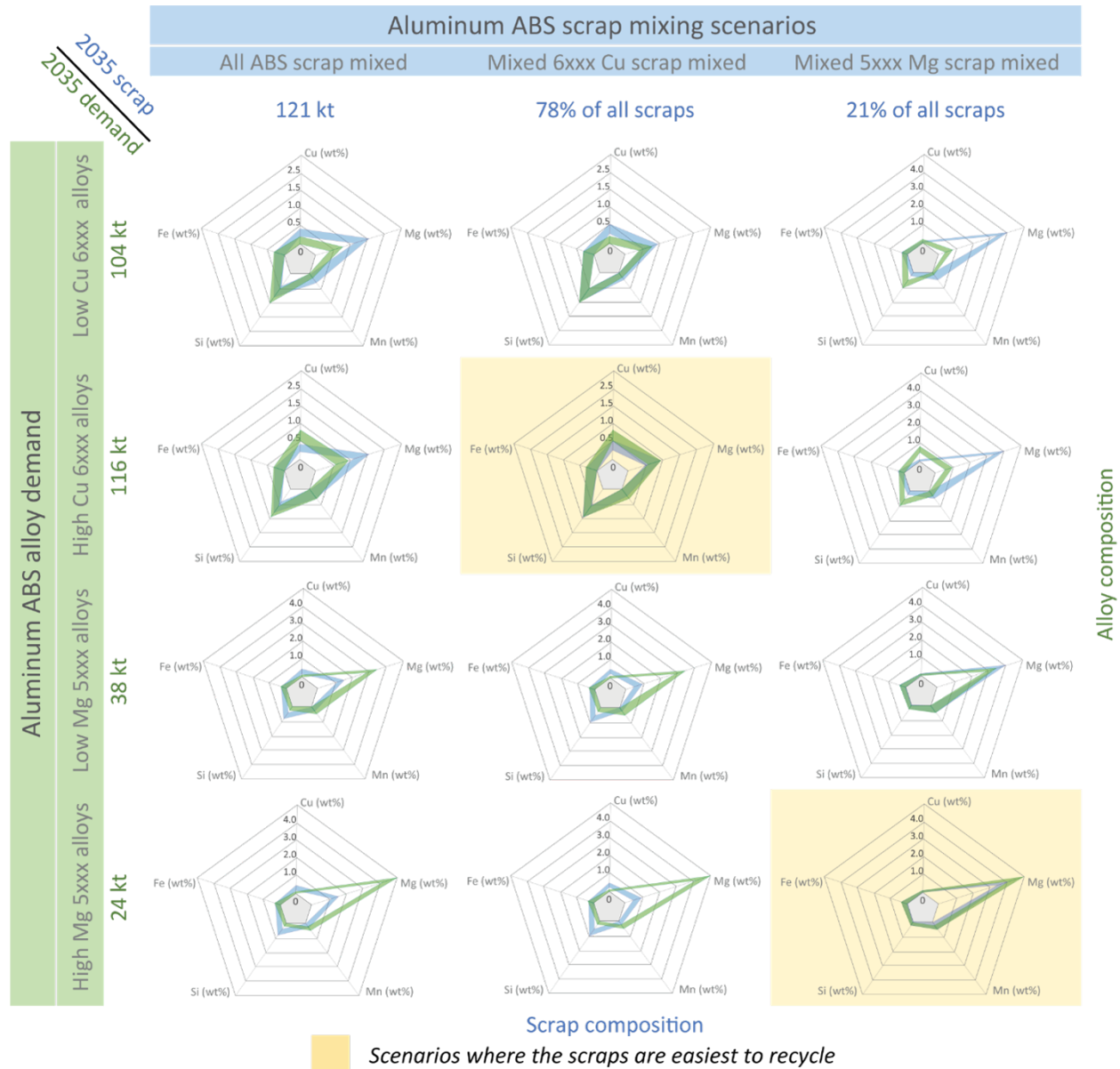


Figure 4.12: Summary of 2035 (baseline scenario) aluminum ABS compositional limits and estimated mixed scrap and new alloy compositions and quantities for the four vehicles in this study. The blue x-axis represents different scrap mixtures and the blue ring-shaped radar plots represent the lower and upper bound composition for five key alloying elements. The green y-axis represents new aluminum ABS alloy demand and the green ring-shaped radar plots represent the lower and upper compositional limit for the same five key alloying elements.

Closed loop recycling of aluminum ABS scrap is best facilitated by complete segregation of the four aluminum ABS alloys (see Table 4.4); however, given the difficulties of sheet alloy separation (Modaresi and Muller, 2012) then it is likely that some sheet alloy mixing will occur during recycling. To evaluate the potential for closed loop recycling under different sheet mixing conditions, Figure 4.12 shows the possible composition of mixed sheet scraps compared to the original sheet alloys.

The green ring-shape radar plots in Figure 4.12 present the upper and lower composition limits for copper, magnesium, manganese, silicon and iron in the four types of aluminum ABS used in the F-Series, Expedition and Navigator vehicles that can be found in the Ford engineering material specification documents (Ford, 2014 and 2020). These five alloying elements have been selected because they have narrow but varying compositional limits across all aluminum ABS alloys in this section. Copper increases alloy strength and facilitates precipitation hardening but may also reduce ductility and corrosion resistance. Magnesium is the major alloying element in 5xxx and 6xxx series wrought alloys used to increase strength. Silicon in 6xxx series aluminum makes for precipitation hardening heat-treatable alloys (Schlesinger, 2014). Iron is one of the most troublesome impurities in aluminum ABS because it promotes the formation of intermediate phases that reduce ductility (De Moraes, et al., 2006). Manganese increases strength through strain hardening by cold rolling, stretching, or drawing while it can also reduce ductility and corrosion resistance (Goel et al., 2014). Note that the composition limits of chromium, zinc, and titanium are identical across all the studied aluminum ABS alloys (Table 4.4) and are not discussed here.

The blue ring-shape radar plots in Figure 4.12 show the elemental composition of aluminum ABS scrap after different levels of sheet mixing that are likely to occur during scrap processing. No tramp element or casting/extrusion alloy contamination is considered in Figure 4.12. The mixed aluminum ABS scrap compositions are calculated for 2035 because this is the year in which the scrap availability from the current vehicle fleet will peak; however, additional scrap composition calculations shown in Section C5 of the SI show that only minimal changes are likely in mixed scrap composition between now and 2050. The DMFA results (see Figure 4.10) show that the total of all 6xxx series (high and low copper) scraps is consistently higher than the 5xxx series (high and low Mg) scraps while the total amount of scrap changes significantly over time. For example, in the 2035 baseline scenarios, the results are 98 kt and 27 kt for all 6xxx series and 5xxx series scraps, respectively. In the 2050 baseline scenario results, there are 192 kt and 54 kt of 6xxx series and 5xxx series scraps, respectively.

Figure 4.12 shows that closed loop recycling of aluminum ABS scrap into aluminum ABS alloys will likely require at least separation of the aluminum ABS scrap alloy families (5xxx versus 6xxx) and ideally separation of each individual alloy. Figure 4.12 shows that in the fully mixed aluminum ABS scrap scenario (first column of Figure 4.12); the scrap cannot be easily recycled into any of the original aluminum ABS alloys without significant dilution with primary aluminum and the addition of alloying elements. This is because the composition of the fully mixed scrap (blue areas in the first column of Figure 4.12) falls outside of the compositional tolerance of all the aluminum ABS alloys (green areas in rows 1-4). For example, the copper content in the fully mixed alloy scrap stream (0.21-0.43 wt.%) is lower than the composition limits for the high copper aluminum ABS alloy (0.5-0.8 wt.%); whereas, the magnesium content of the fully mixed alloy scrap stream (1.12-1.58



wt.%) is above the limits of the high copper aluminum ABS alloy (0.55-0.95 wt.%). Columns 2 and 3 in Figure 4.12 show the estimated composition of the scrap flow assuming all aluminum-copper scraps (6xxx series) or all aluminum-magnesium scraps (5xxx series) are mixed up, respectively. Comparing the composition of mixed aluminum-copper alloy (6xxx) scraps (column 2) and the aluminum-copper aluminum ABS alloys, the scraps can be recycled into the high copper alloy (row 2) with a <0.3 wt.% addition of copper. Similarly, mixed aluminum-magnesium aluminum ABS (5xxx) scraps (column 3) can be recycled into the high magnesium alloy (row 4) with <1 wt.% addition of magnesium.

In order to realize closed loop recycling of the aluminum sheet, emerging separation technologies such as LIBS could be implemented to separate alloy families and individual alloys (Gaustad et al., 2012; Zhu and Cooper, 2020). In LIBS, a focused laser pulse vaporizes a small sample of the scrap surface, and atomic emission from the resulting plasma is used to identify the metal compositions. Currently, the industrial application of LIBS is inhibited by its high cost and low throughput speed: millions of dollars of capital investment are needed for an installed capacity of just 5 tons/hr (Zhu and Cooper, 2021). Other options to increase the recycling of aluminum ABS scraps include the design for dismantling which can increase the separation by alloy family or by individual alloys, and increased research on design for recycling that uses impurity tolerant alloys in new vehicle production. There is also the potential for recyclers to work with OEMs to identify component alloys. (Semi-)automated dismantling equipment could then be used to separate the high-value sheet aluminum alloys from other vehicle components. Automated component separation has already been demonstrated for other product systems, e.g., hard drives (Simon et al., 2017) and smart phones (Laser and Stowell, 2019).

#### 4.2.4.3 Planning for the Sheet Scrap Wave

Limited demand for low quality casting alloys has already constrained the domestic U.S. aluminum recycling rate. This problem will be exacerbated as aluminum ABS intensive vehicles start to reach EOS and enter a recycling system currently configured for producing casting alloys. The present work is a first step towards planning for that coming wave of U.S. aluminum ABS scrap, finding that the supply of aluminum scrap from vehicles for U.S. recycling is likely to double by the mid-2030s. Both U.S. recyclers and automotive manufacturers can take actions to help ensure this wave of scrap is recycled into high value aluminum ABS. For U.S. recyclers, increasing investment in new scrap separation and refining technologies (see section 4.2) will be needed to ensure alloy separation and tramp element removal. Automotive manufacturers could further embrace *Design for Recycling*, ensuring easy separation of individual alloys or at least alloy families. Manufacturers and recyclers could directly collaborate to make car redesign and recycling technology investment decisions based on recycling experiments of early prototype builds. All these actions could be

further stimulated by government research and development funding or financial incentives such as tax breaks for recyclers who invest in separation and refining technology.

### **4.3 Emerging Aluminum Separation and Refining Technologies**

*The work in Section 4.3 has yet to be published as either a journal or conference article; however, it is included in this thesis for completeness as it begins to address the recycling constraint barriers discussed in Sections 4.1 and 4.2.*

Analysis of the U.S. aluminum recycling industry and the automotive aluminum sheet market reveals that the chemical compositional mismatch between the available scrap streams and the demand for metal constrains current and future U.S. EOL aluminum recycling rates. To solve the compositional mismatch problem, scrap separation and refining technologies have been proposed and developed in previous studies as potential solutions. To understand the efficacy of emerging aluminum scrap separation and refining technologies in the optimal aluminum reverse supply chain, we have developed a recycling technology catalog. The catalog data is combined with the linear blending optimization model to quantitatively evaluate the potential of emerging recycling technologies in improving future EOL automotive aluminum closed-loop recycling rates.

The recycling technology catalog was developed by reviewing 46 academic papers and 8 grey literature sources. In total, three separation technologies and eight refining technologies are investigated in the catalog.

Separation:

- Color sorting and etching
- Hot crush
- Laser induced breakdown spectroscopy

Refining:

- Basic melting: reverberatory furnace
- Fluxing
- Hoopes process
- Low temperature electrolysis
- Fractional crystallization
- Vacuum distillation

- Electro-refining for Mg removal
- Membrane purification

For each separation and refining technology, the catalog includes information about the separation and refining potentials (i.e., the ability to separate a material stream into its constituent parts), material losses, costs, energy consumptions, emissions, and describes the likely use of each technology in parallel or in a series with other recycling technologies. Details of how this information is derived from the literature are explained in the following sections and appendix D. The above technologies are selected based on a review of the last 30 years of literature on aluminum recycling technologies and preliminary discussions with global recycling producers e.g., Rio Tinto. Most research developments of the aluminum recycling technologies happened before or at the beginning of the 21st century while recently, these technologies are attracting more attentions from the industry. Section 4.3.1 summarizes the methodology used to develop the recycling technology catalog and summary of key technologies. Section 4.3.2 presents the modified linear optimization model and how the separation and refining technologies could be used to increase the closed loop recycling rate of EOL aluminum ABS scraps using DMFA results from section 4.2.

#### **4.3.1 Summary of the Aluminum Separation and Refining Technology Catalog**

During typical aluminum recycling today, the process starts with the shredding of raw scrap from collected vehicles or scrap stored on site at the scrap yard. The shredding operation turns raw scrap into manageable dimensions so that the shredded chips can be processed by the following operations. Common *separation* processes (solid-state sorting of scraps) (e.g., air separation, magnetic separation, and eddy current separation) are used to remove the most nonmetallic and ferrous tramp elements from the shredded aluminum scrap. Additional emerging (solid-state) *separation* and/or (liquid-state) *refining* technologies can be used to further purify the scraps. The resulting molten scrap charge is mixed with virgin metals to produce new alloys demanded by the market. The flow of scraps during this recycling process is summarized in Figure 4.12. We define "process coupling" during the recycling process as when a refining technology is implemented after an additional separation process. Process coupling contributes to the diversity of scrap process routes and can potentially increase the recycling rate at lower energy consumption. The final step of the recycling process is to melt the scrap, adjust the composition with virgin metal, and cast it into an ingot or parts.

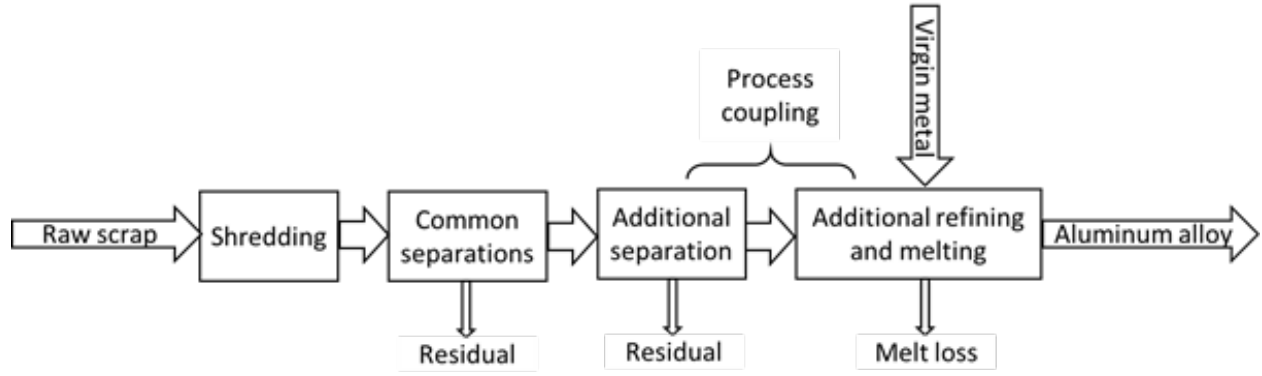


Figure 4.13: Flowchart of the aluminum recycling process

The focus of this study is the third and fourth steps of the recycling process as shown in Figure 4.13. The system boundary of each technology model includes the utilities and consumables used on site, human labor, machinery, and maintenance. Consumption of raw scrap (its cost and environmental impacts) is modeled separately in the linear optimization model and thus not included in the emerging technology models. The performance of each technology is measured along five dimensions: separation and refining potential, process yield ratio, cost, emission, and current industrial use.

The separation or refining potential is the ability of a technology to separate scrap alloys and/or remove impurities. In this work, the separation or refining potential of a technology is represented by the elemental composition of the processed scraps, which depends on the separation and/or refining technology used and the composition of the incoming scrap streams. The composition of incoming scrap depends on the alloy breakdown of the scrap stream and the quantity of tramp element contamination, both of which may change over time. For a separation process (e.g., LIBS process), the chemical compositions of the separated scraps are assumed to be the same as those of the corresponding pure alloy stream. For example, if  $a$  kt of mixed low Cu and high Cu scraps are separated by the LIBS process, then the separated scraps will contain  $b$  kt of low Cu scraps and  $c$  kt of high Cu scraps. The mass of separated scraps and input scraps satisfy the mass conservation and the ratio of  $b$  to  $c$  depends on the ratio in the mixed Cu scraps which can be derived from the DMFA results.

$$a \text{ kt} \cdot \text{comp}_{k, \text{mixed Cu scraps}} \rightarrow b \text{ kt} \cdot \text{comp}_{k, \text{low Cu}} + c \text{ kt} \cdot \text{comp}_{k, \text{high Cu}} \quad (4.12)$$

$$a = \alpha_{LIBS} * (b + c) \quad (4.13)$$

If there is contamination in the input scrap stream, it is assumed that the contamination remains in the separated scraps. This assumption is made because the contaminant is likely firmly attached

to the scrap and unlikely to have been separated in the upstream separation processes. For example, if the mixed Cu alloying aluminum autobody sheet scrap is contaminated with 1% iron (unremoved rivets), the composition of mixed Cu scraps before separation is modeled as:

$$comp_{k=iron,mixed\ Cu\ scraps\ 1\%\ Fe\ contaminate} = comp_{k=iron,mixed\ Cu\ scraps\ uncontaminated} + 1\% \quad (4.14)$$

The composition of separated low Cu and high Cu scraps are modeled as:

$$comp_{k=iron,low\ Cu\ 1\%\ Fe\ contaminate} = comp_{k=iron,low\ Cu} + 1\% \quad (4.15)$$

$$comp_{k=iron,high\ Cu\ 1\%\ Fe\ contaminate} = comp_{k=iron,high\ Cu} + 1\% \quad (4.16)$$

For a refining process, the chemical composition of the refined scrap is a function of the input scrap composition. For example, if the Hoopes process is used to refine scrap with chemical composition  $comp_{k,input}$  where  $k$  indicates the alloy elements, then the  $comp_{k=aluminum,refined}$  of the Hoopes process equals 99.97% and the alloying element composition is calculated using the Equation 4.17. As the scrap composition changes over time, the refined scrap aluminum content always equals 99.97% while the other alloy content changes following the same calculation. If the scraps are contaminated by any trace elements, the trace element content increases in the input scrap stream. The refined scrap aluminum content still equals 99.97% and the other alloy content is calculated using the same procedure as in Equation 4.17.

$$comp_{k,refined} = comp_{k,input} * (100\% - comp_{aluminum,refined}) \quad (4.17)$$

During a separation or refining process, materials may be lost due to the removal of contaminants (e.g., removal of steel rivets and surrounding aluminum sheet) or melting (e.g., oxidation of exposed aluminum melt). Process yield quantifies the ratio of the mass of material recovered to the mass of material input and indicates the level of material loss of technology. In this study, the process yield ratio is expressed as  $\alpha$  [%] which is used in the cost and energy estimations later. The process yield of technology is assumed to be the same irrespective of scrap input  $s$  or alloy demand  $d$  and may change over time (year  $t$ ).

The cost of a separation or refining technology includes both variable costs such as utilities (e.g., electricity and natural gas), consumables (e.g., salt), etc., and fixed costs such as machinery. For a typical separation process such as color sorting and etching, the lifetime cost ( $C_{total}$ [\$]) of processing a total amount of  $x_{total}$ [metric ton] aluminum scraps is as follows:

$$C_{total} = x_{total} \times (c_{utilities} + c_{consumables} + c_{labor}) + C_{machinery} + C_{maintenance\&repair} \quad (4.18)$$

Where  $c_{utilities}$ [\$/metric ton input],  $c_{consumables}$ [\$/metric ton input], and  $c_{labor}$ [\$/metric ton input] are the specific costs per metric ton aluminum scrap of utilities (e.g., electricity), consumables (e.g., etching chemicals) and operating labor respectively,  $C_{machinery}$ [\$] is the investment of the construction and machinery and  $C_{maintenance\&repair}$ [\$] is the lifetime maintenance and repair cost. For a separation technology, the machinery costs and utilities or consumables used are usually identifiable from academic and grey papers or specifications of similar machines in other markets (e.g., sewage water vacuum evaporator to approximate aluminum vacuum distillation for zinc removal) and the energy column of the catalog records the utilities consumed per metric ton input of the technology. Specifically, the electricity cost is modeled at 6.91 cents/kWh and the natural gas cost is modeled at \$4.14/1000 cubic feet. The labor cost is modeled at a constant value of \$10.8/metric ton of scrap input for separation technologies according to Pressley et al. (2015)'s analysis of aluminum separation facilities in the U.S. Maintenance and repair cost is approximated as 56% of machinery cost according to Enparantza et al. (2006)'s life cycle analysis of industrial machines. The value of  $x_{total}$  is estimated from throughput rate  $t$  [metric ton/hr], process yield ratio  $\alpha$  [%] and machine life  $m$  [hr] as shown in Equation 4.19.

$$x_{total} = \frac{t}{\alpha} \times m \quad (4.19)$$

Throughput rate and process yield ratios are both process specific data obtained from literature or machine specification reviews. For example, the yield of the Hoopes process is assumed to be 95% according to DeYoung et al. (2010). For machine lifetime estimates, Erumban (2008) found that the average service life of industrial machines is around 30 years, and each machine is assumed to operate at 300 days/year and 18 hrs/day which gives the total machine life in hours. The lifetime cost  $C_{total}$  is then converted to unit mass based specific cost  $c_{total}$ [\$/metric ton input] by amortizing it among  $x_{total}$  metric tons of material as shown in Equation 4.20.

$$c_{total} = \frac{C_{total}}{x_{total}} = c_{utilities} + c_{consumables} + c_{labor} + \frac{C_{machinery} + C_{maintenance\&repair}}{x_{total}} \quad (4.20)$$

The specific cost of a refining technology can be calculated similarly using Equation 4.20. In the case of coupled processes, where a separation technology is followed by a refining technology, the cost of the coupled processes is computed as Equation 4.21. The inclusion of the separation technology yield ratio ( $\alpha_{separation}$ ) accounts for the material loss during the separation process. The

cost data is collected to prepare for future analysis of potential cost savings or industry investment needed to switch from current recycling routines to emerging technologies as part of a future Department of Energy project. In this case study of U.S. aluminum ABS recycling, the cost data is not used.

$$C_{total\_coupled\_process} = C_{separation} + \alpha_{separation} \times C_{refining} \quad (4.21)$$

The specific energy  $e_{total}$  [MJ/kg of scrap input] from a separation or refining technology is quantified by the process energy (utilities) and embodied energy of materials.

$$e_{total} = e_{utilities} + e_{consumables} \quad (4.22)$$

For coupled separation and refining process, the combined specific energy is calculated as Equation 4.23.

$$e_{total\_coupled\_process} = e_{separation} + p_{separation} \times e_{refining} \quad (4.23)$$

Information about the level of industrial use of each technology is collected as a reference for analyzing its potential future market share. For example, hot crush is one of the technologies that has only been mentioned in academic research papers and not used in the industry. Thus, its industrial use is assumed to be currently zero and recorded as "laboratory scale". Other levels of industrial use considered in this analysis include: "some industrial uses" (e.g., LIBS separation process which has been deployed in pilot scrap processing facilities (Steinert, 2018)) and "widely used" (reverberatory furnace melting which is the most widely used recycling technology in the U.S.).

For each technology parameter, a data confidence level—high (H), medium (M), or low (L)—is assigned according to three measures: (1) date of the data sources (e.g., post 2010 vs. pre-2000) (2) integrity of the data source (e.g., peer-reviewed vs. anecdotal); and (3) the degree to which (proxy) data from multiple sources is required to calculate the technology parameter. For example, the heating system for the semi-solid hot crush process was modeled using proxy reverberatory furnace data which is assigned a score of 2 in third measurement category. The weighted scores in the three measurement categories are summed up to get a total score. If the total score is higher than 90%, it is assigned a confidence level of high(H). Similarly, if the score is within 70% - 90%, it is assigned a confidence level of medium (M) and a low (L) if less than 70%. A data source with a confidence level of high is assumed to vary within 10% of the nominal value, and a similar 20% or 30% variation is assumed for medium or low confident data sources respectively. Table 4.6 below is the example weighting rubric for assigning the confidence level to each data source. The data confidence measurement will be used for future sensitivity analysis of the reverse aluminum supply chain optimization.

Table 4.6: data confidence level measuring rubric

		technology parameter			
data confidence criteria	score range	weight	cost of Labor	refining potential of fractional crystallization	cost of electro-refining technology for Mg removal
date of the data source	3: post 2010	33.33%	3	1	3
	2: 2000-2010				
	1: pre-2000				
integrity of the data	2: peer-reviewed	33.33%	2	2	2
	1: anecdotal				
degree to which (proxy) data from multiple sources is required	3: research and industry data (no approximation needed)	33.33%	1	2	3
	2: approximated with aluminum related process or extrapolated from experimental data				
	1: approximated with other processes				
		weighted total score (%)	77%	67%	100%
		confidence level	medium	low	high

#### 4.3.1.1 Color Sorting and Etching

Color sorting and etching has been widely used in industry to separate metal scraps since the 1970s (Bell et al. 2003; Wyss and Schultz 1999). However, it was not used to separate aluminum scraps by alloy groups until 1999 (Bell et al. 2003; Wyss and Schultz 1999). During the color sorting process, scraps are treated with chemical solutions, e.g., sodium hydroxide solution, under controlled temperatures to produce different surface colors according to their alloy compositions. An optical sensor and automated sorting mechanism are then used to separate the color etched scraps into alloy groups. In the case of similar alloy compositions, more than one round of chemical treatment can be applied to produce distinctive surface colors and further distinguish the scraps. Wyss and Schultz (1999) used two rounds of solution treatment to produce distinguishable color on the surface of 2xxx, 3xxx, 5xxx, 6xxx, and 7xxx wrought aluminum scraps which were then detected by an industrial level CCD camera. According to Brown (1982), the yield ratio of industrial



level color sorter can be higher than 99%. The cost of color sorting and etching is estimated at around \$13/metric ton aluminum input while the energy consumption is estimated at around 400 Wh/metric ton aluminum input.

Compared to traditional separation methods (e.g., air separation and magnetic separation), the major advantage of color sorting is its ability to separate scrap by alloy families and manage a scrap of various sizes and shapes (Gausted et al., 2012). However, color sorting has not been widely adopted in the aluminum recycling industry because of the high investment requirement and the inaccuracy in sorting the etched scraps (Steinert, 2019; Rio Tinto, 2019). Inaccuracies may be caused by coating and surface finish of the scraps, temperature control, and chemical solution choices (Wyss and Schultz, 1999; Bell et al., 2003; Gausted et al., 2012).

#### **4.3.1.2 Hot Crush**

Hot crush is a technique that separates casting and wrought aluminum scraps based on their distinguishing thermal-mechanical behaviors at sub-melting point temperatures (Ambrose et al. 1983; Duane 1985; Brown et al., 1985). Within the temperature range between 525°C and 625°C, casting aluminum alloys become more brittle (which is called hot shortness) while wrought aluminum alloys are still ductile. Based on these thermal-mechanical behaviors, Ambrose et al. (1983), Duane (1985), Brown et al. (1985) designed and tested the hot crush process where the mixed casting and wrought aluminum alloys are heated to 525 - 625°C and crushed using jaw crushers or other smashing mechanism. The casting alloys can be crushed into smaller pieces while wrought metal remains in the original size. Subsequent screening and sorting operations then separate the wrought scraps from casting scraps based on sample size. Duane et al. (1985) estimated that the yield rate of the hot crush process is around 97% and the loss mainly occurs due to oxidation in the furnace heating operation. The cost and energy consumption of hot crush are estimated at around \$70/metric ton aluminum input and 867 kWh/metric ton aluminum input respectively.

The hot crush process relies on the thermal-mechanical behaviors of aluminum alloys rather than chemical solution treatment, reducing the need for subsequent surface cleaning and drying. Major disadvantages of the hot crush technique include (1) high energy cost compared to traditional separation techniques in order to reach sub-melting temperature; (2); long preheating time (1 hr. to 6 hrs.) for homogeneous scrap temperature (Duane, 1985) (3) complexity of screening mechanism design for different wrought and cast scrap mixture; (4) potential contamination in sorted wrought scrap due to melted casting alloys (Ambrose et al. 1983; Duane 1985). No industrial usage has been found for hot crush technique in the aluminum recycling industry.

### **4.3.1.3 Laser-Induced Breakdown Spectroscopy (LIBS)**

Laser-induced breakdown spectroscopy (LIBS) process separates aluminum scraps by individual alloy type (Gausted et al., 2012). During the LIBS process, elements on the scrap surface are excited by the energetic laser pulse. The emitted light from the scrap is captured to produce spectrums which are analyzed to identify the chemical composition of the specific scrap. The LIBS technology was first invented by the Los Alamos National Laboratory in the 1980s (Javaid and Essadiqi, 2003). Currently, it has been applied to metal scrap sorting by U.S. companies such as Huron Valley Steel (Gesing and Wolanski, 2001) and Austin AI (Austin AI, 2019) as well as EU companies such as Constellium, TriTech and Steinert (Rio Tinto, 2019; Steinert, 2019). According to Gesing et al. (2010), for a single pass sorting of three-alloy mixture, the recovery rate for each alloy ranges from 96% to 99%. Campanella et al. (2017) tested the LIBS system with uncleaned aluminum scraps and achieved yield ratios between 47% and 90% under various experimental setups. We approximate the yield ratio of the LIBS process as the average of all data sources at 83%. The cost of LIBS is estimated at around \$10/metric ton aluminum input while the energy consumption is estimated at around 640 Wh/metric ton aluminum input.

LIBS process requires no heat treatment or chemical solution treatment. However, in order for the pulse laser to reach the surface of the scrap for accurate detection, the scrap must be cleaned and de-coated before screening. Scrap size is another factor that limits sorting accuracy because if the scrap size is too small, it may bypass the laser detector or be incorrectly identified according to Gesing et al. (2010). LIBS process throughput rate is limited by the conveyor system design and sorting requirement. Current LIBS sorters usually can sort a mixture of two or three alloys at a time. In the case of complex EOL scrap streams, more than one round of sorting is required to separate the scraps into individual groups (Gesing et al., 2010; Austin AI, 2019).

### **4.3.1.4 Basic Refining: Reverberatory Furnace**

A reverberatory furnace is a type of large scale natural-gas-fired smelting furnace that is commonly used in secondary aluminum production in the U.S. In a reverberatory furnace, aluminum scraps are charged into the hearth (bottom of the furnace) directly or from sidewalls, and the heat generated from burning the natural gas transfers directly to the aluminum scrap by radiation and convection. Common aluminum secondary production remelts the solid aluminum scrap mixture in a reverberatory furnace to form a molten aluminum charge. The molten aluminum charge has a homogenous chemical composition which can be estimated from the weighted average of the chemical composition of input scrap. Melting loss occurs in a reverberatory furnace due to oxidation of molten aluminum that is directly exposed to the air-fuel combustion mixture. The yield rate of reverberatory melting is estimated at 96% (Deyoung et al., 2011; Schlesinger, 2014; Milford et al.,

2011). The cost and energy consumption of reverberatory furnace melting are estimated at around \$262/metric ton aluminum input and 1543 kWh/metric ton aluminum input respectively.

Reverberatory furnace melting is a batch process that has higher productivity and lower maintenance cost compared to the other common re-melting furnace, i.e., the rotary furnace. However, it may suffer from low energy efficiency because of the stationary heat transfer design (Li et al., 2006). A recent study has suggested that adding oxygen to aid the natural gas burning in the reverberatory furnace can increase the furnace energy efficiency compared to traditional air-fuel combustion (Gangoli et al., 2017).

#### **4.3.1.5 Fluxing for Magnesium Removal**

Fluxing is a commonly used technique to prevent metal oxidation and to remove inclusions, alkali metals, and magnesium in aluminum recycling (Utigard et al., 1998; Utigard et al., 2001; Williams, et al., 2016)). Chlorine gas, a typical fluxing gas, reacts with magnesium in the molten aluminum charge and forms magnesium chloride which is then removed as part of the dross (Tiwari, 1982; Fu and Evan, 2007; Qian et al., 1998). Dross is the semi-solid floating layer formed during the re-melting process that contains a mixture of molten aluminum, various oxides, chloride compounds, etc. Lately, the use of chlorine as the fluxing agent has been gradually abandoned because of health concerns related to its toxicity (Schlesinger, 2014). In addition to chlorine gas, solid chlorine or fluoride containing fluxes, e.g.,  $\text{AlCl}_3$ ,  $\text{AlF}_3$  and  $\text{NaAlF}_4$  can be used to remove magnesium in the form of chloride or fluoride dross (Majidi, et al., 2007; Leboeuf et al., 2016; Gaustad et al., 2012). However,  $\text{AlF}_3$  is expensive for secondary aluminum production and use of fluoride-based salts also presents potential workplace hygiene concerns (Gaustad et al., 2012). The cost of fluxing is estimated at around \$142/metric ton aluminum input. Fluxing is usually performed on melted scraps and the additional energy to melting is minimal.

Fluxing process often requires a large amount of gas or salt to enable efficient removal, e.g., 2.95 kg of chlorine is needed to remove 1.0 kg of magnesium (Schlesinger, 2014). The chemicals used (e.g., chlorine as fluxing gas,  $\text{AlCl}_3$ ) or produced (e.g., HCl vapors generated during the fluxing process) in the fluxing process present health and environmental concerns (Gaustad et al., 2012). In addition, the reaction of salts with the alloying elements may produce new contamination in the alloys. and generate large amounts of salt cakes (e.g., 200-500 kg per metric ton of aluminum produced) which contain mostly nonmetallic salt that requires further waste treatment (Utigard et al., 1998).

#### **4.3.1.6 Hoopes Process**

The Hoopes process is a three-layer electrolysis process that refines liquid aluminum to produce high purity products (higher than 99.97 wt.% aluminum content) such as 1xxx series foil (Gaustad et al., 2012). It was first developed by J.W. Hoopes et al. in the early nineteenth century as a primary aluminum refining technology (Lindsay, 2014). In the Hoopes process, the molten aluminum scrap forms the anode layer and the pure aluminum concentrates at the cathode layer. The remaining elements are lost in the electrolyte layer (Gaustad et al., 2012). The yield ratio of the Hoopes process is modeled at 95% according to DeYoung et al. (2011). The cost of the Hoopes process is estimated at around \$1165/metric ton aluminum input while the energy consumption is estimated at around 17,500 kWh/metric ton aluminum input.

The Hoopes process is energy intensive as it requires high operation temperature (between 700°C and 900°C) and high electricity input to enable electrolyzing of molten aluminum. According to Hammer et al. (2014), the environmental saving of Hoopes refining is only 17% of primary aluminum production. The Hoopes process suffers from low productivity and its market share is very limited in the current aluminum primary or secondary industry (Rio Tinto, 2019).

#### **4.3.1.7 Low Temperature Electrolysis**

Low temperature electrolysis is an electro-refining process that produces high purity aluminum at a lower temperature (around 100°C) compared to traditional electrolysis (e.g., the Hoopes process that usually operates at 700-800°C) (Endo, et al., 2014; Gaustad et al., 2012; Kamavaram et al., 2005). Instead of using cryolite as the electrolyte, which is a common practice in the Hall Heroult primary aluminum production process, room-temperature-ionic-liquids are used in low temperature electrolysis to enable electro-deposition of pure aluminum (Pradhan and Reddy, 2014). The common setup for low temperature electrolysis has three layers: the scrap aluminum anode, the pure aluminum or copper cathode, and the room-temperature-ionic-liquid as electrolyte. Purified aluminum is electro-deposited on the cathode which removes tramp elements such as manganese, iron, silicon, copper, zinc, nickel, and lead (Gaustad et al., 2012). The cost of low temperature electrolysis is estimated at around \$387/metric ton aluminum input and the energy consumption is estimated at around 4950 kWh/metric ton aluminum input.

Low temperature electrolysis saves energy compared to traditional electro-refining technologies, e.g., the Hall Heroult process and the Hoopes process. In laboratory tests, the energy consumption ranges between 3.2 and 6.7 kWh/metric ton aluminum according to Kamavaram et al. (2005). It also avoids possible toxic or harmful gas emissions compared to fluxing. However, the low temperature electrolysis may suffer from low processing rate, e.g., the experimental purification rate is only around 0.003 g/hr according to Kamavaram et al. (2005). Low temperature electrolysis is still at

experimental stage and no industry usage of low temperature electrolysis has been found (Rio Tinto, 2019).

#### **4.3.1.8 Fractional Crystallization**

Fractional crystallization is a popular method for ore and primary metal refining invented in the nineteenth century (Muniz-Lerma et al., 2017; Gaustad et al., 2012; Drini et al., 2005; Kahveci and Unal, 2000; Sillenkens, 1999). Several studies investigate the usage of fractional crystallization to purify and produce high-purity aluminum metals with 99.99 wt.% or higher aluminum content (Muniz-Lerma et al., 2017; Drini et al., 2005; Kahveci and Unal, 2000; Sillenkens, 1999). During the fractional crystallization process, the surface of scrap melt is cooled in a controlled manner (usually by air blow/quench) to allow for the formation of aluminum crystals, leaving the impurities in the remaining melt. A continuous filtering mechanism is used to collect the purified aluminum. In theory, the fractional crystallization process can remove most eutectic impurities such as silicon, iron, copper, nickel, magnesium, gallium and zinc from the aluminum melt (Drini et al., 2005; Sillenkens, 1999). Yield rate of fractional crystallization ranges between 40% and 80% based on different experimental setups (Muniz-Lerma et al., 2017; Drini et al., 2005; Kahveci and Unal, 2000; Sillenkens, 1999). The cost of fractional crystallization is estimated at around \$172/metric ton aluminum input and the energy consumption is estimated at around 2300 kWh/metric ton aluminum input.

Due to the fact that metal tends to form solid solutions, the crystallization process has to be repeated in order to achieve desired purity. There is also a large amount of unavoidable yield loss during the fractional crystallization process since downgraded impure aluminum is created in each cycle of the crystallization. In addition, this refining technique requires a large equipment capacity to allow consistent crystallization to happen. Due to the low productivity, high investment requirement and yield loss, fractional crystallization has only been seen in few aluminum primary facilities (Rio Tinto, 2019).

#### **4.3.1.9 Vacuum Distillation**

Vacuum distillation removes impurities, e.g., lithium, magnesium, manganese, and zinc from aluminum baths under reduced pressure based on distinct boiling point differences between impurity elements and aluminum (Gaustad et al., 2012). Molten aluminum that enters the vacuum furnace is held at certain temperatures, e.g., 30 mins at 750°C to 900°C, to allow impurity elements e.g., zinc, to vaporize. Ithaki, Arakawa and Murata (2000) experimentally reduced the zinc content in the aluminum bath from 3 wt.% to less than 0.1 wt.% and collected the zinc vapor at water-cooled flanges. According to Gilstad (2013), the yield ratio of distillation process, which is similar to

that of the fractional crystallization process, is modeled at 80%. The cost of vacuum distillation is estimated at around \$212/metric ton aluminum input while the energy consumption is estimated at around 3841 kWh/metric ton aluminum input.

A major advantage of vacuum distillation is that the vaporized impurity elements, such as zinc, can be collected and reused which adds to the economic value of the technology. However, the effectiveness of impurity removal is limited by pressure and the ratio of free surface to the volume of aluminum melt (Gaustad et al., 2012). No industrial usage of vacuum distillation in the aluminum recycling industry has been found (Rio Tinto, 2019).

#### **4.3.1.10 Electro-Refining for Magnesium Removal**

The electro-refining for magnesium technique was developed by Gesing and Das from Phinix, LLC and MER Corporation under a US DOE project (Gesing and Das, 2017; Gesing, Das and Loutfy, 2016). This process is designed to extract magnesium from molten aluminum scrap by integrating an electro-refining cell in a reverberatory furnace (Gesing and Das, 2017; Gesing, Das and Loutfy, 2016). The aluminum scrap melt circulates through the electro-refining cell and excessive magnesium (with minor aluminum content) deposits on the cathode which can be removed as a continuously cast solid rod. A selected electrolyte ( $\text{NaCl-SrCl}_2\text{-MgCl}_2$  and  $\text{LiF-MgF}_2$ ) allows for the separation of magnesium from aluminum melt by density and has the potential to remove lithium, sodium, calcium, strontium from the scrap aluminum melt. The theoretical purity of the refined aluminum product ( $3 \times 10^{-5}$  mol pct.) can meet the chemical composition requirement for both wrought and casting aluminum alloys (Gesing and Das, 2017; Gesing, Das and Loutfy, 2016). The cost of electro-refining for magnesium technique is estimated at around \$272/metric ton aluminum input while the energy consumption of electro-refining for magnesium technique is estimated at around 2500 kWh/metric ton aluminum input.

Major advantages of the electro-refining for magnesium technique include (1) reclaiming alloyed magnesium (2) replacing conventional chlorination refining process and avoiding associate health and environmental concerns. Disadvantages of this process include possible moisture or residual contaminations e.g., sodium in the processed scraps (Gesing and Das, 2017; Gesing, Das and Loutfy, 2016). This technology has only been tested in laboratory and no industry usage has been found (Das, 2019).

#### **4.3.1.11 Membrane Purification Cell**

Membrane purification cell is an electro-refining process that uses a horizontal membrane cell anode to replace the aluminum-copper alloy anode in a typical Hoopes process (DeYoung et al., 2011). It can remove common contaminants in aluminum scraps such as copper, silicon, iron,

manganese, etc. According to DeYoung et al. (2011), the membrane purification technology has lower energy consumption and emission compared to the Hoopes process. The cost and energy consumption of membrane purification technology are estimated at around \$446/metric ton aluminum input and 6393 kWh/metric ton aluminum input respectively.

Compared to other refining processes, membrane purification cell has a relatively low melt loss (yield ratio around 95%) due to the enclosed melting chamber design that prevents exposure of molten aluminum to the combustion product or atmosphere. The membrane cell can serve as both a purification system and an electric melting system to save the operation cost of re-melting furnaces (DeYoung et al., 2011). Similar to other electro-refining processes, the membrane purification cell is likely to suffer from low production rate. No industry usage has been found for the process (Rio Tinto, 2019).

### 4.3.2 Applying Emerging Recycling Technologies to Upcoming U.S. ABS Scrap for Closed-Loop Recycling

We combine the technology catalog with the modified linear programming model introduced in Section 4.1 to evaluate the potential of emerging recycling technologies on the upcoming stream of the U.S. aluminum ABS scrap. Equation 4.24-4.29 shows the modified linear programming model.

$$\text{Minimize : } \sum_{d=1}^D \sum_{s=1}^S \sum_{p=1}^P \alpha_{d,s,p} \cdot \theta_{d,s,p} \cdot \text{energy}_{d,s,p}, \text{ for each year} \quad (4.24)$$

$$\sum_{s=1}^S \sum_{p=1}^P \alpha_{d,s,p} \theta_{d,s,p} \geq \text{Alloy\_demand}_d, \text{ for each } d \quad (4.25)$$

$$\sum_{d=1}^D \sum_{p=1}^P \theta_{d,s,p} \leq \text{Metal\_source}_s, \text{ for each } s \quad (4.26)$$

$$\frac{\sum_{s=1}^S \theta_{d,s,p} * \alpha_{d,s,p} * \text{comp\_lower}_{k,s,p}}{\sum_{s=1}^S \theta_{d,s,p} * \alpha_{d,s,p}} \geq \text{comp\_limit\_min}_{d,k}, \text{ for each } [d,p] \quad (4.27)$$

$$\frac{\sum_{s=1}^S \theta_{d,s,p} * \alpha_{d,s,p} * \text{comp\_upper}_{k,s,p}}{\sum_{s=1}^S \theta_{d,s,p} * \alpha_{d,s,p}} \leq \text{comp\_limit\_max}_{d,k}, \text{ for each } [d,p] \quad (4.28)$$

$$\sum_{s=\text{scraps}} \theta_{d,s,p} \geq a * \sum_s \theta_{d,s,p}, \text{ for each } [d,p] \quad (4.29)$$

The objective function is shown in Equation 4.24, subject to the inequality constraints shown in Equation 4.25-4.29. For each year between 2021 and 2050, we minimize the total energy needed to produce the demanded alloys (total of  $D$  alloy types) as predicted in the DMFA section. The total energy includes the embodied energy of scrap (GREET, 2020) and virgin metals (Ashby, 2012) as well as process energy derived in the technology catalog. In this case study,  $D = 6$  which are low Cu alloy, high Cu alloy, low Mg alloy, high Mg alloy (shown in Figure 4.11 in Section 4.2.5), extrusion (A6082), and casting (A356.0). The quantity, yield ratio, and energy consumption of metal source  $s$  used to produce new alloy  $d$  through technology  $p$  [Mt] are represented by  $\theta_{d,s,p}$ ,  $\alpha_{d,s,p}$  and  $energy_{d,s,p}$ , respectively. There is a total of  $S$  metal source types. Among all the metal sources,  $s=1$  represents unalloyed primary aluminum,  $s=2:6$  represents the five alloying elements and the rest of  $s$  to  $S$  represents the scrap sources (aluminum ABS scrap, extrusion scrap, casting scrap or mixture of scraps).

There are four groups of inequality constraints: alloy demand, scrap supply, alloy chemistry, and economic furnace constraints. The alloy demand constraints (Equation 4.26) ensure that the production of each new metal alloy,  $d$ , is greater than or equal to alloy demand ( $Alloy\_demand_d$ ). The scrap supply constraints (Equation 4.27) ensure that the quantity of a used scrap source does not exceed the amount available ( $Metal\_source_s$ ). The alloy chemistry constraints ensure that the elemental composition of the new metal alloys falls between the lower bound (Equation 4.28) and upper bound (Equation 4.29) of that specified by ANSI/ISO standards. The  $comp\_lower_{k,s,p}$  and  $comp\_upper_{k,s,p}$  represent the lower and upper bound concentration of element  $k$  in metal source  $s$  processed by technology  $p$ . The economic furnace constraints (Equation 4.30) ensure that the scrap content in a recycling furnace is no less than the required weight fraction  $a$ , which eliminates the scenario where the optimization model simulates any alloy production that contains only a small fraction (e.g., 5%) of scrap in recycling furnaces. This is an unrealistic and economically infeasible scenario as it corresponds to buying and remelting mainly primary materials. Details about how the constraints are implemented are explained in Section 4.3.2.1.

The raw scrap inputs to the model are the aluminum ABS scraps disassembled from EOL aluminum bodied vehicles. The examined vehicles have a body-on-frame design of which the aluminum castings are located in the vehicle frame (Section 4.2). If shredding together, the cast aluminum could be mixed (as is currently the case) with the sheet and extrusion aluminum from the vehicle body. If unbolted, the cast aluminum frame could be separated from the sheet and extrusion aluminum body structure. Based on the vehicle material composition, we define four scrap mixing scenarios for the optimization analysis:

- All aluminum automotive body and chassis scrap (aluminum ABS, extrusion and casting scraps) mixed together,



- Aluminum automotive body and chassis scrap separated by wrought and cast family
- Aluminum automotive scraps separated by sheet (aluminum ABS), extrusion and cast
- Aluminum automotive scraps separated by alloy (aluminum low Cu, high Cu, low Mg, high Mg, extrusion and casting alloys)

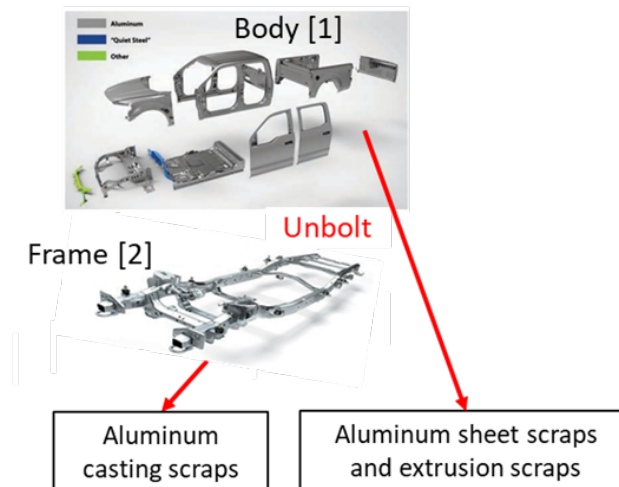


Figure 4.14: Illustration of the Ford vehicle structure (figure constructed from SAE, 2015 and Darby, 2015)

In addition to scrap mixing, scrap contamination can also contribute to the compositional mismatch problem (Section 4.1). Potential contaminations of the EOL scrap stream from the aluminum-bodied vehicles include the mixing of steel rivet and copper wiring. According to Chappuis (2015) and GREET (Argonne, 2020), the steel content in aluminum-bodied vehicle body and chassis is between 7-9%, and the copper content is around 4%. In reality, even though the shredded scraps usually have gone through magnetic separation, eddy current separation, or other separation processes, there is still the possibility of steel and copper scraps that have remained undetected during separation (Kelly et al., 2017). To analyze the contamination's impact on the recycling rate, we define four scrap contamination scenarios (each applies to the four scrap mixing scenarios defined above).

- Base case no contamination scenario
- 1% iron contamination due to remaining steel scraps from rivet
- 1% copper contamination due to remaining copper scraps from wiring
- 1% iron contamination and 1% copper contamination

The 16 scrap scenarios (4 mixing scenarios x 4 contamination scenarios) are combined with four recycling technology scenarios to evaluate the effectiveness of recycling technologies in separating and refining mixed and/or contaminated scraps and improving the recycling rate of EOL ABS scraps:

- If only dilution through the reverberatory furnace is available.
- If dilution and a separation technology are available.
- If dilution and a refining technology are available.
- If dilution, a separation and a refining technology are all available.

The first technology scenario setting is based on the current recycling practice that most recyclers only dilute the scraps with primary unalloyed aluminum and need alloying elements to meet the desired chemical composition requirements of alloy products. The second to fourth scenarios respectively examine the effectiveness of representing separation, refining, and coupled process with separation and refining technologies.

#### 4.3.2.1 Implementing the Optimization Model using MATLAB

In order to implement the optimization model, the MATLAB linprog function is used. MATLAB linprog function is a linear programming solver that finds the minimum of a problem specified by:

$$\min_x f^T x \quad (4.30)$$

$$A \cdot x \leq b \quad (4.31)$$

$$A_{eq} \cdot x = b_{eq} \quad (4.32)$$

$$lb \leq x \leq ub \quad (4.33)$$

Where  $f$ ,  $x$ ,  $b$ ,  $b_{eq}$ ,  $lb$ , and  $ub$  are the objective function, design variables, inequality constraint vector, equality constraint vector, variable lower bound and upper bound, respectively.  $A$  and  $A_{eq}$  are the inequality and equality constraint matrices. In order to model the five inequality constraints of the problem (Equation 4.25 - 4.29), the coefficients  $A$  and  $b$  are needed. Dimension of matrix  $A$  and  $b$  depends on the number of constraints and the size of the design variable. In this analysis, the design variable is represented by  $\theta$ , which is a K-by-1 array where value of K depends on the recycling technology scenarios and the number of alloy product types. The number of design variable elements needed for each recycling technology is defined as  $K_p$ , representing the liquid metal alloying and scrap flows to the recycling process and  $K = D * \sum_p K_p$ . For example, in the

primary production, only the major alloying elements and primary aluminum are needed (first row in Figure 4.15), thus  $K_1 = 6$ . For secondary production with only dilution, not only the alloying elements and primary Al ingot but also EOL scraps are needed (second row in Figure 4.15), thus  $K_2 = 6+18=24$ . Although there are only six types of pure alloy scrap streams as defined in the scrap mixing scenario, we set up the design variable that can potentially incorporate all possible scrap mixtures scenarios to prepare for future research.

	Primary/alloying element	Unprocessed scrap	Process 1 scrap	Process 2 scrap
Primary production	Cu Mg Mn Si Fe Al			
Dilution	Cu Mg Mn Si Fe Al	scrap		
Refining	Cu Mg Mn Si Fe Al	scrap	Scrap refined	
Separation	Cu Mg Mn Si Fe Al	scrap	Scrap separated	
Separation and refining	Cu Mg Mn Si Fe Al	scrap	Scrap separated	Scrap separated and refined

Figure 4.15: Illustration of design variable setup

The 18 types of pure scrap stream and mixed scrap streams included in the design variable are as follows:

- low Cu
- high Cu
- low Mg
- high Mg
- extrusion
- casting
- mixed Cu
- mixed Mg
- Cu+extrusion
- Mg+extrusion

- Cu+casting
- Mg+casting
- Cu+extrusion +casting
- Mg+extrusion +casting
- All ABS scrap mixed
- ABS +extrusion
- ABS+casting
- ABS +extrusion +casting

Each cell named "scrap", "scrap refined", "scrap separated", or "scrap separated and refined" in Figure 4.15 contains all 18 types of scrap streams. The difference between unprocessed scrap and refined scrap is their composition. For example, unprocessed ABS scrap has 0.15-0.35% Cu, 1.2-1.7% Mg, 0.02-0.29% Mn, 0.38-0.78% Si, 0-0.31% Fe, and 96-98% Al while Hoopes process purified ABS scraps contain 99.9% Al and less than 0.1% of alloying element contents. For separated scrap, we model the LIBS separation process which separate mixed scraps into individual alloys. The pure scrap stream in the separation process represents the separated scrap and the mixed scrap streams represent the input scrap to the process. The separated output scrap and the mixed input scrap stream are mass balanced based on the scrap mix ratio in the original scrap supply (Equation 4.12).

If refining technology is available when recycling, not only pure alloying elements, primary Al, and unprocessed EOL scraps but also refined EOL scrap are available, thus  $K_3 = 6+18+18=42$ . Similarly, for secondary production when separation technology is available,  $K_4 = 6+18+18=42$ . For secondary production when both separation and refining technologies are available,  $K_5 = 6+18+18+18=60$ . For the four recycling technology scenarios, the corresponding design variable K value is as follows:

- $K = D*(K1+K2) = 6*30=180$ . If only dilution through the reverberatory furnace is available.
- $K = D*(K1+K2+K3) = 432$ . If dilution and a separation technology are available.
- $K = D*(K1+K2+K4) = 432$ . If dilution and a refining technology are available.
- $K = D*(K1+K2+K3+K4+K5) = 1044$ . If dilution, a separation, and a refining technology are all available.

In technology scenarios 3 and 4 that include the separation process, the matrix A for the scrap supply constraint needs to be set so that the sum of scraps that are separated but not recycled and the scraps that are separated and recycled cannot exceed the amount of scraps input to the separation process. Also, the input scraps of separation process need to meet the original scrap supply constraint. This splits the scrap supply constraint into two parts. The first part (Equation 4.34) ensures that the scrap that is separated and recycled by all separation processes  $p$  is no more than the mixed scraps flowing into the system.

$$\sum_p \frac{x_{i=separated\ scrap,p}}{\alpha_{i,p}} \leq \sum_p x_{i=mixed\ scraps,p} * ratio_{alloy_i} \quad (4.34)$$

The second part of the scrap supply constraint ensures that the scrap (excluding the separated scraps to avoid double counting as they are constrained by the mixed scrap supply constraint and Equation 4.34 above) flowing into all recycling systems does not exceed the total scrap supply (the original scrap supply constraint Equation 4.26). The corresponding matrix A is the coefficient matrix derived through factorization of the constraint Equation 4.34 (summing of specific elements in design variable  $\theta$  is replaced by the dot product of a vector with value 1s at the specific indices and the design variable).

#### 4.3.2.2 Preliminary Analysis Results for U.S. Aluminum ABS Scrap Recycling

Table 4.7-4.10 shows the preliminary analysis for the U.S. aluminum ABS scrap recycling in 2050 using a minimum energy consumption optimization approach and the DMFA results in Section 4.2.4. A total of 64 scenarios are considered (4 contamination scenarios x 4 scrap mixing scenarios x 4 recycling technology scenarios). For each scenario, we calculate the recycling rate (RR: mass ratio of scrap recycled to the scrap supply for each scrap stream accounting recycling yield losses), recycled content (RC: mass ratio of scraps to primary and secondary alloy product), and cumulative energy demand (CED) needed to fulfill the 2050 automotive aluminum demand for the aluminum intensive vehicles (including primary and secondary production). A 50% furnace constraint is applied ( $a = 50\%$ ) to ensure economic operation of the recycling process. In the scrap mixing scenarios where scraps are assumed to be pre-separated (e.g., ABS scrap separated from casting scraps), and the energy consumption of pre-separation are not considered. This is to incorporate the potential disassembly operations like unbolting of chassis from vehicle body before shredding. The estimated CED in these scenarios is thus a lower bound estimation of reality.

Table 4.7: 2050 recycling rate (RR) and recycled content (RC) of six major aluminum alloys and scraps without contamination

Base case no contamination scenarios													
		Scrap mixing scenario 1: all automotive scraps mixed	Scrap mixing scenario 2: automotive scraps separated by wrought and cast		Scrap mixing scenario 3: automotive scraps separated by sheet (ABS), extrusion and cast			Scrap mixing scenario 4: all automotive scraps separated by alloys					
Recycling technology scenarios	Scenario outputs	Scrap stream 1: ABS +extrusion +casting	Scrap stream 1: ABS + extrusion	Scrap stream 2: Casting	Scrap stream 1: ABS	Scrap stream 2: Extrus.	Scrap stream 3: Casting	Scrap stream 1: Low Cu	Scrap stream 2: High Cu	Scrap stream 3: Low Mg	Scrap stream 4: High Mg	Scrap stream 5: Ex-trus.	Scrap stream 6: Casting
BAU recycling	RR	0%	26%	98%	39%	98%	98%	98%	98%	98%	98%	98%	98%
	Low Cu RC	0%	0%	0%	0%	0%	0%	74%	1%	0%	0%	0%	1%
	High Cu RC	0%	60%	0%	89%	0%	0%	0%	72%	0%	1%	0%	1%
	Low Mg RC	0%	0%	0%	0%	0%	0%	2%	0%	74%	12%	0%	0%
	High Mg RC	0%	0%	0%	0%	0%	0%	0%	0%	0%	51%	0%	0%
	Extrusion RC	0%	0%	0%	0%	75%	0%	0%	0%	0%	1%	75%	1%
	Casting RC	0%	7%	78%	11%	0%	78%	0%	0%	0%	0%	0%	77%
	CED (PJ)	9.60E+04	5.98E+04		4.26E+04			2.54E+04					
Deploy Hoopes scrap refining technology	RR	95%	95%	98%	95%	98%	98%	98%	98%	98%	98%	98%	98%
	Low Cu RC	100%	70%	0%	70%	0%	0%	58%	0%	0%	0%	0%	0%
	High Cu RC	54%	99%	0%	99%	0%	3%	23%	74%	0%	0%	0%	3%
	Low Mg RC	0%	50%	0%	50%	0%	1%	0%	0%	70%	8%	0%	1%
	High Mg RC	0%	49%	0%	49%	1%	1%	0%	0%	0%	62%	1%	1%
	Extrusion RC	98%	15%	55%	15%	62%	17%	8%	0%	6%	0%	62%	17%
	Casting RC	92%	9%	69%	9%	2%	73%	0%	0%	0%	0%	2%	73%
	CED (PJ)	3.94E+04	3.22E+04		2.88E+04			2.54E+04					
Deploy LIBS scrap separation technology	RR	95%	95%	98%	95%	98%	98%	98%	98%	98%	98%	98%	98%
	Low Cu RC	51%	60%	0%	60%	0%	0%	58%	0%	0%	0%	0%	0%
	High Cu RC	96%	98%	0%	98%	0%	3%	23%	74%	0%	0%	0%	3%
	Low Mg RC	0%	55%	0%	55%	0%	1%	0%	0%	70%	8%	0%	1%
	High Mg RC	73%	41%	0%	41%	1%	1%	0%	0%	0%	62%	1%	1%
	Extrusion RC	99%	21%	77%	21%	62%	17%	8%	0%	6%	0%	62%	17%
	Casting RC	82%	10%	66%	10%	2%	73%	0%	0%	0%	0%	2%	73%
	CED (PJ)	3.12E+04	2.90E+04		2.72E+04			2.54E+04					
Deploy LIBS and Hoopes scrap technologies	RR	96%	96%	98%	96%	98%	98%	98%	98%	98%	98%	98%	98%
	Low Cu RC	48%	60%	0%	60%	0%	0%	58%	0%	0%	0%	0%	0%
	High Cu RC	99%	98%	0%	98%	0%	3%	23%	74%	0%	0%	0%	3%
	Low Mg RC	7%	55%	0%	55%	0%	1%	0%	0%	70%	8%	0%	1%
	High Mg RC	98%	41%	0%	41%	1%	1%	0%	0%	0%	62%	1%	1%
	Extrusion RC	99%	21%	77%	21%	62%	17%	8%	0%	6%	0%	62%	17%
	Casting RC	81%	10%	66%	10%	2%	73%	0%	0%	0%	0%	2%	73%
	CED (PJ)	2.90E+04	2.81E+04		2.68E+04			2.54E+04					

Table 4.8: 2050 recycling rate (RR) and recycled content (RC) of six major aluminum alloys and scraps with 1% Fe contamination

Contamination scenario 1: 1% Fe													
		Scrap mixing scenario 1: all automotive scraps mixed	Scrap mixing scenario 2: automotive scraps separated by wrought and cast		Scrap mixing scenario 3: automotive scraps separated by sheet (ABS), extrusion and cast			Scrap mixing scenario 4: all automotive scraps separated by alloys					
Recycling technology scenarios	Scenario outputs	Scrap stream 1: ABS +extrusion +casting	Scrap stream 1: ABS + extrusion	Scrap stream 2: Casting	Scrap stream 1: ABS	Scrap stream 2: Extrus.	Scrap stream 3: Casting	Scrap stream 1: Low Cu	Scrap stream 2: High Cu	Scrap stream 3: Low Mg	Scrap stream 4: High Mg	Scrap stream 5: Ex-trus.	Scrap stream 6: Casting
BAU recycling	RR	0%	0%	0%	0%	0%	0%	0%	0%	0%	0%	0%	0%
	Low Cu RC	0%	0%	0%	0%	0%	0%	0%	0%	0%	0%	0%	0%
	High Cu RC	0%	0%	0%	0%	0%	0%	0%	0%	0%	0%	0%	0%
	Low Mg RC	0%	0%	0%	0%	0%	0%	0%	0%	0%	0%	0%	0%
	High Mg RC	0%	0%	0%	0%	0%	0%	0%	0%	0%	0%	0%	0%
	Extrusion RC	0%	0%	0%	0%	0%	0%	0%	0%	0%	0%	0%	0%
	Casting RC	0%	0%	0%	0%	0%	0%	0%	0%	0%	0%	0%	0%
	CED (PJ)	9.60E+04	9.60E+04		9.60E+04			9.60E+04					
Deploy Hoopes scrap refining technology	RR	95%	95%	98%	95%	98%	98%	98%	98%	98%	98%	98%	98%
	Low Cu RC	98%	98%	0%	98%	0%	0%	71%	27%	0%	0%	0%	0%
	High Cu RC	52%	52%	0%	52%	0%	0%	0%	30%	22%	0%	0%	0%
	Low Mg RC	0%	0%	0%	0%	0%	0%	0%	0%	0%	0%	0%	0%
	High Mg RC	0%	0%	0%	0%	0%	0%	0%	0%	0%	0%	0%	0%
	Extrusion RC	96%	96%	0%	96%	0%	0%	0%	0%	16%	80%	0%	0%
	Casting RC	90%	17%	74%	17%	11%	74%	0%	0%	6%	0%	11%	74%
	CED (PJ)	4.76E+04	4.76E+04		4.76E+04			4.80E+04					
Deploy LIBS scrap separation technology	RR	0%	0%	0%	0%	0%	0%	0%	0%	0%	0%	0%	0%
	Low Cu RC	0%	0%	0%	0%	0%	0%	0%	0%	0%	0%	0%	0%
	High Cu RC	0%	0%	0%	0%	0%	0%	0%	0%	0%	0%	0%	0%
	Low Mg RC	0%	0%	0%	0%	0%	0%	0%	0%	0%	0%	0%	0%
	High Mg RC	0%	0%	0%	0%	0%	0%	0%	0%	0%	0%	0%	0%
	Extrusion RC	0%	0%	0%	0%	0%	0%	0%	0%	0%	0%	0%	0%
	Casting RC	0%	0%	0%	0%	0%	0%	0%	0%	0%	0%	0%	0%
	CED (PJ)	9.60E+04	9.60E+04		9.60E+04			9.60E+04					
Deploy LIBS and Hoopes scrap technologies	RR	96%	96%	98%	96%	98%	98%	98%	98%	98%	98%	98%	98%
	Low Cu RC	98%	98%	0%	98%	0%	0%	71%	27%	0%	0%	0%	0%
	High Cu RC	52%	52%	0%	52%	17%	0%	0%	30%	5%	0%	17%	0%
	Low Mg RC	0%	0%	0%	0%	0%	0%	0%	0%	0%	0%	0%	0%
	High Mg RC	0%	0%	0%	0%	0%	0%	0%	0%	0%	0%	0%	0%
	Extrusion RC	96%	96%	0%	96%	16%	0%	0%	0%	0%	80%	16%	0%
	Casting RC	90%	17%	74%	17%	0%	74%	0%	0%	17%	0%	0%	74%
	CED (PJ)	4.76E+04	4.76E+04		4.76E+04			4.76E+04					

Table 4.9: 2050 recycling rate (RR) and recycled content (RC) of six major aluminum alloys and scraps with 1% Cu contamination

Contamination scenario 2: 1% Cu													
		Scrap mixing scenario 1: all automotive scraps mixed	Scrap mixing scenario 2: automotive scraps separated by wrought and cast		Scrap mixing scenario 3: automotive scraps separated by sheet (ABS), extrusion and cast			Scrap mixing scenario 4: all automotive scraps separated by alloys					
Recycling technology scenarios	Scenario outputs	Scrap stream 1: ABS +extrusion +casting	Scrap stream 1: ABS + extrusion	Scrap stream 2: Casting	Scrap stream 1: ABS	Scrap stream 2: Extrus.	Scrap stream 3: Casting	Scrap stream 1: Low Cu	Scrap stream 2: High Cu	Scrap stream 3: Low Mg	Scrap stream 4: High Mg	Scrap stream 5: Ex-trus.	Scrap stream 6: Casting
BAU recycling	RR	0%	0%	0%	0%	0%	0%	0%	0%	0%	0%	0%	0%
	Low Cu RC	0%	0%	0%	0%	0%	0%	0%	0%	0%	0%	0%	0%
	High Cu RC	0%	0%	0%	0%	0%	0%	0%	0%	0%	0%	0%	0%
	Low Mg RC	0%	0%	0%	0%	0%	0%	0%	0%	0%	0%	0%	0%
	High Mg RC	0%	0%	0%	0%	0%	0%	0%	0%	0%	0%	0%	0%
	Extrusion RC	0%	0%	0%	0%	0%	0%	0%	0%	0%	0%	0%	0%
	Casting RC	0%	0%	0%	0%	0%	0%	0%	0%	0%	0%	0%	0%
	CED (PJ)	9.60E+04	9.60E+04		9.60E+04			9.60E+04					
Deploy Hoopes scrap refining technology	RR	95%	95%	98%	95%	98%	98%	98%	98%	98%	98%	98%	98%
	Low Cu RC	98%	98%	0%	98%	0%	0%	71%	27%	0%	0%	0%	0%
	High Cu RC	52%	52%	0%	52%	0%	0%	0%	30%	0%	22%	0%	0%
	Low Mg RC	0%	0%	0%	0%	0%	0%	0%	0%	0%	0%	0%	0%
	High Mg RC	0%	0%	0%	0%	0%	0%	0%	0%	0%	0%	0%	0%
	Extrusion RC	96%	96%	0%	96%	0%	89%	0%	0%	0%	7%	0%	89%
	Casting RC	90%	17%	74%	17%	11%	60%	0%	0%	19%	0%	11%	60%
	CED (PJ)	4.76E+04	4.76E+04		4.76E+04			4.76E+04					
Deploy LIBS scrap separation technology	RR	0%	0%	0%	0%	0%	0%	0%	0%	0%	0%	0%	0%
	Low Cu RC	0%	0%	0%	0%	0%	0%	0%	0%	0%	0%	0%	0%
	High Cu RC	0%	0%	0%	0%	0%	0%	0%	0%	0%	0%	0%	0%
	Low Mg RC	0%	0%	0%	0%	0%	0%	0%	0%	0%	0%	0%	0%
	High Mg RC	0%	0%	0%	0%	0%	0%	0%	0%	0%	0%	0%	0%
	Extrusion RC	0%	0%	0%	0%	0%	0%	0%	0%	0%	0%	0%	0%
	Casting RC	0%	0%	0%	0%	0%	0%	0%	0%	0%	0%	0%	0%
	CED (PJ)	9.60E+04	9.60E+04		9.60E+04			9.60E+04					
Deploy LIBS and Hoopes scrap technologies	RR	96%	96%	98%	96%	98%	98%	98%	98%	98%	98%	98%	98%
	Low Cu RC	98%	98%	0%	98%	0%	0%	71%	27%	0%	0%	0%	0%
	High Cu RC	52%	52%	0%	52%	17%	0%	0%	30%	5%	0%	17%	0%
	Low Mg RC	0%	0%	0%	0%	0%	0%	0%	0%	0%	0%	0%	0%
	High Mg RC	0%	0%	0%	0%	0%	0%	0%	0%	0%	0%	0%	0%
	Extrusion RC	96%	96%	0%	96%	16%	0%	0%	0%	0%	80%	16%	0%
	Casting RC	90%	17%	74%	17%	0%	74%	0%	0%	17%	0%	0%	74%
	CED (PJ)	4.76E+04	4.76E+04		4.76E+04			4.76E+04					



Table 4.10: 2050 recycling rate (RR) and recycled content (RC) of six major aluminum alloys and scraps with 1% Fe and 1% Cu contamination

Contamination scenario 3: 1% Fe and 1% Cu													
		Scrap mixing scenario 1: All automotive scraps mixed	Scrap mixing scenario 2: Automotive scraps separated by wrought and cast		Scrap mixing scenario 3: Automotive scraps separated by sheet (ABS), extrusion and cast			Scrap mixing scenario 4: All automotive scraps separated by alloys					
Recycling technology scenarios	Scenario outputs	Scrap stream 1: ABS +extrusion +casting	Scrap stream 1: ABS + extrusion	Scrap stream 2: Casting	Scrap stream 1: ABS	Scrap stream 2: Extrus.	Scrap stream 3: Casting	Scrap stream 1: Low Cu	Scrap stream 2: High Cu	Scrap stream 3: Low Mg	Scrap stream 4: High Mg	Scrap stream 5: Ex-trus.	Scrap stream 6: Casting
BAU recycling	RR	0%	0%	0%	0%	0%	0%	0%	0%	0%	0%	0%	0%
	Low Cu RC	0%	0%	0%	0%	0%	0%	0%	0%	0%	0%	0%	0%
	High Cu RC	0%	0%	0%	0%	0%	0%	0%	0%	0%	0%	0%	0%
	Low Mg RC	0%	0%	0%	0%	0%	0%	0%	0%	0%	0%	0%	0%
	High Mg RC	0%	0%	0%	0%	0%	0%	0%	0%	0%	0%	0%	0%
	Extrusion RC	0%	0%	0%	0%	0%	0%	0%	0%	0%	0%	0%	0%
	Casting RC	0%	0%	0%	0%	0%	0%	0%	0%	0%	0%	0%	0%
	CED (PJ)	9.60E+04	9.60E+04		9.60E+04			9.60E+04					
Deploy Hoopes scrap refining technology	RR	95%	95%	98%	95%	98%	98%	98%	98%	98%	98%	98%	98%
	Low Cu RC	98%	98%	0%	98%	0%	0%	71%	27%	0%	0%	0%	0%
	High Cu RC	52%	52%	0%	52%	0%	0%	0%	30%	0%	22%	0%	0%
	Low Mg RC	0%	0%	0%	0%	0%	0%	0%	0%	0%	0%	0%	0%
	High Mg RC	0%	0%	0%	0%	0%	0%	0%	0%	0%	0%	0%	0%
	Extrusion RC	96%	96%	0%	96%	0%	89%	0%	0%	0%	7%	0%	89%
	Casting RC	90%	17%	74%	17%	11%	60%	0%	0%	19%	0%	11%	60%
	CED (PJ)	4.76E+04	4.76E+04		4.76E+04			4.80E+04					
Deploy LIBS scrap separation technology	RR	0%	0%	0%	0%	0%	0%	0%	0%	0%	0%	0%	0%
	Low Cu RC	0%	0%	0%	0%	0%	0%	0%	0%	0%	0%	0%	0%
	High Cu RC	0%	0%	0%	0%	0%	0%	0%	0%	0%	0%	0%	0%
	Low Mg RC	0%	0%	0%	0%	0%	0%	0%	0%	0%	0%	0%	0%
	High Mg RC	0%	0%	0%	0%	0%	0%	0%	0%	0%	0%	0%	0%
	Extrusion RC	0%	0%	0%	0%	0%	0%	0%	0%	0%	0%	0%	0%
	Casting RC	0%	0%	0%	0%	0%	0%	0%	0%	0%	0%	0%	0%
	CED (PJ)	9.60E+04	9.60E+04		9.60E+04			9.60E+04					
Deploy LIBS and Hoopes scrap technologies	RR	96%	96%	98%	96%	98%	98%	98%	98%	98%	98%	98%	98%
	Low Cu RC	98%	98%	0%	98%	0%	0%	71%	27%	0%	0%	0%	0%
	High Cu RC	52%	52%	0%	52%	17%	0%	0%	30%	5%	0%	17%	0%
	Low Mg RC	0%	0%	0%	0%	0%	0%	0%	0%	0%	0%	0%	0%
	High Mg RC	0%	0%	0%	0%	0%	0%	0%	0%	0%	0%	0%	0%
	Extrusion RC	96%	96%	0%	96%	16%	0%	0%	0%	0%	80%	16%	0%
	Casting RC	90%	17%	74%	17%	0%	74%	0%	0%	17%	0%	0%	74%
	CED (PJ)	4.76E+04	4.76E+04		4.76E+04			4.76E+04					

In the business-as-usual (BAU) base case technology scenario (only dilution is available), the recycling rate of *ABS +extrusion+cast scrap* drops to 0% when a 50% furnace constraint is applied (without furnace constraint the recycling rate would be 40% within the current EOL aluminum recycling rate range). This low BAU recycling rate is because of the high Mg (1.2-1.7 wt.%) and low Si (0.4-0.8 wt.%) content in the ABS and extrusion scrap, which is very different from the casting alloy (0.2-0.5 wt.% Mg and 6.5-7.5 wt.% Si) that usually serves as the recycling sink for high impurity scraps. When all scraps are mixed together, the mixed scrap cannot be easily diluted to meet the chemical composition scrap of any of the ABS, extrusion, or casting alloys. However, if the scrap is separated by wrought and cast (unbolting the vehicle body from the frame), recycling rates increase and all scraps could be absorbed by high Cu alloy and casting alloy production. If the scrap is contaminated with 1% Fe or 1% Cu, even if all sheet scraps are separated by alloy, only primary production could meet the new alloy demand (recycling rate of 0%).

In the recycling technology scenario when LIBS is available and there is no contamination in scraps, scraps are separated into individual alloys through the LIBS process and recycled. In the case of scrap contamination, no scrap can be recycled regardless of whether they are individual aluminum alloys or mixed scraps because the modeled LIBS process will not remove the contaminated scraps (e.g., steel rivets that are firmly connected to aluminum sheets). If the contamination can be split from attached aluminum parts or shredded into small enough chunks during the disassembly and shredding process, it is possible for the LIBS process to separate the contaminated scraps from the aluminum scrap streams. Removing contaminated scraps may cause higher losses during the LIBS process (depending on the purity of input scraps) but greatly increase the recycling rates (recycling rate will increase from 0% in the original contamination scenarios to 93-94% assuming only the contaminants are lost during the separation). However, more energy may be needed for disassembling, shredding, and repeated LIBS separation in order to remove the contaminants from the aluminum scrap streams.

In the recycling technology scenario when the Hoopes process is available, all scraps can be recycled because the Hoopes process turns all scraps into very high purity aluminum (Section 4.3.1). However, the energy required to recycle the same amount of scraps using the Hoopes process is much higher than the energy required using the LIBS process although the same recycling rate (100%) is achieved. This is because the Hoopes process is an electrolytic process that is much more energy-intensive than the LIBS process.

In the recycling technology scenario when both the LIBS and the Hoopes processes are available, the scraps can all be recycled with lower energy consumption when only one of the LIBS or the Hoopes process is available. This is because the LIBS or the Hoopes process is selected by the optimization model as needed to not only maximize recycling rate but also minimize alloying element losses. Alloying elements such as copper and magnesium are energy-intensive to produce.

Minimizing alloying element losses reduces alloying element demand and saves the production energy.

#### **4.3.2.3 Section Conclusion, Limitations and Future Work**

From the case study, we found that without emerging aluminum separation and refining technologies, the future (2050) EOL U.S. aluminum ABS recycling rate for the four aluminum intensive vehicles will be far less (0% recycling rate if vehicles are not disassembled by alloy groups and only dilution is available) from desired (90%). The current practice where U.S. aluminum sheet scrap is largely downcycled or exported instead of closed-loop recycled offers partial validation of this preliminary analysis. The two investigated scrap separation and refining technologies can resolve the compositional mismatch problem between scrap and alloy product in most cases with significant energy savings compared to primary production. If the study is extended to recycling of all U.S. vehicles in addition to the four vehicles, a new dynamic flow analysis is needed to study the alloy demand and scrap generation associated with these vehicles. Moving from just aluminum intensive vehicles to all vehicles will likely lead to more diversities in the chemical composition of new alloy demand and vehicle scraps. Serious chemical composition mismatch problems may be observed due to the diverse composition which will make recycling of EOL automotive aluminum even more challenging.

For future research, we will scale up the analysis to incorporate more emerging technologies in the optimization and evaluate their relative performance in improving EOL aluminum recycling rates. EOL scraps in addition to the automotive scraps from the four Ford vehicles will be considered in future analysis. The LIBS process will be scaled up to not only separate the EOL scraps by alloys but also decontaminate the tramp elements in the scraps.

## **Chapter 5**

### **Conclusion and Future Work**

This thesis has investigated opportunities for the U.S. transport and metals industries to reduce emissions, focusing on the decarbonization of U.S. light-duty vehicle (LDV) transport as well as the steel and aluminum industries. This chapter summarizes the contributions of this thesis (Section 5.1) and outlines potential further work (Section 5.2).

#### **5.1 Contributions of this Thesis**

The motivation for this thesis was to investigate how the emissions of the U.S. transport and industry sectors could be reduced to meet the Intergovernmental Panel on Climate Change (IPCC)'s emission target. Given the wide scope of this topic, three areas of focus are identified in Chapter 1 (LDVs, steel industry, and aluminum industry, which are the leading contributors to U.S. transport and industry sector emissions).

Chapter 2 presents a comprehensive hybrid dynamic material flow analysis (DMFA) and life cycle assessment (LCA) model that analyzes the system-level production, use, and disposal emissions associated with the U.S. LDV fleet. This hybrid model overcomes the limitation of typical single-vehicle level LCA studies by incorporating the fleet effect of increasing vehicle demand and the temporal effect of emissions. The analysis shows that decarbonizing U.S. transport will lead to a significant shift towards increased industry emissions. This increase in industry emissions is caused by (1) the increased need to make renewable energy technologies and, (2) an increase in material production and manufacturing as new vehicles are built to replace combustion engine vehicles that are being retired early. Therefore, electrification of the fleet alone is not enough, and other vehicle technology and demand strategies (e.g., early retirement of internal combustion engine vehicles and decarbonization of the electricity) should be pursued concurrently with vehicle electrification to help meet the IPCC's target.

Chapter 3 presents the data reconciliation method for material flow analysis (MFA) studies that streamline data collection and evaluation, network definition and updating, and presentation of the results using a multi-dimensional matrix cataloging system. This model can help MFA

practitioners to quickly produce their own MFA network. The model has already been used to help Yale researchers update the U.S. steel flow network (Reck and Althaf, 2021) and has also been used to produce the first alloy-shape-application MFA for the aluminum extrusion industry by Oberhausen et al. (2021). Within this thesis, the MFA results generated by the model for the U.S. steel sector show that there are opportunities to decrease new steel demand by reducing the quantity of new scraps generated by industry and increasing end-of-life (EOL) recycling. The largest new scrap reduction opportunity exists in fabrication scraps from manufacturing sheet metal into automobile parts. Currently, 46% of U.S. steel scraps are lost/landfill/hibernating which is a potential opportunity for improving EOL recycling. However, there are challenges for U.S. EOL steel recycling due to changing steel demand (e.g., reinforcement bar demand from U.S. construction sector is likely to shrink in the future) and scrap contamination (e.g., copper in steel). Reinforcement bar has served as the reservoir for highly impure copper contaminated steel scraps. Decreasing reinforcement bar demand and increasing copper contamination may cause technical barriers to increasing EOL steel recycling in the U.S.

Chapter 4 shows that the chemical compositional mismatch between the available scrap stream and the new alloys demanded by the industry will ultimately prohibit the U.S. EOL aluminum recycling rate from reaching 90%, which is needed for the aluminum industry to meet the 2 °C target. New opportunities and challenges from the rising automotive aluminum body sheet (ABS) market require manufacturers and recyclers to think ahead about how to recycle increasing ABS scraps. Emerging aluminum separation and refining technologies are reviewed and evaluated to show their potentials in solving the compositional mismatch problem and increase recycling. The developed linear programming model provides future decision makers a useful tool to quantitatively evaluate the impact of scrap collection, compositional mismatch, and emerging scrap separation and refining technologies to increasing the recycling rate using aluminum DMFA as input.

## **5.2 Future Work**

Several opportunities for further research have been identified from the work in this thesis. These are outlined in the sub-sections below.

### **5.2.1 Updating the GREET Life Cycle Analysis Data for Transport Research**

From the review on publications of vehicle LCA studies presented in Section 1.2.1 and Section 2.1, it is found that most U.S. centered vehicle LCA studies directly or indirectly use the life cycle inventory and impact data from the GREET model, which is developed and maintained by the Argonne National Lab. The GREET model provides detailed life cycle inventory data on the material, production, use, and disposal of vehicles and the environmental impacts associated with

the vehicles. However, in GREET’s vehicle material and production model, the effect of material efficiency is unclear. In the GREET model, a loss factor (Equation 5.1) is defined as the ratio between the material embodied in the product plus recycled scraps to the material input and is estimated for most production and fabrication processes (Dai et al., 2017). Despite recognizing scrap generation in common metal fabrication processes, the default loss factors are set to 1, meaning no losses for most processes and components. The GREET model authors argue that the scrap generated in these processes is well sorted and fully recycled within the same facility and therefore, there is no problem with using a loss factor of 1. However, even if the scraps can be fully recycled, we believe the no-loss assumption will only be true if the recycling is perfect, meaning no material or energy losses.

$$Loss\ factor = \frac{Material\ embeded\ in\ product + Recycled\ scraps}{Material\ input} \quad (5.1)$$

However, most fabrication scraps cannot be directly reused as input material in reality and there are unavoidable energy consumption and material losses during recycling. Fabrication and machining scraps are usually mixed alloy scraps sometimes covered in cutting fluid and coolant, preventing them from being easily recycled. Most fabrication scraps are sent to external recyclers, who clean and remelt the scraps to cast them into new billets for fabrication processes or directly into casting products. Without a clear understanding of the material efficiency, the estimated vehicle life cycle impact may not accurately reflect the real-world impact. Therefore, one direction of future transport research could be updating the process material efficiency data for the GREET model. In a preliminary analysis, we assign a 25% yield loss to all steel and aluminum fabrication processes in the GREET model (changing the loss factors to 1.3), which is reasonable (and conservative) given expected material utilization in processes such as stamping, extrusion, casting, and machining.

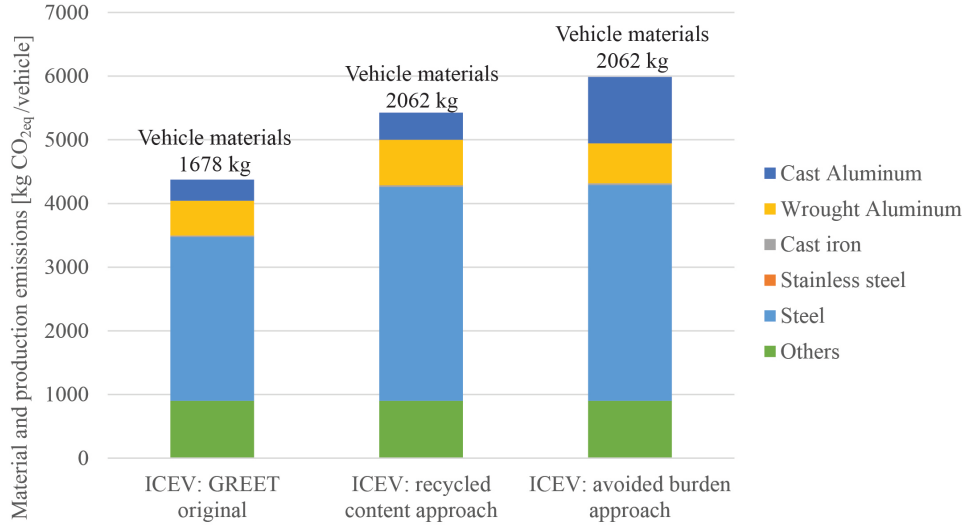


Figure 5.1: vehicle production GHG emissions before and after updating the steel and aluminum fabrication yield

Figure 5.1 shows the material consumption in a passenger car before and after the yield loss update using the avoided burden approach and the recycled content approach. The avoided burden approach (also called substitution approach) awards the benefit of recycled scraps to the product but give it no credit for recycled content at the start of life (Ashby, 2013). The recycled content approach allocate the full credit for recycled content to the product at the start of life while giving no credit for recycling the scraps (Ashby, 2013). Equation 5.2 and 5.3 describes how to calculate the environmental impact of a product with mass  $m$  using the two approaches.

$$(Impact_{total})_{avoided\ burden} = m(rI_{rc} + (1 - r)(I_m + I_d)) \quad (5.2)$$

$$(Impact_{total})_{recycled\ content} = m(RI_{rc} + (1 - R)I_m + (1 - r)I_d) \quad (5.3)$$

Where  $R$  is the recycled content of product material input and its value for the five key materials in vehicle production is acquired from the GREET model.  $r$  is the fraction of scraps that will be recycled and is assumed to be 25%.  $I_{rc}$ ,  $I_m$ , and  $I_d$  are the emission factors of recycling, primary production and disposing of the vehicle materials. Figure 5.2 shows the definitions of all the variables in the product system.

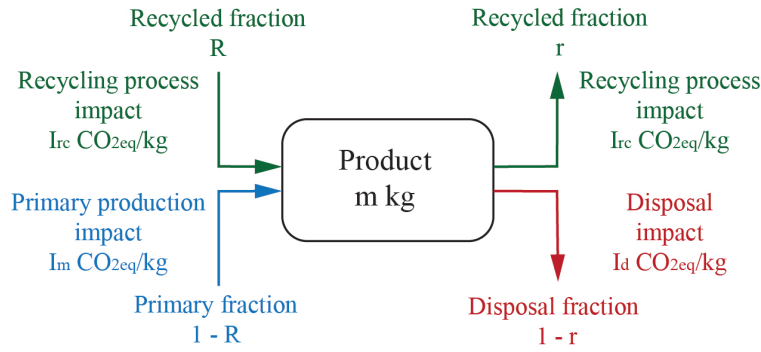


Figure 5.2: The material flows during product life, adapted from Ashby (2013) and Hammond and Jones (2011)

The results in Figure 5.1 show that without correctly accounting for the yield loss during the material production and fabrication process, an LCA can greatly underestimate the production phase emissions by around 24-37%. LCAs are often used by industry and researchers to inform the material selection and estimate the life cycle environmental burdens of vehicles. Inaccuracy in LCA studies could greatly hinder effective decision making for the automotive industry’s climate mitigation strategies. Thus, updating the material efficiency definitions in the GREET model would be a valuable direction for future research.

### 5.2.2 Data Reconciliation for MFA Analysis: Uncertainties and New Methods

Data scarcity and inconsistency are major hurdles to producing high-quality MFA maps, thus data reconciliation methods are needed. Reconciling the inconsistent and missing data using the nonlinear least-squares method introduced in Chapter 3 produces an internal consistent MFA network (i.e. reconciled MFA variable values) based on the structural and mass conservation constraints. Depending on the data availability, some of the MFA variable values may have multiple sources of data records, while others may lack data and are calculated based on the constraints. Understanding the level of conflict in the data records will guide future data collection and improvement processes. One potential way of demonstrating this level of data conflict in the reconciled MFA network is to compare the residual value calculated for each MFA variable in the nonlinear least-squares method. The residual for each MFA variable is defined as  $r_{i,j} = (x_i - \hat{x}_{i,j})/\hat{x}_{i,j}$  which is the normalized difference between MFA variable  $x_i$  and data record  $\hat{x}_{i,j}$ . Figure 5.3 is an illustration of the weighted residual values of optimized MFA variables in the 2014 steel Sankey diagram. Weighted residual close to 1 means more conflicting data records.

Reconciling the inconsistent and missing MFA data can be computation heavy. Even the data reconciliation method proposed in Chapter 3 of the thesis requires hours of computational time when few new data sources are added and cannot quantitatively compute the uncertainties. To



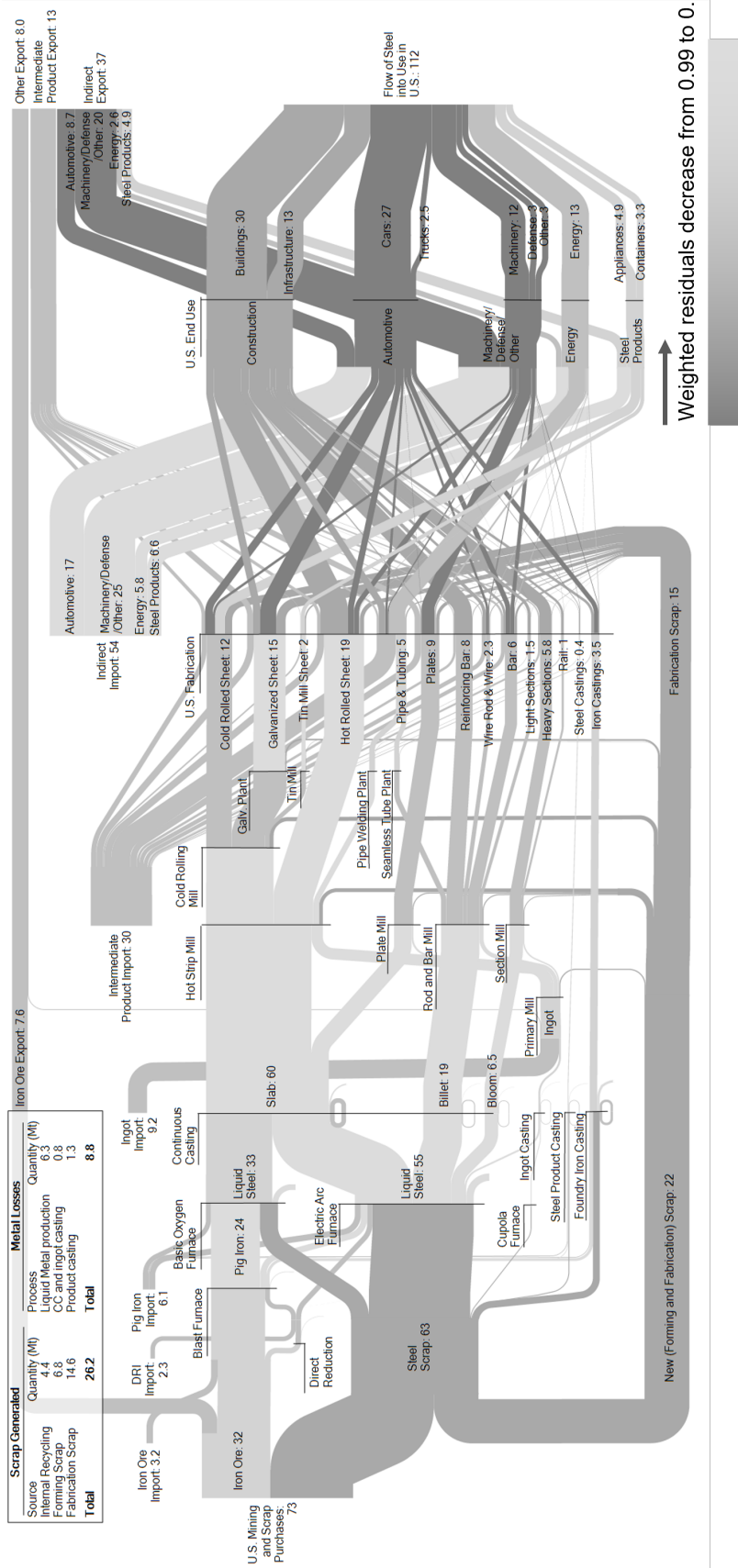


Figure 5.3: Level of conflict in the data records (darker grey means more conflicting data records and lightest grey means lacking data)

improve the updatability of a MFA network, a formal Bayesian inference approach could be a potential solution.

Bayesian inference is based on the Bayes' rule that predicts the posterior density  $p(\theta|D)$  (distribution of interested variables) based on prior density  $p(\theta)$ , likelihood function  $p(D|\theta)$  and evidence  $p(D)$ . The advantage of using Bayesian inference is to be able to quantify uncertainty and optimize the collection of new MFA data records (Atkinson et al., 2007; Chaloner and Verdinelli, 1995).

$$P(\theta|D) = \frac{P(D|\theta) P(\theta)}{P(D)} \quad (5.4)$$

Unlike nonlinear least-squares optimization, which intrinsically assumes that the data follows normal distribution, the Bayesian inference allows the use of any probability distribution to represent data record uncertainties. Bayesian inference can also be used to quantify not only data uncertainty but also structural uncertainty in the MFA models: Bayesian model selection and model averaging could be used to select among candidate model structures and calculate MFA parameter (flow) values based on the uncertainty calculation. Model structure uncertainty in MFA refers to the uncertainty pertaining to the existence of flows between nodes in the network structure. For example, in the steel flow network shown in Chapter 3, we deemed it unlikely that a flow exists linking the basic oxygen furnace (BOF) to the rod and bar mill. The MFA results, however, would look very different if this assumption were false: if steel from the BOF (emissions-intensive primary production) is actually used in the rod and bar mill, then increased material efficiency in the mill (or downstream) will lead to greater emissions savings than if only supplied with recycled steel.

A challenge in the use of Bayesian inference is the construction of priors and probability distributions for the evidence when data records are rarely presented with any uncertainty information. For lack of better information, Gaussian uncertainty ranges (e.g.,  $\pm 10\%$ ) have been assumed in previous work (e.g., by Lupton and Allwood, 2017); however, priors could be defined using expert elicitation (Laner, et al., 2014) or historical MFAs. The data noise could be modeled as a random variable, which is also learned through the Bayesian inference process.

### 5.2.3 Design for Recycling of Aluminum Autobody Sheet

Due to the vehicle lightweighting trend, the embodied energy and emissions of vehicles increases as energy-intensive materials such as aluminum auto body sheet (ABS) are used to replace mild steel. This presents an opportunity for recyclers to shift towards high-value recycling into wrought alloys and for carmakers to increase the EOL recycled content of their sheet (on average, currently  $\approx 0\%$  and  $\approx 14\%$  for U.S. aluminum and steel ABSs respectively derived from the GREET model (Argonne, 2020) and DMFA in Chapter 3 and 4), reducing their material costs and energy burden. However,

currently, the aluminum and steel sheets are not effectively recycled in the U.S. – often shredded together as a whole vehicle and only separated by ferrous and non-ferrous scraps. Shredded and contaminated EOL metal (e.g., mixed aluminum alloys with steel rivets and mixed steel alloys with embedded copper wiring) is often exported, downcycled to castings, or recycled as reinforcement bar.

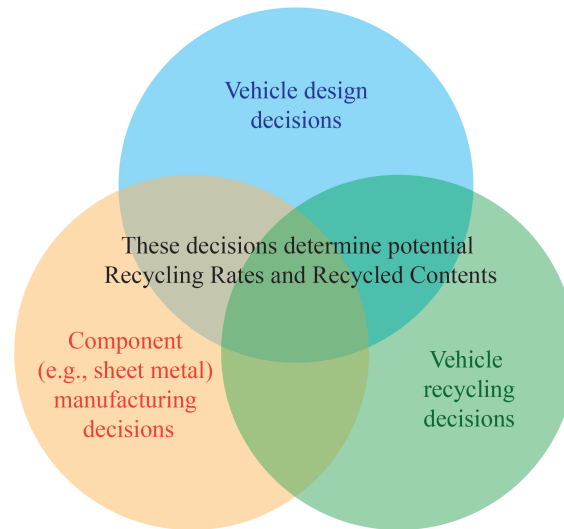


Figure 5.4: Coordinating between vehicle design, vehicle manufacturing, and vehicle recycling is needed to increase recycling

Previous design for recycling research has often consisted of guidelines/check-lists (Bras, 1997) that, while useful for relative design assessment, prevents a quantitative understanding of vehicle design changes, trade-offs, and optimal system design. The optimization framework introduced in chapter 4 could be extended to accommodate the coupled effects (see Figure 5.4) of **sheet metal manufacturing processing decisions** (which will determine the sheet metal composition constraints and final sheet properties), the **vehicle design decisions** (which will determine the upstream sheet metal property specification as well as the downstream ability to separate the sheet metal from sources of contamination such as rivets and other alloys), and the **recycling processing decisions** (which will determine the ability to separate the different materials at vehicle EOL for a given vehicle design). This cross life cycle optimization approach could reveal new low-cost, optimal methods for increasing automotive sheet metal recycling rates and recycled contents.

## Appendix A

### Reducing greenhouse gas emissions from U.S. light-duty transport in line with the 2 degrees Celsius target

This document contains information useful to understanding the themes, calculations, and numbers introduced in the main manuscript. This document is 50 pages long and contains 15 tables and 25 figures.

To determine the contribution of U.S. LDVs (produced and imported for domestic consumption, not including exported vehicles) to the global emissions, we estimate the 2015 U.S. LDVs production, use, and disposal emissions compared to the global emissions. According to the Emissions Database for Global Atmospheric Research<sup>1</sup>, the global anthropogenic GHG emissions excluding land-use, land-use change, and forestry (LULUCF) reaches around 49 Gt CO<sub>2</sub> eq. in 2015. Among all the emission sectors, transport accounts for 27% of the emissions.

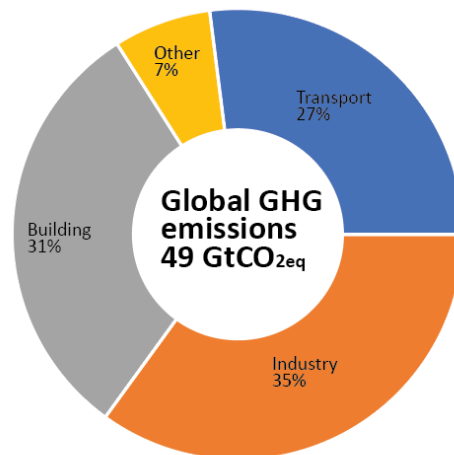


Figure A.1: Global GHG emissions by economic sectors in 2015

According to U.S. Environmental Protection Agency (EPA)<sup>2</sup>'s report, the U.S. emitted 6676 million metric tons (Mt) CO<sub>2</sub> eq. of GHGs in 2015 excluding LULUCF emissions. Figure A.1 below shows the 2015 U.S. GHG emissions by economic sectors. Among all the economic sectors,

the transportation sector accounts for around 28% of the U.S. GHG emissions. According to the EPA (2020)<sup>2</sup>, the largest sources of transportation greenhouse gas emissions in 2018 were passenger cars (41.2 percent); light-duty trucks, which include sport utility vehicles, pickup trucks, and minivans (17.4 percent); freight trucks (23.2 percent); commercial aircraft (6.9 percent); pipelines (2.6 percent); other aircraft (2.4 percent); rail (2.3 percent); and ships and boats (2.2 percent). These figures include direct CO<sub>2</sub>, CH<sub>4</sub>, and N<sub>2</sub>O emissions from vehicle use phase: fossil fuel combustion used in transportation, indirect emissions from electricity use and emissions from non-energy use (i.e., lubricants) used in transportation, as well as HFC emissions from mobile air conditioners and refrigerated transport allocated to these vehicle types. Around 97% of the transport CO<sub>2</sub> emissions are from fuel combustion<sup>2</sup>. EPA (2020)<sup>2</sup> accounted for the GHG emissions in the transportation sector due to combustion and electricity and show that around 99.7% of transport sector emissions are from fossil fuel combustion and only 0.3% are from electricity generation from various sources.

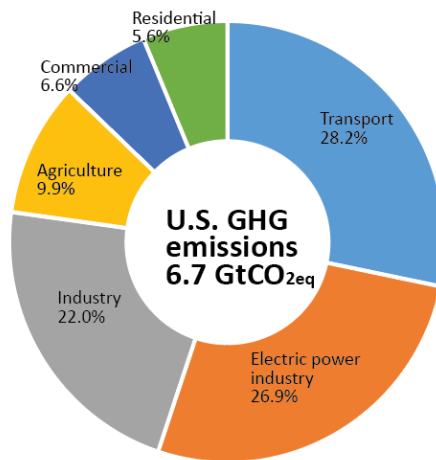


Figure A.2: U.S. GHG emissions by economic sectors in 2015

Since the EPA’s transportation sector emissions only include emissions from vehicle use phase fuel combustion and electricity generation (1083.9 Mt CO<sub>2</sub> eq.), we estimated the fuel production from fuel uses, and vehicle production and disposal emissions from vehicle production and disposal data. According to GREET (2020)<sup>3</sup>, for every kg CO<sub>2</sub> eq. emitted from burning gasoline, an additional 16% are emitted from fuel production. Therefore, 182 Mt CO<sub>2</sub> eq. are emitted in 2015 due to fuel production for U.S. LDV use of which more than 94% are domestic produced in the U.S.<sup>4</sup>. According to EPA (2018), 9,676,333 passenger cars (73% are imported<sup>5</sup>) and 7,101,536 light trucks (43% are imported<sup>5</sup>) are produced for U.S. consumption in 2015. Production of one passenger car and light truck accounts for 6 t of CO<sub>2</sub> eq. emissions and 8 t of CO<sub>2</sub> eq. respectively<sup>3</sup>. Therefore, the total vehicle production emissions are around 125.5 Mt CO<sub>2</sub> eq. According to Bureau

of Transportation Statistics<sup>6</sup>, 11,047,000 motor vehicles are scrapped in 2014 of which 54% are LDVs (and we assume that the 2015 scrappage are similar). For each vehicle scrapped, 0.2 t of CO<sub>2</sub> eq. are emitted during disassembly. Therefore, 2.2 Mt CO<sub>2</sub> eq. are emitted from U.S. LDVs disposal in 2015. In total, 1394 Mt CO<sub>2</sub> eq. are emitted in 2015 attributable to the U.S. LDVs. Compared to global GHG, the U.S. LDV sector accounts for 1.39 Gt/49 Gt = 2.84% of the global GHG emissions in 2015.

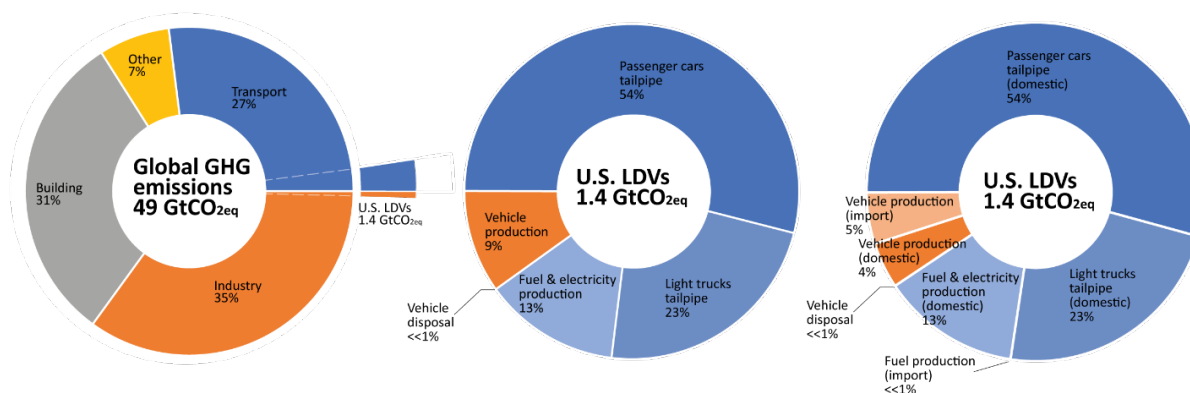


Figure A.3: Global GHG emissions (left), U.S. transport GHG emissions (middle) and U.S. transport GHG emissions splitting domestic and import(right) in 2015

## A.1 Calculating cumulative emissions budget and global mean temperature rises.

In order to determine the cumulative emissions reduction budget in line with IPCC's 2°C target and U.S. LDV sector's contribution to the global mean temperature rises, we apply the concept of global warming potentials (GWP) factors and global temperature change Potential (GTP). Section S1.1 summarizes the rationales of GWP and GTP and the parameter values used in this analysis. Section S1.2 summarizes how we define the emissions reduction budget based on IPCC recommendation. Section 1.3 estimate the remaining temperature rise budget corresponding to IPCC.

### A.1.1 Summary of radiative forcing, GWP, and GTP concept

Imbalance of the incoming energy to earth from sunlight and outgoing energy loss from the earth causes the climate change. This energy imbalance and its impact to the Earth's climate is measured by forcings from both externally and by human activities such as solar irradiance, landscape change and emissions of anthropogenic greenhouse gasses and aerosols, etc<sup>7</sup>. The impact of the forcing agents is amplified by the climate system and the process is called climate feedback.

In order to understand the long-term changes in climate, the global mean surface temperature is used as the primary index. The contribution to global mean surface temperature changes of

different agents are quantified using the “radiative forcing” concept. Traditional definition of the radiative forcing is *as the instantaneous change in energy flux at the tropopause resulting from a change in a component external to the climate system*<sup>7</sup>. However, in current climate change studies, the “adjusted radiative forcing” is used. It focuses on the energy imbalance in the Earth and troposphere system and is most relevant to surface temperature change<sup>7</sup>. The radiative forcing concept conceptualizes the Earth’s climate as a closed system with a detectable metric of change: global mean surface temperature<sup>7</sup>. Equation S1 – 3 shows the examples of calculating the forcing  $RF(t)$  for carbon dioxide [CO<sub>2</sub>], nitrous oxide [CH<sub>4</sub>] and methane [N<sub>2</sub>O] respectively as a function of time, t, and in units of W m<sup>-2</sup>.

$$RF_{CO_2}(t) = C_{CO_2} \ln \ln \left[ \frac{CO_2(t)}{CO_2(t_0)} \right] \quad (\text{A.1})$$

$$RF_{CH_4}(t) = C_{CH_4} \left( \sqrt{M} - \sqrt{M_0} \right) - (f(M, N_0) - f(M_0, N_0)) \quad (\text{A.2})$$

$$RF_{N_2O}(t) = C_{N_2O} \left( \sqrt{N} - \sqrt{N_0} \right) - (f(M_0, N) - f(M_0, N_0)) \quad (\text{A.3})$$

Where  $C_X$  is a constant (in units of W m<sup>-2</sup>) derived for the simple climate model,  $CO_2(t)$  (in units of ppm) is the atmospheric concentration of  $CO_2$  for year  $t$  and  $CO_2(t_0)$  is the atmospheric concentration of  $CO_2$  for year  $t_0$ . For methane and nitrous oxide,  $M$  is CH<sub>4</sub> in ppb,  $N$  is N<sub>2</sub>O in ppb and the subscript 0 denotes the unperturbed molar fraction for the species being evaluated. However, note that for the CH<sub>4</sub> forcing  $N_0$  should refer to present-day N<sub>2</sub>O, and for the N<sub>2</sub>O forcing  $M_0$  should refer to present-day CH<sub>4</sub><sup>8</sup>. Among all the radiative forcings, well-mixed greenhouse gases (GHG: CO<sub>2</sub>, N<sub>2</sub>O, CH<sub>4</sub> and chlorofluorocarbons [CFCs]) lead to the largest positive forcing since 1750 according to IPCC<sup>7</sup>.

In order to quantitatively compare the radiative consequences of emissions of different gases, the GWP concept is developed based on the radiative forcing model. GWP is defined as the time-integrated RF due to a pulse emission of a given component, relative to a pulse emission of an equal mass of CO<sub>2</sub>. The equation for calculating GWP of a gas species  $X$  is expressed as equation 4<sup>8</sup>.

$$GWP(X) = \frac{\int_0^{timehorizon} RF_X(t) dt}{\int_0^{timehorizon} RF_{CO_2}(t) dt}$$

Where  $RF(t)$  is the time decay profile for the gas following its release into the atmosphere. Scaling the radiative impact of other forcings by that of CO<sub>2</sub> makes it easier to compare forcings quantitatively to each other, but this approach has been criticized because it depends on how well the radiative impact of CO<sub>2</sub> is understood and the time horizon over which the GWP is calculated (note about 100 year). A direct interpretation is that the GWP is an index of the total energy added to the climate system by a component in question relative to that added by CO<sub>2</sub>. However, the GWP does not lead to equivalence with temperature or other climate variables<sup>9</sup>. Thus, the name ‘Global

Warming Potential' may be somewhat misleading.

Another metric, the GTP, is developed by Shine et al. (2005) to quantify the impact of an emission pulse relative to that of CO<sub>2</sub> to the global mean surface temperature<sup>10</sup>. To calculate the global mean temperature change, the absolute GTP (AGTP) concept is adopted by Joos et al. (2013)<sup>11</sup>. Figure A.4 shows the temperature response due to 1-kg pulse emissions of GHG with a range of lifetimes.

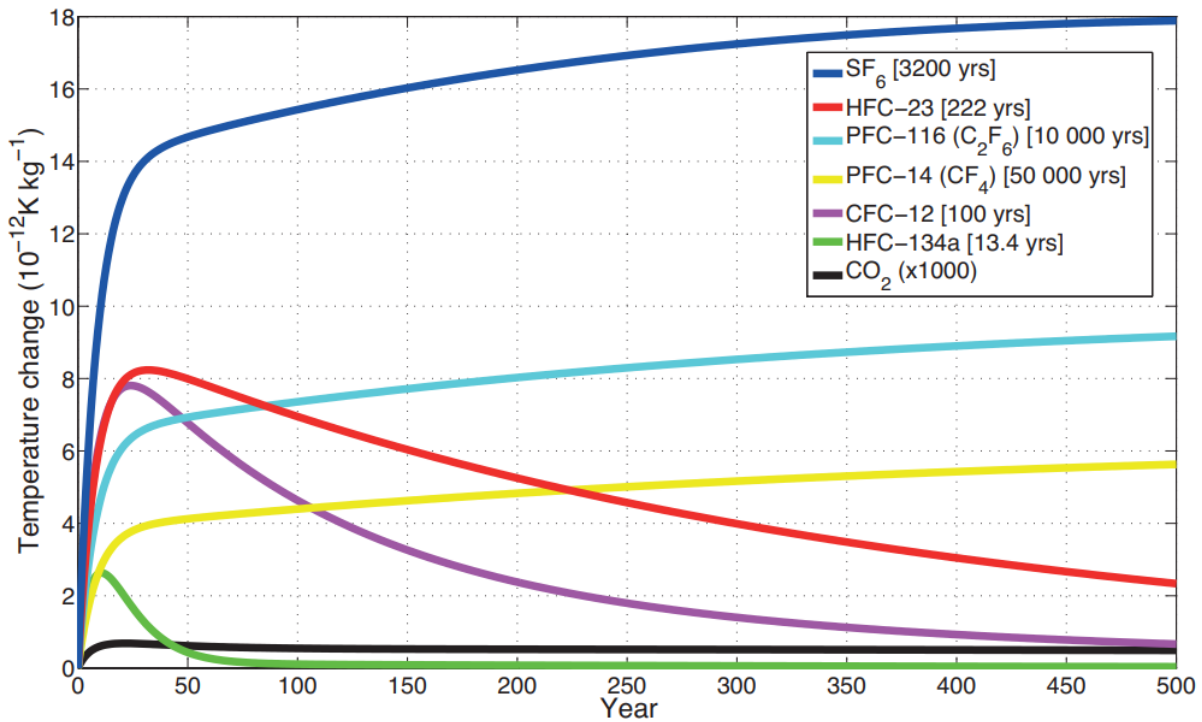


Figure A.4: Figure A.4 Temperature response due to 1-kg pulse emissions of greenhouse gases with a range of lifetimes (given in parentheses). Calculated with a temperature impulse response function taken from Boucher and Reddy (2008) which has a climate sensitivity of 1.06 K

Equation 5 shows the calculation of the global mean temperature change due to any given emission scenario using a convolution of the emission scenarios and  $AGTP_i$ <sup>12</sup>.

$$\Delta T(t) = \sum_i \int_0^t E_i(s) AGTP_i(t-s) ds$$

Comparing to GWP, GTP is an end-point metric that is based on temperature change for a selected year, t, and is sensitive to the time when emission happens. The concept of GTP is used in this study to more accurately reflect the impact of direct emissions during all life stages of a product.

Although there are a number of GHGs that are emitted from human activities, in general, CO<sub>2</sub>, CH<sub>4</sub>, and N<sub>2</sub>O are regarded as the major GHGs<sup>8,13-14</sup> which are the focus of this analysis. To



calculate the annual and cumulative GHG emissions from the three GHGs, we use the GWP100 factor conversion. The global mean temperature rises are estimated from annual emissions of each gasses and the AGTP profiles using Equation S5. Table A.1 shows the corresponding GWP100 factor and temperature responses of the three gasses used in this analysis<sup>8,15</sup>.

Table A.1: GWP and AGTP of CO<sub>2</sub>, CH<sub>4</sub>, and N<sub>2</sub>O

Common name	GWP 100 according to IPCC (2014) <sup>8</sup>	AGTP (Absolute Global Temperature change Potential)
Carbon dioxide (CO <sub>2</sub> )	1	
Methane (CH <sub>4</sub> )	28	
Nitrous oxide (N <sub>2</sub> O)	265	

### A.1.2 U.S. LDVs emissions budget in line with the 2oC target

The 2014 IPCC AR5 Synthesis show the changes in GHG needed by 2050 (and 2100) relative to 2010 emissions to limit global warming at different levels (IPCC, 2014: Table A.PM.1<sup>8</sup>). To limit global warming likely below 2°C above pre-industrial temperatures, the GHG concentration needed to be within 430-480 ppm CO<sub>2</sub>eq. in 2100 (the RCP2.6 scenario) which corresponds to annual GHG emissions reduction by 41-72% by 2050 from 2010 level. Without carbon capture and storage, IPCC recommends a 60-70% reduction of transport emissions by 2050 from 2010 level (IPCC, 2014: Figure A.PM.7<sup>8</sup>). Later in the 2018 IPCC report (Global Warming of 1.5 °C<sup>16</sup>), it states that *for limiting global warming to below 2°C CO<sub>2</sub> emissions are projected to decline by about 25% by 2030 in most pathways (10–30% interquartile range) and reach net zero around 2070 (2065–2080 interquartile range). Non-CO<sub>2</sub> emissions in pathways that limit global warming to 1.5°C show deep*

reductions that are similar to those in pathways limiting warming to 2°C. Figure A.PM.1<sup>16</sup> also indicates that annual emissions need to decrease linearly to achieve the emission reduction target.

In this analysis, we define the emissions reduction budget based on the IPCC recommendation to achieve a 70% of U.S. LDVs emissions by 2050 from the 2010 level. To estimate the quantitative emissions budget, the 2010 emissions information is needed. Using the same calculation process as in Section S1, the 2010 GHG emissions attributable to the U.S. LDV sector is estimated as 1.41 Gt CO<sub>2</sub> eq. including vehicle production, use and disposal. The 2010-2050 cumulative emissions budget is therefore calculated as the sum of the linearly extrapolated emissions from 2010 to 70% reduced by 2050 (0.42 Gt CO<sub>2</sub> eq.). The emissions that have already taken place between 2010 and 2020 (14.4 Gt CO<sub>2</sub> eq.) are deducted from the sum. The final 2021-2050 cumulative emission budget for the U.S. LDV sector to achieve a 70% reduction by 2050 is around 23.1 Gt CO<sub>2</sub> eq. Figure A.5 shows the 2010-2050 cumulative emissions budget (grey area) and annual emissions budgets.

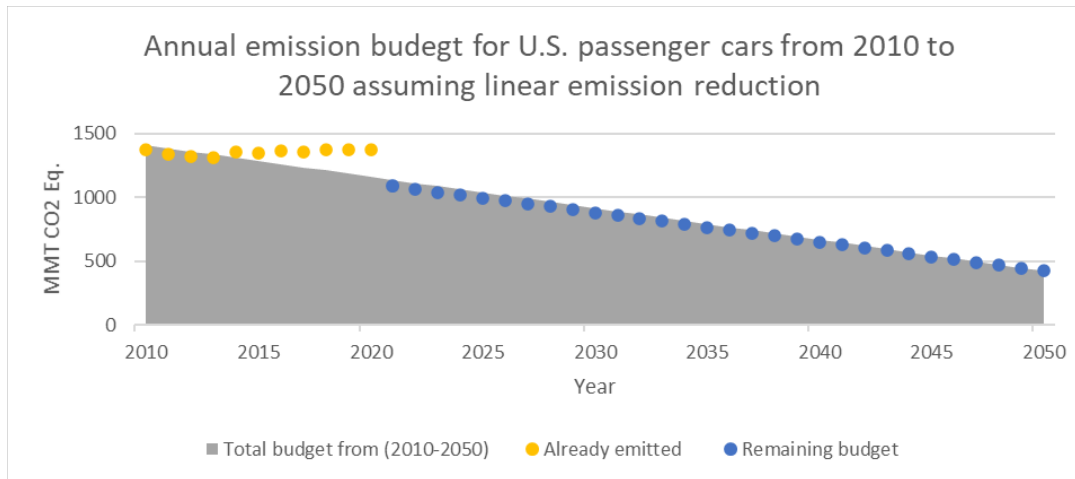


Figure A.5: Emission budget to achieve 70% reduction by 2050 from 2010 level in line with the 2°C target

### A.1.3 Remaining temperature budget

The IPCC (2014)<sup>8</sup> recommends that global mean surface temperature rises remain below 2°C by the end of the century to avoid the worst consequences. From the most recent IPCC report (2018)<sup>16</sup>, at least 1.13 °C of global warming will be reached by 2020. The remaining 2021-2050 global temperature budget is therefore 0.87 °C. The 2021-2050 U.S. temperature budget is 1.66E-3 °C calculated from the annual emissions assumed in the cumulative emission budget (S2.1) using Equation S5.

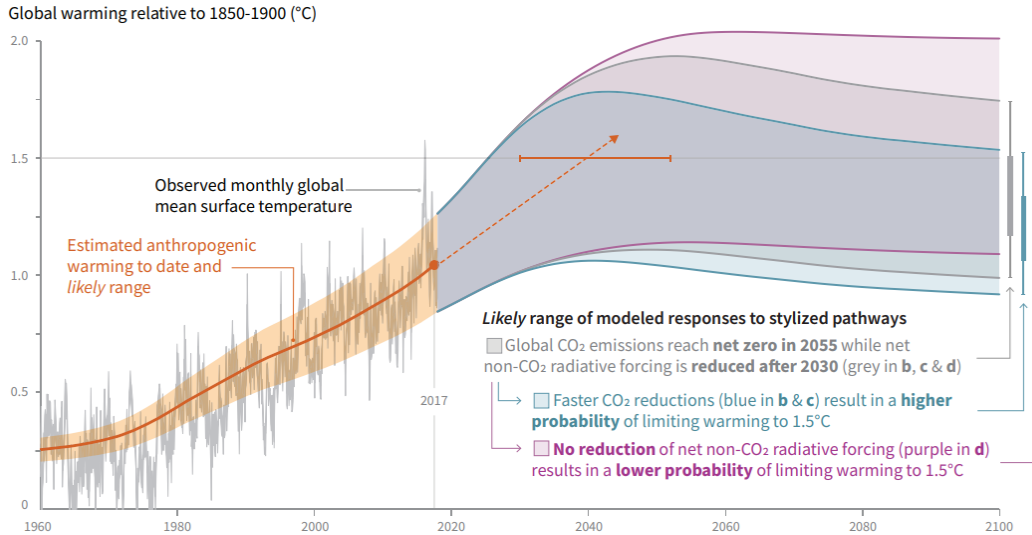


Figure A.6: Global mean surface temperature rises according to IPCC (2018)

## A.2 U.S. light-duty vehicle dynamic material flow analysis (DMFA)

Dynamic material flow analysis (DMFA) is a method to quantify the stocks and flows of materials in a defined temporal and economic or geographic boundaries. In this work, we use DMFA to estimate the vehicle production, stock and EOL flows, which are later combined with vehicle life cycle inventory and life cycle impact analysis to estimate the vehicle material flows and GHG emissions.

### A.2.1 Estimating historical vehicle fleet size and age distributions

A flow driven DMFA is firstly conducted to estimate historical LDVs fleet size and age distributions up to year 2018 based on EPA (2020) automotive trends report<sup>17</sup>. Table A.2 shows the historical LDVs production (including domestically produced vehicles, and all vehicles produced outside the U.S. and imported for U.S. consumption) and the ratio of production by vehicle size class according to EPA (2020)<sup>17</sup>. Ratio of production by vehicle size class is assumed constant as 2018 data for year 2019-2050. The car SUV and truck SUV are grouped into the SUV category. Minivan/Van and pickup are grouped into the light truck category.

Table A.2: Historical U.S. LDV production (EPA, 2020)

	U.S. LDV production (in 1,000 units)	Car (Sedan/ Wagon)	SUV1 (Car SUV)	SUV2 (Truck SUV)	Light truck 1 (Minivan/ Van)	Light truck 2 (Pickup)
1975	10224	80.6%	0.1%	1.7%	4.5%	13.1%
1976	12334	78.8%	0.1%	1.9%	4.1%	15.1%
1977	14123	80.0%	0.1%	1.9%	3.6%	14.3%
1978	14448	77.3%	0.1%	2.5%	4.3%	15.7%
1979	13882	77.8%	0.1%	2.8%	3.5%	15.9%
1980	11306	83.5%	0.0%	1.6%	2.1%	12.7%
1981	10554	82.7%	0.0%	1.3%	2.3%	13.6%
1982	9732	80.3%	0.1%	1.5%	3.2%	14.8%
1983	10302	77.7%	0.3%	2.5%	3.7%	15.8%
1984	14020	76.1%	0.4%	4.1%	4.8%	14.6%
1985	14460	74.6%	0.6%	4.5%	5.9%	14.4%
1986	15365	71.7%	0.4%	4.6%	6.8%	16.5%
1987	14865	72.2%	0.6%	5.2%	7.5%	14.4%
1988	15295	70.2%	0.7%	5.6%	7.4%	16.1%
1989	14453	69.3%	0.7%	5.7%	8.8%	15.4%
1990	12615	69.8%	0.5%	5.1%	10.0%	14.5%
1991	12573	67.8%	1.8%	6.9%	8.2%	15.3%
1992	12172	66.6%	2.0%	6.2%	10.0%	15.1%
1993	13211	64.0%	3.6%	6.3%	10.9%	15.2%
1994	14125	59.6%	2.3%	9.1%	10.0%	18.9%
1995	15145	62.0%	1.5%	10.5%	11.0%	15.0%
1996	13144	60.0%	2.2%	12.2%	10.7%	14.9%
1997	14458	57.6%	2.5%	14.5%	8.8%	16.7%
1998	14456	55.1%	3.1%	14.7%	10.3%	16.7%
1999	15215	55.1%	3.2%	15.4%	9.6%	16.7%
2000	16571	55.1%	3.7%	15.2%	10.2%	15.8%
2001	15605	53.9%	4.8%	17.3%	7.9%	16.1%
2002	16115	51.5%	3.7%	22.3%	7.7%	14.8%
2003	15773	50.2%	3.6%	22.6%	7.8%	15.7%

2004	15709	48.0%	4.1%	25.9%	6.1%	15.9%
2005	15892	50.5%	5.1%	20.6%	9.3%	14.5%
2006	15104	52.9%	5.0%	19.9%	7.7%	14.5%
2007	15276	52.9%	6.0%	21.7%	5.5%	13.8%
2008	13898	52.7%	6.6%	22.1%	5.7%	12.9%
2009	9316	60.5%	6.5%	18.4%	4.0%	10.6%
2010	11116	54.5%	8.2%	20.7%	5.0%	11.5%
2011	12018	47.8%	10.0%	25.5%	4.3%	12.3%
2012	13449	55.0%	9.4%	20.6%	4.9%	10.1%
2013	15198	54.1%	10.0%	21.8%	3.8%	10.4%
2014	15512	49.2%	10.1%	23.9%	4.3%	12.4%
2015	16739	47.2%	10.2%	28.1%	3.9%	10.7%
2016	16278	43.8%	11.5%	29.1%	3.9%	11.7%
2017	17016	41.0%	11.5%	31.8%	3.6%	12.1%
2018	16259	36.7%	11.3%	35.1%	3.1%	13.9%
2019-2050		36.7%	11.3%	35.1%	3.1%	13.9%

Figure A.7 shows the historical vehicle production by powertrains (assuming the same for cars, SUVs and light trucks) according to EPA (2020)<sup>17</sup>. In this analysis, 10 vehicle powertrains are considered including gasoline ICEVs (which can be retrofitted to use bioethanol gasoline<sup>18</sup>), 100-mile BEVs, 200-mile BEVs, 300-mile BEVs, 10-mile all-electric range gasoline plug-in hybrid electric vehicles (PHEVs), 40-mile all-electric gasoline PHEVs, hybrid electric vehicles (HEVs), FCVs, compressed natural gas vehicles (CNGVs) and diesel ICEVs. Until 2018, more than 97% of U.S. LDVs sold are gasoline ICEVs. HEVs, BEVs, PHEVs and fuel flex vehicles that run on ethanol-gasoline blend (combined into gasoline ICEVs due to similar production emissions) are among the most popular vehicle powertrains in the remaining 3% of the sales recently.

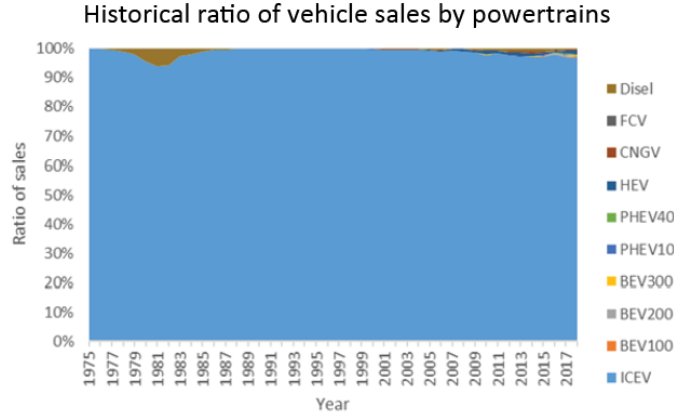


Figure A.7: Historical vehicle ratio of sales by powertrains

Equations S6 shows how the fleet size and age composition,  $Fleetsize_{t,a}$ , is estimated, where  $t$  is the year between 1975 and 2018 and  $a$  is the age of vehicle in the fleet.

$$Fleetsize_{t,a} = Prod_{t-a} \times (1 - F_{t,a})$$

$F_{t,a}$  is the cumulative distribution function of the vehicle lifespans which is based on Liao et al. (2021)'s analysis of historical and future U.S. car and light truck lifespan distributions (survivability)<sup>19</sup>. Without additional data availability, we assume that the SUV lifespan distribution is the average of cars and light trucks. Table A.3 lists the historical vehicle lifespan distribution (1975-2018) as well as future lifespan following a Gamma distribution used in this analysis.

Table A.3: LDV lifespan distribution parameters

Year	Cars			SUV			Light truck		
	Mean lifespan	Shape parameter K	Scale parameter $\theta$	Mean lifespan	Shape parameter K	Scale parameter $\theta$	Mean lifespan	Shape parameter K	Scale parameter $\theta$
1975	12.2	6.1	2	14.245	5.75	2.5	16.29	5.4	3
1976	12.43	6.2	2	14.41	5.85	2.5	16.39	5.5	3
1977	12.65	6.3	2	14.57	5.9	2.5	16.49	5.5	3
1978	12.86	6.4	2	14.725	5.95	2.5	16.59	5.5	3
1979	13.06	6.5	2	14.87	6.05	2.5	16.68	5.6	3
1980	13.25	5.8	2.3	15.005	5.7	2.65	16.76	5.6	3
1981	13.43	5.8	2.3	15.14	5.7	2.65	16.85	5.6	3

1982	13.6	5.9	2.3	15.265	5.75	2.65	16.93	5.6	3
1983	13.77	6	2.3	15.385	5.85	2.65	17	5.7	3
1984	13.92	6.1	2.3	15.5	5.9	2.65	17.08	5.7	3
1985	14.07	6.1	2.3	15.61	5.9	2.65	17.15	5.7	3
1986	14.22	6.2	2.3	15.72	5.95	2.65	17.22	5.7	3
1987	14.36	6.2	2.3	15.82	6	2.65	17.28	5.8	3
1988	14.49	8.1	1.8	15.92	6.95	2.4	17.35	5.8	3
1989	14.62	8.1	1.8	16.015	6.95	2.4	17.41	5.8	3
1990	14.74	8.2	1.8	16.105	7	2.4	17.47	5.8	3
1991	14.86	8.3	1.8	16.195	7.05	2.4	17.53	5.8	3
1992	14.97	8.3	1.8	16.275	7.1	2.4	17.58	5.9	3
1993	15.08	8.4	1.8	16.36	7.15	2.4	17.64	5.9	3
1994	15.19	8.4	1.8	16.44	7.15	2.4	17.69	5.9	3
1995	15.29	8.5	1.8	16.515	7.2	2.4	17.74	5.9	3
1996	15.39	8.6	1.8	16.59	7.25	2.4	17.79	5.9	3
1997	15.48	8.6	1.8	16.66	7.25	2.4	17.84	5.9	3
1998	15.58	8.7	1.8	16.73	7.35	2.4	17.88	6	3
1999	15.66	8.7	1.8	16.795	7.35	2.4	17.93	6	3
2000	15.75	8.8	1.8	16.86	7.4	2.4	17.97	6	3
2001	15.83	8.8	1.8	16.925	7.4	2.4	18.02	6	3
2002	15.91	8.8	1.8	16.985	7.4	2.4	18.06	6	3
2003	15.99	8.9	1.8	17.045	7.45	2.4	18.1	6	3
2004	16.07	8.9	1.8	17.105	7.45	2.4	18.14	6	3
2005	16.14	9	1.8	17.155	7.55	2.4	18.17	6.1	3
2006	16.21	9	1.8	17.21	7.55	2.4	18.21	6.1	3
2007	16.28	9	1.8	17.265	7.55	2.4	18.25	6.1	3
2008	16.35	9.1	1.8	17.315	7.6	2.4	18.28	6.1	3
2009	16.42	9.1	1.8	17.37	7.6	2.4	18.32	6.1	3
2010	16.48	9.2	1.8	17.415	7.65	2.4	18.35	6.1	3
2011	16.54	9.2	1.8	17.46	7.65	2.4	18.38	6.1	3
2012	16.6	9.2	1.8	17.51	7.65	2.4	18.42	6.1	3
2013	16.66	9.3	1.8	17.555	7.75	2.4	18.45	6.2	3
2014	16.72	9.3	1.8	17.6	7.75	2.4	18.48	6.2	3
2015	16.77	9.3	1.8	17.64	7.75	2.4	18.51	6.2	3

2016	16.83	9.4	1.8	17.685	7.8	2.4	18.54	6.2	3
2017	16.88	9.4	1.8	17.72	7.8	2.4	18.56	6.2	3
2018	16.93	9.4	1.8	17.76	7.8	2.4	18.59	6.2	3
2019	16.98	9.4	1.8	17.8	7.8	2.4	18.62	6.2	3
2020	17.03	9.5	1.8	17.84	7.85	2.4	18.65	6.2	3
2021	17.08	9.5	1.8	17.875	7.85	2.4	18.67	6.2	3
2022	17.13	9.5	1.8	17.915	7.85	2.4	18.7	6.2	3
2023	17.17	9.5	1.8	17.945	7.85	2.4	18.72	6.2	3
2024	17.22	9.6	1.8	17.985	7.95	2.4	18.75	6.3	3
2025	17.26	9.6	1.8	18.015	7.95	2.4	18.77	6.3	3
2026	17.3	9.6	1.8	18.045	7.95	2.4	18.79	6.3	3
2027	17.34	9.6	1.8	18.08	7.95	2.4	18.82	6.3	3
2028	17.38	9.7	1.8	18.11	8	2.4	18.84	6.3	3
2029	17.42	9.7	1.8	18.14	8	2.4	18.86	6.3	3
2030	17.46	9.7	1.8	18.17	8	2.4	18.88	6.3	3
2031	17.46	9.7	1.8	18.17	8	2.4	18.88	6.3	3
2032	17.46	9.7	1.8	18.17	8	2.4	18.88	6.3	3
2033	17.46	9.7	1.8	18.17	8	2.4	18.88	6.3	3
2034	17.46	9.7	1.8	18.17	8	2.4	18.88	6.3	3
2035	17.46	9.7	1.8	18.17	8	2.4	18.88	6.3	3
2036	17.46	9.7	1.8	18.17	8	2.4	18.88	6.3	3
2037	17.46	9.7	1.8	18.17	8	2.4	18.88	6.3	3
2038	17.46	9.7	1.8	18.17	8	2.4	18.88	6.3	3
2039	17.46	9.7	1.8	18.17	8	2.4	18.88	6.3	3
2040	17.46	9.7	1.8	18.17	8	2.4	18.88	6.3	3
2041	17.46	9.7	1.8	18.17	8	2.4	18.88	6.3	3
2042	17.46	9.7	1.8	18.17	8	2.4	18.88	6.3	3
2043	17.46	9.7	1.8	18.17	8	2.4	18.88	6.3	3
2044	17.46	9.7	1.8	18.17	8	2.4	18.88	6.3	3
2045	17.46	9.7	1.8	18.17	8	2.4	18.88	6.3	3
2046	17.46	9.7	1.8	18.17	8	2.4	18.88	6.3	3
2047	17.46	9.7	1.8	18.17	8	2.4	18.88	6.3	3
2048	17.46	9.7	1.8	18.17	8	2.4	18.88	6.3	3
2049	17.46	9.7	1.8	18.17	8	2.4	18.88	6.3	3



2050	17.46	9.7	1.8	18.17	8	2.4	18.88	6.3	3
------	-------	-----	-----	-------	---	-----	-------	-----	---

Figure A.8 shows the estimated fleet size and age distribution between 1975 and 2018 using the above-described method assuming 1974 fleet size starts from 0. The resulting fleet size in 2018 is around 252 million units which is consistent with EIA (2019)<sup>20</sup>.

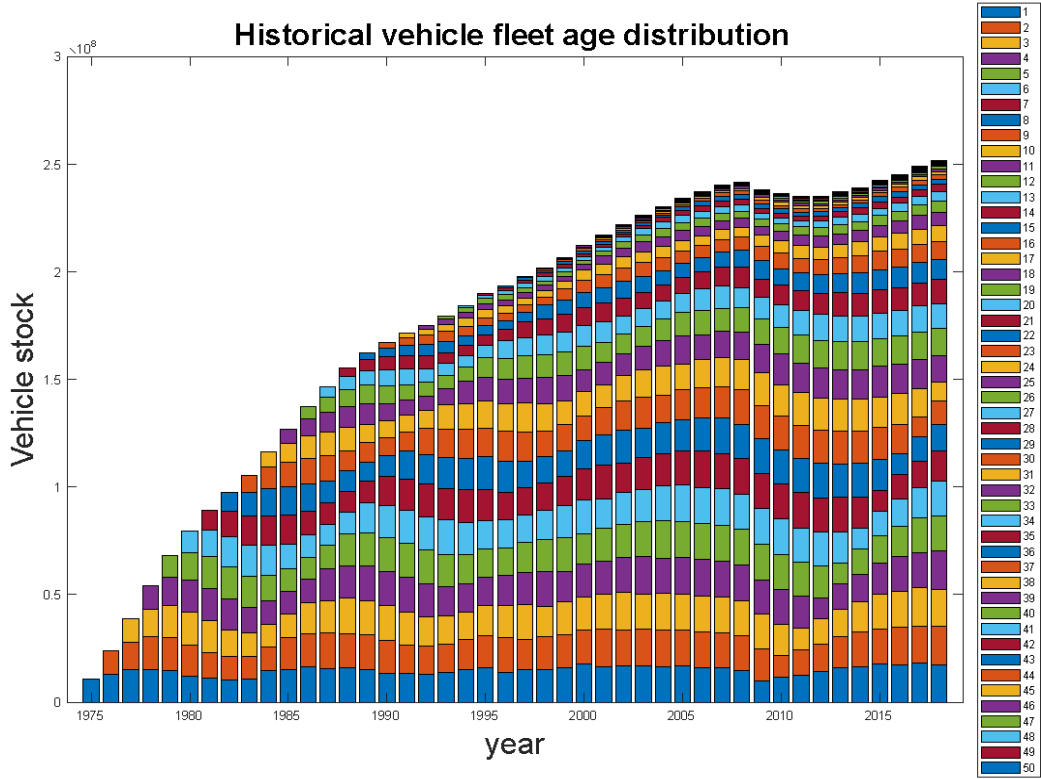


Figure A.8: Estimated historical vehicle fleet age distribution.

**A.2.2 Estimating future LDV production, fleet size and disposal**

From 2019 and onwards, the future vehicle fleet size, production for U.S. sales and scrappage are estimated using a stock-driven DMFA method from aggregate LDV vehicle travel demand and annual *km traveled per vehicle* (Equation 4-6 in the main manuscript).

We reference EIA’s (2020)<sup>21</sup> estimation of future aggregate LDV vehicle travel demand from 2019-2050 which aligns well with the FHWA (2018)’s predicted future LDV transport demand prediction<sup>22</sup>.

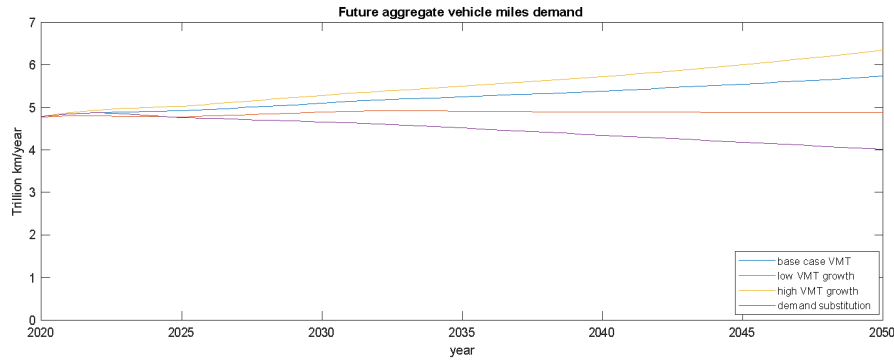


Figure A.9: Future aggregate vehicle travel demand

The annual *km traveled per vehicle* of age  $a$  years is assumed to be a function of the km traveled at age 1 year (Figure A.10). Ratios of annual *km traveled per vehicle* of age  $a$  years with respect to age 1 year are derived from Table E1.5-2 in the *Interim Joint Technical Assessment Report* for CAFE standard by EPA and NHTSA (2016)<sup>23</sup>.

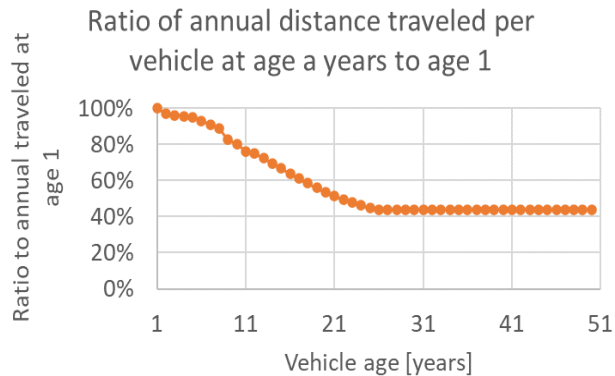


Figure A.10: Ratio of annual km traveled per vehicle with respect to vehicle age  $a$ .

The vehicle lifespan distribution is modeled when predicting future vehicle production (base case, early ICEV retirement at 20 years, and early ICEV retirement at 10 years) and scrappage (Equation 4 and 5 in the main manuscript). The base case vehicle lifespan is from Liao et al. (2021) shown in Table A.3<sup>19</sup>. In the early retirement simulations, the same lifespan distributions from the base case are assumed for all vehicles except for ICEVs that reach early retirement age.

Figure A.11 shows the resulting future vehicle sales prediction. Note that in the early retirement cases starting in 2023, after every 10 or 20 years, there is a jump in the annual vehicle production which is due to additional vehicles produced to maintain the fleet size in the corresponding vehicle travel demand case.

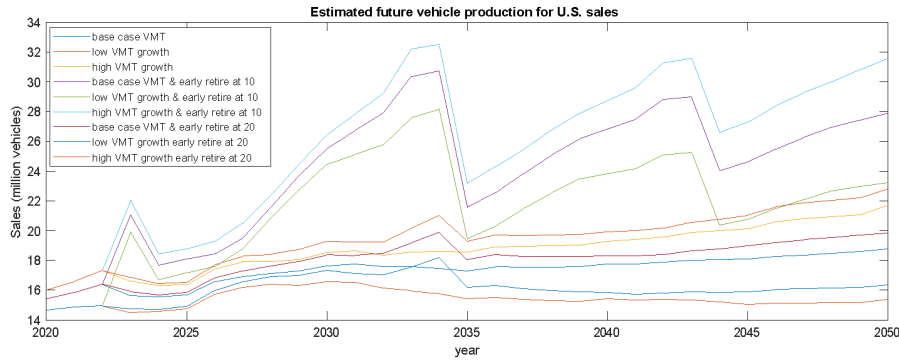


Figure A.11: Estimated future vehicle production for U.S. sales.

In the demand substitution case, which is built on the base case LDV vehicle travel demand, we consider the shift towards public and physical transportation that could potentially reduce both the aggregate and the per-vehicle travel demand. A maximum vehicle travel demand reduction of 50% of U.S. urban LDV transport (accounting for 70% of total U.S. LDV travel) is deemed possible in Replogle et al. (2014)’s analysis<sup>24</sup>. This is achieved in their study through a combined increase in public transportation, walking, and cycling. A similar level of 30% LDV travel reduction has been assumed in Wang et al. (2020)’s analysis of California delivered through smart growth urban planning<sup>25</sup>. Therefore, in the demand reduction case, we assume from 2023 to 2050, 0% to 30%, and linearly increasing between, LDV travel is replaced (45% by public transportation, 35% by cycling and 20% by walking) using a constant occupancy rate of 1.63<sup>26</sup>. The breakdown of the replacement between public transport, cycling and walking is informed by Buehler and Pucher’s (2011) analysis of the German and the UK transportation system so that the resulting U.S. travel breakdown becomes similar to Germany and UK by 2050<sup>27</sup>. The 2050 U.S. per-vehicle miles travels will then reduce to 8,557 vehicle-miles/year which is still higher than Germany, France and Canada (7,715 miles/year in Germany, 8,480 miles/year in France and 7,289 miles/year in Canada<sup>28</sup>) due to higher current U.S. per-person miles travel. The demand reduction case doubles the public transportation demand by 2050 from the 2020 level while the target per capita 2050 public transportation demand is still 20% lower than average public transportation demand in OECD European countries in 2010<sup>24</sup>. For each mile of LDV vehicle travel demand replaced, there are potential increases in dietary emissions and public transportation emissions.

To investigate the potential increase in the dietary emissions due to increased walking and cycling in the travel demand substitution case, we compare the average daily calorie intake with the dietary energy intake recommended by the United States Department of Agriculture (USDA)<sup>29</sup>. According to Alexandrou et al. (2013), the U.S. average energy input for a typical American diet for the year 2004 is 3,679 kcal/capita/day which is well over the average value of 2,100 kcal/capita/day recommended by United States Department of Agriculture (USDA)<sup>29</sup>. The additional energy intake

could be used to support 57 km of cycling (115 kJ/km according to Higgins, 2005) or 31 km of walking (215 kJ/km according to Higgins<sup>30</sup>) per day per capita. Based on the 2019 U.S. population of 3.28E8, cycling or walking using the excess food energy could replace 89% or 48% of 2019 LDV travel demand. This is well over the required increase in cycling (11%) and walking (6%) in the vehicle travel demand substitution case. Therefore, we decided to not add additional dietary emissions to the cumulative emission calculation in the vehicle travel demand substitution case. Due to lack of information, we also do not include the potential infrastructure and urban planning emissions changes due to increased public transport and personal exercise.

The public transportation life cycle emissions (kg CO<sub>2</sub> eq./km) data are taken from Logan et al. (2020)<sup>31</sup>, Replogle et al. (2014)<sup>24</sup>, Chester and Cano (2016)<sup>32</sup> and Chan et al. (2013)<sup>33</sup> which is around 25% of LDV life cycle emissions. This 25% of LDV travel emissions by public transportation include vehicle cycle (material extraction and vehicle production) as well as emissions from vehicle operation which is consistent with reviews of multiple studies of public transit system<sup>24,31-33</sup>. Although we did not include the new infrastructure construction and operation emissions in this analysis, Chester and Cano (2016) showed in their study that the infrastructure construction and operation emissions accounts for less than 20% of the life cycle emissions<sup>32</sup>. The demand substitution case assumes no changes in vehicle sales or fleet size, rather, only a reduction in the LDV per-vehicle travel demand.

To determine the sales of vehicles of each powertrain, we apply the sales share of alternative fuel vehicles parameter to the estimated future production in each year. Seven sales shares of alternative fuel vehicles parameters are considered. A base case equals the EIA (2020) prediction that sales of alternative fueled vehicles will increase from 6% in 2020 to 16% of new LDV sales by 2050<sup>21</sup>. The EIA (2020) prediction is selected because it reflects the current trends of U.S. vehicle sales compared to recent sales data (its 6% sales of alternative fuel vehicles align with Argonne's monthly sales data that the share of HEV in LDV sales is 3.16%, and the share of PHEVs and BEVs together is 1.91% of total LDV sales in August 2020)<sup>21</sup>. All other cases simulate a constant increase in the sales share of a single powertrain from the 2020 value. Four cases simulate a 100% sales share by 2050 for HEVs, PHEV40s (already proven and popular technologies), biofuel fuel flex vehicles (a 100% biofuel share is deemed feasible by McCollum and Yang<sup>34</sup>), and BEV300s (BEV300 2050) respectively. Figure A.12 and S13 shows the seven sales share of alternative fuel vehicles parameters of car and light trucks. It is assumed that the sales share of alternative fuel vehicles parameter of SUVs takes the average of car and light truck.

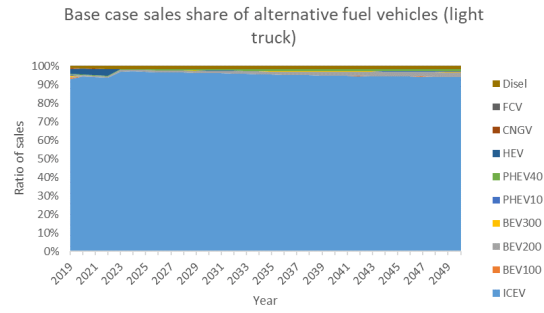
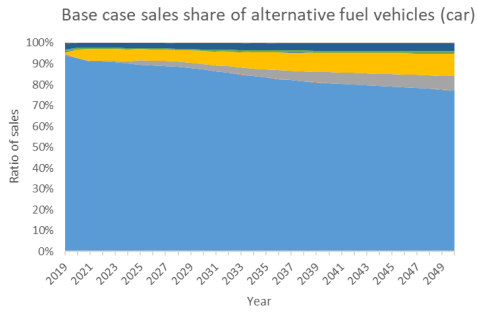
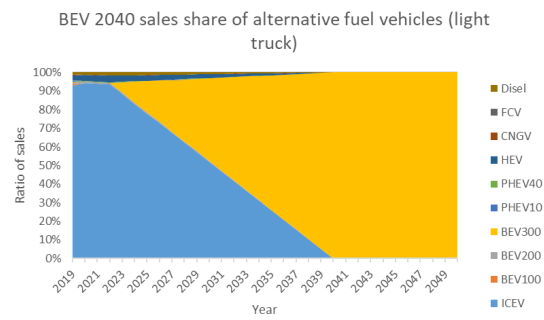
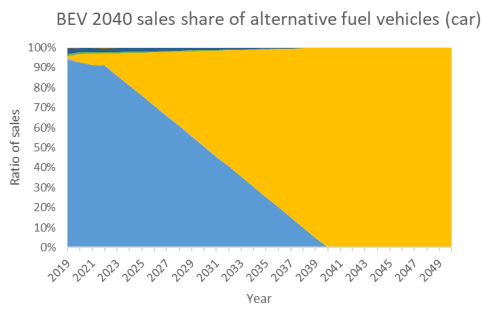
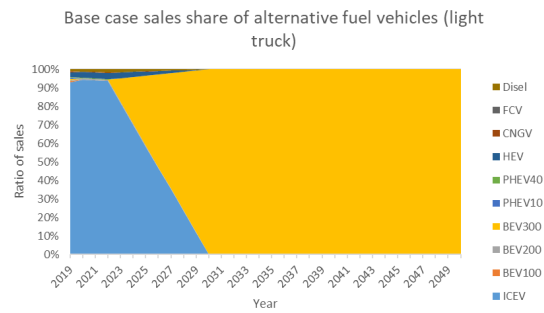
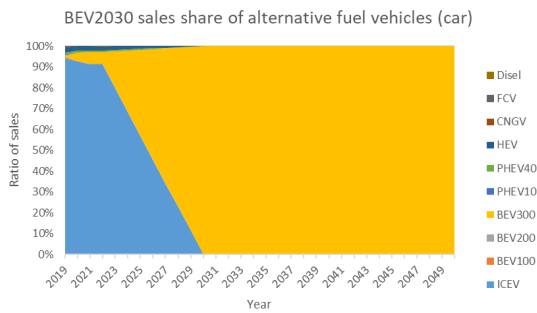
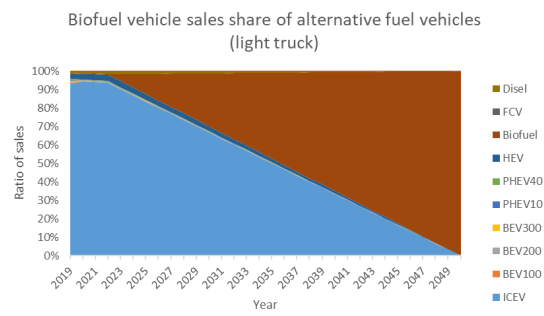
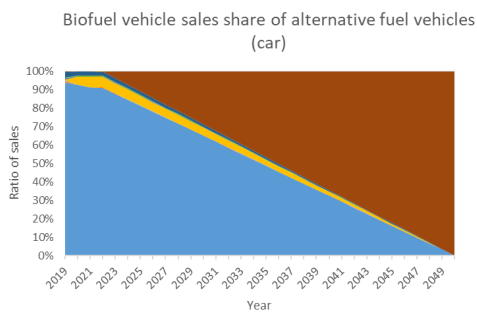


Figure A.12: Base case sales share of alternative fuel vehicles



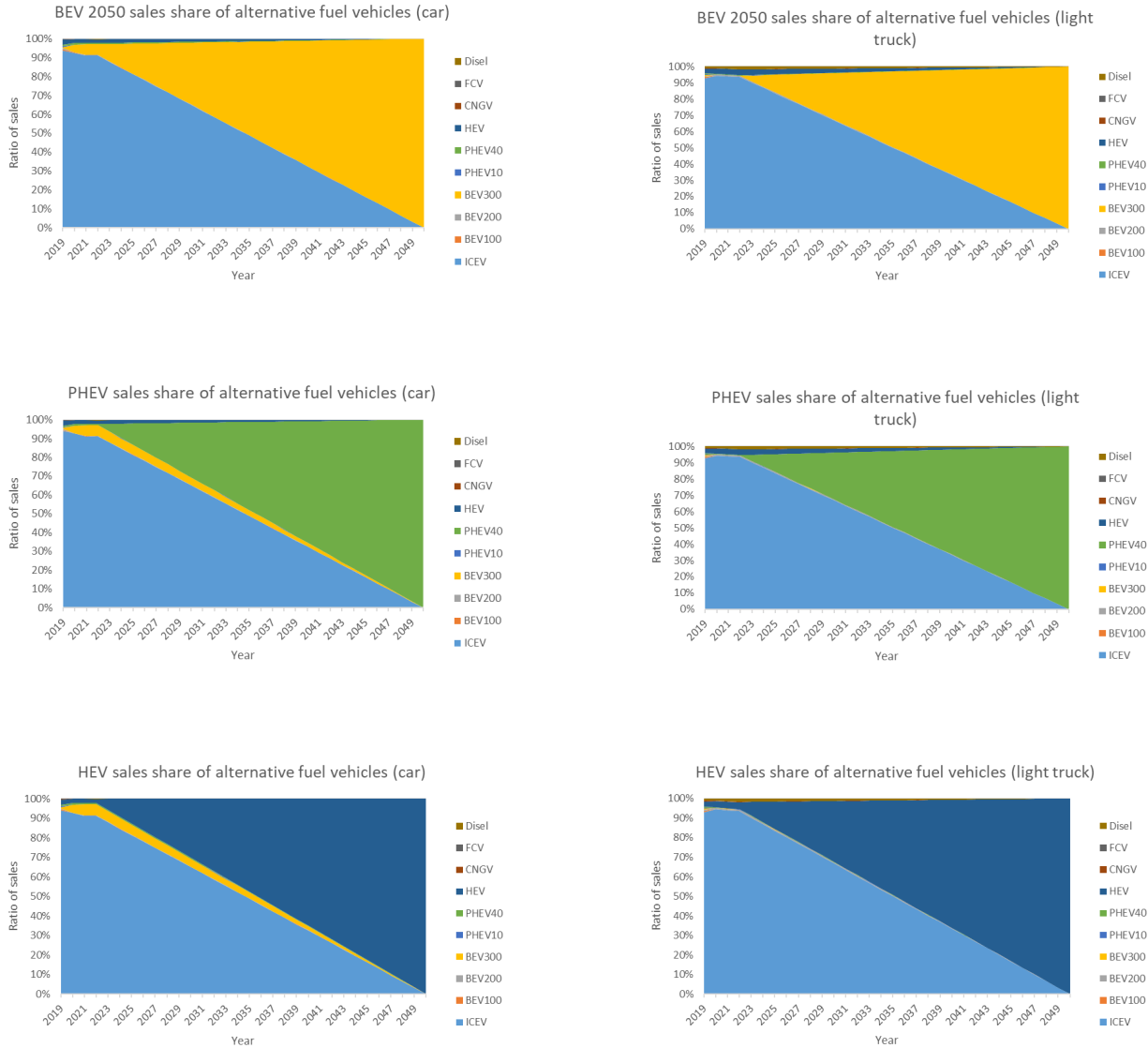


Figure A.18: Vehicle sales share of alternative fuel vehicles

### A.2.3 Recycling rate

Two recycling scenarios are considered in this study for 13 vehicle materials and vehicle batteries. The first recycling scenario (base case) assumes that the current EOL closed-loop recycling rates (RR) according to Keoleian et al. (2012)<sup>35</sup>'s study of vehicle materials life cycle are continued to 2050 and we estimate the recycled contents for each material through annual scrap availability and material demand derived from dynamic material analysis shown in Table A.4. The second recycling scenario (high) assumes that EOL closed-loop RRs increase linearly from current values (third column in Table A.4) to 90% (unless otherwise specified in Tale S4).

Table A.4: 2020 Recycled content and EOL closed loop recycling rates

	2020 Recycled Content	2020 EOL recycling rate	2050 EOL recycling rate – base case constant as 2020	2050 EOL recycling rate – 90% recycling rate by 2050
Steel	26%	30%	30%	90%
Stainless steel	0%	0%	0%	90%
HSS/AHSS	26%	30%	30%	90%
Cast iron	100%	100%	100%	100%
Wrought Aluminum	11%	12%	12%	90%
Cast Aluminum	85%	95%	95%	95%
Copper/Brass	0%	0%	0%	90%
Zinc	0%	0%	0%	0%
Magnesium	52%	58%	58%	90%
Glass	0%	0%	0%	0%
Average Plastic	0%	0%	0%	0%
Rubber	0%	0%	0%	0%
Carbon Fiber-Reinforced Plastic for General Use	0%	0%	0%	90%
Lead-Acid (ICEV)	35%	90%	90%	90%
Lead-Acid (other)	35%	90%	90%	90%
Ni-MH	0%	0%	0%	0%
Li-ion (BEV100)	0%	0%	0%	90%
Li-ion (BEV200)	0%	0%	0%	90%
Li-ion (BEV300)	0%	0%	0%	90%
Li-ion (PHEV10)	0%	0%	0%	90%

### A.3 Vehicle LCA

According to the international standard for life cycle assessment (ISO 14040:2006<sup>36</sup>), LCA addresses the environmental impacts throughout a product’s life cycle, e.g. use of resources and the environmental consequences of releases. As one of the most popular environmental analysis tools, it has been widely used by researchers across the world for light-duty vehicle impact analysis. According to our review, many of the vehicle LCAs looking at U.S. light-duty vehicle sectors are based on the greenhouse gases, regulated emissions, and energy use in transportation (GREET) model developed by the Argonne national lab<sup>35,37-44</sup>. The GREET model simulates the energy and emissions associated with the production, use and end-of-life of both fuel (fuel cycle) and vehicle (vehicle cycle). In this study, we use the GREET model as the starting point for modeling the

current life cycle impact of all vehicles of the three sizes and ten powertrains. The scope of LCA for each vehicle model covers its production including raw material production and manufacturing; use, e.g., fuel supply (well-to-pump) and combustion (pump-to-well), electricity charging for BEV; and end-of-life treatment. The functional unit is the lifetime of one vehicle. The environmental benefits of using recycled materials are modeled using the recycled content method based on the recycling rates defined in Section S3.3.

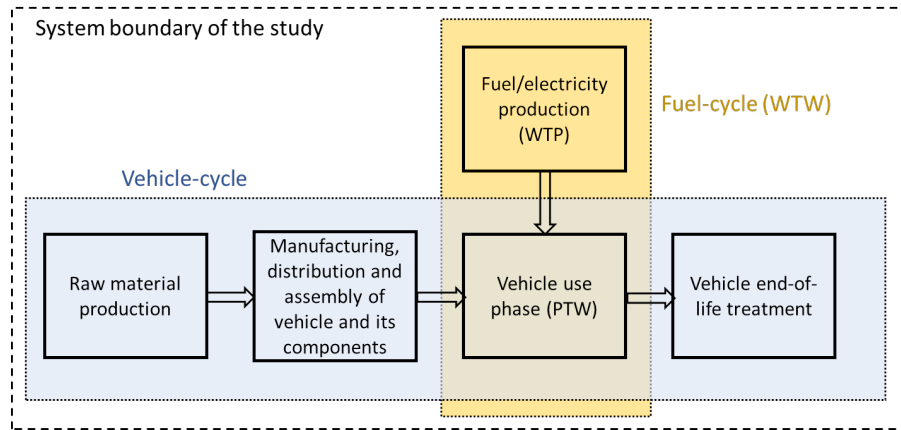


Figure A.19: System boundary of the product-level LCA study

Section S4.1 discusses how the vehicle technology scenarios are used to estimate vehicle production energy. Section S4.2 discusses how vehicle technology scenarios are used to estimate the use phase energy. Section S4.3 discusses vehicle disposal energy and emissions factors used to convert vehicle production, use and disposal energy to emissions impact.

### A.3.1 Vehicle production impact

Vehicle production emissions are dominated by vehicle design and material choices. The GREET model<sup>37</sup> provides a detailed bill of materials and emission factors for materials used in vehicle production. For ICEVs, the vehicle structure and powertrain dominate the vehicle production. However, for electric vehicles, battery production may have comparable impact compared to the vehicle structure. Therefore, we separately consider the vehicle production impact from structure (S4.1.1) and battery (S4.1.2).

#### A.3.1.1 vehicle structure

For each vehicle model, the current vehicle material composition is obtained from the GREET model. Various studies have investigated the theoretical potential of vehicle lightweighting with material substitutions. For example, DOE (2015)<sup>45</sup> summarized in the Quadrennial Technology



Review that a whole vehicle weight reduction opportunities of 17%, 28%, or 36% respectively if advanced high-strength steel (AHSS), aluminum, or CFRP materials were applied to the greatest extent possible. Kim et al., (2010) estimated 6-19% vehicle lightweighting is achievable using HSS, and 6-23% lightweighting is achievable using aluminum<sup>46</sup>. Therefore, we define three vehicle lightweighting scenarios to achieve 10% lightweighting by 2050 (baseline scenario using high-strength steel (HSS)), 20% using aluminum, and 30% using carbon-fiber-reinforced plastic (CFRP) respectively. The 10% reduction level using HSS based on the average range of Kim et al., (2010)<sup>46</sup>, Kelly et al.(2015)<sup>47</sup>, and Milovanoff et al. (2019)<sup>48</sup>. Similarly, the 20% reduction levels using aluminum are based on the average of Kim et al., (2010)<sup>46</sup>, Kelly et al.(2015)<sup>47</sup>, and Milovanoff et al. (2019)<sup>48</sup>. The maximum level of 30% lightweighting using CFRP was based on the average of DOE (2015)<sup>45</sup> and Kelly et al.(2015)<sup>47</sup>. The baseline vehicle lightweight scenario is assumed to achieve 10% lightweighting by 2050 from 2010 by replacing 50% mild steel with high-strength steel (HSS) using a substitution factor of 0.67 combining analysis by Kim et al., (2010)<sup>46</sup>, Kelly et al.(2015)<sup>47</sup>, and Milovanoff et al. (2019)<sup>48</sup>. The moderate vehicle lightweight scenario achieves 20% lightweighting by replacing 80% mild steel with wrought aluminum using a substitution factor of 0.55 derived from Kim et al., (2010)<sup>46</sup>, Kelly et al.(2015)<sup>47</sup>, and Milovanoff et al. (2019)<sup>48</sup>. The high vehicle lightweight scenario achieves 30% lightweighting by replacing 80% mild steel and all aluminum with carbon-fiber-reinforced plastic (CFRP) with a substitution factor of 0.5 according to DOE (2015)<sup>45</sup> and Kelly et al.(2015)<sup>47</sup>. In all the mass reduction levels, a stepwise adoption function is assumed, i.e., 50% of the mass reduction occurs in 2020-2030, 33% of the mass reduction occurs in 2030-2040 and the rest occurs in 2040-2050 to account for the increasing difficulty of mass reduction as vehicle lightweight design approaching the potential limit. The vehicle composition between 2020 and 2050 are therefore calculated as linear extrapolation between current composition and end point composition following the assumed stepwise adoption function. Figure A.15-17 show vehicle material composition in the baseline, moderate and high lightweight scenarios.

In addition to vehicle lightweighting, there are other trends in vehicle design that may affect vehicle production impacts. Examples include the addition of safety and comfort accessory features and vehicle horsepower increase. However, comparing the impact of material substitution, their impacts are likely to be dominated in the operation phase while the impact in the vehicle production phase is negligible. Therefore, we only considered their impacts on the vehicle operation phase.

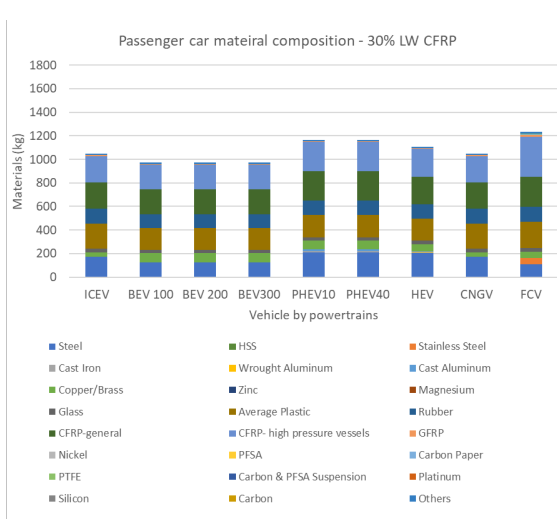
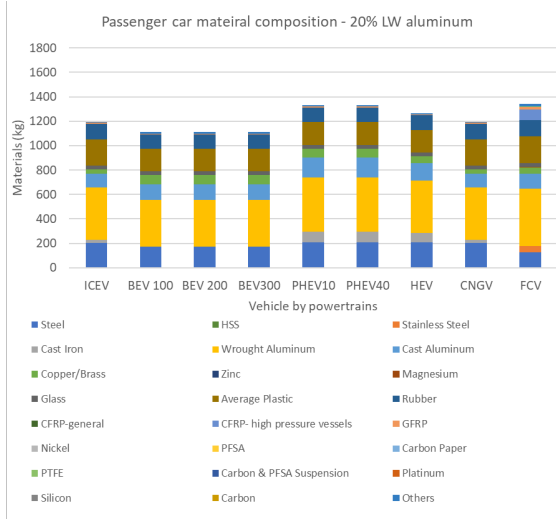
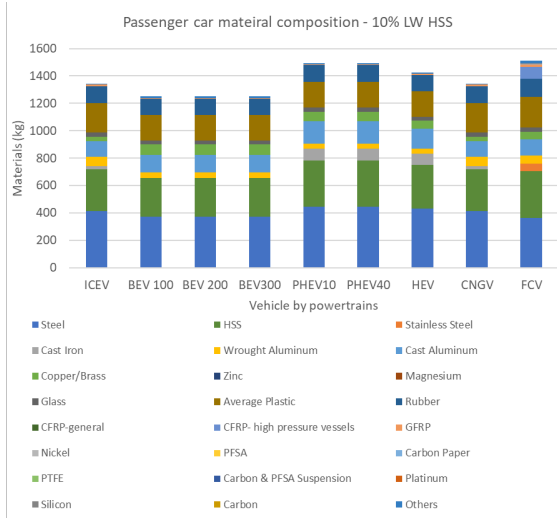
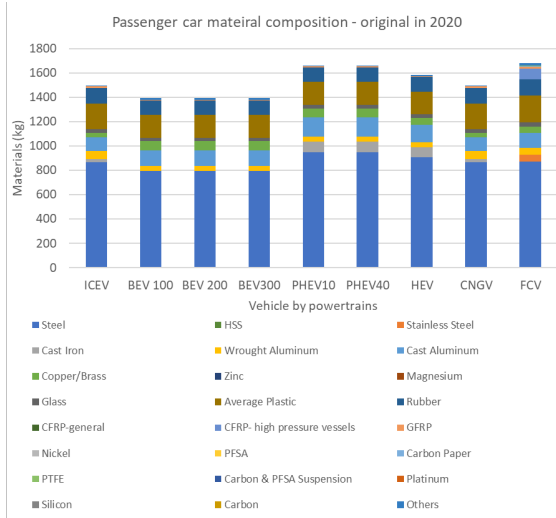


Figure A.21: passenger car material composition

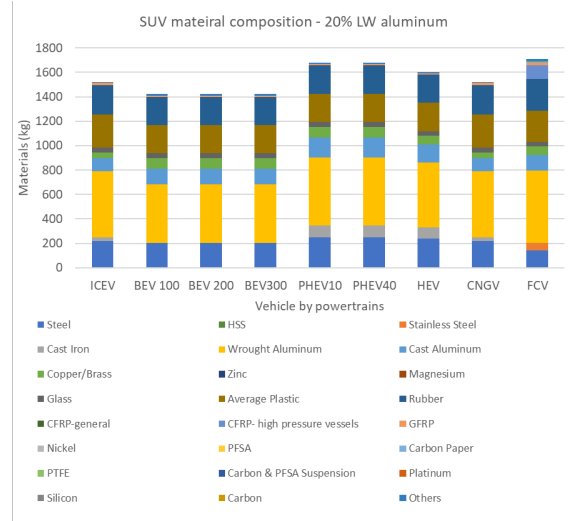
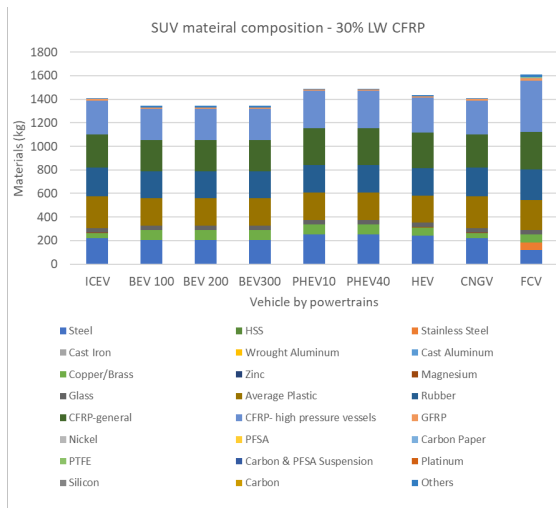
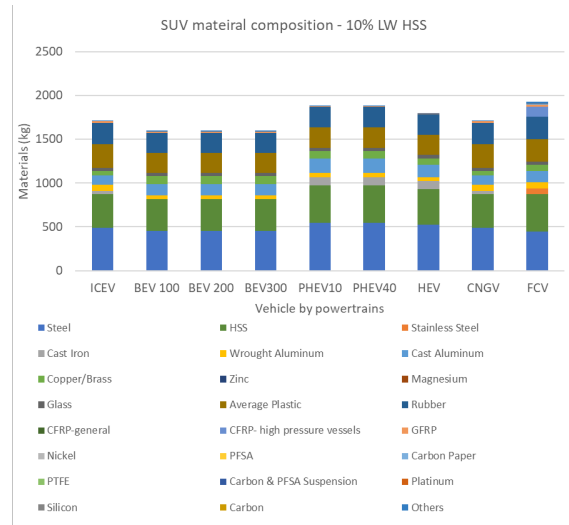
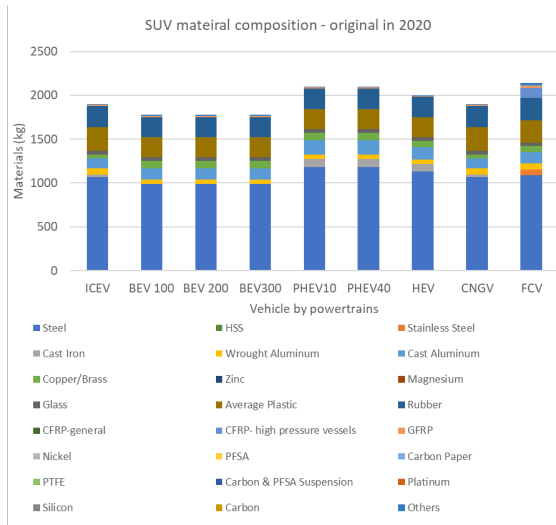


Figure A.23: SUV material composition



Figure A.25: Light truck material composition

### A.3.1.2 Batteries

Three types of batteries are commonly used in modern LDVs: Lead-Acid batteries for vehicle starter and accessory features, Ni-MH batteries for most HEVs and FCVs and Li-ion batteries for electric vehicles. The GREET model provided a detailed battery LCA analysis for all three types of batteries which is referenced in this analysis. For Li-ion batteries, various types of cathodes are available. Currently, the lithium nickel manganese cobalt oxide-based Li-ion battery (60% Ni, 20%Mn, 20% Co: NMC622) is widely used in many BEV and PHEV models while NMC 811 are projected to be taking over the market in the future<sup>48,50</sup>. According to the GREET model, the environmental impact associated with a Li-ion battery is mainly from the energy and emission-intensive materials and battery assembly phases. Among all the components of the battery assembly,

the battery (electrode, separator, cell container), electrode paste, and battery management system together contributes to more than 50% of the battery-related GHG emissions. Energy demands for co-precipitation and calcination are the major contributor to the total energy use and GHG emissions of the cathode powder production, whereas the production of upstream materials, especially those containing cobalt and nickel, dominates the rest of the impact categories. In order to reduce the energy and emissions associated with the Li-ion batteries, Dunn et al. (2015)<sup>51</sup> pointed out that recycling of the cathode material is a potential approach since it can greatly reduce the use of a solvent in cathode material production and process heat requirements. To recycle EV batteries, disassembly of the battery packs from the vehicle, and recovery of the battery materials are the main challenges. The battery disassembly process requires high-voltage training and insulated tools to prevent electrocution of operators or short-circuiting of the batteries which can be cost and environmental-inefficient. Current traction Li-ion batteries usually contain multiple precious materials, e.g., cobalt, nickel, manganese, in a complex layered structure which makes direct separation either expensive, energy-intensive or infeasible. Pyrometallurgical processes to recover metal materials, e.g., cobalt, copper, nickel, and iron, cannot recover lithium or aluminum and need follow-up leaching and purification steps. Both battery disassembly and material recovery processes may lead to chemical hazards due to flammable electrolyte, toxic and carcinogenic electrolyte additives, and the potentially toxic or carcinogenic electrode materials<sup>51,52</sup>.

In this analysis, we assumed the major improvement of emission and energy consumption for battery manufacturing comes from reduced battery weight due to energy density increases and the recycling of the battery packs. The system level energy density of the Li-ion battery is assumed to increase from 150 Wh/kg in 2020 to 235 Wh/kg by 2025. This is based on review of current automotive Li-ion batteries status and predictions on future battery status in various studies<sup>49,50,53-56</sup>, as a goal for commercialization batteries set by USABC. Ambrose et al. (2020)<sup>53</sup> assumed an average battery density of 138 Wh/kg in 2018 with an improvement of 6–8% per year according to US DRIVE (2013). By 2020, the battery density should reach at least 150 Wh/k. As for future battery specific energy, Ambrose et al. (2020)<sup>53</sup> assumed an energy density of 208 Wh/kg by 2025. Schmuch et al. (2019)<sup>49</sup> and Gallagher et al. (2019)<sup>56</sup> both mentioned that a 235 Wh/kg is widely acknowledged as a target value in order to allow mass adoption of long ranged electric vehicles. USABS (2020)<sup>54</sup> set the 235 Wh/kg system level energy density as the goal in 2020's request for proposal information. Ding et al. (2019)<sup>50</sup> suggested that switching to the NMC 811 chemistry could achieve the the 235 Wh/kg system level energy density while further increase would require switching to other battery chemistry or structure, e.g., Li-S, Li-air, or solid-state batteries, etc. However, there is limited information about their commercialization progress or environmental impact for laboratory scale technology like Li-S, Li-air or solid-state batteries . To avoid the high uncertainty associated with future battery chemistry and structure, we assume all EV batteries share

a constant battery energy density and specific power from 2025 and onward. The energy density of lead-acid batteries for ICEVs and nickel metal hydride (NiMH) traction batteries (for HEVs and FCVs) are assumed constant according to Ding et al. (2019)<sup>50</sup> and Xu et al.(2017)<sup>57</sup>. Table A.5 summarizes the current and 2025 vehicle battery configurations.

Table A.5: 2020 vehicle battery configurations summary

	Battery pack capacity (kWh)		
	passenger car	SUV	light truck
Ni-MH (HEV/FCV)	41	58	58
Li-Ion (BEV100)	24	29	34
Li-Ion (BEV200)	48	58	67
Li-Ion (BEV300)	72	86	101
Li-Ion (PHEV10)	4	5	6
Li-Ion (PHEV40)	16	19	22
	Battery power (kW)		
	passenger car	SUV	light truck
Ni-MH (HEV/FCV)	32	45	53
Li-Ion (BEV100)	347	416	499
Li-Ion (BEV200)	347	416	499
Li-Ion (BEV300)	347	416	499
Li-Ion (PHEV10)	81	98	117
Li-Ion (PHEV40)	81	98	117
	2020 battery mass (kg)		
	passenger car	SUV	light truck
Lead-Acid (ICEV)	17	24	28
Lead-Acid (other)	10	16	16
Ni-MH (HEV/FCV)	40	57	66
Li-Ion (BEV100)	173	208	250
Li-Ion (BEV200)	347	416	499
Li-Ion (BEV300)	520	624	749
Li-Ion (PHEV10)	54	65	78
Li-Ion (PHEV40)	217	260	312
	2025 battery mass (kg)		
	passenger car	SUV	light truck
Lead-Acid (ICEV)	17	24	28
Lead-Acid (other)	10	16	16
Ni-MH (HEV/FCV)	40	57	66
Li-Ion (BEV100)	111	133	159
Li-Ion (BEV200)	221	266	319
Li-Ion (BEV300)	332	398	478
Li-Ion (PHEV10)	18	22	27
Li-Ion (PHEV40)	74	89	106

Two levels of battery recycling, assuming we can achieve 0%, or 90% close-loop EOL recycling rates by 2050, are defined as in Section S3.2. A 0% EOL recycling rate is the continuation of the current vehicle Li-ion recycling situation where only experimental or laboratory scale recycling facilities are available. In order to estimate the corresponding environmental impact changes due to battery recycling, we reference the GREET 2020 battery recycling sub-model. It consists of the energy and emission-related to four battery material recycling approaches that retrieve cathode materials. Among the four approaches, direct physical separation has the highest potential in retrieving critical elements, e.g., lithium, cobalt, nickel, etc. and minimize the environmental impacts, therefore, it is chosen as the candidate approach in all the recycling scenarios which can reduce 30% of Li-ion production emissions/kg. The recycling of NiHM batteries is not considered in this study as Silvestri et al. (2020)<sup>58</sup> showed that the NiHM recycling processes can increase the total GHG emissions by up to 20% despite decreases in cumulative energy demand.

### **A.3.2 Use phase impact**

In this analysis, we consider three fuel economy improvement scenarios which correspond to around 1.5%/year, 4%/year, and 5%/year fuel economy improvements from 2020 to 2050 by physical-based fuel economy estimation considering technology readiness. Historically, the U.S. average new LDV fleet fuel economy has been required to improve at around 4-5%/year according to the NHTSA's CAFE standard. However, the recent SAFE rule has relaxed the requirement to 1.5%/year from 2020 level for the 2021-2026 model years. The future fuel economy improvements are assumed to be driven by different levels of design improvements and technology adoptions. Table A.6 below summarizes the levels of (1) vehicle light-weighting effort, (2) engine, motor and transmission efficiency, (3) drag and friction improvement, (4) auxiliary power, and functions in the three fuel economy scenarios.

Various simulation tools have been developed for the PTW analysis including ADVISOR, AVL CRUISE, IGNITE by Ricardo Software, GT-Power, FASTSim, etc. The first three vehicles/powertrain simulation tools offer capabilities to calculate energy flows in a conventional vehicle and alternative-fueled vehicles considering both powertrain and auxiliary components while the GT-Power focused on engine simulation and related fuel economy impact<sup>65</sup> Researchers have implemented these vehicle simulation tools to investigate the relationship between vehicle curb weight, powertrain configuration, auxiliary components, and the fuel economy. For example, Cheah (2010)<sup>66</sup> indicated that the relationship between fuel consumption and the curb weight of the vehicle is approximately linear based on ADVISOR simulations. On average across all vehicle models, every 100 kg weight reduction will achieve a reduction of 0.53 L/100 km in fuel consumption. The Joint Research Centre of the European (JEC) published WTW reports based on AVL CRUISE simulations and predicted the potential improvement in auxiliaries, weight reduction, vehicle aerodynamics, and



Table A.6: Fuel economy scenarios and associated technical parameters

	Vehicle technology scenario changes from 2020 to 2050			Reference
	Base case Fuel Economy Improvement	Moderate Fuel Economy Improvement	High Fuel Economy Improvement	
Vehicle and battery light-weighting	-10%	-20%	-30%	45- 48, 53
Powertrain (engine, transmission or motor) efficiency	ICEV: +30% BEV: +20% PHEV: +28% HEV: +33% FCV: +7% CNGV: +30% Diesel: +30%	ICEV: +45% BEV: +33% PHEV: +42% HEV: +49% FCV: +20% CNGV: +45% Diesel: +45%	ICEV: +60% BEV: +44% PHEV: +56% HEV: +65% FCV: +32% CNGV: +60% Diesel: +60%	49, 60- 64
Wheel tire coefficient of friction	+9%	+21%	+35%	64
Aerodynamics drag	+9%	+21%	+35%	64
Accessory power	0%	-30%	-40%	64

rolling resistance as well as the impact to fuel economies for EU vehicles<sup>65</sup>). FASTSim is the latest simulation tool developed by NREL for simplified vehicle simulation based on technology attributes. It provides default vehicle attributes data for all vehicle models considered in this study currently and allows users to adjust technology attributes based on predicted technology changes. Therefore, we chose the FASTSim simulator for estimating fuel economy improvement. The vehicle attributes data derived from Table A.5 above for each vehicle model are imported to the FASTSim simulator.

Table A.8: Summary of pathway vehicle life cycle parameters, vehicle technology scenario and electricity emissions scenarios (continued)

HEV	base case	0.70	0.4	0.32	600	0.637	0.364	0.41	600
	moderate	0.70	0.4	0.32	600	0.553	0.316	0.46	420
	high	0.70	0.4	0.32	600	0.455	0.26	0.50	360
FCV	base case	0.70	0.4	0.28	600	0.637	0.364	0.37	600
	moderate	0.70	0.4	0.28	600	0.553	0.316	0.41	420
	high	0.70	0.4	0.28	600	0.455	0.26	0.46	360
CNGV	base case	0.70	0.4	0.19	600	0.637	0.364	0.25	600
	moderate	0.70	0.4	0.19	600	0.553	0.316	0.28	420
	high	0.70	0.4	0.19	600	0.455	0.26	0.31	360
Diesel ICEV	base case	0.70	0.4	0.25	600	0.637	0.364	0.30	600
	moderate	0.70	0.4	0.25	600	0.553	0.316	0.33	420
	high	0.70	0.4	0.25	600	0.455	0.26	0.36	360

The vehicle attributes data are inputted into FASTSim simulator (Fig. S11). For other vehicle attributes that FASTSim requires while we predict that will not have major impact in future fuel economies, the default values are kept.

Table A.7: vehicle technical parameters in 2020 and 2050

		wheel tire coefficient of friction	Cd (drag coefficient)	Powertrain efficiency	auxiliary power	wheel tire coefficient of friction	Cd (drag coefficient)	Powertrain efficiency	auxiliary power
		Value in 2020				Value in 2050			
Gasoline ICEV	base case	0.70	0.4	0.19	600	0.637	0.364	0.25	600
	moderate	0.70	0.4	0.19	600	0.553	0.316	0.28	420
	high	0.70	0.4	0.19	600	0.455	0.26	0.31	360
BEV100	base case	0.70	0.4	0.60	600	0.637	0.364	0.73	600
	moderate	0.70	0.4	0.60	600	0.553	0.316	0.80	420
	high	0.70	0.4	0.60	600	0.455	0.26	0.86	360
BEV200	base case	0.70	0.4	0.60	600	0.637	0.364	0.73	600
	moderate	0.70	0.4	0.60	600	0.553	0.316	0.80	420
	high	0.70	0.4	0.60	600	0.455	0.26	0.86	360
BEV300	base case	0.70	0.4	0.60	600	0.637	0.364	0.73	600
	moderate	0.70	0.4	0.60	600	0.553	0.316	0.80	420
	high	0.70	0.4	0.60	600	0.455	0.26	0.86	360
PHEV10	base case	0.70	0.4	0.30	600	0.637	0.364	0.39	600
	moderate	0.70	0.4	0.30	600	0.553	0.316	0.44	420
	high	0.70	0.4	0.30	600	0.455	0.26	0.48	360
PHEV40	base case	0.70	0.4	0.30	600	0.637	0.364	0.39	600
	moderate	0.70	0.4	0.30	600	0.553	0.316	0.44	420
	high	0.70	0.4	0.30	600	0.455	0.26	0.48	360

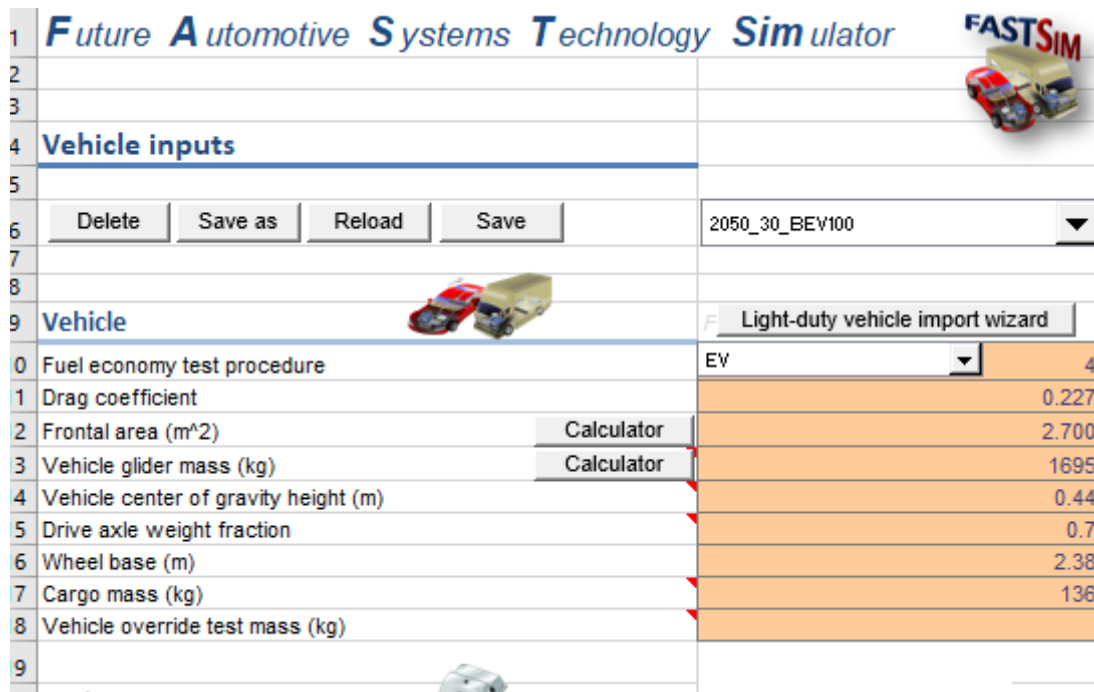
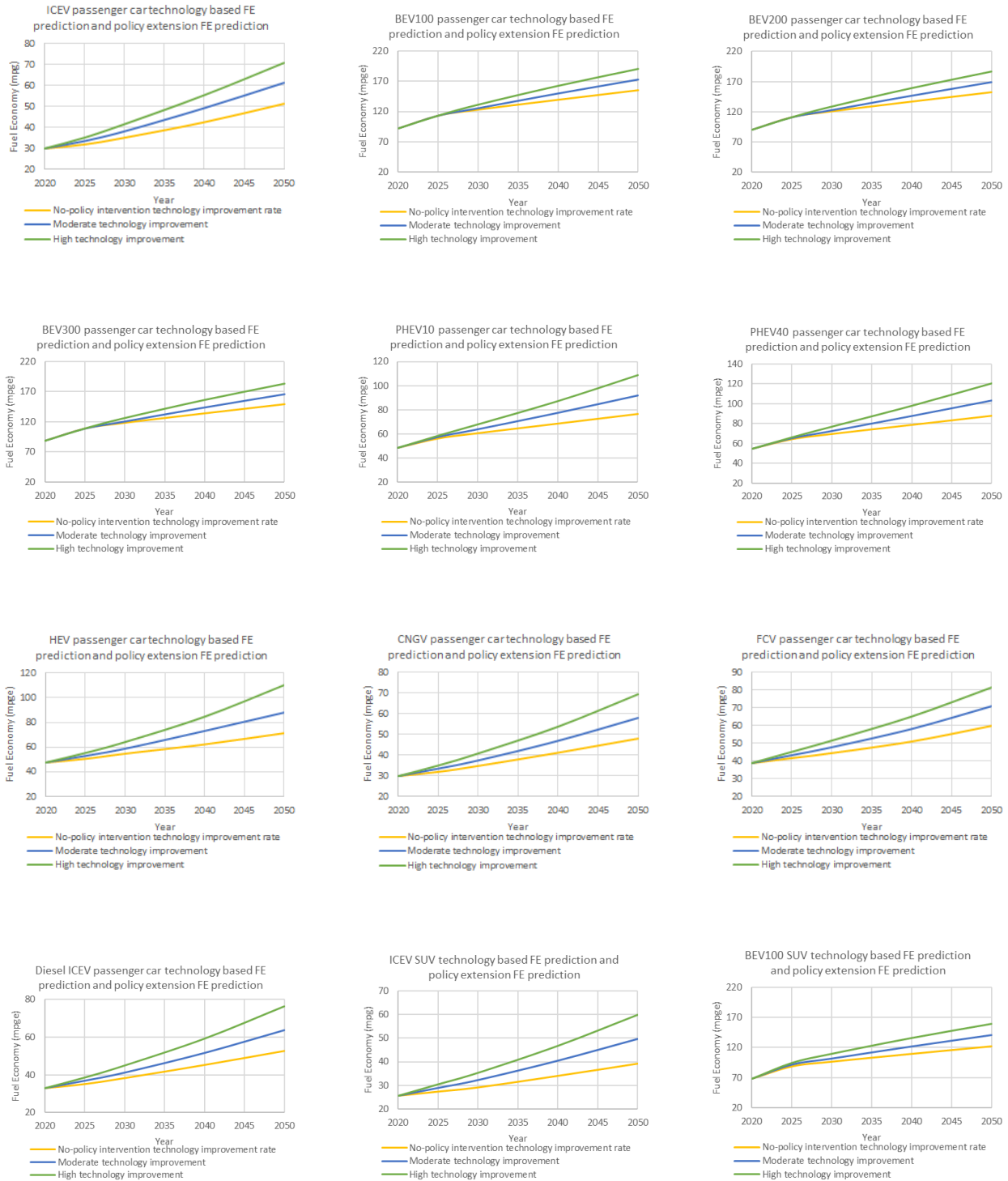
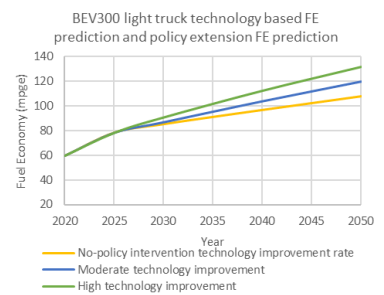
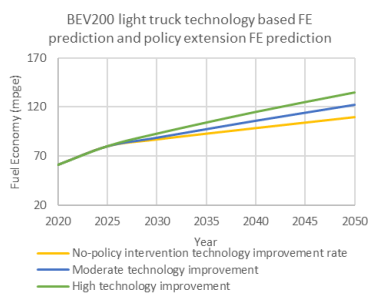
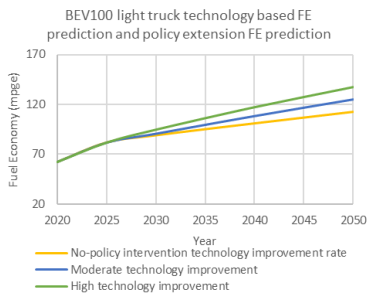
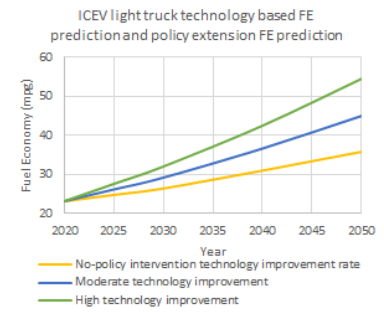
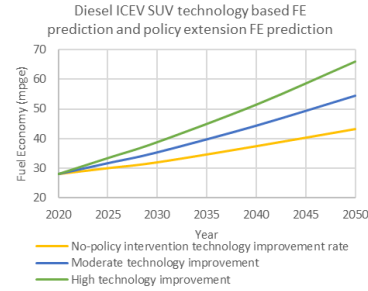
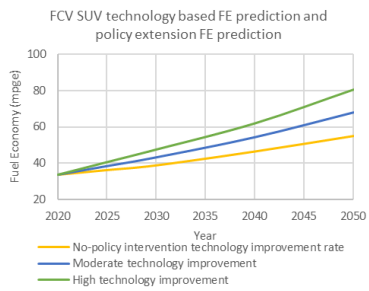
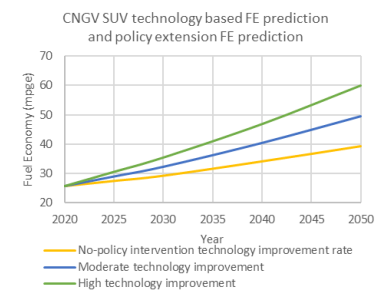
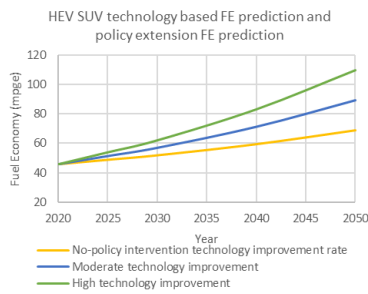
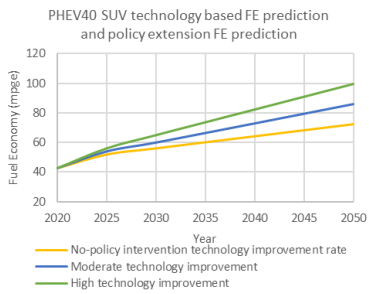
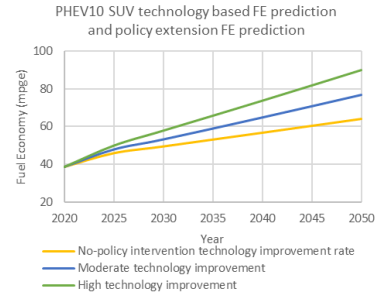
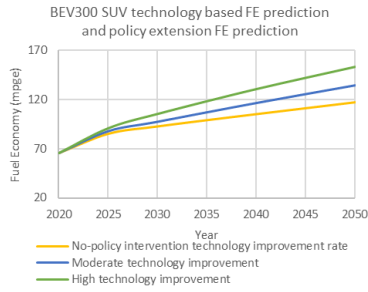
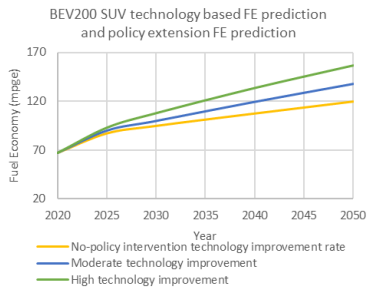


Figure A.26: FASTSim UI

We read the adjusted fuel economy predicted in FASTSim and Fig. S12 shows the predicted vehicle fuel economies in the three scenarios for each vehicle model (passenger car and light truck, separately mainly due to weight difference).





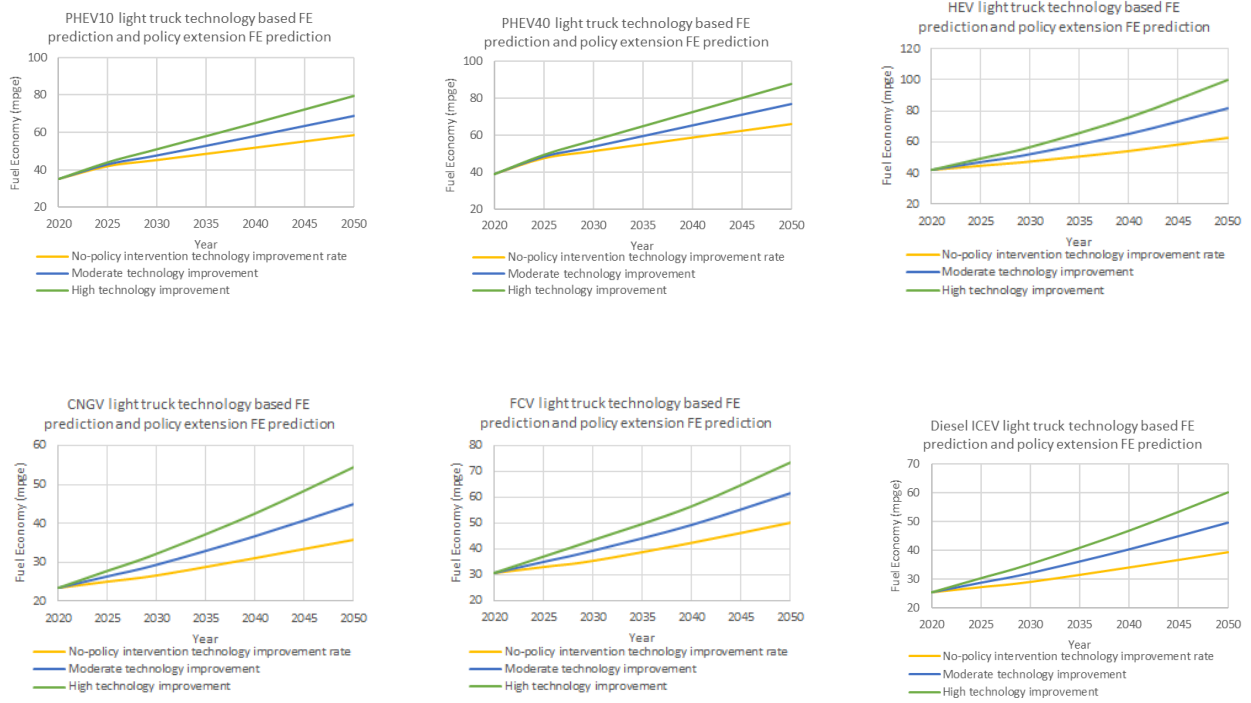


Figure A.36: fuel economy improvement estimations of passenger car, SUVs and light trucks by powertrains

We compared the FASTSim vehicle simulation method with our own physical-based model (Equations S7 and S8) for verification.

$$E_{thrust\ energy/mile} = \frac{\int_0^{x_{ftp75\ test}} (\mu mg + ma + \frac{1}{2}\rho v^2 C_d A_f) dx}{x_{ftp75\ test}} \quad (A.4)$$

$$FE = \frac{\eta_{engine} E_{fuel/gallon}}{E_{thrust\ energy/mile} + E_{auxiliary}} \quad (A.5)$$

Where  $E_{thrustenergy/mile}$  is the average energy that is needed for the engine to provide enough thrust force to move the vehicle under the required driving condition in the FTP75 test (EPA required combined city and highway test procedures).  $\mu$  is the friction between the vehicle tire and the ground.  $m$  is the vehicle mass.  $C_d$  is the drag coefficient of the vehicle.  $A_f$  is the frontal area of the vehicle.  $a$ ,  $v$ ,  $x$  are the acceleration, velocity, and distance traveled by the vehicle calculated from the FTP75 test cycle? In addition for the engine to provide enough thrust energy, it also needs to supply the auxiliary energy that is needed by the air conditioning system, the electric power required by the on-board battery to drive other accessory functions, e.g. speakers, lights, displays, etc.  $FE$  is the fuel economy of the vehicle model.  $\eta_{engine}$  is the engine efficiency that is changing over time based on the scenario technology assumptions.  $E_{fuel/gallon}$  is the energy contained in one gallon of fuel. A 70% reduction factor is applied to the fuel economy values from EIA (2020) to account for

Table A.10: Fuel emissions intensities

	Emissions intensity (g/gallon eq.)		
	CO2	CH4	N2O
Gasoline	9,570.0	12.1	0.3
Natural gas	4,978.4	121.6	1.1
Hydrogen	7,066.7	0.1	0.0
Diesel	9,595.5	17.2	0.2
Bioethanol corn starch	5,948.6	13.4	6.3
Bioethanol cellulosic switchgrass	2,230.7	5.0	2.4

the difference between laboratory test results and on-road efficiencies. For 2020 light trucks and passenger cars, the estimated fuel economy between FASTSim and the simplified physical models are small.

Table A.9: comparison between FASTSim and Physical based model fuel economy prediction

	ICEV	
	LT - 2020	Passenger car - 2020
70% EIA in AEO (2020) FE (mpg)	22.19	30.03
Physical based model FE (mpg)	23.25	29.93
FASTSim FE (mpg)	21.91	28.01
Diff between Physical based model & FASTSim(%)	5.8%	6.4%

### A.3.3 Emissions factors

The emissions factors of fuel sources are needed to determine materials emissions intensity and convert vehicle production, use and disposal energy to emissions impact. The following sections describe the data sources of fuel and electricity emissions intensity and materials emissions factors. For the vehicle disposal phase, we account for the energy needed to disassemble the vehicle, i.e., 1.1 MJ/kg of vehicle mass for disassembly.

#### A.3.3.1 Electricity and fuel emissions intensities

We reference the GREET model for fuel sources emissions intensities including motor gasoline, hydrogen, natural gas, and diesel for vehicle use phase. The emissions intensity of bioethanol are from EPA (2011)<sup>67</sup>. The emission intensity of gasoline, natural gas, hydrogen and diesel are assumed constant over the length of the study. Bioethanol emission intensity will change as the production approach transitions from corn starch to cellulosic switchgrass.

Currently, the U.S. electricity grid GHG intensity is around 421 g CO<sub>2</sub>eq/kWh of which around 17% of electricity is generated from renewable sources<sup>20</sup>. Various U.S. electric companies, e.g.,

Table A.11: Electricity emissions intensity changes

	2020	2035	2050
Grid carbon value –base case 30% reduction of grid GHG intensity by 2050 (gCO <sub>2</sub> e/kWh)	421	320	294
Grid carbon value – 50% reduction of grid GHG intensity by 2050 (gCO <sub>2</sub> e/kWh)	421	319	211
Grid carbon value – 80% reduction of grid GHG intensity by 2050 (gCO <sub>2</sub> e/kWh)	421	258	84

Pacific Gas and Electric, Duke Energy, etc., have proposed a low carbon grid plan to reduce the grid GHG emissions by 2050. Various studies have shown that 80-100% of renewable grids are feasible<sup>68-70</sup>. In this analysis, three levels of electricity GHG intensity scenarios are assumed which corresponds to base case 30% reduction (derived from EIA Annual Energy Outlook Table 8<sup>21</sup>), 50% reduction, and 80% reduction of the grid intensity. In the 50% reduction, and 80% reduction case, a linear decrease in electricity grid carbon intensity from 2020 to 2050 is assumed. The GHG impact of average U.S. produced electricity under the three decarbonization scenarios is presented in Table A.4.

### A.3.3.2 Material emissions factors

Based on the vehicle composition, we estimate the vehicle structure production emissions by multiplying the material weight with emission factors of each type of the materials according to GREET<sup>37</sup> and Ashby<sup>71</sup>. We use a recycled content method to account for recycling rate changes in the production emissions. The change of recycled contents are described in Section 3.2 above.

$$EF_{average} = (1 - RC) \times EF_{primary} + RC \times EF_{secondary} \quad (A.6)$$

For each vehicle, three composition scenarios are defined assuming they change linearly from 2020 compositions to 2050 compositions which depend on the base case, moderate and high vehicle lightweighting scenarios. We reference the GREET model's energy intensity (mmBTU/kg material product used in a vehicle) and vehicle assembly (mmBTU/vehicle vehicle assembled) for all primary vehicle materials. The GREET model's information on electricity vs. non-electricity energy consumption allows us to split energy intensity by electrical and non-electrical components for electricity decarbonization analysis discussed later. The energy intensity of secondary vehicle materials (including recycled Li-ion battery production) are derived from GREET<sup>37</sup> and Ashby<sup>71</sup> and are also categorized by electrical and non-electrical components. Table A.5 and S6 shows the emissions factor of vehicle materials, assembly and batteries.

Table A.12: Primary material emission factor related to electricity

	Primary- electricity			
	CH4 (gram/vehicle)	N2O(gram/vehicle)	CO2(gram /vehicle)	Electricity (kWh/vehicle)
Steel	0.64	0.01	381.95	6
Stainless steel	1.00	0.01	602.16	3
Cast iron	0.11	0.00	63.21	3
Wrought Aluminum	1.95	0.02	1270.60	18
Cast Aluminum	2.11	0.02	1376.42	21
Copper/Brass	1.07	0.01	647.39	6
Zinc	1.74	0.02	1043.88	6
Magnesium	5.63	0.05	3378.34	32
Glass	0.25	0.00	146.88	3
Average Plastic	0.54	0.01	324.05	12
Rubber	0.27	0.00	160.89	6
Carbon Fiber-Reinforced Plastic for General Use	3.32	0.03	1990.55	38
Carbon Fiber-Reinforced Plastic for High Pressure Vessels	6.51	0.06	3910.36	64
Glass Fiber-Reinforced Plastic	1.11	0.01	663.44	12
Nickel	5.63	0.06	3623.39	32
PFSA (Nafion117 Sheet)	0.53	0.01	316.23	3
Carbon Paper	26.93	0.25	16169.42	261
PTFE	0.54	0.01	326.01	15
Carbon & PFSA Suspension (Nafion Dry Polymer)	0.52	0.01	309.28	3
Platinum	60.91	0.66	41626.03	144
Silicon	109.73	1.03	65942.10	457
Carbon	2.19	0.03	1482.26	12
Others	0.00	0.00	0.00	0
assembly emissions per lb	0.26	0.00	154.70	0
assembly energy per vehicle (kWh/vehicle)	0.00	0.00	0.00	3246



Table A.13: Primary material emission factor not related to electricity

	Primary- non-electricity			Electricity (kWh/vehicle)
	CH4 (gram/vehicle)	N2O(gram/vehicle)	CO2(gram /vehicle)	
Steel	1.33	0.01	904.37	-
Stainless steel	0.31	0.00	152.30	-
Cast iron	1.81	0.01	331.13	-
Wrought Aluminum	2.67	0.03	1903.61	-
Cast Aluminum	3.07	0.04	2151.51	-
Copper/Brass	1.00	0.01	588.58	-
Zinc	0.15	0.00	85.75	-
Magnesium	7.56	0.11	4125.90	-
Glass	1.02	0.01	579.19	-
Average Plastic	7.77	0.11	1039.36	-
Rubber	2.42	0.04	1472.49	-
Carbon Fiber-Reinforced Plastic for General Use	13.87	0.18	5877.39	-
Carbon Fiber-Reinforced Plastic for High Pressure Vessels	21.62	0.30	10181.25	-
Glass Fiber-Reinforced Plastic	3.62	0.04	1259.96	-
Nickel	6.52	0.23	2837.85	-
PFSA (Nafion117 Sheet)	0.55	0.01	237.51	-
Carbon Paper	82.96	1.17	40353.62	-
PTFE	4.84	0.08	3066.34	-
Carbon & PFSA Suspension (Nafion Dry Polymer)	0.54	0.01	232.08	-
Platinum	7.69	0.04	5370.69	-
Silicon	37.89	0.73	18430.87	-
Carbon	2.13	0.01	558.74	-
Others	0.00	0.00	0.00	-
assembly emissions per lb	0.35	0.01	151.05	-
assembly energy per vehicle (kWh/vehicle)	-	-	-	-

Table A.14: Secondary material emission factor related to electricity

	Secondary- electricity			
	CH4 (gram/vehicle)	N2O(gram/vehicle)	CO2(gram /vehicle)	Electricity (kWh/vehicle)
Steel	0.71	0.01	425.60	3
Stainless steel	1.00	0.01	602.16	3
Cast iron	0.01	0.00	3.16	0
Wrought Aluminum	0.31	0.00	191.97	3
Cast Aluminum	0.30	0.00	187.78	3
Copper/Brass	0.27	0.00	161.85	0
Zinc	0.29	0.00	173.98	0
Magnesium	0.00	0.00	0.00	0
Glass - no recycling	0.25	0.00	146.88	3
Average Plastic (assume ABS)	0.02	0.00	10.80	0
Carbon Fiber-Reinforced Plastic for General Use	1.99	0.02	1194.33	23

Table A.15: Secondary material emission factor not related to electricity

	Secondary-non- electricity			
	CH4 (gram/vehicle)	N2O(gram/vehicle)	CO2(gram /vehicle)	Electricity (kWh/vehicle)
Steel	0.26	0.00	123.57	-
Stainless steel	0.31	0.00	152.30	-
Cast iron	0.09	0.00	16.56	-
Wrought Aluminum	0.96	0.01	476.89	-
Cast Aluminum	1.19	0.02	579.29	-
Copper/Brass	0.25	0.00	147.14	-
Zinc	0.02	0.00	14.29	-
Magnesium	0.50	0.01	212.59	-
Glass - no recycling	1.02	0.01	579.19	-
Average Plastic (assume ABS)	0.26	0.00	34.65	-
Carbon Fiber-Reinforced Plastic for General Use	8.32	0.11	3526.44	-

Table A.16: Battery emission factor separated by non-electricity and electricity related based on current electricity intensity.

Primary- non-electricity				
	CH4 (gram/kg battery)	N2O (gram/kg battery)	CO2 (gram/kg battery)	electricity (kWh/kg battery)
Lead-Acid	5.60E+00	2.10E-02	1.10E+03	-
Ni-MH	7.30E+00	1.10E-01	3.10E+03	-
Li-ion (NMC622)	1.20E+01	1.40E-01	6.30E+03	-
Li-ion (NMC811)	1.28E+01	1.50E-01	6.74E+03	-
Secondary-non- electricity				
	CH4 (gram/kg battery)	N2O (gram/kg battery)	CO2 (gram/kg battery)	electricity (kWh/kg battery)
Lead-Acid	3.10E+00	1.40E-02	6.20E+02	-
Li-ion (NMC622)	7.80E+00	9.10E-02	4.20E+03	-
Li-ion (NMC811)	8.35E+00	9.74E-02	4.49E+03	-
Primary- electricity				
	CH4 (gram/kg battery)	N2O (gram/kg battery)	CO2 (gram/kg battery)	electricity (kWh/kg battery)
Lead-Acid	3.70E+00	0.00E+00	7.40E+02	0.00E+00
Ni-MH	4.80E+00	7.60E-02	2.00E+03	8.90E+00
Li-ion (NMC622)	9.40E+00	1.10E-01	5.10E+03	2.30E+01
Li-ion (NMC811)	1.01E+01	1.18E-01	5.46E+03	2.46E+01
Secondary- electricity				
	CH4 (gram/kg battery)	N2O (gram/kg battery)	CO2 (gram/kg battery)	electricity (kWh/kg battery)
Lead-Acid	3.10E+00	1.40E-02	6.20E+02	4.20E+00
Li-ion (NMC622)	3.30E+00	3.90E-02	1.80E+03	8.50E+00
Li-ion (NMC811)	3.53E+00	4.17E-02	1.93E+03	9.10E+00

### A.3.4 Life cycle emissions of vehicle

Combining above vehicle material composition, production, use and disposal energy data with material and fuel emissions factors, we can estimate the life cycle emissions of all vehicles at each year of its life cycle. Figure A.37-39 shows the per-vehicle life cycle emissions of all powertrains.

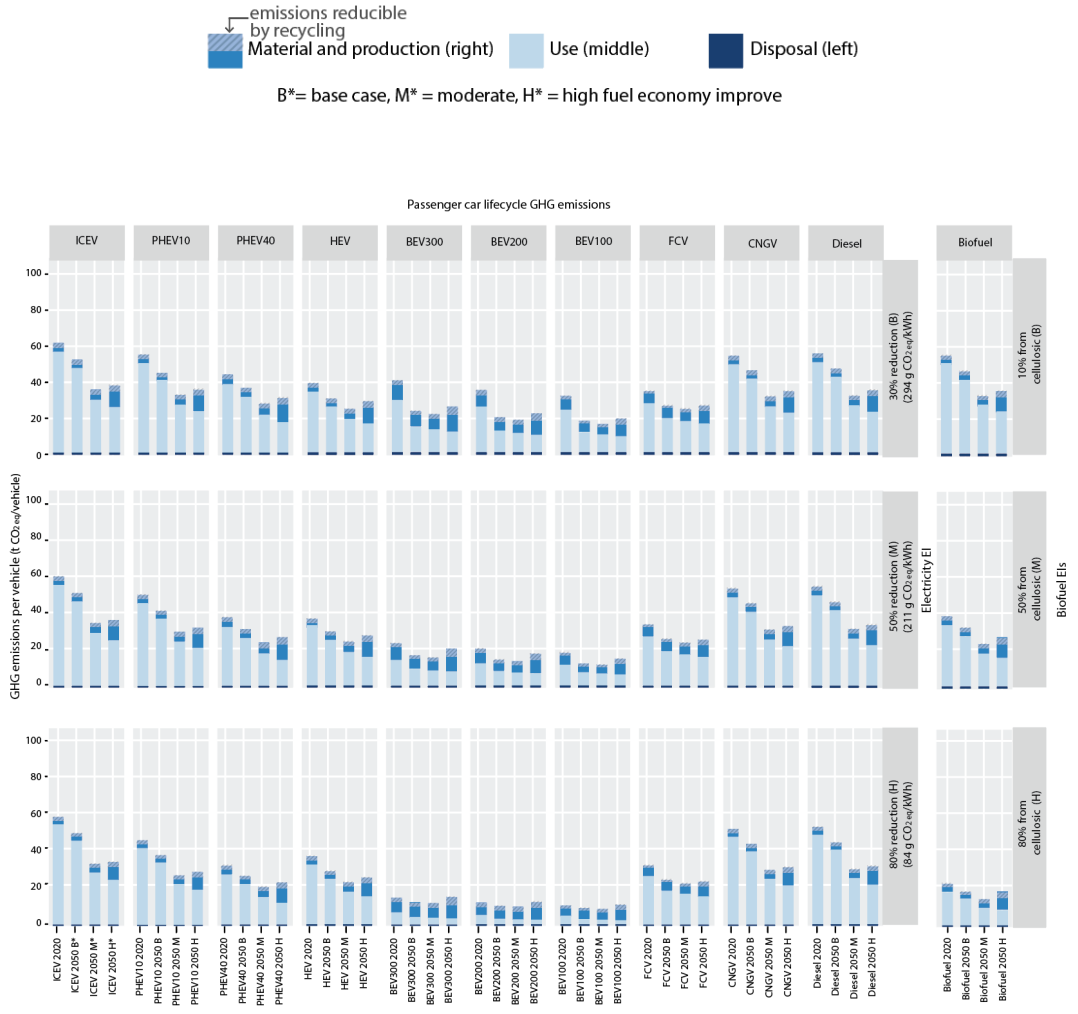
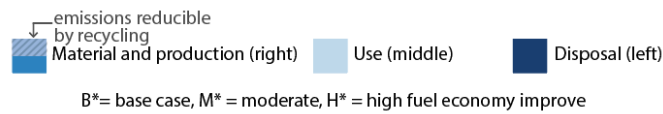


Figure A.37: Life cycle GHG emissions for passenger car simulated using base case vehicle lifespans and electricity GHG intensities that are constant throughout the life cycle. The hatched area represents the emissions that could theoretically be reduced if the recycled contents of all vehicle materials increase to 90%.



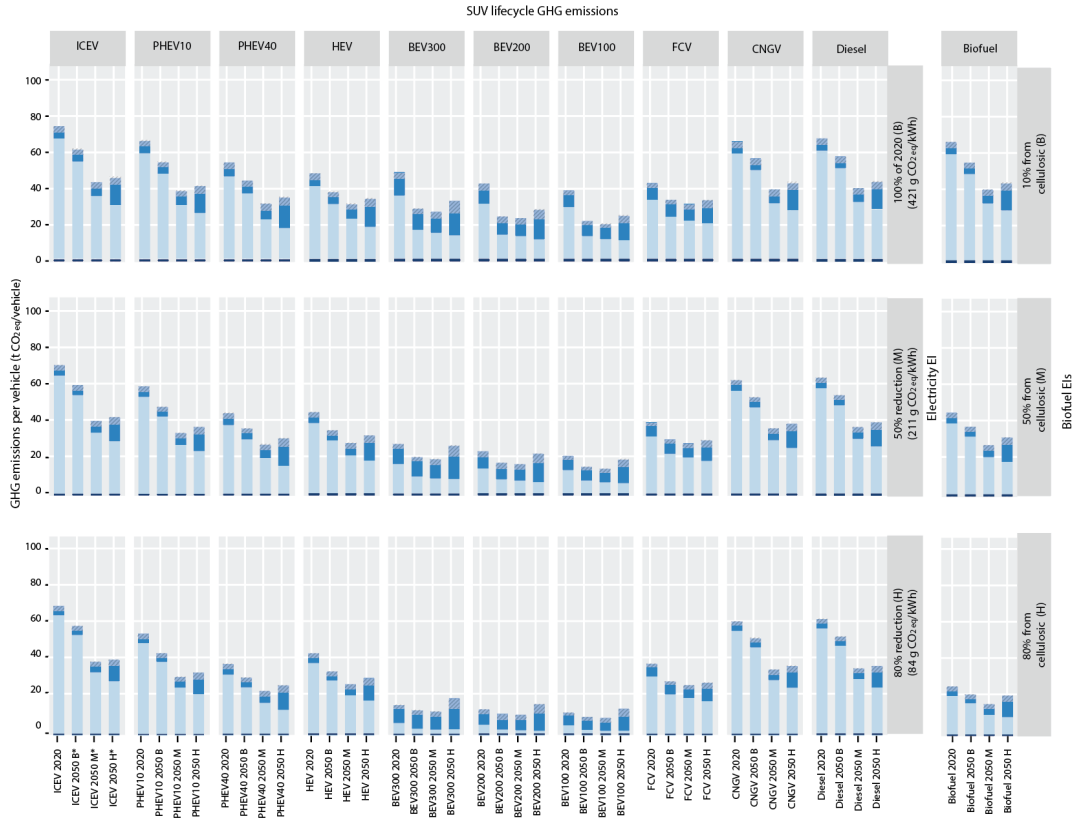


Figure A.38: Life cycle GHG emissions for SUV simulated using base case vehicle lifespans and electricity GHG intensities that are constant throughout the life cycle. The hatched area represents the emissions that could theoretically be reduced if the recycled contents of all vehicle materials increase to 90%.

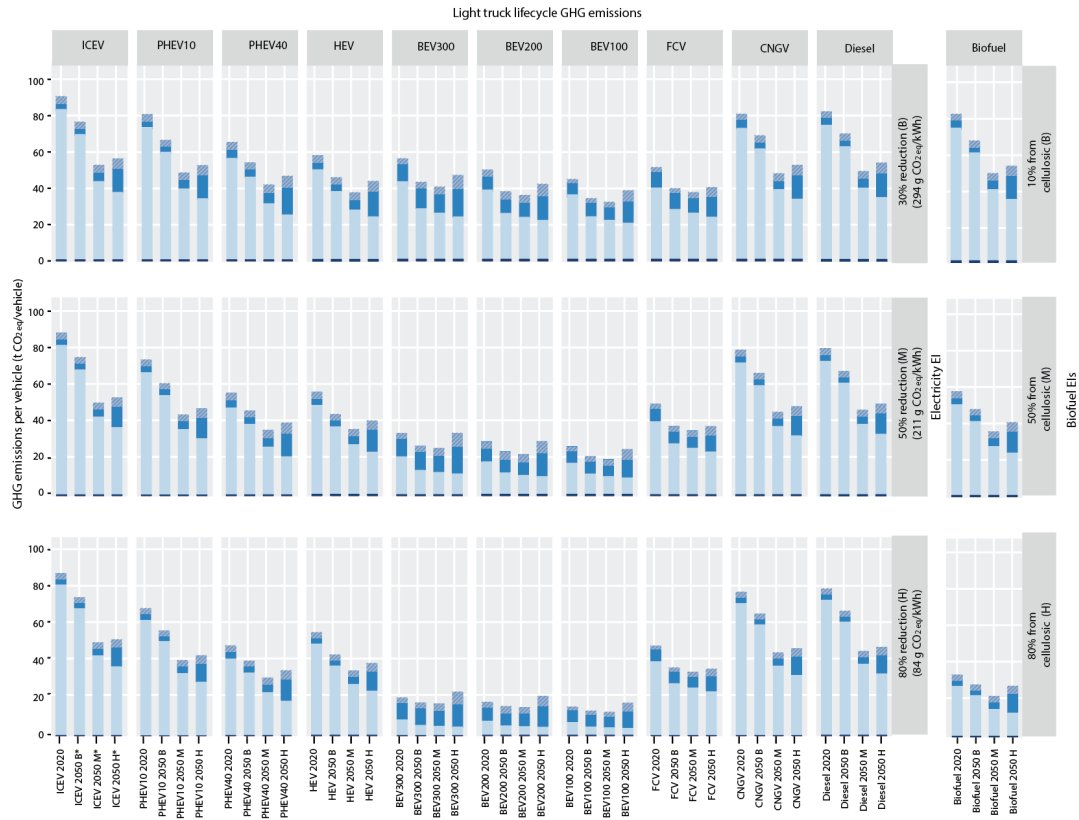


Figure A.39: Life cycle GHG emissions for light truck simulated using base case vehicle lifespans and electricity GHG intensities that are constant throughout the life cycle. The hatched area represents the emissions that could theoretically be reduced if the recycled contents of all vehicle materials increase to 90%.

## A.4 Simulation results

This section summarizes the detailed emissions results in the simulated pathways.

### A.4.1 Pathway summary

In this analysis, we simulated 1512 future pathways. Table A.13 summarizes all the vehicle technology scenarios and electricity emissions scenarios in the simulative pathways.

Table A.17: Summary of vehicle life cycle parameters, vehicle technology scenarios and electricity emissions scenarios in the stimulated pathways

	Vehicle life cycle parameters				Vehicle technology	Electricity emissions
	Vehicle travel demand	Sales ratio of vehicle powertrains	Vehicle lifespans	Recycling rates	scenario	scenarios
Level 1	Base case (+0.7%/year)	Base case (EIA, 2020 deployment)	Base case (Liao et al., 2021)	Base case constant EOL RR	Base case	Base case 30% EIS reduction
Level 2	Low growth (+0.1%/year)	Flex fuel biofuel vehicles 100% by 2050	ICEVs retire at age 20 and older	High (Increase linearly from current EOL RR to 90% by 2050)	Moderate	50% EIS reduction
Level 3	High growth (+1%/year)	PHEV40s 100% by 2050	ICEVs retire at age 10 and older	-	High	80% EIS reduction
Level 4	-	HEVs 100% by 2050	-	-	-	-
Level 5	-	BEV300s 100% by 2050	-	-	-	-
Level 6	-	BEV300s 100% by 2040	-	-	-	-
Level 7	-	BEV300s 100% by 2030	-	-	-	-

#### A.4.2 Additional results: cumulative emissions and temperature wedge plot

Figure A.40 shows the annual emissions results in the BAU pathway, moderate and high fuel economy pathways (the rest of the parameters and scenario assumptions are the same as the BAU pathway).

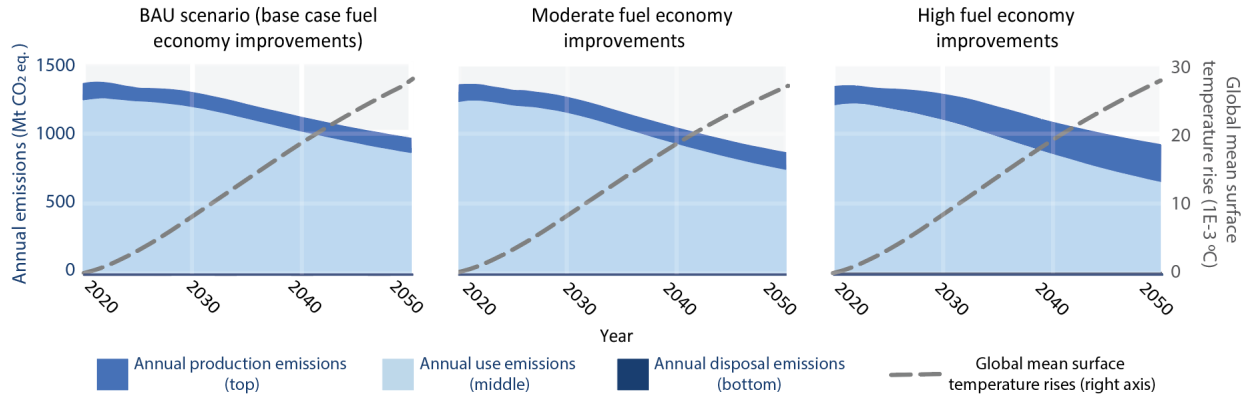


Figure A.40: (Left) Annual U.S. LDV emissions for the BAU pathway. (Middle) Annual U.S. LDV emissions for the moderate (fuel economy improvement) vehicle technology scenario (all other scenarios and parameter value being base case). (Right) Annual U.S. LDV emissions for the high (fuel economy improvement) vehicle technology scenario (all other scenarios and parameter values being base case)

Figure A.41 shows the lower bound, base case and upper bound emissions pathways in Figure 2.1. Table A.14 summarizes the life cycle parameters, vehicle technology scenarios and electricity emissions scenarios correspond to the low, base case and upper bound emission pathways.



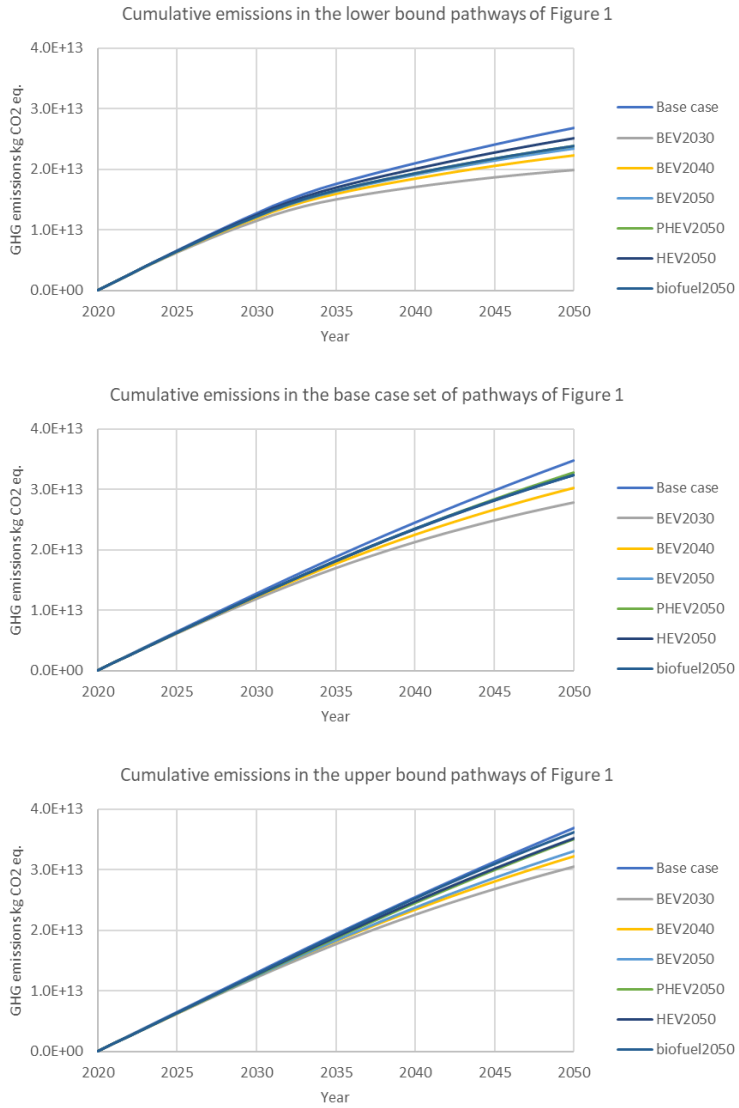


Figure A.41: The lower bound, base case and upper bound set of scenarios shown in Figure 1 of the main manuscript.

Table A.15 shows the cumulative emissions breakdown by gas species and vehicle size class in the above emission pathways.

Table A.18: Summary of pathway vehicle life cycle parameters, vehicle technology scenario and electricity emissions scenarios

		Vehicle life cycle parameters				Vehicle technology scenario	Electricity emissions scenarios
Dominant vehicle powertrains		Vehicle travel demand	Sales ratio of vehicle powertrains	Vehicle lifespans	Recycling rates	Fuel economy	Electricity emissions intensities
Base case	Lower bound	Low growth (+0.1%/year)	Base case (EIA, 2020 deployment)	ICEVs retire at age 10 and older	High (Increase linearly from current EOL RR to 90% by 2050)	Moderate	80% EIs reduction
	Base case	Base case (+0.7%/year)	Base case (EIA, 2020 deployment)	Base case (Liao et al., 2021)	Base case constant EOL RR	Base case	Base case
	Upper bound	High growth (+1%/year)	Base case (EIA, 2020 deployment)	Base case (Liao et al., 2021)	Base case constant EOL RR	High	Base case
BEV2030	Lower bound	Low growth (+0.1%/year)	BEV300s 100% by 2030	ICEVs retire at age 10 and older	High (Increase linearly from current EOL RR to 90% by 2050)	Moderate	80% EIs reduction
	Base case	Base case (+0.7%/year)	BEV300s 100% by 2030	Base case (Liao et al., 2021)	Base case constant EOL RR	Base case	Base case
	Upper bound	High growth (+1%/year)	BEV300s 100% by 2030	Base case (Liao et al., 2021)	Base case constant EOL RR	High	Base case
BEV2040	Lower bound	Low growth (+0.1%/year)	BEV300s 100% by 2040	ICEVs retire at age 10 and older	High (Increase linearly from current EOL RR to 90% by 2050)	Moderate	80% EIs reduction
	Base case	Base case (+0.7%/year)	BEV300s 100% by 2040	Base case (Liao et al., 2021)	Base case constant EOL RR	Base case	Base case
	Upper bound	High growth (+1%/year)	BEV300s 100% by 2040	Base case (Liao et al., 2021)	High (Increase linearly from current EOL RR to 90% by 2050)	High	Base case
BEV2050	Lower bound	Low growth (+0.1%/year)	BEV300s 100% by 2050	ICEVs retire at age 10 and older	High (Increase linearly from current EOL RR to 90% by 2050)	Moderate	80% EIs reduction
	Base case	Base case (+0.7%/year)	BEV300s 100% by 2050	Base case (Liao et al., 2021)	Base case constant EOL RR	Base case	Base case
	Upper bound	High growth (+1%/year)	BEV300s 100% by 2050	Base case (Liao et al., 2021)	Base case constant EOL RR	High	Base case

Table A.19: Summary of pathway vehicle life cycle parameters, vehicle technology scenario and electricity emissions scenarios (continued)

PHEV	Lower bound	Low growth (+0.1%/year)	PHEV40s 100% by 2050	ICEVs retire at age 10 and older	High (Increase linearly from current EOL RR to 90% by 2050)	Moderate	80% EIs reduction
	Base case	Base case (+0.7%/year)	PHEV40s 100% by 2050	Base case (Liao et al., 2021)	Base case constant EOL RR	Base case	Base case
	Upper bound	High growth (+1%/year)	PHEV40s 100% by 2050	Base case (Liao et al., 2021)	Base case constant EOL RR	High	Base case
HEV	Lower bound	Low growth (+0.1%/year)	HEVs 100% by 2050	ICEVs retire at age 10 and older	High (Increase linearly from current EOL RR to 90% by 2050)	Moderate	80% EIs reduction
	Base case	Base case (+0.7%/year)	HEVs 100% by 2050	Base case (Liao et al., 2021)	Base case constant EOL RR	Base case	Base case
	Upper bound	High growth (+1%/year)	HEVs 100% by 2050	Base case (Liao et al., 2021)	Base case constant EOL RR	High	Base case
Biofuel	Lower bound	Low growth (+0.1%/year)	Flex fuel biofuel vehicles 100% by 2050	ICEVs retire at age 10 and older	High (Increase linearly from current EOL RR to 90% by 2050)	Moderate	80% EIs reduction
	Base case	Base case (+0.7%/year)	Flex fuel biofuel vehicles 100% by 2050	Base case (Liao et al., 2021)	Base case constant EOL RR	Base case	Base case
	Upper bound	High growth (+1%/year)	Flex fuel biofuel vehicles 100% by 2050	Base case (Liao et al., 2021)	Base case constant EOL RR	High	Base case

Table A.20: Cumulative emissions equivalent breakdown

Cumulative emissions equivalent breakdown								
	CO2	CH4	N2O	Total	Passenger car	SUV	Light truck	Total
BAU	93.8%	5.5%	0.7%	100.0%	33%	46%	20%	100.0%
BEV2050	94.0%	5.3%	0.7%	100.0%	33%	46%	20%	100.0%
BEV2040	94.1%	5.3%	0.7%	100.0%	33%	46%	20%	100.0%
BEV2030	94.1%	5.3%	0.6%	100.0%	33%	46%	20%	100.0%
Biofuel2050	90.9%	5.3%	3.8%	100.0%	33%	46%	20%	100.0%
HEV2050	93.8%	5.5%	0.7%	100.0%	33%	46%	20%	100.0%
PHEV2050	93.9%	5.4%	0.7%	100.0%	33%	46%	20%	100.0%

Figure A.42 shows the global mean temperature rises corresponding to the U.S. LDVs.

Figure A.43 below shows the raw data for the cumulative emissions and temperature rises used to construct Figure 4 in the main manuscript.

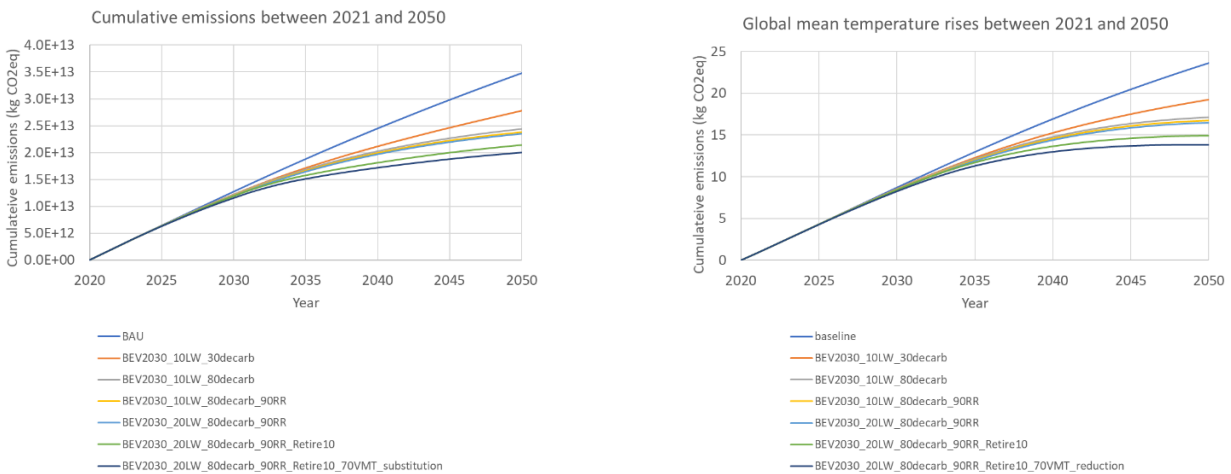
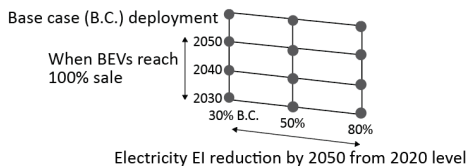
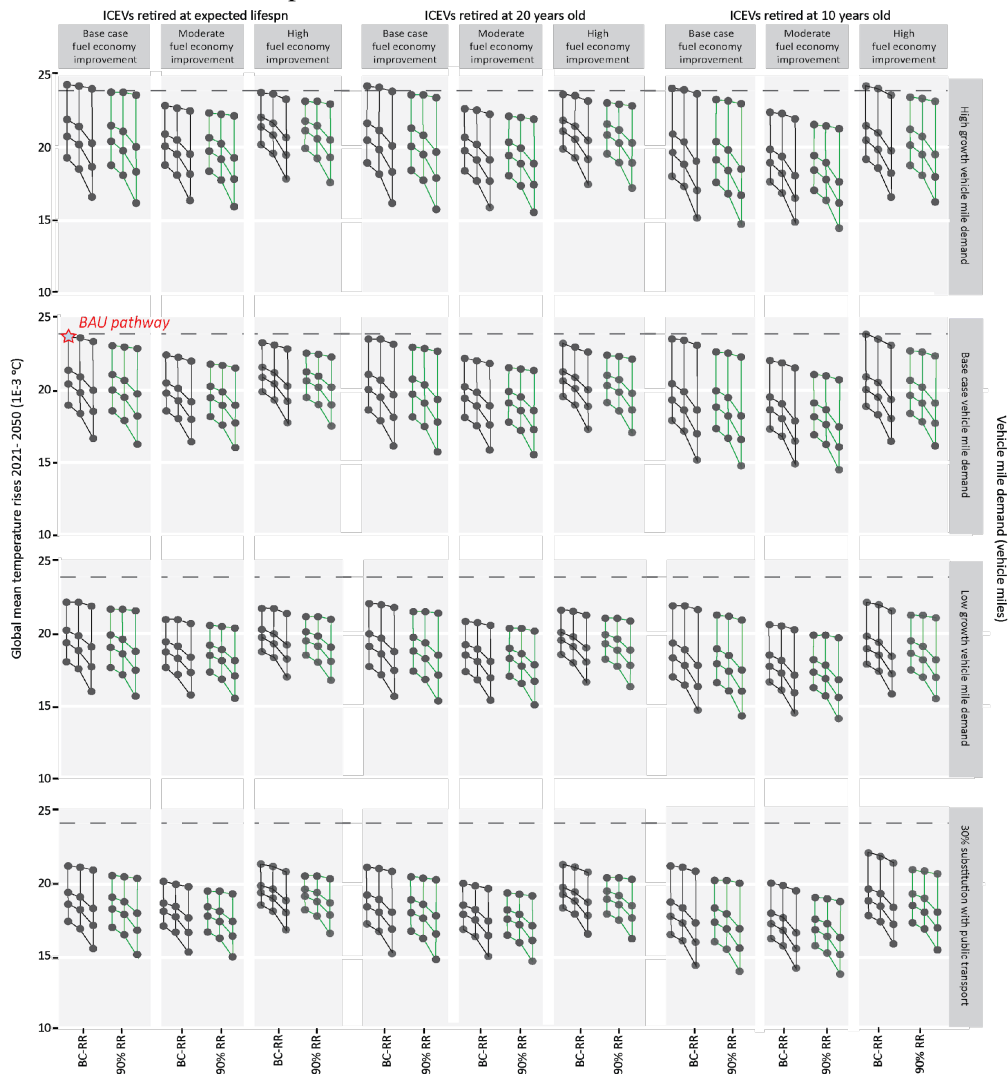


Figure A.43: Cumulative emissions and temperature rises corresponds to Figure 4 in the main manuscript.

Figure A.44 shows the separate impact of vehicle structural material recycling and battery recycling on 2021-2050 cumulative production emissions in the pathways that have BEV300 reach 100% of sales by 2030 and base case, moderate or high fuel economy improvements (that corresponds to 10%, 20% or 30% lightweighting by 2050).



(a) The horizontal position of a node on a flag corresponds to the Electricity emissions scenario and the vertical position of the node corresponds to the Sales share of alternative fuel vehicles.



(b) Global temperature attributable to U.S. LDVs.

Figure A.42: Global temperature rises for varying vehicle life cycle parameters, vehicle technology scenarios, and electricity emissions scenarios. The higher dashed horizontal lines refer to BAU temperature rises. BC-RR: base case recycling rates. 90% RR: 90% recycling rates. The numbered arrows correspond to the cumulative emissions wedge plot shown in Figure 4.

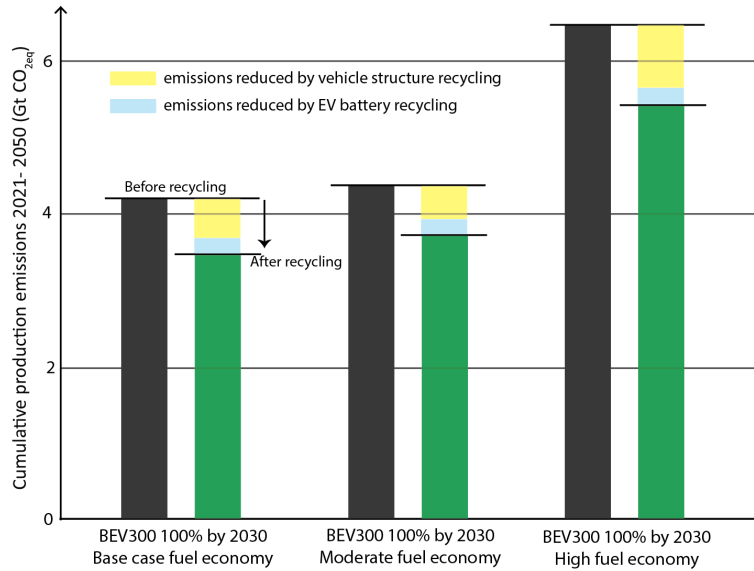


Figure A.44: Cumulative production emissions before and after recycling

### A.5 Reference:

[1] Emissions Database for Global Atmospheric Research (EDGAR ) Crippa, M., Oreggioni, G., Guizzardi, D., Muntean, M., Schaaf, E., Lo Vullo, E., Solazzo, E., Monforti-Ferrario, F., Olivier, J.G.J. and Vignati, E., 2019. Fossil CO<sub>2</sub> and GHG emissions of all world countries. Luxemburg: Publication Office of the European Union.

[2] EPA. 2020. Automotive trends report. Retrieved from: <https://www.epa.gov/automotive-trends>. Last accessed on May 15th, 2021.

[3] GREET, 2020. Argonne National Lab. Retrieved from: <https://greet.es.anl.gov/>. Last accessed on May 15th, 2021.

[4] EIA, 2021. Monthly Energy Review, Table 1.1. Last accessed on May 15th, 2021.

[5] Wagner, I. 2019. U.S. sales of domestic and imported light vehicles - by type 2016. Retrieved from: Statista.com. Last accessed on May 15th, 2021.

[6] BTU, 2016. Motor Vehicles Scrapped. <https://www.bts.gov/content/motor-vehicles-scrapped>. Last accessed on May 15th, 2021.

[7] National Research Council. (2005). Radiative Forcing of Climate Change: Expanding the Concept and Addressing Uncertainties. In *Radiative Forcing of Climate Change*. Washington, DC: The National Academies Press.

[8] Myhre, G., D. Shindell, F.-M. Bréon, W. Collins, J. Fuglestedt, J. Huang, D. Koch, J.-F. Lamarque, D. Lee, B. Mendoza, T. Nakajima, A. Robock, G. Stephens, T. Takemura and H. Zhang, 2013: Anthropogenic and Natural Radiative Forcing. In: *Climate Change 2013: The*

Physical Science Basis. Contribution of Working Group I to the Fifth Assessment Report of the Intergovernmental Panel on Climate Change [Stocker, T.F., D. Qin, G.-K. Plattner, M. Tignor, S.K. Allen, J. Boschung, A. Nauels, Y. Xia, V. Bex and P.M. Midgley (eds.)]. Cambridge University Press, Cambridge, United Kingdom and New York, NY, USA.

[9] Fuglestedt, J., Berntsen, T., Myhre, G., Rypdal, K., and Skeie, R. B. (2008). Climate forcing from the transport sectors. *Proc. Natl. Acad. Sci. U. S. A.*, 105(2), 454–458.

[10] Shine, K. P., Fuglestedt, J. S., Hailemariam, K., and Stuber, N. (2005). Alternatives to the Global Warming Potential for comparing climate impacts of emissions of greenhouse gases. *Clim. Change*, 68(3), 281–302.

[11] Joos, F., Roth, R., Fuglestedt, J.S., Peters, G.P., Enting, I.G., Bloh, W.V., Brovkin, V., Burke, E.J., Eby, M., Edwards, N.R. and Friedrich, T., 2013. Carbon dioxide and climate impulse response functions for the computation of greenhouse gas metrics: a multi-model analysis. *Atmospheric Chemistry and Physics*, 13(5), pp.2793-2825.

[12] Berntsen, T. and Fuglestedt, J., 2008. Global temperature responses to current emissions from the transport sectors. *Proceedings of the National Academy of Sciences*, 105(49), pp.19154-19159.

[13] Bauer, N., Rose, S.K., Fujimori, S., Van Vuuren, D.P., Weyant, J., Wise, M., Cui, Y., Daioglou, V., Gidden, M.J., Kato, E. and Kitous, A., 2018. Global energy sector emission reductions and bioenergy use: overview of the bioenergy demand phase of the EMF-33 model comparison. *Climatic Change*, pp.1-16.

[14] Kumar, V., Sharma, A., Soni, J.K. and Pawar, N., 2017. Physiological response of C3, C4 and CAM plants in changeable climate. *The Pharma Innovation*, 6(9, Part B), p.70.

[15] Karstensen, J., Peters, G.P. and Andrew, R.M., 2015. Uncertainty in temperature response of current consumption-based emissions estimates. *Earth System Dynamics*, 6(1), pp.287-309.

[16] IPCC, 2018: Global Warming of 1.5°C. An IPCC Special Report on the impacts of global warming of 1.5°C above pre-industrial levels and related global greenhouse gas emission pathways, in the context of strengthening the global response to the threat of climate change, sustainable development, and efforts to eradicate poverty [Masson-Delmotte, V., P. Zhai, H.-O. Pörtner, D. Roberts, J. Skea, P.R. Shukla, A. Pirani, W. Moufouma-Okia, C. Péan, R. Pidcock, S. Connors, J.B.R. Matthews, Y. Chen, X. Zhou, M.I. Gomis, E. Lonnoy, T. Maycock, M. Tignor, and T. Waterfield (eds.)]. In Press.

[17] EPA. 2020. Automotive trends report.

[18] Fuel Flex kit. N.d. Retrieved on January, 15th., 2021.

[19] Liao, Jiankan., Zhu, Yongxian., Cooper, R. Daniel., 2021. Reducing emissions by using products more intensively. *Journal of Industrial Ecology* (Submitted).

[20] EIA, 2019. Annual Energy Outlook 2020. Energy Information Administration, Washington,

DC. Retrieved from: <https://www.eia.gov/outlooks/aeo/>.

[21] EIA, 2020. Annual Energy Outlook 2020. Energy Information Administration, Washington, DC. Retrieved from: <https://www.eia.gov/outlooks/aeo/>.

[22] FHWA. (2018). FHWA Forecasts of Vehicle Miles Traveled (VMT): Spring 2018.

[23] EPA and NHTSA. 2016. Interim Joint Technical Assessment Report: Light-Duty Vehicle Greenhouse Gas Emission Standards and Corporate Average Fuel Economy Standards for Model Years 2017-2025. Table E1.5-1.

[24] Replogle, M.A. and Fulton, L.M., 2014. A global high shift scenario: impacts and potential for more public transport, walking, and cycling with lower car use.

[25] Wang, T., Jiang, Z., Zhao, B., Gu, Y., Liou, K.N., Kalandiyur, N., Zhang, D. and Zhu, Y., 2020. Health co-benefits of achieving sustainable net-zero greenhouse gas emissions in California. *Nature Sustainability*, pp.1-9.

[26] BTU, 2017. Vehicle Occupancy Per Vehicle Mile by Daily Trip Purpose. Last accessed on May 15th, 2021.

[27] Buehler, R. and Pucher, J., 2011. Sustainable transport in Freiburg: lessons from Germany's environmental capital. *International Journal of Sustainable Transportation*, 5(1), pp.43-70.

[28] FHWA. 2018. FHWA Forecasts of Vehicle Miles Traveled (VMT): Spring 2018.

[29] Alexandrou, A., Tenbergen, K. and Adhikari, D., 2013. Energy balance of a typical US diet. *Foods*, 2(2), pp.132-142.

[30] Higgins, P.A., 2005. Exercise-based transportation reduces oil dependence, carbon emissions and obesity. *Environmental Conservation*, pp.197-202.

[31] Logan, K.G., Nelson, J.D. and Hastings, A., 2020. Electric and hydrogen buses: Shifting from conventionally fuelled cars in the UK. *Transportation Research Part D: Transport and Environment*, 85, p.102350.

[32] Chester, M.V. and Cano, A., 2016. Time-based life-cycle assessment for environmental policymaking: Greenhouse gas reduction goals and public transit. *Transportation Research Part D: Transport and Environment*, 43, pp.49-58.

[33] Chan, S., Miranda-Moreno, L.F., Alam, A. and Hatzopoulou, M., 2013. Assessing the impact of bus technology on greenhouse gas emissions along a major corridor: A lifecycle analysis. *Transportation Research Part D: Transport and Environment*, 20, pp.7-11.

[34] McCollum, D. and Yang, C., 2009. Achieving deep reductions in US transport greenhouse gas emissions: Scenario analysis and policy implications. *Energy Policy*, 37(12), pp.5580-5596.

[35] Keoleian, G. A., and Sullivan, J. L. (2012). Materials challenges and opportunities for enhancing the sustainability of automobiles. *MRS Bull.*, 37(4), 365–372.

[36] ISO 14040:2006. Environmental management — Life cycle assessment — Principles and framework.



[37] Argonne National Laboratory, 2020. GREET Model (<http://greet.es.anl.gov/>). Last Accessed: March 15th, 2021.

[38] Hawkins, T. R., Gausen, O. M., and Stromman, A. H. (2012). Environmental impacts of hybrid and electric vehicles-a review. *Int. J. Life Cycle Assess.*, 17, 997–1014.

[39] Hawkins, T. R., Singh, B., Majeau-Bettez, G., and Strømman, A. H. (2013). Comparative Environmental Life Cycle Assessment of Conventional and Electric Vehicles. *J. Ind. Ecol.*

[40] Lewis, A. M., Kelly, J. C., and Keoleian, G. A. (2014). Vehicle lightweighting vs. electrification: Life cycle energy and GHG emissions results for diverse powertrain vehicles. *Appl. Energy*, 126, 13–20.

[41] Ma, H., Balthasar, F., Tait, N., Riera-Palou, X., and Harrison, A. (2012). A new comparison between the life cycle greenhouse gas emissions of battery electric vehicles and internal combustion vehicles. *Energy Policy*, 44, 160–173.

[42] Majeau-Bettez, G., Hawkins, T. R., and Strømman, A. H. (2011). Life Cycle Environmental Assessment of Lithium-Ion and Nickel Metal Hydride Batteries for Plug-In Hybrid and Battery Electric Vehicles. *Environ. Sci. Technol.*, 45(10), 4548–4554.

[43] Palazzo, J., and Geyer, R. 2019. Consequential life cycle assessment of automotive material substitution: Replacing steel with aluminum in production of north American vehicles. *Environ. Impact Assess. Rev.*, 75, 47–58.

[44] Samaras, C., Meisterling, A., and Meisterling, K. (2008). Life Cycle Assessment of Greenhouse Gas Emissions from Plug-in Hybrid Vehicles: Implications for Policy. *Environ. Sci. Technol.*, 42(9), 3170–3176.

[45] Department of Energy (DOE). 2015. Quadrennial Technology Review 2015. <https://www.energy.gov/quadrennial-technology-review-2015>. Last Accessed: March 15th, 2021.

[46] Kim, H.J., Keoleian, G.A. and Skerlos, S.J., 2011. Economic assessment of greenhouse gas emissions reduction by vehicle lightweighting using aluminum and high-strength steel. *Journal of Industrial Ecology*, 15(1), pp.64-80.

[47] Kelly, J.C., Sullivan, J.L., Burnham, A. and Elgowainy, A., 2015. Impacts of vehicle weight reduction via material substitution on life-cycle greenhouse gas emissions. *Environmental science & technology*, 49(20), pp.12535-12542

[48] Milovanoff, A., Kim, H.C., De Kleine, R., Wallington, T.J., Posen, I.D. and MacLean, H.L., 2019. A Dynamic Fleet Model of US Light-Duty Vehicle Lightweighting and Associated Greenhouse Gas Emissions from 2016 to 2050. *Environmental science & technology*, 53(4), pp.2199-2208.

[49] Schmuch, R., Wagner, R., Hörpel, G., Placke, T. and Winter, M., 2018. Performance and cost of materials for lithium-based rechargeable automotive batteries. *Nature Energy*, 3(4), pp.267-278.

[50] Ding, Y., Cano, Z.P., Yu, A., Lu, J. and Chen, Z., 2019. Automotive Li-ion batteries: current status and future perspectives. *Electrochemical Energy Reviews*, 2(1), pp.1-28.

[51] Dunn, J. B., Gaines, L., Barnes, M., Wang, M., and Sullivan, J. 2012. Material and energy flows in the materials production, assembly, and end-of-life stages of the automotive lithium-ion battery life cycle.

[52] Harper, G., Sommerville, R., Kendrick, E., Driscoll, L., Slater, P., Stolkin, R., . . . Anderson, P. (2019). Recycling lithium-ion batteries from electric vehicles. *Nature*, 575(7781), 75–86.

[53] Ambrose, H., Kendall, A., Lozano, M., Wachche, S. and Fulton, L., 2020. Trends in life cycle greenhouse gas emissions of future light duty electric vehicles. *Transportation Research Part D: Transport and Environment*, 81, p.102287.

[54] USABC., 2020. Development of advanced high-performance batteries for electric vehicle (ev) applications request for proposal information (RFPI)

[55] Tyson, Madeline, Charlie Bloch. 2019. Breakthrough Batteries: Powering the Era of Clean Electrification. Rocky Mountain Institute. <http://www.rmi.org/breakthrough-batteries>

[56] Gallagher, K.G., Trask, S.E., Bauer, C., Woehrle, T., Lux, S.F., Tschetch, M., Lamp, P., Polzin, B.J., Ha, S., Long, B. and Wu, Q., 2015. Optimizing areal capacities through understanding the limitations of lithium-ion electrodes. *Journal of The Electrochemical Society*, 163(2), p.A138.

[57] Xu, J., Lin, F., Doeff, M.M. and Tong, W., 2017. A review of Ni-based layered oxides for rechargeable Li-ion batteries. *Journal of Materials Chemistry A*, 5(3), pp.874-901.

[58] Silvestri, L., Forcina, A., Arcese, G. and Bella, G., 2020. Recycling technologies of nickel–metal hydride batteries: An LCA based analysis. *Journal of Cleaner Production*, 273, p.123083.

[59] Ahmadi, S., Bathaee, S.M.T. and Hosseinpour, A.H., 2018. Improving fuel economy and performance of a fuel-cell hybrid electric vehicle (fuel-cell, battery, and ultra-capacitor) using optimized energy management strategy. *Energy Conversion and Management*, 160, pp.74-84.

[60] Grunditz, E., 2016. Design and assessment of battery electric vehicle powertrain, with respect to performance, energy consumption and electric motor thermal capability. Chalmers University of Technology.

[61] Shabbir, W. and Evangelou, S.A., 2014. Real-time control strategy to maximize hybrid electric vehicle powertrain efficiency. *Applied energy*, 135, pp.512-522.

[62] Thomas, J., 2014. Drive cycle powertrain efficiencies and trends derived from EPA vehicle dynamometer results. *SAE International Journal of Passenger Cars-Mechanical Systems*, 7(2014-01-2562), pp.1374-1384.

[63] Philips, P. and Megli, T., 2017. Powertrain efficiency in the US fleet on regulatory drive cycles and with advanced technologies. *SAE International Journal of Fuels and Lubricants*, 10(2), pp.537-555.

[64] Moawad, Ayman., Kim, Namdoo., Shidore, Neeraj., and Rousseau, Aymeric. 2016. Assessment of Vehicle Sizing, Energy Consumption and Cost Through Large Scale Simulation of Advanced Vehicle Technologies. United States.

[65] JRC, R.E., HASS, H., LARIVÉ, J.F., Jrc, L.L., Maas, H. and Rickeard, D., 2014. WELL-TO-WHEELS Report Version 4. a JEC WELL-TO-WHEELS ANALYSIS. Institute for Energy and Transport, Joint Research Centre, Luxembourg: Publications Office of the European Union, 2014.

[66] Cheah, L.W., 2010. Cars on a diet: the material and energy impacts of passenger vehicle weight reduction in the US (Doctoral dissertation, Massachusetts Institute of Technology).

[67] EPA. 2020. Lifecycle Greenhouse Gas Results. Retrieved from:<https://www.epa.gov/fuels-registration-reporting-and-compliance-help/lifecycle-greenhouse-gas-results>.

[68] Cochran, J., Denholm, P., Speer, B. and Miller, M., 2015. Grid integration and the carrying capacity of the US grid to incorporate variable renewable energy (No. NREL/TP-6A20-62607). National Renewable Energy Lab.(NREL), Golden, CO (United States).

[69] Heard, B.P., Brook, B.W., Wigley, T.M. and Bradshaw, C.J., 2017. Burden of proof: A comprehensive review of the feasibility of 100% renewable-electricity systems. *Renewable and Sustainable Energy Reviews*, 76, pp.1122-1133.

[70] Connolly, D., Lund, H., Mathiesen, B.V. and Leahy, M., 2011. The first step towards a 100% renewable energy-system for Ireland. *Applied Energy*, 88(2), pp.502-507.

[71] Ashby, M.F. and Cebon, D., 1993. Materials selection in mechanical design. *Le Journal de Physique IV*, 3(C7), pp.C7-1.

[72] Masson-Delmotte, V., Zhai, P., Pörtner, H.O., Roberts, D., Skea, J., Shukla, P.R., Pirani, A., Moufouma-Okia, W., Péan, C., Pidcock, R. and Connors, S., 2018. Global warming of 1.5 C. An IPCC Special Report on the impacts of global warming of, 1, pp.1-9.

[73] Hawkins, T.R., Singh, B., Majeau-Bettez, G. and Strømman, A.H., 2013. Comparative environmental life cycle assessment of conventional and electric vehicles. *Journal of Industrial Ecology*, 17(1), pp.53-64.

[74] Bauer, C., Hofer, J., Althaus, H.J., Del Duce, A. and Simons, A., 2015. The environmental performance of current and future passenger vehicles: Life cycle assessment based on a novel scenario analysis framework. *Applied energy*, 157, pp.871-883.

[75] Messagie, M., Boureima, F.S., Coosemans, T., Macharis, C. and Mierlo, J.V., 2014. A range-based vehicle life cycle assessment incorporating variability in the environmental assessment of different vehicle technologies and fuels. *Energies*, 7(3), pp.1467-1482.

[76] Ma, H., Balthasar, F., Tait, N., Riera-Palou, X. and Harrison, A., 2012. A new comparison between the life cycle greenhouse gas emissions of battery electric vehicles and internal combustion vehicles. *Energy policy*, 44, pp.160-173.

[77] EPA and NHTSA. 2016. Interim Joint Technical Assessment Report: Light-Duty Vehicle

Greenhouse Gas Emission Standards and Corporate Average Fuel Economy Standards for Model Years 2017-2025. Table E1.5-1.

[78] Farrington, R. and Rugh, J., 2000. Impact of vehicle air-conditioning on fuel economy, tailpipe emissions, and electric vehicle range (No. NREL/CP-540-28960). National Renewable Energy Lab., Golden, CO (US).

[79] Wolfram, P., Tu, Q., Heeren, N., Pauliuk, S. and Hertwich, E.G., 2020. Material efficiency and climate change mitigation of passenger vehicles. *Journal of Industrial Ecology*.

[80] Heywood, J., MacKenzie, D., Akerlind, I.B., Bastani, P., Berry, I., Bhatt, K., Chao, A., Chow, E., Karplus, V., Keith, D. and Khusid, M., 2015. On the road toward 2050: Potential for substantial reductions in light-duty vehicle energy use and greenhouse gas emissions. Massachusetts Institute of Technology Sloan Automotive Laboratory, Engineering System Division.

[81] Kim, H.J., Keoleian, G.A. and Skerlos, S.J., 2011. Economic assessment of greenhouse gas emissions reduction by vehicle lightweighting using aluminum and high-strength steel. *Journal of Industrial Ecology*, 15(1), pp.64-80.

[82] Luk, J.M., Kim, H.C., De Kleine, R., Wallington, T.J. and MacLean, H.L., 2017. Review of the fuel saving, life cycle GHG emission, and ownership cost impacts of lightweighting vehicles with different powertrains. *Environmental science & technology*, 51(15), pp.8215-8228.

[83] Black, F.M., High, L.E. and Lang, J.M., 1980. Composition of automobile evaporative and tailpipe hydrocarbon emissions. *Journal of the Air Pollution Control Association*, 30(11), pp.1216-1220.

[84] Greene, D.L. and DeCicco, J., 2000. Engineering-economic analyses of automotive fuel economy potential in the United States. *Annual Review of Energy and the Environment*, 25(1), pp.477-535.

[85] Javid, R.J. and Nejat, A., 2017. A comprehensive model of regional electric vehicle adoption and penetration. *Transport Policy*, 54, pp.30-42. [86] Mayyas, A., Omar, M., Hayajneh, M. and Mayyas, A.R., 2017. Vehicle's lightweight design vs. electrification from life cycle assessment perspective. *Journal of Cleaner Production*, 167, pp.687-701.

[87] Miotti, M., Supran, G.J., Kim, E.J. and Trancik, J.E., 2016. Personal vehicles evaluated against climate change mitigation targets. *Environmental science & technology*, 50(20), pp.10795-10804.

[88] NHTSA and EPA, 2020. Corporate Average Fuel Economy. Retrieved on June, 20th, 2020. <https://www.nhtsa.gov/laws-regulations/corporate-average-fuel-economy>. Last Accessed: March 15th, 2021.

[89] California Air Resources Board, 2017. Advanced Clean Cars Program. Retrieved on June, 20th, 2020. <https://ww2.arb.ca.gov/our-work/programs/advanced-clean-cars-program/about>. Last Accessed: March 15th, 2021.

- [90] Vermont Department of Environmental Conservation, 2020. ZERO EMISSION VEHICLES.
- [91] McCollum, D. and Yang, C., 2009. Achieving deep reductions in US transport greenhouse gas emissions: Scenario analysis and policy implications. *Energy Policy*, 37(12), pp.5580-5596.
- [92] Greene, D.L., Park, S. and Liu, C., 2014. Public policy and the transition to electric drive vehicles in the US: The role of the zero emission vehicles mandates. *Energy Strategy Reviews*, 5, pp.66-77.
- [93] Bastani, P., Heywood, J.B. and Hope, C., 2012. The effect of uncertainty on US transport-related GHG emissions and fuel consumption out to 2050. *Transportation Research Part A: Policy and Practice*, 46(3), pp.517-548.
- [94] Replogle, M.A. and Fulton, L.M., 2014. A global high shift scenario: impacts and potential for more public transport, walking, and cycling with lower car use.
- [95] Supekar, S.D. and Skerlos, S.J., 2017. Analysis of costs and time frame for reducing CO2 emissions by 70% in the US auto and energy sectors by 2050. *Environmental science & technology*, 51(19), pp.10932-10942.
- [96] Zhu, Y., Chappuis, L.B., De Kleine, R., Kim, H.C., Wallington, T.J., Luckey, G. and Cooper, D.R. 2020 The coming wave of aluminum sheet scrap from vehicle recycling in the United States. *Resources, Conservation and Recycling*, 164, p.105208.
- [97] Kelly, J.C., Sullivan, J.L., Burnham, A. and Elgowainy, A., 2015. Impacts of vehicle weight reduction via material substitution on life-cycle greenhouse gas emissions. *Environmental science & technology*, 49(20), pp.12535-12542.
- [98] Elgowainy, A., Han, J., Ward, J., Joseck, F., Gohlke, D., Lindauer, A., Ramsden, T., Bidy, M., Alexander, M., Barnhart, S. and Sutherland, I., 2018. Current and future United States light-duty vehicle pathways: Cradle-to-grave lifecycle greenhouse gas emissions and economic assessment. *Environmental science & technology*, 52(4), pp.2392-2399.
- [99] Ellingsen, L.A.W., Singh, B. and Strømman, A.H., 2016. The size and range effect: lifecycle greenhouse gas emissions of electric vehicles. *Environmental Research Letters*, 11(5), p.054010.
- [100] Karabasoglu, O. and Michalek, J., 2013. Influence of driving patterns on life cycle cost and emissions of hybrid and plug-in electric vehicle powertrains. *Energy policy*, 60, pp.445-461.
- [101] Lewis, A.M., Kelly, J.C. and Keoleian, G.A., 2014. Vehicle lightweighting vs. electrification: life cycle energy and GHG emissions results for diverse powertrain vehicles. *Applied Energy*, 126, pp.13-20.
- [102] Majeau-Bettez, G., Hawkins, T.R. and Strømman, A.H., 2011. Life cycle environmental assessment of lithium-ion and nickel metal hydride batteries for plug-in hybrid and battery electric vehicles. *Environmental science & technology*, 45(10), pp.4548-4554.
- [103] Dai, Q., Kelly, J.C., Gaines, L. and Wang, M., 2019. Life cycle analysis of lithium-ion batteries for automotive applications. *Batteries*, 5(2), p.48.

[104] Harper, G., Sommerville, R., Kendrick, E., Driscoll, L., Slater, P., Stolkin, R., Walton, A., Christensen, P., Heidrich, O., Lambert, S. and Abbott, A., 2019. Recycling lithium-ion batteries from electric vehicles. *Nature*, 575(7781), pp.75-86.

[105] Ciez, R.E. and Whitacre, J.F., 2019. Examining different recycling processes for lithium-ion batteries. *Nature Sustainability*, 2(2), pp.148-156.

[106] Field, F., Kirchain, R., and Clark, J., 2000. Life-Cycle Assessment and Temporal Distributions of Emissions Developing a Fleet-Based Analysis (Vol. 4).

[107] Kim, H.-J. J., McMillan, C., Keoleian, G. A., and Skerlos, S. J., 2010. Greenhouse Gas Emissions Payback for Lightweighted Vehicles Using Aluminum and High-Strength Steel. *Journal of Industrial Ecology*, 14(6), 929–946.

[108] Zhu, Y., Skerlos, S., Xu, M. and Cooper, D.R., 2020. System level impediments to achieving absolute sustainability using LCA. *Procedia CIRP*, 90, pp.399-404.

[109] Sutherland, J.W., Skerlos, S.J., Haapala, K.R., Cooper, D., Zhao, F. and Huang, A., 2020. Industrial Sustainability: Reviewing the Past and Envisioning the Future. *Journal of Manufacturing Science and Engineering*, 142(11).

[110] Sterner, E.O. and Johansson, D.J., 2017. The effect of climate–carbon cycle feedbacks on emission metrics. *Environmental Research Letters*, 12(3), p.034019.

[111] Argonne National Laboratory, 2020. GREET Model (<http://greet.es.anl.gov/>). Last Accessed: March 15th, 2021.

[112] Onat, N.C., Kucukvar, M., Tatari, O. and Egilmez, G., 2016. Integration of system dynamics approach toward deepening and broadening the life cycle sustainability assessment framework: a case for electric vehicles. *The International Journal of Life Cycle Assessment*, 21(7), pp.1009-1034.

[113] Milovanoff, A., Kim, H.C., De Kleine, R., Wallington, T.J., Posen, I.D. and MacLean, H.L., 2019. A Dynamic Fleet Model of US Light-Duty Vehicle Lightweighting and Associated Greenhouse Gas Emissions from 2016 to 2050. *Environmental science & technology*, 53(4), pp.2199-2208.

[114] Milovanoff, A., Posen, I.D. and MacLean, H.L., 2020. Electrification of light-duty vehicle fleet alone will not meet mitigation targets. *Nature Climate Change*, 10(12), pp.1102-1107.

[115] Allwood, J.M., Cullen, J.M. and Milford, R.L., 2010. Options for achieving a 50% cut in industrial carbon emissions by 2050. *Environmental science & technology*, 44 (6), pp.1888-1894.

[116] Modaresi, R., Pauliuk, S., Løvik, A.N. and Muller, D.B., 2014. Global carbon benefits of material substitution in passenger cars until 2050 and the impact on the steel and aluminum industries. *Environmental science & technology*, 48(18), pp.10776-10784.

[117] Serrenho, A.C., Norman, J.B. and Allwood, J.M., 2017. The impact of reducing car weight on global emissions: the future fleet in Great Britain. *Philosophical Transactions of the Royal*

Society A: Mathematical, Physical and Engineering Sciences, 375(2095), p.20160364.

[118] U.S. EPA. 2020. Automotive trends report. Supplemental Table E. Detailed Real-World Fuel Economy, CO2 Emissions, and Vehicle Attribute and Technology Data.

[119] Levasseur, A., Cavalett, O., Fuglestvedt, J.S., Gasser, T., Johansson, D.J., Jørgensen, S.V., Raugei, M., Reisinger, A., Schivley, G., Strømman, A. and Tanaka, K., 2016. Enhancing life cycle impact assessment from climate science: Review of recent findings and recommendations for application to LCA. *Ecological Indicators*, 71, pp.163-174.

[120] Fuel Flex kit. N.d. Retrieved on January, 15th., 2021.

[121] U.S. EIA, 2020. Annual Energy Outlook. Table 38. Light-Duty Vehicle Sales by Technology Type. Last Accessed: March 15th, 2021.

[122] Liao, Jiankan., Zhu, Yongxian., Cooper, R. Daniel., 2021. Reducing emissions by using products more intensively. *Journal of Industrial Ecology* (Submitted)

[123] Federal Highway Administration (FHWA)., 1969-2019. Traffic Volume Trends. Highway Statistics. Last Accessed: March 15th, 2021.

[124] FHWA. 2018. FHWA Forecasts of Vehicle Miles Traveled (VMT): Spring 2018. Last Accessed: March 15th, 2021.

[125] Sager, J., Apte, J.S., Lemoine, D.M. and Kammen, D.M., 2011. Reduce growth rate of light-duty vehicle travel to meet 2050 global climate goals. *Environmental Research Letters*, 6(2), p.024018.

[126] Chester, M.V. and Cano, A., 2016. Time-based life-cycle assessment for environmental policymaking: Greenhouse gas reduction goals and public transit. *Transportation Research Part D: Transport and Environment*, 43, pp.49-58.

[127] Chan, S., Miranda-Moreno, L.F., Alam, A. and Hatzopoulou, M., 2013. Assessing the impact of bus technology on greenhouse gas emissions along a major corridor: A lifecycle analysis. *Transportation Research Part D: Transport and Environment*, 20, pp.7-11.

[128] Logan, K.G., Nelson, J.D. and Hastings, A., 2020. Electric and hydrogen buses: Shifting from conventionally fuelled cars in the UK. *Transportation Research Part D: Transport and Environment*, 85, p.102350.

[129] Greenblatt, J.B. and Saxena, S., 2015. Autonomous taxis could greatly reduce greenhouse-gas emissions of US light-duty vehicles. *Nature Climate Change*, 5(9), pp.860-863.

[130] Kopelias, P., Demiridi, E., Vogiatzis, K., Skabardonis, A. and Zafiropoulou, V., 2020. Connected and autonomous vehicles—Environmental impacts—A review. *Science of the total environment*, 712, p.135237.

[131] Fagnant, D.J. and Kockelman, K.M., 2014. The travel and environmental implications of shared autonomous vehicles, using agent-based model scenarios. *Transportation Research Part C: Emerging Technologies*, 40, pp.1-13.

[132] Harper, C.D., Hendrickson, C.T., Mangones, S. and Samaras, C., 2016. Estimating potential increases in travel with autonomous vehicles for the non-driving, elderly and people with travel-restrictive medical conditions. *Transportation research part C: emerging technologies*, 72, pp.1-9.

[133] Miller, S.A. and Heard, B.R., 2016. The environmental impact of autonomous vehicles depends on adoption patterns.

[134] Taiebat, M., Brown, A.L., Safford, H.R., Qu, S. and Xu, M., 2018. A review on energy, environmental, and sustainability implications of connected and automated vehicles. *Environmental science & technology*, 52(20), pp.11449-11465.

[135] Transportation Research Center at Argonne National Laboratory. 2020. Light Duty Electric Drive Vehicles Monthly Sales Updates.

[136] Van Haaren, Rob. 2011. "Assessment of electric cars' range requirements and usage patterns based on driving behavior recorded in the National Household Travel Survey of 2009." *Earth and Environmental Engineering Department, Columbia University, Fu Foundation School of Engineering and Applied Science, New York* 51 (2011): 53.

[137] Accenture. 2011. Plug-in electric vehicles Changing perceptions, hedging bets. Accenture end-consumer survey on the electrification of private transport.

[138] Office of Governor Gavin Newsom. 2020. Governor Newsom Announces California Will Phase Out Gasoline-Powered Cars and Drastically Reduce Demand for Fossil Fuel in California's Fight Against Climate Change. Last Accessed: March 15th, 2021.

[139] Norwegian EV policy. Norway is leading the way for a transition to zero emission in transport. <https://elbil.no/english/norwegian-ev-policy/>. Last Accessed: March 15th, 2021.

[140] Twidale, Susanna., 2020. Britain to ban new petrol cars by 2030 on road to net zero emissions. Reuters. <https://www.reuters.com/article/us-climate-change-britain/britain-to-ban-new-petrol-cars-by-2030-on-road-to-net-zero-emissions-idUSKBN27X2Z0>. Last Accessed: March 15th, 2021.

[141] BloombergNEF. 2020. Electric Vehicle Outlook 2020. <https://bnef.turtl.co/story/evo-2020/page/3/1>. Last Accessed: March 15th, 2021.

[142] Morrison, G.M., Allan, A. and Carpenter, R., 2010. Abating greenhouse gas emissions through cash-for-clunker programs. *Transportation research record*, 2191(1), pp.111-118.

[143] Milford, R.L., Allwood, J.M. and Cullen, J.M., 2011. Assessing the potential of yield improvements, through process scrap reduction, for energy and CO<sub>2</sub> abatement in the steel and aluminium sectors. *Resources, Conservation and Recycling*, 55(12), pp.1185-1195.

[144] Allwood, J.M., Cullen, J.M. and Milford, R.L., 2010. Options for achieving a 50% cut in industrial carbon emissions by 2050. *Environmental science & technology*, 44 (6), pp.1888-1894.

[145] Ayres RU. 1999. The second law, the fourth law, recycling and limits to growth. *Ecological*



Economics 29: 473–483.

[146] Ahmadi, S., Bathaee, S.M.T. and Hosseinpour, A.H., 2018. Improving fuel economy and performance of a fuel-cell hybrid electric vehicle (fuel-cell, battery, and ultra-capacitor) using optimized energy management strategy. *Energy Conversion and Management*, 160, pp.74-84.

[147] Grunditz, E., 2016. Design and assessment of battery electric vehicle powertrain, with respect to performance, energy consumption and electric motor thermal capability. Chalmers University of Technology.

[148] Shabbir, W. and Evangelou, S.A., 2014. Real-time control strategy to maximize hybrid electric vehicle powertrain efficiency. *Applied energy*, 135, pp.512-522.

[149] Thomas, J., 2014. Drive cycle powertrain efficiencies and trends derived from EPA vehicle dynamometer results. *SAE International Journal of Passenger Cars-Mechanical Systems*, 7(2014-01-2562), pp.1374-1384.

[150] Philips, P. and Megli, T., 2017. Powertrain efficiency in the US fleet on regulatory drive cycles and with advanced technologies. *SAE International Journal of Fuels and Lubricants*, 10(2), pp.537-555.

[151] Ambrose, H., Kendall, A., Lozano, M., Wachche, S. and Fulton, L., 2020. Trends in life cycle greenhouse gas emissions of future light duty electric vehicles. *Transportation Research Part D: Transport and Environment*, 81, p.102287.

[152] Department of Energy (DOE). 2015. Quadrennial Technology Review 2015. Last Accessed: March 15th, 2021.

[153] Moawad, Ayman., Kim, Namdoo., Shidore, Neeraj., and Rousseau, Aymeric. 2016. Assessment of Vehicle Sizing, Energy Consumption and Cost Through Large Scale Simulation of Advanced Vehicle Technologies. United States.

[154] Schmuch, R., Wagner, R., Hörpel, G., Placke, T. and Winter, M., 2018. Performance and cost of materials for lithium-based rechargeable automotive batteries. *Nature Energy*, 3(4), pp.267-278.

[155] USABC., 2020. Development of advanced high-performance batteries for electric vehicle (ev) applications request for proposal information (RFPI)

[156] Xu, J., Lin, F., Doeff, M.M. and Tong, W., 2017. A review of Ni-based layered oxides for rechargeable Li-ion batteries. *Journal of Materials Chemistry A*, 5(3), pp.874-901.

[157] Ding, Y., Cano, Z.P., Yu, A., Lu, J. and Chen, Z., 2019. Automotive Li-ion batteries: current status and future perspectives. *Electrochemical Energy Reviews*, 2(1), pp.1-28.

[158] NREL, 2020. FASTSim vehicle simulation tool.

[159] EPA, 1999. Federal Test Procedure (FTP/EPA75) drive cycle. Last Accessed: March 15th, 2021.

[160] Brooker, A., Gonder, J., Wang, L., Wood, E., Lopp, S., Ramroth, L., 2015. FASTSim: A

Model to Estimate Vehicle Efficiency, Cost and Performance. SAE World Congress 2015; Detroit, MI, USA, 2015-01-0973.

[161] EPA. 2020. Lifecycle Greenhouse Gas Results. Last Accessed: March 15th, 2021.

[162] EPA, 2019. Final Rulemaking for Modifications to Fuel Regulations to Provide Flexibility for E15 and to Elements of the Renewable Identification Number Compliance System.

[163] Garside, M. 2020. U.S. distribution of ethanol production by feedstock type 2019. Statista. Last Accessed: March 15th, 2021.

[164] EPA. 2007. Energy Independence and Security Act of 2007. Last Accessed: March 15th, 2021.

[165] DOE, 2016. 2016 BILLION-TON REPORT Advancing Domestic Resources for a Thriving Bioeconomy.

[166] U.S. EIA, 2020. Annual Energy Outlook. Table 8. Electricity Supply, Disposition, Prices, and Emissions.

[167] Pacific Gas and Electric. 2017. PG&E Renewable Energy Deliveries Grow; GHG-Free Portfolio Is Nearly 70 Percent. Last accessed: March 15th, 2021.

[168] Cochran, J., Denholm, P., Speer, B. and Miller, M., 2015. Grid integration and the carrying capacity of the US grid to incorporate variable renewable energy (No. NREL/TP-6A20-62607). National Renewable Energy Lab.(NREL), Golden, CO (United States).

[169] Heard, B.P., Brook, B.W., Wigley, T.M. and Bradshaw, C.J., 2017. Burden of proof: A comprehensive review of the feasibility of 100% renewable-electricity systems. *Renewable and Sustainable Energy Reviews*, 76, pp.1122-1133.

[170] Pleßmann, G., Erdmann, M., Hlusiak, M. and Breyer, C., 2014. Global energy storage demand for a 100% renewable electricity supply. *Energy Procedia*, 46(0), pp.22-31.

[171] Connolly, D., Lund, H., Mathiesen, B.V. and Leahy, M., 2011. The first step towards a 100% renewable energy-system for Ireland. *Applied Energy*, 88(2), pp.502-507.

[172] Shinnar, R., 2003. The hydrogen economy, fuel cells, and electric cars. *Technology in society*, 25(4), pp.455-476.

[173] Edwards, M.R. and Trancik, J.E., 2014. Climate impacts of energy technologies depend on emissions timing. *Nature Climate Change*, 4(5), pp.347-352.

[174] Mian, A. and Sufi, A., 2012. The effects of fiscal stimulus: Evidence from the 2009 cash for clunkers program. *The Quarterly journal of economics*, 127(3), pp.1107-1142.

[175] Ke, W., Zhang, S., He, X., Wu, Y. and Hao, J., 2017. Well-to-wheels energy consumption and emissions of electric vehicles: Mid-term implications from real-world features and air pollution control progress. *Applied Energy*, 188, pp.367-377.

[176] Biden, Joe. 2021. The Biden Plan for a Clean Energy Revolution and Environmental Justice. Last Accessed: May 15th, 2021.

[177] Buehler, R., 2011. Determinants of transport mode choice: a comparison of Germany and the USA. *Journal of transport geography*, 19(4), pp.644-657.

[178] Ercan, T., Onat, N.C. and Tatari, O., 2016. Investigating carbon footprint reduction potential of public transportation in United States: A system dynamics approach. *Journal of Cleaner Production*, 133, pp.1260-1276.

[179] Craglia, M. and Cullen, J., 2020. Do vehicle efficiency improvements lead to energy savings? The rebound effect in Great Britain. *Energy Economics*, 88, p.104775.

[180] NHTSA. 2017. Summary of Travel Trends 2017 National Household Travel Survey. Last Accessed: March 15th, 2021.

[181] Duffin, Erin. 2020. Work situation of adults in the United States during the COVID-19 outbreak as of April 2020.

[182] Statista. 2021. What percentage of your workforce will remain permanently remote post-COVID who were not remote before COVID? Last Accessed: March 15th, 2021.

[183] Saevarsdottir, G., Kvande, H. and Welch, B.J., 2020. Aluminum production in the times of climate change: The global challenge to reduce the carbon footprint and prevent carbon leakage. *JOM*, 72(1), pp.296-308.

[184] Cooper, D.R., Rossie, K.E. and Gutowski, T.G., 2017. The energy requirements and environmental impacts of sheet metal forming: An analysis of five forming processes. *Journal of Materials Processing Technology*, 244, pp.116-135.

[185] Raykar, S.S.S., 2015. Analysis of energy use and carbon emissions from automobile manufacturing (Doctoral dissertation, Massachusetts Institute of Technology). Last Accessed: March 15th, 2021.

[186] Colias, Mike. 2018. America Has Fallen Out of Love With the Sedan. *The Wall Street Journal*. Last Accessed: March 15th, 2021.

## Appendix B

### Mapping the annual flow of steel in the United States

This document contains information useful to understanding the themes, calculations, and numbers introduced in the main manuscript. This document is 116 pages long and contains 24 tables and 14 figures. All data refers to U.S. steel flows in 2014 unless otherwise stated. The final 2014 U.S. steel flows.(xlsx file) and reconciliation Matlab code (.m file) can be downloaded from: [http://remade.engin.umich.edu/temp\\_during\\_review.htm](http://remade.engin.umich.edu/temp_during_review.htm)

#### B.1 Data Reconciliation

In section 2.4 of the main paper, we introduced a nonlinear least squares optimization method to reconcile collected steel flow data and to produce a mass balanced network. This B1 section will review existing formal reconciliation methods, present the flexible and updateable cataloguing method used in this analysis, describe the optimization setup, generation of the initial values used in the optimization, reconciled results, and analysis of corresponding residuals.

##### B.1.1 Review of formal reconciliation methods for material flows

Data scarcity and inconsistency are major hurdles in conducting MFAs. Although data records from various sources (e.g., government reports, academic and grey papers, etc.) are often collected in order to model all the processes and products in a material flow network, information could still be missing for one or more variables in the network. In addition, due to the abundance of data sources, the collected data records often contradict each other, e.g., violating conservation of mass<sup>1,2</sup>. Several data reconciliation methods have been applied to adjust the collected data records and achieve consistency in the material flow network. These include nonlinear least squares optimization<sup>3-6</sup>, Bayesian updating<sup>1,2,7,8</sup> and physical input-output tables<sup>9-12</sup>. A brief review of each method is presented below.

### **B.1.1.1 Least squares optimization method**

Least squares optimization is one of the earliest and most used methods in data reconciliation for MFAs and other resource flow studies<sup>13</sup> due to its simplicity and ease of use. In the least squares optimization method, the reconciliation is achieved by minimizing the objective function which is the sum of squared residuals between measured data records and the final MFA variables<sup>3</sup>. Ploeg (1988) implemented the general nonlinear least squares method to recover uncollected data in his multisectoral econometric model<sup>14</sup>. The popularity of the nonlinear least squares method is highlighted by Narasimhan and Jordache (1999) in their data reconciliation book<sup>15</sup> and by Brunner and Rechberger (2017) in their MFA handbook<sup>16</sup>. Other applications of least squares optimization in data reconciliation can be found in many MFA studies<sup>17-19</sup> including the MFA software named substance flow analysis, STAN<sup>3,20</sup>. However, a major limitation of the least squares optimization method as commonly applied is that instead of reconciling multiple collected data records for the same variable, these multiple data records are transformed into a mean and a standard deviation which leads to loss in the resolution of collected information. Another limitation of the least squares optimization as commonly applied is due to the linearization of nonlinear constraints, e.g., transforming yield ratio constraint to mass balance of input to product and scraps<sup>19-21</sup>. This is common because the linearization reduces the computational complexity. However, it may also lead to imprecise solutions.

Recently, Kopec et al. (2016) proposed a weighted nonlinear least squares method that allows nonlinear constraints and reconciliation of multiple data records per variable<sup>6</sup>. The weight of each residual is determined by the quality of the corresponding data record in a 1-100 scale<sup>6</sup>. Kopec et al. (2016) demonstrate their method by conducting a case study which re-examines Cullen et al. (2012)'s global steel flows. They present high level results and the improved objective function in order to demonstrate the utility of the proposed method. However, they show neither detailed guidelines about how this reconciliation method could be implemented nor results of the actual reconciled MFA network. In addition, their quality measuring system is not clearly defined which makes it difficult to be reused in other studies and likely leads to inconsistent data weighting.

### **B.1.1.2 Bayesian inference**

Bayesian inference is another data reconciliation method that adjusts the variable estimates based on a priori constraints<sup>22</sup>. It is a probabilistic method that allows the use of arbitrary probability distributions to represent data record uncertainties<sup>1,7,22-24</sup>. According to Wang and Romagnoli (2003), historical data forms the prior knowledge (prior distribution) of the MFA variables and the result of Bayesian inference is updated when a new measurement data comes in<sup>22</sup>. However, as indicated in Lupton and Allwood (2017)'s study, it is not always possible to understand the

probability distribution of an MFA variable in the case of lacking information<sup>23</sup>. In their global steel flow case study, they have to assume Gaussian or uniform Dirichlet distributions for the majority of the data records<sup>23</sup>. An alternative to the probabilistic method is the fuzzy-set method in which a fuzzy interval, instead of a probability distribution, is used to express the variable uncertainty<sup>13</sup>. Without a systematic framework of assigning uncertainty distributions (or fuzzy intervals in the fuzzy set method) to each data record, the Bayesian inference results could be biased due to improper distribution choices. In addition, Bayesian inference can be computationally expensive, e.g., the supporting information of Lupton and Allwood (2017) suggest that a 24 variable case study took 30 minutes on a 2 GHz Intel i5 laptop.

### **B.1.1.3 Input-output table**

Input-output tables (IOT) were first developed by Leontief (1936) in order to study the economic interactions between different sectors of an economy<sup>9,25</sup>. As such, the IOT entries are in monetary units, e.g., United State dollars<sup>26</sup> and the method is well-known in balancing economic and social flows<sup>6,27</sup>. Recently, the IOT has been applied in MFA studies due to its ease of application<sup>9–12</sup>. These types of IOTs are called physical input output tables (PIOTs)<sup>9</sup>. The basic constraint in the PIOTs is that the total input should satisfy final demand which is a simplified form of mass conservation<sup>12</sup>. A common PIOT table consists the flows from all the processes and products to subsequent processes<sup>9,10</sup> similar to the left portion of the matrix catalogue example shown in Figure 1 of the main article. However, due to the simplified mass conservation setup, the PIOTs cannot incorporate nonlinear constraints e.g., yield ratio or other nonlinear variable related constraints which are abundant in this article's steel flow study.

### **B.1.2 A flexible and updatable cataloguing method (this analysis)**

The cataloguing method used in this article's analysis is summarized in Figure 1 of the main article. The matrix shown in Figure 1 is a base template that is repeated many times in the code used to define the reconciliation and run the optimization. The different copies of the matrix are used to define different parameters of the steel flow (e.g., the existence or not of a flow between two nodes or the upper bound on a flow) and to enter the data records. Figure B.1 shows the multi-dimensional matrices used to define the flow and catalogue the data records. Alongside the schematic in Figure B.1, are definitions and examples.

Figure B.2 shows the set of tasks a practitioner must perform in order to use the cataloguing system to perform a formally reconciled MFA.

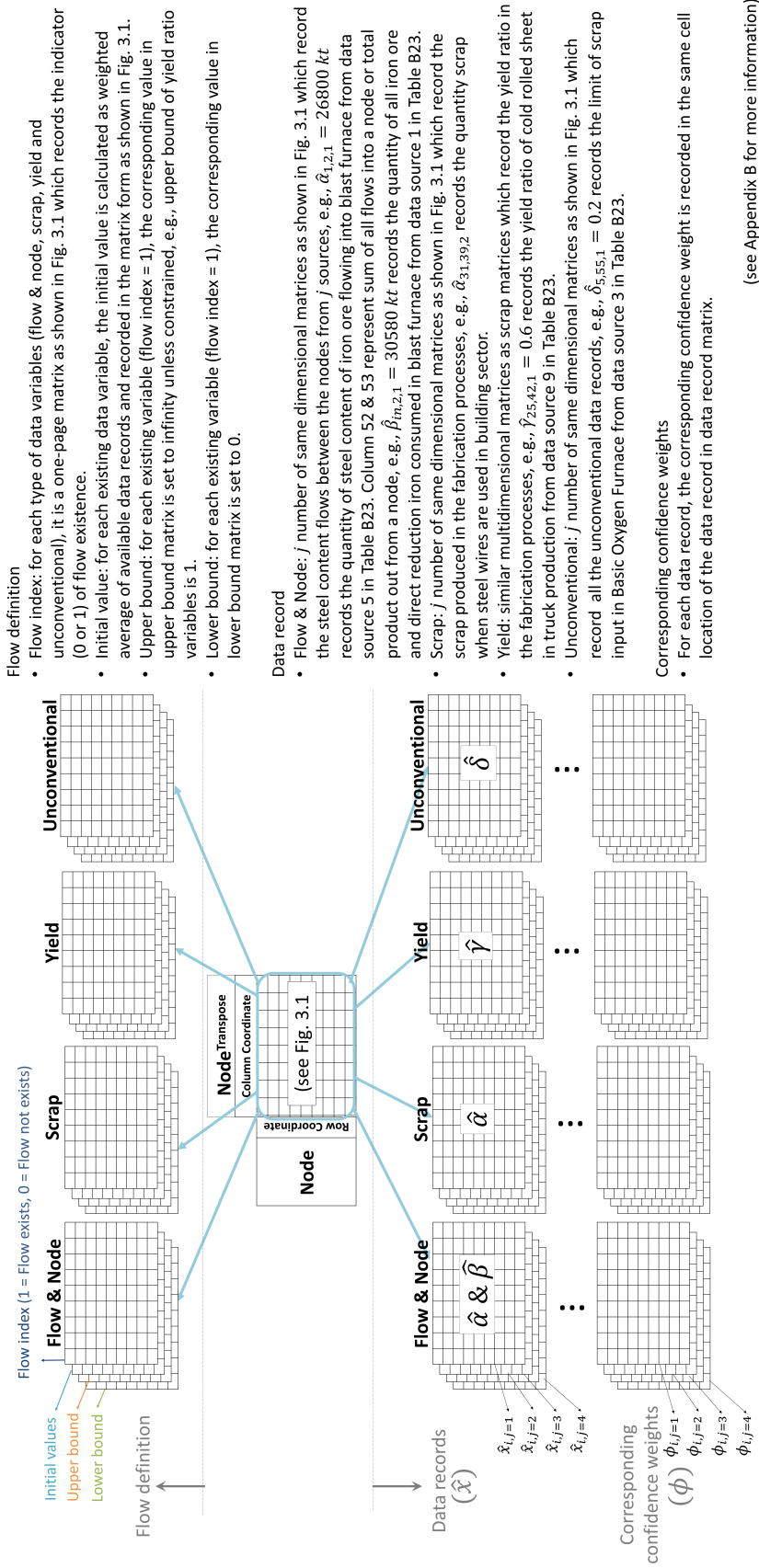


Figure B.1: The multi-dimensional matrix-based cataloging system used for setting up the reconciliation

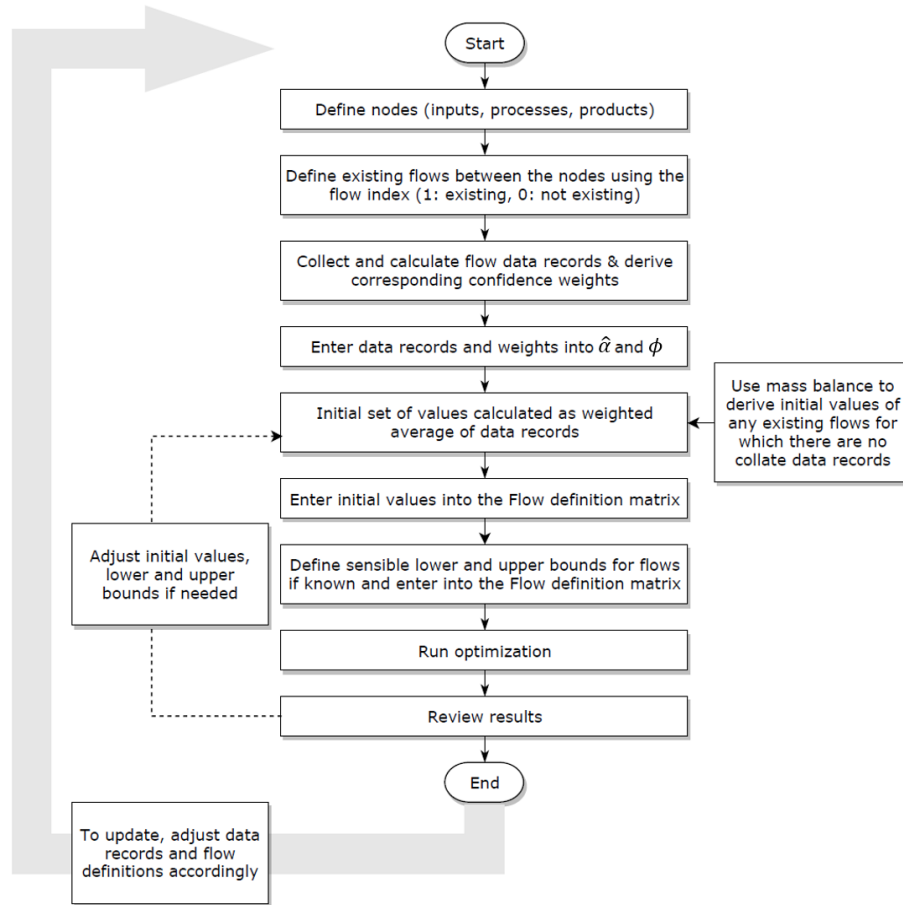


Figure B.2: A flow chart showing the tasks a practitioner must follow in order to produce a material map using the cataloguing structure shown in Figure B.1

### B.1.3 Nonlinear least squares optimization method

As shown in equation 1 of the manuscript,  $x_i$  was used to represent different MFA variables. Because empirical data sources refer to a range of MFA variables, as summarized in Table B.1, different elements within the  $x_i$  vector represent flow ( $\alpha_{k,l}$ ), node ( $\beta_k$ ), yield ratio ( $\gamma_{k,l}$ ) or unconventional data ( $\delta_m$ ).



Table B.1: Type of MFA Variables

Sub - categories of $x_i$	Variable Type	Symbol	Examples from collected data
	Flow and scrap: steel content (product or scrap) flows from node $k$ to node $l$ .	$\alpha_{k,l,product}$ , $and \alpha_{k,l,scrap}$	Pig iron flows out from blast furnace (node $k$ ) to export (node $l$ ): USGS iron and steel yearbook shows 7 kt. USGS iron and steel scrap shows 6.77 kt. and WorldSteel shows 52 kt.
	Node: sum of all flows into a node $m$ or total product out from node $k$ (excluding scraps and loss in case of output node).	$\beta_{k,in}$ and $\beta_{k,out}$	Pig iron produced out from blast furnace (node $k$ ). USGS iron and steel yearbook shows 29400 kt and WorldSteel shows 29374 kt.
	Yield ratio: percentage of product output to material input associated with the flow from node $k$ to node $l$ or the ratio of node output to node input.	$\gamma_k$ $or \gamma_{k,l}$	Yield ratio of direct reduction process is around 99.3% (Cullen, 2013) or yield ratio of using cold rolled sheet (node $k$ ) to produce car panels (node $l$ ) is 60% (Cullen, 2013).
	Unconventional: data referring to one or more of the above variables such as data on the sum of a subset of flows or ratios between subsets of flows.	$\delta_m$	Sum of all welded and seamless pipes and tubes is 4718 kt (WorldSteel).

The objective function is shown below along with the mass conservation constraints defined using the sub-categorical variables.

Objective function:

minimize:

$$\sum_i^I \frac{\sum_j^{J_i} \Phi_{i,j} \cdot (r_{i,j})^2}{J_i} \quad (B.1)$$

Where  $r_{i,j} = \frac{x_i - \hat{x}_{i,j}}{\hat{x}_{i,j}}$  is the residual between MFA variable and data value.

Subject to: **mass conservation**

For each node  $k$ :

$$\sum_l \alpha_{k,l} = \sum_m \alpha_{m,k} = \beta_{k,in} = \beta_{k,out} + \sum_{scrap+loss} \alpha_{k,l} \quad (B.2)$$

This constraint ensures that all materials flowing into a node (steel making or forming process) equal the sum of product, loss and scrap, e.g. sum of iron ore (iron content within iron ore), direct reduction iron and steel scraps going to blast furnace equals the amount of pig iron produced in

blast furnace plus the loss associated with the process. The mass conservation constraint establishes the link between node variables and flow variables, so the overall flow network is maintained.

For each node  $k$  :

$$\gamma_k = \frac{\beta_{k,out}}{\beta_{k,in}} \quad (\text{B.3})$$

Which constrains the overall yield ratio of a steelmaking or forming process. For processes that use the same input material but exhibit different yield ratios depending on the product made, e.g. forming using cold rolled sheet to produce car panels versus forming using cold rolled sheet to produce domestic kitchen appliance panels, a specific yield ratio is defined for each of the process outputs, as shown below.

For each flow  $k$  to  $l$ :

$$\gamma_{k,l} = \frac{\alpha_{k,l,product}}{\alpha_{k,l,product} + \alpha_{k,l,scrap}} \quad (\text{B.4})$$

These flow specific yield ratio constraints only apply to the intermediate products to end-use products section of the network from line 24 to line 35 and lines 37 and 38 of the matrix catalog as shown in Figure B.4 in B3.1.

For each unconventional variable:

$$\delta_m = \sum_{some} \alpha_{k,l} \quad (\text{B.5})$$

or

$$\delta_m = \frac{\sum_{some} \alpha_{k,l}}{\sum_{some} \alpha_{k,l}} \quad (\text{B.6})$$

The form of the unconventional constraints vary from one to another and the equations above only demonstrate two examples. An explanation of each unconventional data point can be found in the data list in B3.2.

Lastly:

$$0 \leq \gamma_{k,l} \leq 1 \quad (\text{B.7})$$

$$x_i = \{\alpha_{k,l}, \beta_k, \gamma_{k,l}, \delta_m\} \geq 0 \forall i \quad (\text{B.8})$$

$$lb_i \leq x_i \leq ub_i \text{ for some } i \quad (\text{B.9})$$

These additional boundary constraints are used to narrow the solution space to speed up the optimization and they also incorporate existing empirical estimations of some MFA variable, e.g. yield ratio of any process is always between 0 and 1.

#### B.1.4 Initial values used in the formal reconciliation optimization

An important input to the data reconciliation algorithm is the set of initial values used for all MFA variables including flow, node, yield ratio, etc. As we are performing a nonlinear optimization, wildly inaccurate initial values will likely result in the optimization starting in a ‘well of attraction’ far from the global minimum; therefore, the subsequent local minimum found by the optimization will likely be far (in terms of objective function and the values of the flow variables) from the truly best solution. In order to leverage all known data records, the initial values used in this analysis were, where available, the weighted mean of the recorded data. The weight for each data record is equal to the weight recorded in Table B.23. For example, the value in the initial guess for the flow of hot rolled sheet into infrastructure is given by equation B1:

$$\begin{aligned} \text{Flow}_{24,40} &= \text{HR sheet to infrastructure} \\ &= \frac{(0.25 \times 6123) + (0.417 \times 616) + (0.333 \times 385)}{0.25 + 0.417 + 0.333} \\ &= 1916 \text{ kt} \end{aligned} \tag{B.10}$$

Where no recorded data could be found, an initial MFA variable can typically be calculated using simple mass balance. For example, there is no recorded data to use as an initial value for the flow of *ingots, billets, blooms, and slabs* into the primary mill (flow coordinate: 36,18) but is instead calculated to be 10,431 kt by knowing that it must equal the total flow into *ingots, billets, blooms, and slabs* from domestic ingot casting (1,110 kt) and imports (9,610 kt) minus the flow of *ingots, billets, blooms, and slabs* to export (289 kt). Data records do exist for these three other flows.

The only wider assumption needed in order to generate a set of initial values is that the size of the relative flows from the primary mill to the hot strip mill, plate mill, bar/rod mill, and section mill in 2014 was equal to the relative size of all steel flows passing through these four types of mill. For example, according to the initial set of values there is a total of 97,677 kt of steel passing through the four forming mills, of which 60% passed through the hot strip mill; therefore, it was assumed that 60% of the output from the primary mill flowed into the hot strip mill, and so on for the other types of forming mill.

This initial set is not a feasible solution (violating mass balance); thus, the initial constraint violation recorded by MATLAB is equal to 10,900 kt. The initial set of values used in this study is shown in Table B.2 (see <https://pubs.acs.org/doi/abs/10.1021/acs.est.9b01016>).

### B.1.5 Derivation of an informally reconciled steel map

An informally reconciled U.S. 2014 steel map was derived and is available for download at [http://remade.engin.umich.edu/temp\\_during\\_review.htm](http://remade.engin.umich.edu/temp_during_review.htm). This manual, informally reconciled steel map was not needed in order to derive the final steel map shown in Figure 2 of the main article. However, it was derived in order to compare the final steel map variables derived using the informal and formal techniques (see Figure B.4).

The informal reconciliation stated by gathering intermediate product information from the USGS Iron and Steel Minerals Yearbook<sup>28</sup> in the following categories: tin mill products, galvanized products, hot rolled sheet and strip, cold rolled sheet and strip, pipe and tube, rod and bar products, rebar, light sections, heavy sections, rail, steel castings and iron castings. There are several reasons for using intermediate goods as the starting point: the USGS reports detailed production, import, and export data for these products; intermediate products represent the finest resolution of the overall steel life-cycle; and intermediate product data can be extrapolated backward to the production phase and forward through end-use.

The USGS data for intermediate products is then filled into the corresponding section of the catalog matrix (section from 24,39 to 35,47 and 37,39 to 38,47) and used to derive upstream and downstream values together with other data, specifically import, export, and yield values. For example, USGS<sup>28</sup> reports that around 20640 kt of hot rolled sheet and strips are produced in the U.S. which is set as the value for variable x(14,24,1).

Using the intermediate product data and yield data for specific processes, upstream continuous casting, liquid steel production, scrap and loss data can be extrapolated. Where needed, data points regarding each specific upstream step can be used to inform the extrapolation. For example, the amount of continuous cast slab produced can be back-calculated using the total of the intermediate products created from slab and the yield ratios for the processes that transform slab to those products. However, liquid steel to CC slab is provided by both the BOF and EAF and the proportion of one or the other is not known. To achieve a good estimate that satisfies mass conservation, the USGS data point for BOF steel produced ( $\approx 33$  Mt) is allocated to CC Slab and the balance is met using EAF steel. In this way, the initial values for BOF steel to CC Slab will match the USGS recorded data<sup>28</sup> and the initial values for EAF steel to CC Slab will only vary slightly from the USGS recorded<sup>28</sup>. A similar method is employed to adjust the iron ore, DRI, and scrap inputs to match what is required by mass balance. Iron ore and DRI data, including corresponding import and export values from USGS, are used directly in the initial value set. Since the scrap flow data from multiple sources are conflicting with each other and the USGS provides a minimum scrap consumption as 58Mt<sup>28</sup>, we adjusted the scrap flow into each furnace to satisfy mass conservation constraints.

To create the downstream section of the set of initial values, the flows of intermediate products to end-use goods sectors are estimated based on methods used in the existing literature; e.g., Cullen

et al. (2013). The Supplementary Information from Cullen’s work outlines a detailed approach for estimating flows from intermediate products to end-use goods. To create the set of initial values (as well as a set of data for use in the reconciliation), this method was followed with changes made to adapt it to the U.S. manufacturing sector in 2014.

### B.1.6 Optimization results

MATLAB’s fmincon solver with interior-point algorithm is used to conduct the optimization (Byrd et al., 1999; Matlab, 2013). It took 450 iterations for the objective function to converge (Figure B.3: 30 hours using an Intel(R) Core™ i7-6600U CPU, 2.81 GHz, with 16 GB of RAM). The optimization reduced the objective function by 20% from 18.5 at the initial set of values to 14.7. A smaller objective value indicates that the solution is a better fit to the available data than the manually derived initial set of values. A list of optimization results for all MFA variables and their corresponding weighted residuals are shown in Table B.2 next to the initial set of values. Table B.3, Table B.4 and Table B.5 summarize the number of variables, number of constraints and number of data records by categories respectively.

Table B.2: Summary of Variables

Type of variables	Quantity
Flow between nodes (excluding scrap & loss)	181
Flows to scrap node	78
Flows to loss node	11
Yield ratio	83
Node variable	78
Unconventional variable	33
Total non-zero existing	464
Existing zero variables (e.g., flows direct from BF to cars)	10755
Total	11219

Table B.3: Summary of Constraints

Type of constraint	Quantity
Mass conservation	133
Yield ratio	165
Unconventional variable	33
Boundary constraints	184
Constraining non-existing flow/scrap/loss to zeros	8799
Total	9314

Table B.4: Summary of Data Sources

Type of data	Quantity
Flow	156
Scrap	0
Loss	0
Yield ratio	78
Node variable	17
Unconventional variable	42
Total	293

Figure B.3 shows the evolution of the objective function value and maximum constraint violation versus the number of iterations in the optimization solving process. Both objective function value and maximum constraint violation change minimally after 450 iterations which is the sign of convergence.

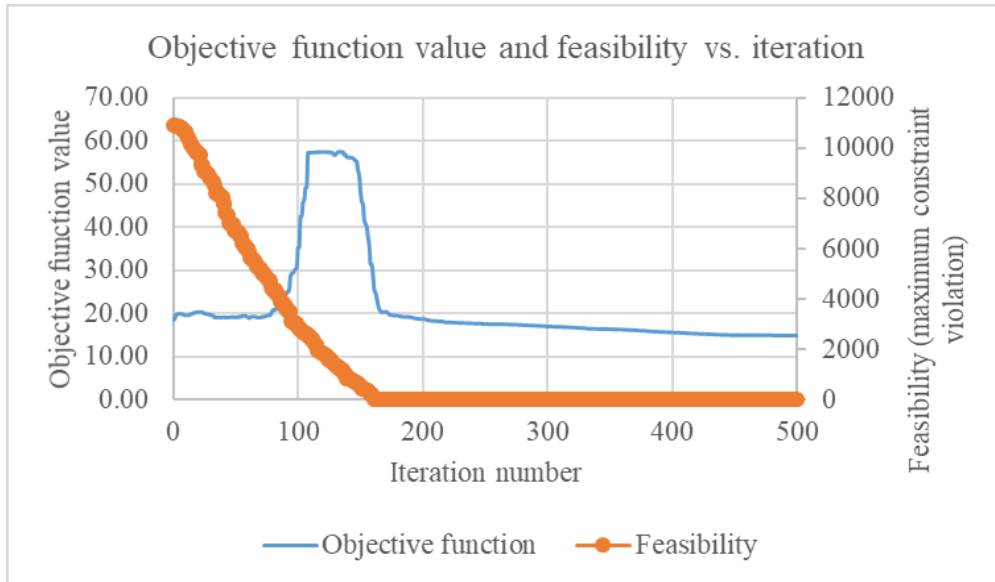


Figure B.3: Objective function value and maximum constraint violation versus the number of iterations

Figure B.4 shows the five greatest differences between the final formally reconciled steel map and, on the left hand side, the manual, informally reconciled map derived as described in Section B.1.5 and, on the right hand side, the initial set of MFA variable values used in the formal reconciliation. As shown in Figure B.4, the choice of MFA reconciliation technique has a significant effect on the final MFA variables.

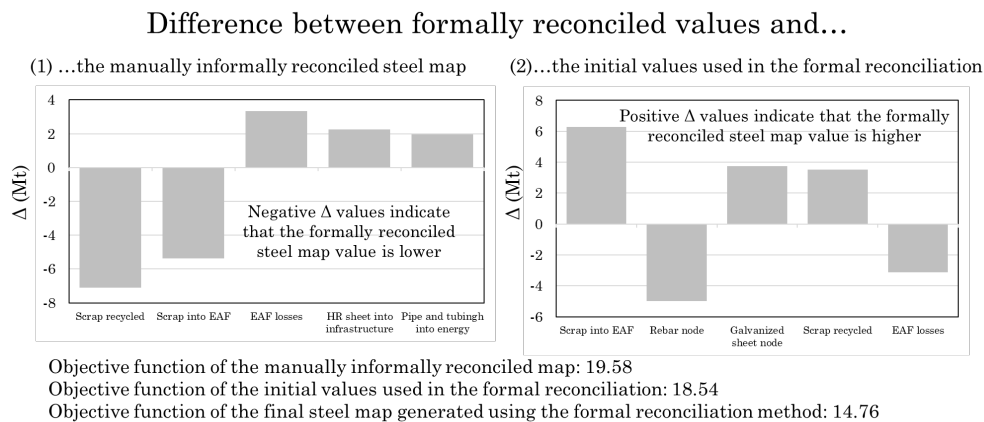


Figure B.4: Greatest differences between the informally (manually) reconciled steel map, the initial values used in the formal reconciliation, and the final formal reconciliation map shown in Figure 2 of the main article

### B.1.7 Residual analysis

The weighted residuals for each MFA variable are shown in Table B.6. Note that for those MFA variables that have no empirical data record, the corresponding residuals are zero and not included in the objective value computation. For MFA variables that have multiple possible values from different data sources, the weighted residual is the weighted sum of normalized residuals according to each data source. We identify the maximum normalized but non-weighted residual for both the set of initial values and the reconciled result as shown in Table B.6.

Table B.5: Summary of residuals

Value	Initial set of values	Optimization result	Optimization residual to USGS data
Objective function	18.54	14.76	3.87
Objective function without confidence value	64.29	38.46	4.23
Maximum non-weighted residual value	6.59 (x38,43,1 iron casting to machinery)	2.66(x38,43,1 iron casting to machinery)	0.93 (x3,6,1 direct reduction to electric arc furnace)

Figure B.5 shows the contribution of different sizes of residual values to the objective function. The largest difference between the initial set of values and the optimization result is that the optimization process reduces the quantity and size of large residuals, shifting to a greater number of small residuals to reduce the overall objective value. For example, the flow from iron casting to machinery equaled 434 Mt in the informally reconciled map (weighted normalized residual: 3.11), and 267 Mt in the formally reconciled map (weighted normalized residual: 0.99).

The ability for the optimization algorithm to simultaneously modify variable values while achieving mass balance constraints would have been very hard to achieve by manual data reconciliation alone.



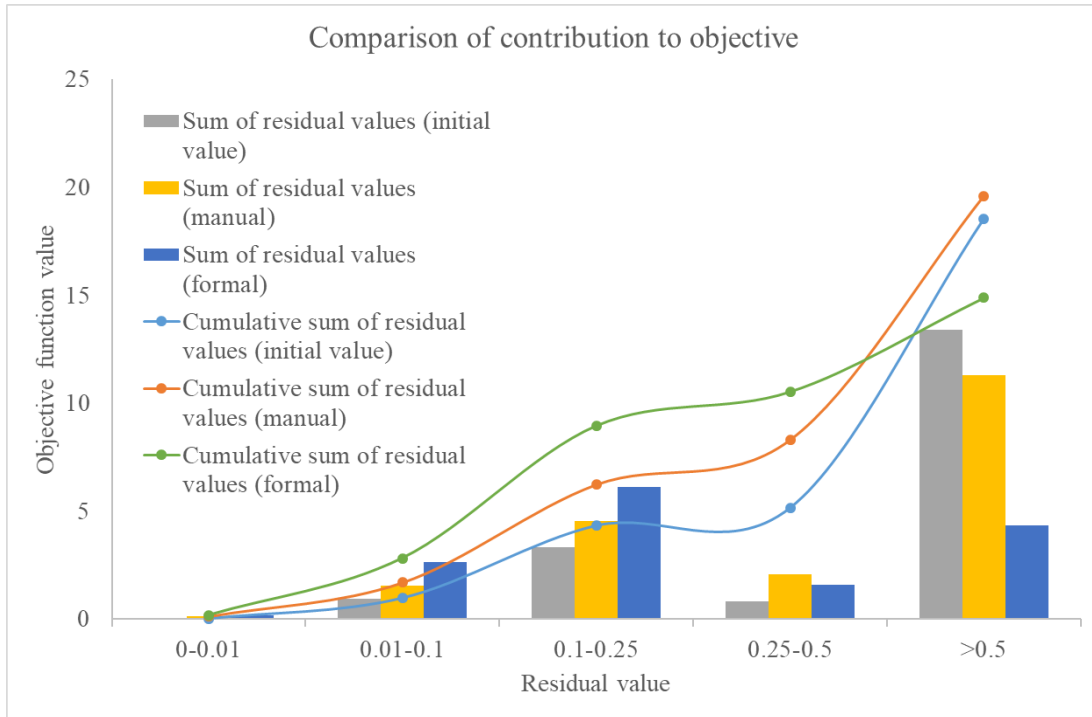


Figure B.5: Size of residuals in initial variable set, final optimized variable set, and informally (manually) reconciled variable set

## B.2 Flow estimate sources and derivations

This B2 section describes the source, and where necessary the derivation, of the empirical data records on the U.S. 2014 steel mass flow used in the reconciliation described in section B1. A summary of all the data records (and sources) used is provided in Table B.23, in Section B3.2.

### B.2.1 Summary of steelmaking and fabrication process yields

The data records for steelmaking process yields used in the reconciliation are shown in the table below.

Table B.6: Steelmaking and fabrication process yields

Steelmaking Process	Coordinate (Table B.23)	Yield Ratio	
Blast Furnace	[2.54]	0.993	All Steel- making Process Yields derived from WSA (2009)
Direct Reduction	3.54	0.993	
Basic Oxygen Furnace	5.54	0.871	
Electric Arc Furnace	6.54	0.889	
Cupola Furnace	7.54	0.871	
CC Slab	8.54	0.965	
CC Billet	9.54	0.975	
CC Bloom	10.54	0.955	
Ingot Casting	11.54	0.98	
Steel Product Casting	12.54	0.522	
Foundry Iron Casting	13.54	0.66	
Hot Strip Mill	14.54	0.96	
Plate Mill	15.54	0.9	
Rod/Bar Mill	16.54	0.94	
Section Mill	17.54	0.9	
Primary Mill	18.54	0.925	
Cold Rolling Mill	19.54	0.951	
Tube Welding Plant	20.54	0.935	
Seamless Tube Plant	21.54	0.922	
Galvanizing Plant	22.54	0.975	
Tin Mill	23.54	0.935	

Additionally, a report prepared for AISI by Energetics, Inc. (2003) reports a range of yield ratios for the BOF of 0.91-0.93 and EAF of 0.92-0.94. The upper limit of these ratios (0.93 for the BOF and 0.94 for the EAF) is used as a maximum value for each furnace type's yield in the reconciliation. The EAF value of 0.94 is also used as the maximum yield for the CF.

### **B.2.2 Liquid steel to continuously cast semi-finished goods**

Liquid steel produced in the BOF and EAF is cast into semi-finished products, of which there are four types: ingot, billet, bloom, and slab. These four categories are distinguished by the general shape and size they're cast in and the types of products they are used to produce. Three of the

four (billet, bloom, and slab) are produced using a continuous casting process and fed directly into further rolling and shaping processes. USGS (2016a) records that 98.5% of U.S. steel production was continuously cast in 2014.

A bottom-up estimate was used to estimate the proportions of each continuously cast product. Slab is rolled and shaped into flat products, such as sheet and plate. Billet is formed into rod and bar products, such as hot rolled bar and wire rod. Bloom is formed into section products, such as heavy sections and rail. USGS and Worldsteel <sup>28,33</sup> both report steel intermediate product production by specific product (e.g., “hot rolled sheet” or “reinforcing bar”) which can then be categorized by the type of semi-finished products used to produce them. Table B.8 shows this categorization and the overall quantities and percent of the total for each category.

Table B.7: Categorization of intermediate products by continuous cast product (USGS, 2016a)

Semi-Finished Product	Intermediate Products	Quantity (kt)	Quantity (%)
Slab	Plate, welded pipe and tube, tin mill products, hot-rolled sheet and strip, cold-rolled sheet and strip, galvanized or coated sheet and strip,	61394	69.8%
Billet	Wire rod, hot-rolled bars, reinforcing bar, cold finished bar, seamless tube, wire, light sections	19822	22.5%
Bloom	Heavy sections, rail	6748	7.7%

The categorizations from Table B.8 are used to determine the structure of the flow network, which in turn will dictate the proportions of slab, billet, and bloom in the final reconciled result. Rather than constrain the proportion with unconventional data to be a certain percentage (for example, using the percentages from Table B.8 as unconventional data), the proportion is determined by the downstream flows from each continuously cast product through mass balance constraints.

For example, in both Figure B.4 and Table B.23, the only outputs from CC Bloom are [10.10]: *Internal recycling*, [10.17]: *CC Bloom to Section Mill*, and [10.51]: *Loss*. The Section Mill then has outputs to [17.34]: *Section Mill to Heavy Sections*, [17.35]: *Section Mill to Rail* and [17.50]: *Scrap*. Therefore, the reconciled results for [17.34] and [17.35] (heavy sections and rail, respectively), the reconciled yields for the section mill and CC Bloom, and mass balance principles can be used to back-calculate the amount of liquid steel input necessary to support that amount of production. The same can be said of liquid steel entering CC Slab and CC Billet, which are likewise determined by mass balance with the intermediate product outputs according to the categories in Table B.8.

Liquid steel includes all production in BOF, EAF and cupola furnace (CF), so the liquid steel allocation must also include which type of furnace is supplying each semi-finished product. Flat

products are the most sensitive to defects due to contamination from tramp elements in recycled steel, so all primary (BOF) steel is assumed to be used for production of slab to maintain the highest possible purity in flat intermediate products<sup>34</sup>. However, BOF production is not enough to fill the demand for flat products as reported by USGS (2016a), so a flow from the EAF to CC Slab is added to the network to supply the balance. Allocation for billet and bloom demand is supplied exclusively by the EAF. Raw steel production in the CF is only around 0.1% of total raw steel production and decreasing each year<sup>35</sup>. The small amount of liquid steel from the CF is sent to ingot casting and the balance of ingot casting demand is met with EAF steel. The network structure is therefore as follows: BOF and EAF to CC Slab; EAF to CC Billet; EAF to CC Bloom; and EAF and CF to Ingot casting. The amounts of liquid steel from each furnace type to each semi-finished product can then be determined by mass balance principles and liquid steel production data by furnace type.

The USGS intermediate product data includes one other product which is not included in the continuous cast categories in Table B.8: ingots, blooms, billets, and slab. It is a small percentage of the overall domestic production (1110 kt of 89100 kt, or 1.2% according to USGS (2016a)), but it is a significant fraction of imported steel (9610 kt of 40200 kt, or 24%). Ingots, blooms, billets, and slab are not truly intermediate products but are instead semi-finished goods similar to CC products. Therefore, they are precursors to the production of true intermediate products and must be routed accordingly in the network. The U.S. Census Bureau (2015) reports that of the 9610 kt imported into the U.S., 9559 kt is billet, bloom, or slab and is thus destined for rolling mills along with domestic semi-finished products. Data records for the reconciliation include the net value of ingot, billet, bloom and slab (1110 kt of production minus 289 kt of export plus 9610 kt of import: 10431 kt, according USGS (2016a)).

No data has been found which divides the net value into individual CC products, so some assumption must be made regarding the proportion of each CC product. It is assumed that the all net imports of ingot, billet, bloom and slab are destined for the primary mill where they are prepared for rolling in subsequent mills. The output of the primary mill is then allocated to the hot strip mill, plate mill, rod/bar mill, and section mill. The proportion of intermediate products downstream of each rolling mill determines the proportion of steel from the primary mill destined for that mill. The following describes which intermediate products are downstream of each rolling mill:

- Hot Strip Mill: Welded pipe and tube, tin mill products, hot-rolled sheet and strip, cold-rolled sheet and strip, galvanized or coated sheet and strip
- Plate Mill: Plate
- Rod/Bar Mill: Wire rod, hot-rolled bars, reinforcing bar, cold finished bar, seamless tube, wire, light sections

- Section Mill: Heavy sections, rail

Mass balance principles are combined with this network structure and the relevant production and yield data to determine the amount of primary mill output destined for each rolling mill. Again, the structure of the reconciliation model automatically determines the proportions based only upon the network structure and mass balance without the addition of unconventional data.

For example, in Figure B.4 and Table B.23, ingots, billets, blooms and slab has two inputs: [11.36] *Ingot casting to Ingots, billets, blooms, and slabs* and [48.36] *Import to Ingots, billets, blooms, and slabs*. Each of these values is reconciled from existing data. Ingots, billets, blooms and slab also has two outputs: [36.18] *Ingots, billets, blooms and slab to Primary mill* and [36.49] *Ingots, billets, blooms and slab to Export*, and the export value is reconciled from existing data. The net value is destined for the Primary mill, where it is divided among [18.14] *Primary mill to Hot strip mill*, [18.15] *Primary mill to Plate Mill*, [18.16] *Primary Mill to Rod/Bar mill* and [18.17] *Primary Mill to Section Mill*. Plates represent approximately 11% of overall intermediate product production (according to data from USGS) so 11% of primary mill output is destined for the section mill. The proportion will vary according to the reconciled downstream results.

### **B.2.3 WSA vs USGS intermediate product data**

Table B.9 (<https://pubs.acs.org/doi/abs/10.1021/acs.est.9b01016>) shows the available data from the USGS and the World Steel Association for production of intermediate products in 2014<sup>28,33</sup>. An important conclusion can be drawn from this comparison. The sum of USGS intermediate products equals the total reported “production of hot rolled products” from the WSA, indicating that the two data sources have good agreement, which is further supported by the almost perfect agreement for data points from similar product categories. What little variance does occur can be attributed to rounding errors. This consistency can be interpreted two ways: either the data from both reporting agencies is independently gathered and near perfectly accurate, or these two reports are generated based on a common set of underlying data. The second interpretation is more likely, and when the references from each reporting agency are compared it is evident that these two reports relied heavily on American Iron and Steel Institute (AISI) data for these specific values. Unfortunately, this common set of data is not publicly available. The USGS data is more complete and is therefore used exclusively for intermediate product values in the reconciliation. This is done to prevent “double counting” of the same data source.

### **B.2.4 Intermediate Products to End-Use Goods**

AISI reports the following in their 2015 Profile of the U.S. steel industry<sup>37</sup>:

Table B.8: AISI Profile steel intermediate use by end-use sector

	Percentage	Value (Mt)
<b>Total apparent steel demand</b>	<b>100%</b>	<b>120</b>
Construction	40%	48
Automotive	26%	31.2
Machinery and equipment	10%	12
Energy	10%	12
Appliances	4%	4.8
Container	4%	4.8
National Defense and Homeland Security	3%	3.6
Other	3%	3.6

This percentage breakdown refers to the total steel inputs to domestic manufacturing in each end-use sector prior to fabrication losses. Only the percentages in the above table are used as unconventional data in the reconciliation (see Table B.23, coordinates [39-47.55]) since the mass value of 120 Mt of intermediate products is subject to reconciliation. Total steel inputs to domestic manufacturing for each end-use sector can be calculated by summing all “flow” data points into that end-use sector except for imports as well as all “scrap” data points associated with that sector. For example, the sum of coordinates [24-38.43.1] and coordinates [24-38.43.2] gives the total intermediate steel destined for manufacturing in the Machinery and Equipment end-use sector.

### **B.2.5 Intermediate Products to End-Use Goods based on Cullen et al. (2012)**

Determining the flows from intermediate products to end-use goods at a higher resolution than described by AISI (2015a) requires extensive use of bottom-up and top-down estimates, which are considered unconventional data

No data sources have been found which give explicit numerical values of flows from intermediate products to end-use goods, such as “Cold Rolled Sheet to Cars.” Determining these flows at a higher resolution than just the AISI overall breakdown therefore requires top-down and bottom-up estimates derived from industry production data and steel product percentage breakdowns from literature (e.g., steel intermediate product use in construction is based on bottom-up percentage estimates of steel use from Moynihan et al. (2012) and Cooper et al. (2012)). As an example, the flow of galvanized sheet into cars for 2014 is not a discrete value found in available data, but must instead be estimated based on bottom-up estimates of steel use in the automotive sector.

The data reconciliation allows for extensive use of unconventional data such that in theory it

would be possible to simply use the percentage breakdowns from the literature as unconventional data to determine intermediate product flows; however, doing so would come at significant computational cost and may lead to problems achieving convergence. Therefore, rather than using the raw percentages from the literature, a combination of top-down and bottom-up estimates are performed based on what data is available for each sector. The resulting numbers from these estimates are then used as data points in the reconciliation with appropriate weighting.

Cullen et al. (2012) outline a useful method of estimating flows from intermediate products to end use goods for their global map of steel production. The methodology is described in detail in the supplementary information for that paper and is a useful starting point for our estimates. Cullen's methodology is followed to determine a set of inputs to the reconciliation, with the following differences:

- The AISI profile intermediate to end-use goods breakdown for the U.S. is used as stated above in Table B.10: Construction 40%; Automotive 26%; Machinery and equipment 10%; Energy 10%; Container 4%; Appliances 4%; National Defense and Homeland Security 3%; and Other 3%.
- Automotive is divided into Cars 24% and Trucks 2% based on OICA statistics and average steel mass per vehicle is derived from U.S. specific sources (detailed further in section B2.6.2).
- The AISI profile doesn't include a section specifically for other transport and the U.S. does not produce ships other than for military applications, so the "ships and other" allocation is applied to Defense and Homeland Security.
- Energy includes oil and gas applications and the USGS (USGS Iron and Steel) details production of line pipe and oil country goods (a subset of pipe and tubing). Therefore, 8245 kt of pipe and tubing is allocated to Energy. The remainder of steel allocated to energy is done according to Cullen et al.'s breakdown for Electrical Equipment.

Some adjustment is necessary to balance the flows, as the percentage of each type of intermediate product is not the same for the U.S. in 2014 as for the world in 2008. The resulting intermediate to end-use goods matrix is shown in Fig S6. Figure B.6a shows the intermediate product to end-use goods matrix as outlined by Cullen with the intermediate products from USGS and Figure B.6b shows the resulting matrix when intermediate products are combined to match the network used in this work. For each cell in the matrix, three numbers are given. The top right is the amount of the specified intermediate product destined for the end-use category. The bottom left is the fabrication yield as described by Cullen. The bottom right is the product of the other two and is the total amount of that intermediate product in the finished goods. Figure B.6b also includes the relevant coordinate

	Total	39	Buildings	40	Infrastructure	41	Cars	42	Trucks	43	Machinery/Equipment	44	Energy	45	Other/Homeland Security	46	Domestic Appliances	47	Containers
		30.214		14.852		27.348		2.058		10.360		11.311		6.742		4.524		4.524	
		0.931	28.141	0.925	13.735	0.677	18.519	0.716	1.474	0.880	9.117	0.926	10.470	0.768	5.175	0.800	3.619	0.700	3.167
HR Sheet	23.643	[24.39]	11.927	[24.40]	6.803			[24.42]	0.235	[24.43]	4.229	[24.44]	0.375			[24.46]	0.076		
24		0.900	10.734	0.900	6.123			0.600	0.141	0.800	3.383	0.800	0.300			0.800	0.061		
CR Sheet	12.361				[25.41]	4.831	[25.42]	1.032								[25.46]	4.351	[25.47]	2.147
25					0.600	2.899	0.600	0.619								0.800	3.481	0.700	1.503
Galvanized	18.690	[26.39]	2.257	[26.40]	0.673	[26.41]	15.760												
26		0.900	2.031	0.900	0.606	0.600	9.456												
Tin mill products	2.474															[27.46]	0.097	[27.47]	2.377
27																0.800	0.078	0.700	1.664
Pipe and Tubing	11.424	[28.39]	0.859	[28.40]	0.557	[28.41]	0.966	[28.42]	0.149	[28.43]	0.212	[28.44]	8.681						
28		0.950	0.816	0.950	0.529	0.950	0.918	0.950	0.142	0.950	0.201	0.950	8.247						
Plates	10.381	[29.39]	0.168	[29.40]	0.043					[29.43]	5.069	[29.44]	0.735	[29.45]	4.366				
29		0.900	0.151	0.900	0.039					0.950	4.816	0.800	0.588	0.750	3.275				
Reinforcing bar	7.827	[30.39]	4.148	[30.40]	3.679														
30		0.950	3.941	0.950	3.495														
Wire	4.418	[31.39]	1.417	[31.40]	0.601	[31.41]	1.010	[31.42]	0.250	[31.43]	0.072	[31.44]	0.382	[31.45]	0.686				
31		0.950	1.346	0.950	0.571	0.900	0.909	0.900	0.225	0.850	0.061	0.850	0.325	0.800	0.549				
Bar	7.079	[32.39]	1.650	[32.40]	0.091	[32.41]	2.215	[32.42]	0.222	[32.43]	0.575	[32.44]	0.636	[32.45]	1.690				
32		0.900	1.485	0.900	0.082	0.800	1.772	0.800	0.178	0.800	0.460	0.800	0.509	0.800	1.352				
Light Shaped Bars	1.961	[33.39]	1.690	[33.40]	0.271														
33		0.950	1.606	0.950	0.257														
Heavy Sections	5.634	[34.39]	4.782	[34.40]	0.852														
34		0.950	4.543	0.950	0.809														
Rail	1.288		[35.40]	1.159					[35.43]	0.129									
35			0.950	1.101					0.950	0.123									
Steel Castings	0.382		[37.40]	0.015	[37.41]	0.287	[37.42]	0.025			[37.44]	0.055							
37		1.000	0.172	1.000	0.015	1.000	0.287	1.000	0.025		1.000	0.055							
Iron Castings	4.368	[38.39]	1.316	[38.40]	0.108	[38.41]	2.279	[38.42]	0.145	[38.43]	0.073	[38.44]	0.447						
38		1.000	1.316	1.000	0.108	1.000	2.279	1.000	0.145	1.000	0.073	1.000	0.447						

Figure B.6: Intermediate products to end-use goods based on Cullen

number in the top left. Three values are recorded in Table B.23 for each coordinate. [XX.XX.1] is the actual flow and matches the bottom right value from Figure B.6b. [XX.XX.2] is the scrap flow and is equal to the top right minus the bottom right numbers from Figure B.6b. Finally, [XX.XX.3] is the yield and is recorded in Figure B.6b. in the bottom left of each cell.

As an example of how these numbers were derived, consider the case of Mechanical Tubing to Cars. In the methodology from the Cullen SI, cells A2 to A20 are taken directly from data for intermediate products. USGS net intermediate product data<sup>28</sup> is directly used in this work. This allows for following the Cullen methodology more closely, but means that the intermediate products numbers in column A of Figure B.3a. do not appear in Table B.23 due to the different intermediate product categories. The net value of mechanical tubing in the US in 2014 as reported by the USGS is 1.209 Mt. Cells B1-K1 are top-down estimates of intermediate product use in each end-use sector,



derived using AISI (2015a) percentages and a bottom-up estimate to determine the breakdown of car production vs. truck production (B2.6.2). Therefore, an estimated 27.348 Mt of intermediate products were used in the production of cars in 2014. Cullen then outlines the derivations of column D, with 5% of steel in cars (the end-use good) coming from seamless tube. An assumption is made that seamless tube is equivalent to mechanical tubing and yield is considered, giving an estimate of 0.966 Mt of mechanical tubing flowing to car manufacturing and 0.918 Mt making it into the final product. Adjustments are made across the matrix as needed to balance the flows (similar to how Cullen et al. balanced the global version) resulting in Figure B.3a. Product categories are then condensed to achieve Figure B.3b. which is used as data in the reconciliation.

According to the weighting criteria set forth in Table 1 of the main text, the weighting for each of these values is 0.25 (single case study, lone data point, scaled from global numbers).

## **B.2.6 Other estimates for intermediate products**

The values set forth in Figure B.6 are a valid starting point for the intermediate to end-use goods allocation, but more U.S. specific data is available. Unlike the manually balanced flows from the Cullen method, the data reconciliation accounts for mass balance so we can simply convert unconventional data to mass values and apply them as conventional data points in the reconciliation without concern for unbalanced flows. The following subsections describe the process used to estimate flows into various end-use sectors.

### **B.2.6.1 Buildings and Infrastructure**

The AISI profile <sup>37</sup> notes that of the 120 million tons of steel intermediate products consumed in the U.S. 40% is used to make construction products. The top-down value for steel use in the U.S. construction sector is therefore 48 million tons of intermediate products (Table B.9). This value is the flow of imported and domestic steel intermediate products into the construction sector not including the scrap generated during fabrication. To avoid double counting of data sources, only the 40% figure from AISI is used as a data point in the reconciliation under coordinate [39.55] (Table B.23).

Construction can be further subdivided into buildings (office buildings, schools, residential construction, etc) and infrastructure (bridges, water and sewage, dams, etc). The U.S. Census Bureau reported annualized and seasonally adjusted construction spending in Dec 2014 as \$689 billion on buildings and \$293 billion on infrastructure <sup>41</sup>. The 2014 spending values are used as a proxy for the amount of steel destined for each construction category, resulting in a 70/30 split between buildings and infrastructure, respectively. Cullen et al (2012) calculated a 60/40 split for buildings and infrastructure in their world steel flow for the year 2008. When compared against

the world value, the value derived from Census Bureau data appears consistent. Both the Census Bureau and Cullen breakdown between buildings and infrastructure are used as unconventional data in the reconciliation, recorded under coordinate [39.55] for buildings and [40.55] for infrastructure in Table B.23.

Moynihan et al. (2012) estimate steel intermediate product use in buildings and infrastructure for the U.K in 2006. That breakdown is shown in Table B.11.

Table B.9: Breakdown of intermediate products in construction applications from Moynihan et al. (2012)

<b>Intermediate Product</b>	<b>To Buildings (kt)</b>	<b>To Infrastructure (kt)</b>	<b>Buildings (%)</b>	<b>Infrastructure (%)</b>
Sections	1600	100	37%	7%
Rebar	800	700	19%	47%
Sheet	1400	100	33%	7%
Rail	0	200	0%	13%
Tubes	500	400	12%	27%
<b>Total</b>	<b>4300</b>	<b>1500</b>		

The overall breakdown between buildings and infrastructure for the U.K. in 2006 is 75/25, which further supports the 70/30 figure derived for the U.S.

Cooper et al. (2012) report an estimated steel use in the global construction sector for 2008. The overall split between buildings and infrastructure is 67/33, which agrees well with other studies and the value arrived at using U.S. Census Bureau data. The breakdown by intermediate product is shown in Table B.12.

Table B.10: Breakdown of intermediate products in construction applications from Cooper et al. (2012)

<b>Intermediate Product</b>	<b>To Buildings (Mt)</b>	<b>To Infrastructure (Mt)</b>	<b>Buildings (%)</b>	<b>Infrastructure (%)</b>
Structural Steel	61	20	17%	11%
Connections	6	2	2%	1%
Rebar	110	98	30%	56%
Sheet	152	6	42%	3%
Rails	0	10	0%	6%
Drawn Wire	8	7	2%	4%
Tube	27	32	7%	18%
<b>Total</b>	<b>364</b>	<b>175</b>		

When these product breakdowns are applied to steel use in the U.S. in 2014, the results are as seen in Table B.13.

Table B.11: Intermediate product use in U.S. construction according to product breakdowns from Moynihan et al. (2012) and Cooper et al. (2012)

Intermediate Product	Moynihan et al.		Cooper et al.	
	To Buildings (Mt)	To Infrastructure (Mt)	To Buildings (Mt)	To Infrastructure (Mt)
Structural Steel	13.4	0.8	5.4	1.8
Connections	-	-	0.5	0.2
Rebar	6.7	5.6	9.7	8.9
Sheet	11.7	0.8	13.4	0.5
Rails	0.0	1.6	0.0	0.9
Drawn Wire	-	-	0.7	0.6
Tube	4.2	3.2	2.4	2.9
Total	36	12	32.16	15.84

These values are used as data points within the data reconciliation and reported in Table B.23. For example, 4.2 Mt (4200 kt) of tube is recorded under coordinate [28.39.1] as “Pipe and Tubing to Buildings.” To align the intermediate product categories from Moynihan et al. and Cooper et al. with those used in this work, the following adjustments were also made:

- “Structural steel” was divided between light shaped bar and heavy sections in the same proportion as values previously found in section B2.5: Buildings 26% light, 74% heavy; Infrastructure 24% light, 76% heavy (e.g. 800 kt of “structural steel” to infrastructure from Table B.13 is divided between coordinates [33.40.1] *Light shaped bars to infrastructure*: 192 kt and [34.40.1] *Heavy Sections to Infrastructure*: 608 kt).
- “Connections” are assumed to be made of plate
- Sheet is similarly divided between HR sheet and galvanized sheet in the same proportion as values from section B2.5: Buildings 84% HR, 16% galvanized; Infrastructure 77% HR, 23% Galvanized (e.g. 13400 kt of “sheet” to buildings from Table B.13 is divided between coordinates [24.39.1] *HR sheet to buildings*: 11256 kt and [26.39.1] *Galvanized to buildings*: 2144 kt)

### B.2.6.2 Automobiles

The AISI profile <sup>37</sup> notes that of the 120 million tons of steel apparent intermediate product demand in the U.S. 26% goes to automotive applications. This includes both cars and trucks. The top-down total for steel use in the U.S. automotive manufacturing sector is therefore 31.2 million tons of intermediate products. This value is the flow of imported and domestic steel intermediate products into the automotive manufacturing sector plus the scrap generation associated with producing automobiles as reported by AISI and is the starting point in top-down estimates of intermediate product usage in the automotive sector.

The bottom-up estimate starts with automotive production statistics. OICA (2016a, 2016b, 2016c) reports annual production statistics of automobiles by country and the following categories:

- **Passenger cars** are motor vehicles with at least four wheels, used for the transport of passengers, and comprising no more than eight seats in addition to the driver's seat.
- **Light commercial vehicles** are motor vehicles with at least four wheels, used for the carriage of goods. Mass given in tons is used as a limit between light commercial vehicles and heavy trucks. This limit depends on national and professional definitions and varies between 3.5 and 7 tons.
- **Heavy trucks** are vehicles intended for the carriage of goods. Maximum authorized mass is over the limit (ranging from 3.5 to 7 tons) of light commercial vehicles. They include tractor vehicles designed for towing semi-trailers.
- **Buses and coaches** are used for the transport of passengers, comprising more than eight seats in addition to the driver's seat, and having a maximum mass over the limit (ranging from 3.5 to 7 tons) of light commercial vehicles.
- **Light vehicles** include passenger cars and light commercial vehicles.
- **Commercial vehicles** include light commercial vehicles, heavy trucks, coaches and buses.

According to EPA statistics <sup>45</sup>, the average mass for U.S. passenger cars in 2014 was 1614 kg. Light commercial vehicles from the same year had an average mass of 2173 kg. Data from AutoSteel <sup>46</sup> indicates the average mass of a heavy truck is 6333 kg. 60% of the mass of a passenger car is steel (Dai et al., 2016). Table B.14 is the result if that same percentage is applied to all other vehicle categories and their respective production and average mass. The automotive sector can then be separated into "cars" (including passenger cars and light commercial vehicles) and trucks (heavy commercial vehicles) using the relative amounts of steel estimated to be going to each category. Using this estimation, 92.4% of steel intermediate products bound for the automotive sector is

used in the production of cars and 7.6% in the production of trucks. These percentages are used as unconventional data records in the reconciliation.

Table B.12: U.S. Production of Vehicles 2014

Vehicle Type	Avg. Mass (kg)	U.S. Production (2014)	Total Vehicle Mass (kt)	Total Steel Mass (kt)
Passenger Cars	1614	4253098	6866	4119
Light Commercial Vehicles	2173	7118288	15466	9280
Heavy Commercial Vehicles	5600	29313	1620	972
Buses and Coaches	-	-	-	-
<b>Total</b>		11660699		14371

Autosteel<sup>46</sup> also reports estimated values of steel to new U.S. light-duty automobiles by intermediate product. These estimations are for how much steel is in the final, finished vehicle, which is lower than the actual steel used in fabricating the vehicle due to manufacturing scrap. To account for manufacturing scrap and convert the steel in the finished product to the input of intermediate steel to manufacturing, the values from Autosteel are divided by approximate yields for each intermediate product. These yields are based on yields used by Cullen et al. (2012) and are specific to each product and its use in the automotive sector.

Table B.15 shows the results if the Autosteel breakdown is applied to the bottom-up estimate using OICA and EPA data and the results if the breakdown is applied to the top-down estimate using AISI data. Calculating the bottom-up values is straightforward: simply multiply the bottom-up estimate of total steel in cars (both passenger cars and light commercial vehicles such as SUV's and pickup trucks) by the percentage in Table B.15. For example, the mass of wire rod contained in finished cars in 2014 is  $(4119+9280)*(3.4\%) = 458$  kt.

Calculating the top-down values involves one more step to account for the manufacturing losses since the Autosteel breakdown is for finished cars and not all intermediate products have the same fabrication yield when used in automotive applications. This requires solving an equation of the form

$$\frac{\alpha_1 x}{y_1} + \frac{\alpha_2 x}{y_2} + \dots + \frac{\alpha_n x}{y_n} = T \quad (\text{B.11})$$

Where  $\alpha_n$  is the percentage from the Autosteel breakdown for a given intermediate product,  $y_1$  is the corresponding yield from Cullen,  $x$  is the total steel embedded in finished cars, and  $T$  is the total steel destined for car production as determined by the top-down estimate. Once  $x$  is calculated, each intermediate product flow can be determined by multiplying  $x$  by the corresponding percentage from the Autosteel breakdown.

Table B.13: Intermediate products embedded in vehicles in 2014

	% of total steel	Bottom Up	Top Down	Fab Yields	Coord
Wire rod	3.4%	458	682	0.9	31.41.1
Plates	0.6%	80	119	0.7	29.41.1
Bar	14.7%	1976	2944	0.8	32.41.1
Light Shaped Bars	0.7%	96	143	0.8	33.41.1
Rebar	0.0%	0	0		
Tube and Pipe	6.4%	861	1283	0.95	28.41.1
Tin mill sheets	0.1%	15	23	0.6	27.41.1
HR Sheet and Strip	17.9%	2402	3578	0.6	24.41.1
CR Sheet and Strip	16.4%	2194	3270	0.6	25.41.1
Galv Sheet and Strip	27.6%	3697	5508	0.6	26.41.1
Iron castings	12.1%	1620	2414	1	38.41.1
<b>Total</b>		13399	19964		

The totals from the bottom up estimate do not agree well with the top down estimate of 28.8 Mt of steel. However, because the data is to be reconciled, these estimates are used as data points and the reconciliation will address the inconsistencies based on the weighting given to each set of data points.

### B.2.6.3 Machinery

Daehn et al. (2017) describes the breakdown for steel in machinery as follows:

Table B.14: Composition of machinery and equipment steel mass by intermediate product as described by Daehn et al. (2017)

<b>Intermediate Product</b>	<b>Percentage in Final goods</b>
Rail	0.6%
Wire Rod	4.5%
HR Bar	20.5%
Plate	17.0%
HRC	17.0%
CRC	10.8%
Electrical Sheet	4.5%
Welded Tube	11.4%
Seamless Tube	2.3%
Cast Iron	8.5%
Cast Steel	2.8%
Total	100%

These are post-fabrication (post-yield) values for global machinery end-use. By applying the same equation used to determine top-down estimates for intermediate products in cars, we have the estimates of steel used in machinery manufacturing shown in Table B.17. The “post-fab” estimates are used as data points in the reconciliation.

Table B.15: Bottom-up estimates of intermediate products used in machinery and equipment manufacturing

	Yield	Pre-Fab	Post-Fab	Coord
Rail	0.95	59	56	35.43.1
Wire	0.8	526	421	31.43.1
Bar	0.8	2397	1917	32.43.1
Plate	0.8	1987	1590	29.43.1
HRC	0.8	1987	1590	24.43.1
CRC	0.6	2385	1431	25.43.1
Pipe & Tubing	0.8	1602	1281	28.43.1
Iron Castings	1	795	795	38.43.1
Steel Castings	1	262	262	37.43.1

#### B.2.6.4 Appliances

AISI (2015) reports that production of domestic appliances made up 4% of the 120 Mt total steel intermediate product use in 2014, resulting in a top-down estimate of 4.8 Mt being used in appliance manufacturing (including fabrication scrap).

Appliance design magazine <sup>49</sup> reports shipments of all major domestic appliances in the United States. AISI gives estimates of the mass of steel in specific types of appliances on their website <sup>50</sup> which are combined with the production data to estimate the amount of steel in finished appliances in 2014. This can be seen in Table B.18.

Table B.16: Total steel mass of appliances sold in the U.S. in 2014

Category	Quantity Sold 2014	Avg steel mass (kg)	Total steel mass (kg)
Electric Cooking	5130600	48.4	248545068
Gas Cooking	3060900	67.8	207427092
Microwave Ovens	9882700	13.1	129102259
Clothes Washers	8681600	40.5	351852037
Electric Dryers	5484800	48.5	266201387
Gas Dryers	1273600	45.5	58000602
Kitchen sink disposals	7128600	3.6	25867829
Dishwashers	6961200	12.3	85727407
Compactors	35100	45.9	1612011
Refrigerators and freezers	11698900	52.5	614231053
Room AC Units and Dehumidifiers	8143000	16.1	131492255
<b>Total</b>	<b>67,481,000</b>		<b>2120059000</b>

By applying the overall fabrication yield for appliances from Cullen et al. <sup>40</sup> we arrive at a total steel flow of 2.65 Mt into appliances (including manf. scrap), which is significantly lower than the top-down estimate. Since no further breakdown is available allocating specific intermediate products, this value is used as a lower bound for the amount of steel flowing to appliances.



### B.2.7 Indirect trade

$$\begin{aligned} \text{Iron intensity of imports} \left( \frac{\text{kg}}{\text{USD}} \right) = & 0.04 + (0.25 \times \text{iron content as mass}\%) \\ & - (0.09 \times \text{fab.index}) \\ & - (0.05 \times \text{energy conversion index}) \end{aligned} \quad (\text{B.12})$$

Data on the indirect import and export of steel goods is provided by the U.N. Comtrade Database<sup>51</sup>. As performed by Wang et al. (2007), in this analysis we consider the trade of 29 product categories. The Comtrade data shows the value of each category in terms of U.S. dollars (USD). In 2014, for 19 of the import categories and 18 of the export categories, the quantity (in kilograms) of the import and export category is also reported. First, a conversion factor from product mass to steel mass was applied using data from page S8 of the supporting information from Wang et al.'s (2007) paper, "Forging the anthropogenic iron cycle"<sup>52</sup>. Wang et al. provide steel content statistics for all 29 product categories used in this analysis. Subsequently, the mass of imported and exported steel can be readily calculated for the 19 import categories and 18 export categories in which product mass flow data is available. The mass flows of the remaining categories is calculated using the regression (empirical) equations shown in equation B2 and B3, which were derived in Cooper et al. (2019).

$$\begin{aligned} \text{Iron intensity of exports} \left( \frac{\text{kg}}{\text{USD}} \right) = & -0.03 + (0.35 \times \text{iron content as mass}\%) \\ & - (0.065 \times \text{fab.index}) \\ & - (0.065 \times \text{energy conversion index}) \end{aligned} \quad (\text{B.13})$$

The estimated indirect steel flows (both imports and exports) are shown in Table B.22. The "Part or Final Product" categories in Table B.22 are color-coded according to end-use category as follows:

Table B.17: End-use categories for part and final product entries from Table B.22

	1	Passenger motor cars, other than buses
Cars	3	Bodies and Parts motor vehicles excl. motorcycles
	12	Internal combustion engines, not for aircraft
	25	Rubber tires and tubes for vehicles and aircraft
	7	Lorries and trucks, including ambulances, etc
Trucks	14	Trailers and other vehicles not motorized and parts
	27	Road tractors for tractor trailer combinations
	2	Machinery and appliances non electrical parts
	6	Machines for special industries
	11	Nuts, bolts, screws, rivets, washers of iron/steel
Machinery and Equipment	19	Metalworking machinery
	20	Office machines
	22	Agricultural machinery and implements
	24	Tools for use in the hand or machinery
	26	Textile and leather machinery
	29	Nails, tacks, staples, spikes, etc of iron and steel
	5	Other electrical machinery and apparatus
Energy	9	Electrical power machinery and switchgear
	21	Telecommunications apparatus
Domestic Appliances	10	Domestic electrical Equipment
	4	Manufactures of metal
Containers	18	Casks, drums, etc
	8	Ships and boats
	13	Wire products excl electric and fencing grills
	15	Scientific, medical, and optical instruments
Other/Defense	16	Metal furniture
	17	Rail and tram cars, not mechanically propelled
	23	Perambulators, toys, games, and sporting goods
	28	Domestic utensils of iron or steel

The total indirect import into each end-use sector is calculated by summing the steel values in each category in Table B.22. The totals are reported in Table B.23 under coordinates [48.41-47].

Table B.18: Degree of fabrication & assembly (high=1; low=0)

<b>Fabrication &amp; Assembly Index (0-1)</b>	<b>Justification</b>	<b>Products</b>
0.00	Products that come straight out of metal forming equipment ready to be shipped to the customer	Nuts, bolts, screws, rivets, washers of iron/steel; Nails, tacks, staples, spikes, etc. of iron or steel
0.25	Products that require minimal, low skill labor to fabricate and/or assemble before shipping to the customer	Manufactures of metal; Casks, drums, etc.; Domestic Utensils of iron or steel; Perambulators, toys, games, and sporting goods; Tools for use in the hand or in machines
0.50	Products that require moderate, medium skill labor to fabricate and/or assemble before shipping to the customer	Metal furniture; Rubber tires and tubes for vehicles and aircraft; Office Machines; Telecommunications apparatus
0.75	Products that require fabrication of many components for a sub-assembly	Bodies and Parts motor vehicles excl. Motorcycles; Internal combustion engines, not for aircraft; Trailers and other vehicles not motorized and parts; Wire products excl. electric and fencing grills; Rail and tram cars, not mechanically propelled
1.00	Products that require extensive, potentially high skill labor, fabrication of hundreds of components	Passenger motor cars, other than buses; Lorries and trucks, including ambulances, etc.; Domestic Electrical Equipment; Agricultural machinery and implements; Road tractors for tractor trailer combinations; Machinery and appliances non electrical parts; Other electrical machinery and apparatus; Machines for special industries; Ships and boats; Electric power machinery and switchgear; Scientific, medical, and optical instruments; Metalworking machinery; Textile and leather machinery

Table B.19: Presence of energy transformation system (no=0; yes=1)

<b>Energy Conversion Index (0-1)</b>	<b>Justification</b>	<b>Products</b>
0.00	Products that contain no energy transformation system	Manufactures of metal; Nuts, bolts, screws, rivets, washers of iron/steel; Trailers and other vehicles not motorized and parts; Metal furniture; Casks, drums, etc.; Rubber tires and tubes for vehicles and aircraft; Domestic Utensils of iron or steel; Nails, tacks, staples, spikes, etc. of iron or steel; Wire products excl. electric and fencing grills; Rail and tram cars, not mechanically propelled; Perambulators, toys, games, and sporting goods; Tools for use in the hand or in machines
0.50	Machines that contain low cost energy conversion systems	Machinery and appliances non electrical parts; Office Machines; Telecommunications apparatus
1.00	Machines that contain multiple energy conversion systems or whose main purpose in energy conversion	Passenger motor cars, other than buses; Bodies and Parts motor vehicles excl. Motorcycles; Lorries and trucks, including ambulances, etc.; Domestic Electrical Equipment; Internal combustion engines, not for aircraft; Agricultural machinery and implements; Road tractors for tractor trailer combinations; Other electrical machinery and apparatus; Machines for special industries; Ships and boats; Electric power machinery and switchgear; Scientific, medical, and optical instruments; Metalworking machinery; Textile and leather machinery

Figure B.7: U.S. imports and exports of 29 product categories in 2014

No.	SITC-1 Code	Parts or Final Product	INDIRECT IMPORTS				INDIRECT EXPORTS				Iron content (mass fraction)	Degree of fabrication & assembly (high=1; low=0)	Presence of energy conversion system (non=0; yes=1)
			Value (USD)	Value (kg)	Steel value (kg)	Steel per dollar (kgs/USD)	Value (USD)	Value (kg)	Steel value (kg)	Steel per dollar (kgs/USD)			
All inferred values are shown highlighted in yellow			Data from U.N. Comtrade database				Data from U.N. Comtrade database						
1	7321	Passenger motor cars, other than buses	15,829,683,632	10,984,590,379	7139983681	0.66	41,063,551,637	4266115844	2764402099	0.045	0.65	1.00	0.00
2	719	Machinery and appliances non electrical parts	115,408,240,243	164,431,602,74	12,332,370,206	0.107	10,119,292,995,968	177,765,328,43	13,323,399,632	0.132	0.75	1	0.5
3	7328	Bodies and Parts motor vehicles excl. Motorcycles	64,536,936,975	5,564,742,863	3895320004	0.060	43,352,885,600	4040704039	2828492827	0.065	0.70	1.00	0.00
4	698	Manufactures of metal	18,505,886,702	540339017	4864823116	0.263	12,428,586,299	3980809757	3582728781	0.288	0.90	0.00	0.00
5	729	Other electrical machinery and apparatus	80,913,183,041	4546399258	2300470092	0.031	69,631,017,549	3358836945	1847371265	0.027	0.55	1	1
6	718	Machines for special industries	27,749,357,244	2979294777	2234331083	0.081	25,679,757,207	3323809475	2484857106	0.097	0.75	1	1
7	7323	Lorries and trucks, including ambulances, etc.	23,240,855,439	3,038,479,499	2430943599	0.105	14,705,720,223	1968055841	1574444673	0.107	0.80	1.00	0.00
8	735	Ships and boats	1,467,646,847	192004566	172804109	0.118	3,400,936,239	567143742	510429366	0.150	0.90	1	1
9	722	Electric power machinery and switchgear	53,119,696,117	1,671,326,766	919229721	0.017	39,460,471,718	1322430060	727336533	0.018	0.55	1	1
10	7290	Domestic Electrical Equipment	19,209,218,371	2,335,755,205	151841208	0.079	3,429,829,837	385241586	250420031	0.073	0.65	0.00	0.00
11	69421	Nuts, bolts, screws, rivets, washers of iron/steel	5,151,972,216	1,540,103,092	1599901000	0.292	3,842,363,862	550035372	53903205	0.140	0.98	0.00	1.00
12	7115	Internal combustion engines, not for aircraft	27,665,403,184	2,458,571,105	122928553	0.044	19,188,633,930	1128730748	564365374	0.029	0.50	1.00	0.00
13	693	Wire products excl. electric and fencing grills	1,601,491,850	690,045,061	621040555	0.388	1,068,227,250	233764811	210388330	0.197	0.90	0.75	0
14	7333	Trailers and other vehicles not motorized and parts	2,747,015,614	795,130,522	39756261	0.145	4,073,835,229	652240454	326120227	0.080	0.50	1.00	0.00
15	861	Scientific, medical, and optical instruments	54,012,732,393	3034841382	1699168790	0.031	59,907,151,260	2889797587	358988662	0.027	0.55	1	1
16	8213	Metal furniture	5,000,937,756	923,851,463	681445862	0.136	1,147,346,765	19168789	134189152	0.117	0.70	0.00	0.00
17	7316	Rail and tram cars, not mechanically propelled	710,802,933	151460230	128741195	0.181	1,140,892,075	293824422	249750738	0.219	0.85	0.75	0
18	69221	Casks, drums, etc.	597,972,516	134,274,558	128903576	0.216	5,827,254,790	1091767905	1048097189	0.180	0.96	0.00	0.00
19	715	Metaworking machinery	6,205,274,155	411,603,144	267542044	0.043	3,487,737,187	331775215	215653889	0.062	0.65	1	1
20	714	Office Machines	115,447,112,479	1133914932	2499971339	0.022	48,287,786,635	0	0	-0.01	0.22	0.5	0.5
21	724	Telecommunications apparatus	142,878,836,129	11882293218	2374458444	0.017	49,968,439,655	30401999	60802194	0.001	0.20	0.5	0.5
22	712	Agricultural machinery and implements	8,120,074,028	786,577,778	550604445	0.068	8,933,387,524	925101319	647570923	0.072	0.70	0.00	1.00
23	894	Perambulators, toys, games, and sporting goods	30,440,743,321	2,134,139,332	426827866	0.014	6,902,197,355	416988835	83397767	0.012	0.20	0.25	0
24	695	Tools for use in the hand or in machines	7,229,465,303	417,240,844	354654717	0.049	4,893,385,923	179835318	152860020	0.031	0.85	0.25	0
25	6291	Rubber tires and tubes for vehicles and aircraft	15,654,791,497	2,792,743,991	418911599	0.027	5,827,254,790	1091767905	163765186	0.028	0.15	1.00	0.00
26	717	Textile and leather machinery	4,228,111,679	362409767	235566349	0.056	1,500,025,994	142691785	92749666	0.062	0.65	1	1
27	7325	Road tractors for tractor trailer combinations	6,931,458,756	1,224,967,134	979973707	0.141	2,800,560,889	601130613	480904490	0.172	0.80	0.75	1
28	69721	Domestic Utensils of iron or steel	2,209,440,313	431,627,554	410046176	0.186	274,241,914	44945792	42698502	0.156	0.95	0	0
29	69411	Nails, tacks, staples, spikes, etc. of iron or steel	788,551,246	553,539,662	524268859	0.688	62,434,487	20164181	19768997	0.217	0.98	0	0
Color key: Domestic Trucks; Machinery and Equipment;			5342018675				3655829643						
Energy; Domestic Appliances; Containers;			50.4				36.5						
Other/Defense:													
Total (Mt)													

### B.3 MFA structure and data cataloging methodology

The flow of steel through the U.S. is modeled as a network of nodes connected by flows of material. Each node is representative of a physical process or product, so the structure of the network is driven by the process of making and fabricating steel.

The network is represented by a matrix of nodes and flows. The matrix is constructed by identifying all nodes needed for the network (in this case 51). The nodes are the rows and (when transposed) the columns of the matrix (See Figure B.7). Every cell in the matrix can then be interpreted as a flow from the row node to the column node. Each node is labeled with a number to simplify labeling to a two-number coordinate of the form [Origin Node].[Destination Node]. For example, a flow from node 2 (blast furnace) into node 5 (basic oxygen furnace) is labeled [2.5] and is recorded in the matrix in the corresponding cell. Using this method, every possible flow can be identified and labeled so data can be cataloged accordingly.

Nodes include all processes (e.g. basic oxygen furnace, hot rolling, tin mill, etc) used in making intermediate steel. Rather than representing each fabrication process as a node and showing intermediate products flowing through fabrication, we have chosen to assign a node to each intermediate product. This makes the resulting Sankey diagram more readable and allows for quantifying production scrap based on intermediate product and process. In some cases, data is available for a specific node and is either total material into that node or the total output (of usable product) from that node. Two columns have been added to accommodate recording this type of data, an input column (52) and an output column (53). For example, if a data source lists the total amount of liquid steel coming out of the EAF, that data point would be listed under [6.53] as an output from the node. If the input were known, it would be listed under [6.52]. An important difference between these

two columns is that the input column includes all steel or iron inputs to the node, while the output column only accounts for the actual product of the node (without including scrap or loss).

### B.3.1 Full matrix

The full matrix is shown in Figure B.7 with each cell labelled using the cataloguing two-coordinate system.

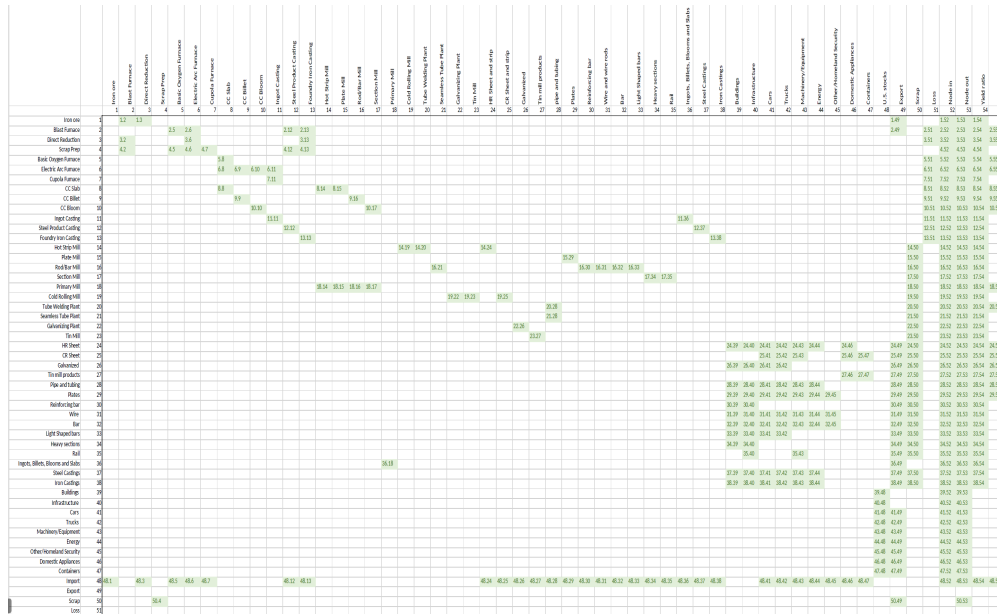


Figure B.8: Network of nodes and flows represented in matrix form

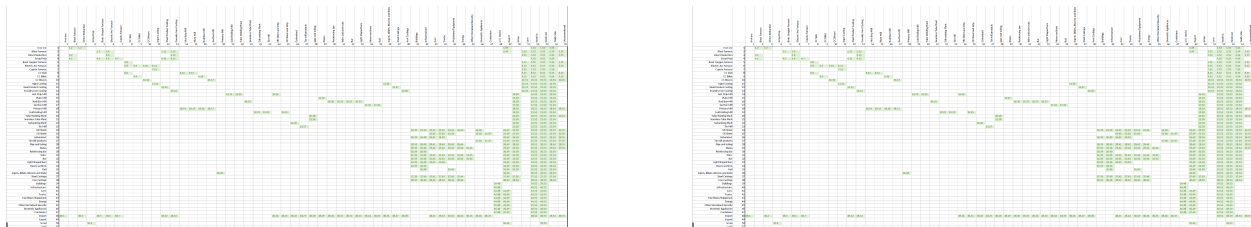


Figure B.9: Network of nodes and flows represented in matrix form

### B.3.2 Matrix node and flow data with weighting

Table B.23 (<https://pubs.acs.org/doi/abs/10.1021/acs.est.9b01016>) presents the complete list of all the data records used in the least squares optimization method used to reconcile all pertinent available data (as described in B1).

Reference used in Table B.23.

1. USGS. (2016). Iron and Steel Scrap. Minerals Yearbook.

2. USGS. (2016). Iron and Steel. Minerals Yearbook.
3. WorldSteel. (2017). Steel Statistical Yearbook 2017.
4. Worldsteel (2009) Yield improvement in the steel industry: working group report 2003—2006. World Steel Association, Brussels.
5. USGS. (2016). Iron Ore. Minerals Yearbook.
6. USGS. (2018). Iron and Steel. Mineral Commodity Summaries.
7. U.S. Department of Commerce. (2018). The Effect of Imports of Steel on the National Security.
8. Daehn, K. E., Cabrera Serrenho, A., & Allwood, J. M. (2017). How Will Copper Contamination Constrain Future Global Steel Recycling? *Environmental Science and Technology*, 51(11), 6599–6606.
9. Cullen, J. M., Allwood, J. M., & Bambach, M. D. (2012). Mapping the global flow of steel: From steelmaking to end-use goods. *Environmental Science and Technology*, 46(24), 13048–13055.
10. Schifo, J. F. and Radia, J. T. (2004). Theoretical/Best Practice Energy Use In Metal Casting Operations. U.S. Department of Energy: Energy Efficiency and Renewable Energy.
11. See Section B2.4-B2.6 for further information concerning intermediate products to end-use goods estimates
12. Moynihan, M. C., & Allwood, J. M. (2012). The flow of steel into the construction sector. *Resources, Conservation and Recycling*, 68, 88–95.
13. See Section B2.7 for further details about indirect trade estimates
14. MIDREX. (2011). World direct reduction statistics. Midrex Technologies, Inc., 12.
15. AISI. (2015a). Profile 2015.
16. Energetics Inc. Steel Industry Technology Roadmap: Barriers and Pathways for Yield Improvements.; For AISI. 2003.

## B.4 U.S. in-use stocks and scrap flows

The figures below were generated from the results of Cooper et al. (2019).

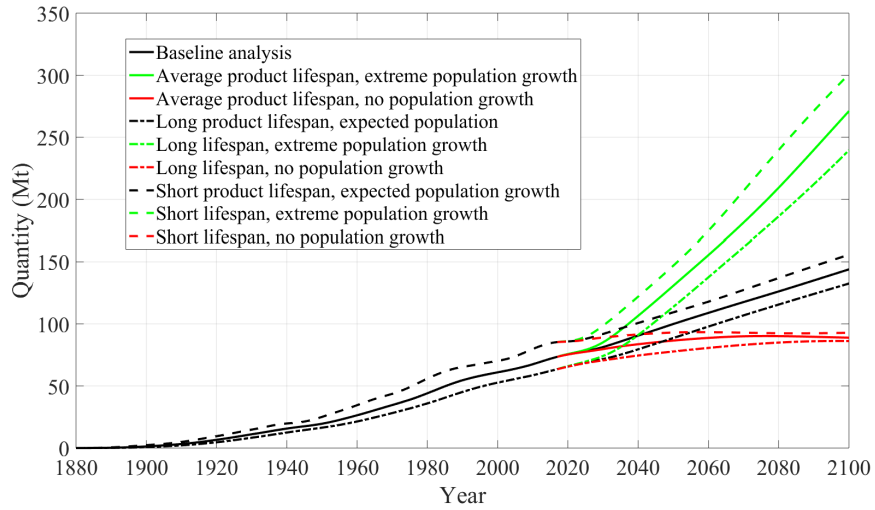


Figure B.10: Historical and future U.S. steel scrap arising aggregated over the end-use sectors

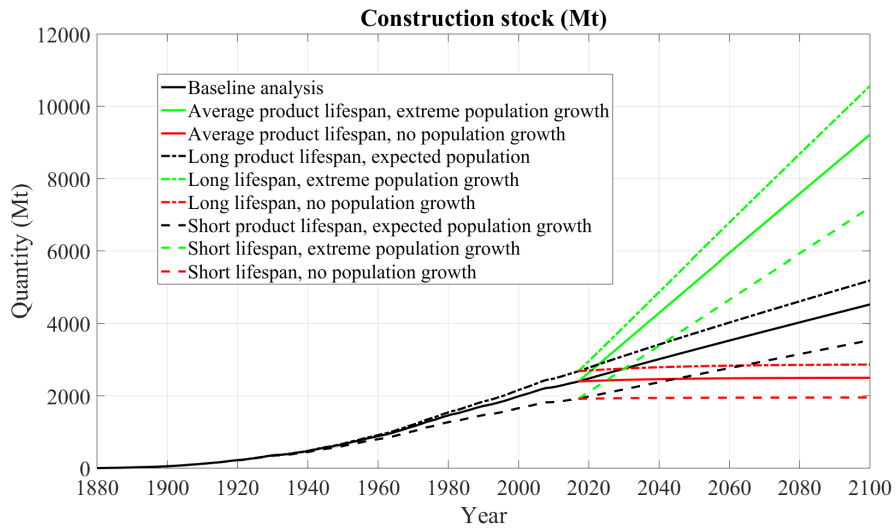


Figure B.11: Absolute steel stocks in the construction sector



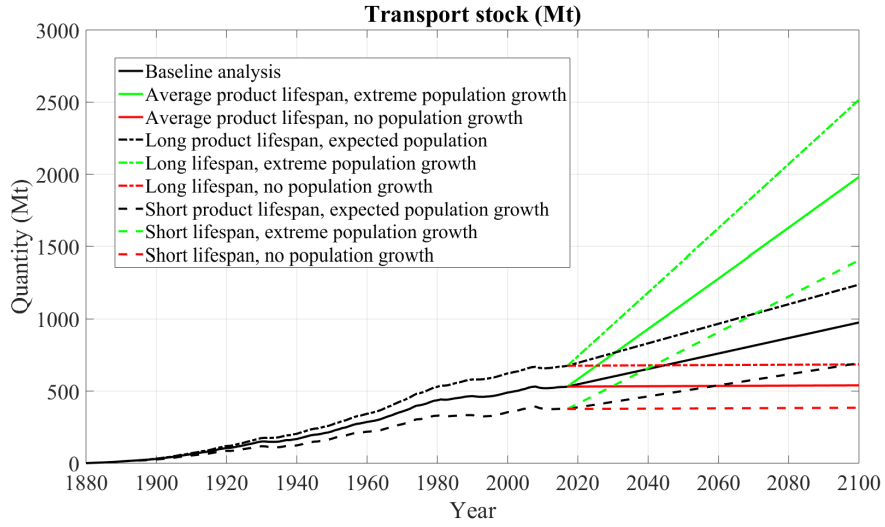


Figure B.12: Absolute steel stocks in the transport sector

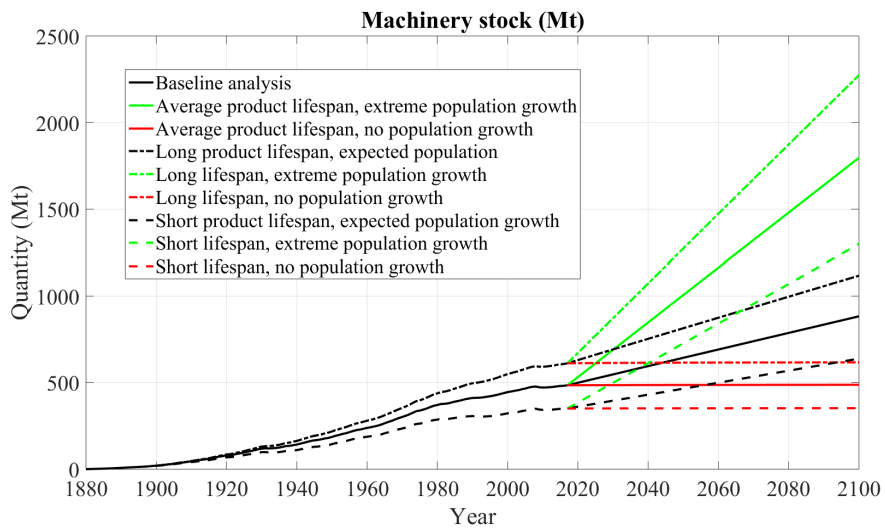


Figure B.13: Absolute steel stocks in the machinery sector

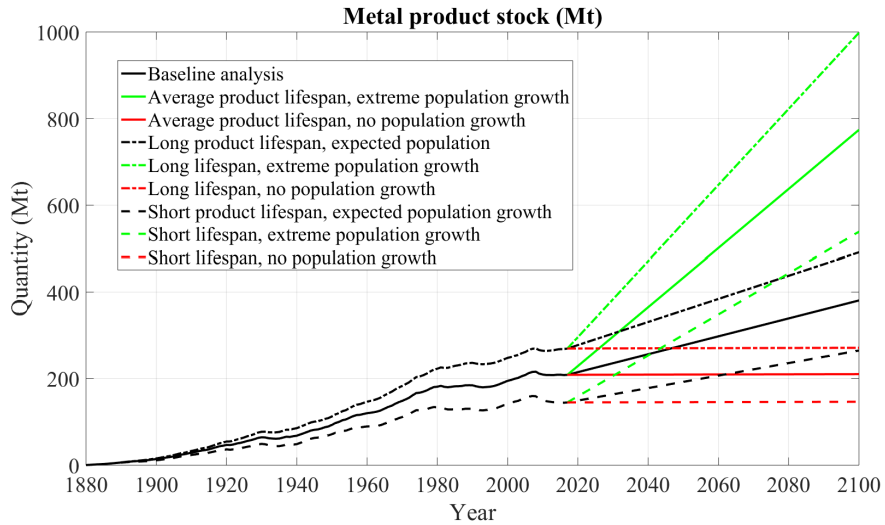


Figure B.14: Absolute steel stocks in the metal goods (products) sector

### B.5 Displacement of steel product imports with domestically recycled material

Table B.24 shows the various steel product import quantities in the final steel map. The green color indicates that the copper tolerance of the product is greater than or equal to 0.2wt.%<sub>Cu</sub>. The blue color indicate that the copper tolerance is less than 0.2wt.%<sub>Cu</sub>. The copper tolerance allocations are informed by the supporting information of Daehn et al. (2017). Of the 29.5 Mt of steel intermediate product imports, approximately 8.4 Mt have a copper tolerance equal to or greater than 0.2wt.%<sub>Cu</sub>.

Table B.20: The quantity and copper tolerance of steel product imports in 2014. Blue: tolerance  $\leq 0.2\text{wt.}\%_{\text{Cu}}$ ; Green: tolerance  $\geq 0.2\text{wt.}\%_{\text{Cu}}$

<b>Steel Intermediate Product</b>	<b>Import quantity (kt)</b>
HR Sheet and strip	3383
CR Sheet and strip	2493
Galvanized	3262
Tin mill products	712
Pipe and tubing	9361
Plates	3134
Reinforcing bar	1175
Wire and wire rods	2051
Bar	1912
Light Shaped bars	166
Heavy sections	940
Rail	397
Steel Castings	160
Iron Castings	302

## **B.6 Construction Consumption versus Prosperity**

One method of assigning responsibility for the materials used by a country is the “material footprint.” This measure accounts for the materials used to make the products that a country consumes (connecting to where they were made). The material footprint of nations is split into four components by Wiedmann et al. (2015): biomass, metal ores, construction, and fossil fuels. For 2008, the annual material footprint for different countries is shown in Figures B13 and B14. The area of a data point in the graph is proportional to the population of the country. The graphs have been constructed by the authors of this article using data from Wiedmann et al. (2015). As can be seen in the graphs, as prosperity (GDP per cap PPP) increases, the absolute demand for construction materials plateaus while overall demand continues to rise.

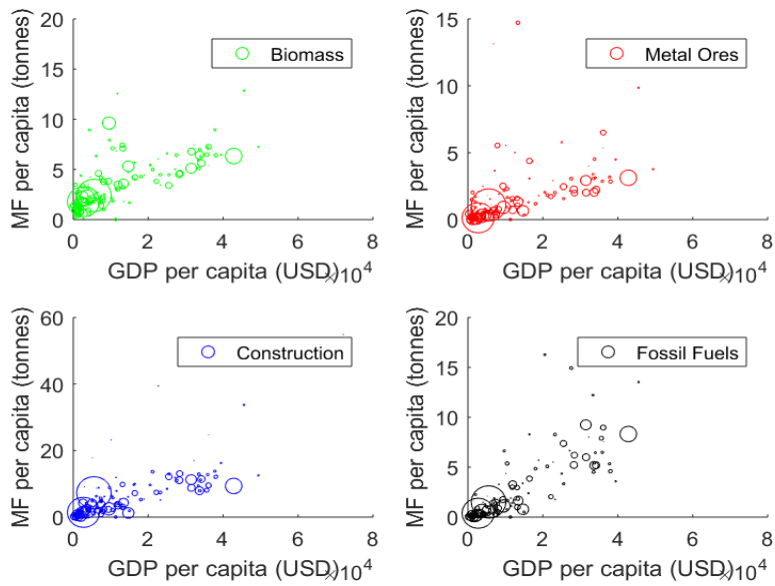


Figure B.15: Absolute material footprint versus prosperity for different countries in 2008

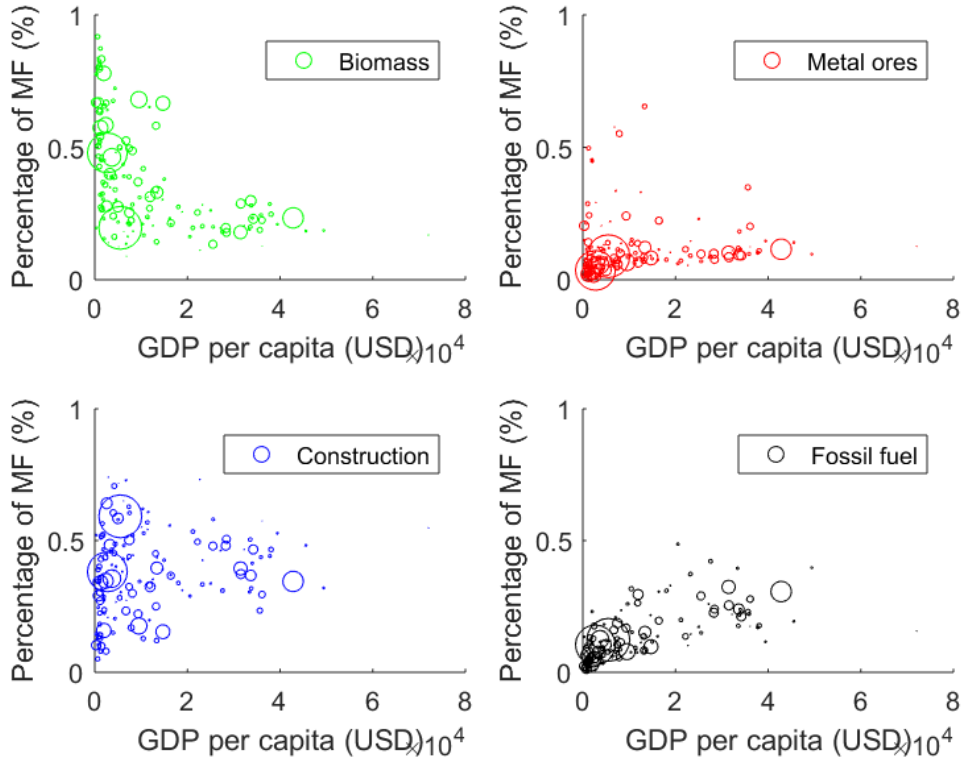


Figure B.16: Relative material footprint versus prosperity for different countries in 2008

## B.7 References

- (1) Cencic, O.; Frühwirth, R. A General Framework for Data Reconciliation-Part I: Linear Constraints. *Comput. Chem. Eng.* **2015**, *75*, 196–208. <https://doi.org/10.1016/j.compchemeng.2014.12.004>.
- (2) Laner, D.; Rechberger, H.; Astrup, T. Systematic Evaluation of Uncertainty in Material Flow Analysis. *J. Ind. Ecol.* **2014**, *18* (6), 859–870. <https://doi.org/10.1111/jiec.12143>.
- (3) Cencic, O. Nonlinear Data Reconciliation in Material Flow Analysis with Software STAN. *Sustain. Environ. Res.* **2016**, *26* (6), 291–298. <https://doi.org/10.1016/J.SERJ.2016.06.002>.
- (4) Crowe, C. M. Reconciliation of Process Flow Rates by Matrix Projection. Part II: The Nonlinear Case. *AIChE J.* **1986**, *32* (4), 616–623. <https://doi.org/10.1002/aic.690320410>.
- (5) Crowe, C. M. Data Reconciliation — Progress and Challenges. *J. Process Control* **1996**, *6* (2–3), 89–98. [https://doi.org/10.1016/0959-1524\(96\)00012-1](https://doi.org/10.1016/0959-1524(96)00012-1).
- (6) Kopec, G. M.; Allwood, J. M.; Cullen, J. M.; Ralph, D. A General Nonlinear Least Squares Data Reconciliation and Estimation Method for Material Flow Analysis. *J. Ind. Ecol.* **2016**, *20* (5), 1038–1049. <https://doi.org/10.1111/jiec.12344>.
- (7) Gottschalk, F.; Sonderer, T.; Scholz, R. W.; Nowack, B. Possibilities and Limitations of Modeling Environmental Exposure to Engineered Nanomaterials by Probabilistic Material Flow Analysis. *Environ. Toxicol. Chem.* **2010**, *29* (5), 1036–1048. <https://doi.org/10.1002/etc.135>.
- (8) Lupton, R. C.; Allwood, J. M. Incremental Material Flow Analysis with Bayesian Inference. *J. Ind. Ecol.* **2018**, *22* (6), 1352–1364. <https://doi.org/10.1111/jiec.12698>.
- (9) Giljum, S.; Hubacek, K. Alternative Approaches of Physical Input-Output Analysis to Estimate Primary Material Inputs of Production and Consumption Activities. *Econ. Syst. Res.* **2004**, *16* (3). <https://doi.org/10.1080/0953531042000239383>.
- (10) Hawkins, T.; Hendrickson, C.; Higgins, C.; H. Scott Matthews. A Mixed-Unit Input-Output Model for Environmental Life-Cycle Assessment and Material Flow Analysis. *Environ. Sci. Technol.* **2007**, *41* (3), 1024–1031. <https://doi.org/10.1021/es060871u>.
- (11) Konijn, P.; de Boer, S.; van Dalen, J. Input-Output Analysis of Material Flows with Application to Iron, Steel and Zinc. *Struct. Chang. Econ. Dyn.* **1997**, *8* (1), 129–153. [https://doi.org/10.1016/S0954-349X\(96\)00063-X](https://doi.org/10.1016/S0954-349X(96)00063-X).
- (12) Weisz, H.; Duchin, F. Physical and Monetary Input-Output Analysis: What Makes the Difference? *Ecol. Econ.* **2006**, *57* (3), 534–541. <https://doi.org/10.1016/J.ECOLECON.2005.05.011>.
- (13) Dubois, D.; Fargier, H.; Ababou, M.; Guyonnet, D. A Fuzzy Constraint-Based Approach to Data Reconciliation in Material Flow Analysis. *Int. J. Gen. Syst.* **2014**, *43* (8), 787–809. <https://doi.org/10.1080/03081079.2014.920840>.
- (14) Ploeg, F. Van Der. Balancing Large Systems of National Accounts. *Comput. Sci. Econ. Manag.* **1988**, *1*, 31–39.

- (15) Narasimhan, S.; Jordache, C. *Data Reconciliation & Gross Error Detection: An Intelligent Use of Process Data.*; 1999.
- (16) Brunner, P. H.; Rechberger, H. *Handbook of Material Flow Analysis: For Environmental, Resource, and Waste Engineers*, Edition, S.; CRC Press, 2017.
- (17) Bagajewicz, M. J. *Smart Process Plants: Software and Hardware Solutions for Data Accuracy: Data Reconciliation, Gross Error Detection, and Instrumentation Upgrade.* McGraw Hill Professional 2009.
- (18) Romagnoli, J. A.; Sanchez, M. C. *Data Processing and Reconciliation for Chemical Process Operations*; Elsevier, 1999; Vol. 2.
- (19) Matyus, T.; Gleiss, A.; Gruber, K.; Bauer, G. Data Reconciliation, Structure Analysis and Simulation of Waste Flows: Case Study Vienna. *Waste Manag. Res.* **2003**, *21* (2), 93–109. <https://doi.org/10.1177/0734242X0302100203>.
- (20) Cencic, O.; Rechberger, H. Material Flow Analysis with Software STAN. *EnviroInfo 2008 - Environ. Informatics Ind. Ecol.* **2008**, *2008*, 440–447.
- (21) Fellner, J.; Aschenbrenner, P.; Cencic, O.; Rechberger, H. Determination of the Biogenic and Fossil Organic Matter Content of Refuse-Derived Fuels Based on Elementary Analyses. *Fuel* **2011**, *90* (11), 3164–3171. <https://doi.org/10.1016/j.fuel.2011.06.043>.
- (22) Wang, D.; Romagnoli, J. A. A Framework for Robust Data Reconciliation Based on a Generalized Objective Function. *Ind. Eng. Chem. Res.* **2003**, *42* (13), 3075–3084.
- (23) Lupton, R. C.; Allwood, J. M. Incremental Material Flow Analysis with Bayesian Inference. *J. Ind. Ecol.* **2017**, *00* (0). <https://doi.org/10.1111/jiec.12698>.
- (24) Laner, D.; Rechberger, H.; Astrup, T. Systematic Evaluation of Uncertainty in Material Flow Analysis. *J. Ind. Ecol.* **2014**, *18* (6), 859–870. <https://doi.org/10.1111/jiec.12143>.
- (25) Leontief, W. Quantitative Input-Output Relations in the Economic System of the United States. **1936**.
- (26) Leontief, W. Environmental Repercussions and the Economic Structure: An Input-Output Approach. *Rev. Econ. Stat.* **1970**, *52* (3), 262–271.
- (27) Tukker, A.; Poliakov, E.; Heijungs, R.; Hawkins, T.; Neuwahl, F.; Rueda-Cantuche, J. M.; Giljum, S.; Moll, S.; Oosterhaven, J.; Bouwmeester, M. Towards a Global Multi-Regional Environmentally Extended Input-Output Database. *Ecol. Econ.* **2009**, *68* (7), 1928–1937. <https://doi.org/10.1016/J.ECOLECON.2008.11.010>.
- (28) USGS. *Iron and Steel*; 2016.
- (29) Matlab. *Fmincon Nonlinear Optimization Documentation*; Matlab, 2013.
- (30) Byrd, R. H.; Hribar, M. E.; Nocedal, J. An Interior Point Algorithm for Large-Scale Nonlinear Programming. *SIAM J. Optim.* **1999**, *9* (4), 877–900.
- (31) WorldSteel. *Yield Improvement in the Steel Industry: Working Group Report 2003 - 2006*;

Brussels, 2009.

- (32) Energetics, I. *Steel Industry Technology Roadmap: Barriers and Pathways for Yield Improvements*; 2003.
- (33) WorldSteel. *Steel Statistical Yearbook 2017*; 2017.
- (34) Pretorius, E. Personal Communication with the Authors, April 27. 2018.
- (35) USGS. *Iron and Steel Scrap*; 2016.
- (36) U.S. Census Bureau. *U.S. Imports for Consumption of Steel Products*; 2015.
- (37) AISI. Profile 2015. *Arlingt. Virginia* **2015**, 10.
- (38) Moynihan, M. C.; Allwood, J. M. The Flow of Steel into the Construction Sector. *Resour. Conserv. Recycl.* **2012**, 68, 88–95. <https://doi.org/10.1016/j.resconrec.2012.08.009>.
- (39) Cooper, D. R.; Allwood, J. M. Reusing Steel and Aluminum Components at End of Product Life. *Environ. Sci. Technol.* **2012**, 46 (18), 10334–10340. <https://doi.org/10.1021/es301093a>.
- (40) Cullen, J. M.; Allwood, J. M.; Bambach, M. D. Mapping the Global Flow of Steel: From Steelmaking to End-Use Goods. *Environ. Sci. Technol.* **2012**, 46 (24), 13048–13055. <https://doi.org/10.1021/es302433p>.
- (41) U.S. Census Bureau. *December 2014 Construction at \$982.1 Billion Annual Rate*; 2015.
- (42) OICA. Cars. <https://doi.org/10.1016/j.jbiosc.2008.09.016>.
- (43) OICA. *Heavy Trucks*; 2016.
- (44) OICA. *Light Commercial Vehicles*; 2016.
- (45) EPA. *Light-Duty Automotive Technology, Carbon Dioxide Emissions, and Fuel Economy Trends: 1975 Through 2012*; 2018. <https://doi.org/10.1002/yd.31>.
- (46) Schnatterly, J. Watching Our Weight: Steel Content of N. American Auto. Autosteel 2010.
- (47) Dai, Q.; Kelly, J. C.; Elgowainy, A. *Vehicle Materials: Material Composition of U.S. Light-Duty Vehicles*; 2016.
- (48) Daehn, K. E.; Cabrera Serrenho, A.; Allwood, J. M. How Will Copper Contamination Constrain Future Global Steel Recycling? *Environ. Sci. Technol.* **2017**, 51 (11), 6599–6606. <https://doi.org/10.1021/acs.est.7b00997>.
- (49) Appliance Design. Shipments. 2015.
- (50) AISI. The New Steel. Appliance Recycling for Environmentally Friendly Consumers. 2015.
- (51) U.N. UN Comtrade Database.
- (52) Wang, T.; Müller, D. B.; Graedel, T. E. Forging the Anthropogenic Iron Cycle. *Environ. Sci. Technol.* **2007**, 41 (14), 5120–5129. <https://doi.org/10.1021/es062761t>.
- (53) Cooper, D.; Ryan, N.; Zhu, Y.; Syndergaard, K. The Potential for Material Independence and Circularity in the U.S. Steel Sector. *Submitt. to J. Ind. Ecol.* **2019**.

(54) Wiedmann, T. O.; Schandl, H.; Lenzen, M.; Moran, D.; Suh, S.; West, J.; Kanemoto, K. The Material Footprint of Nations. *Proc Natl Acad Sci U S A* **2015**, *112* (20), 6271–6276. <https://doi.org/10.1073/pnas.1220362110>.



## Appendix C

### The coming wave of aluminum sheet scrap from vehicle recycling in the U.S.

#### C.1 Vehicle longevity study

This section summarizes the methods for estimating the vehicle survival rate and lifespan distributions.

##### C.1.1 Vehicle survival rate

A survival rate curve shows the fraction of vehicles produced for model year,  $t_0$ , that will still be in the vehicle fleet at age,  $a$ , in year  $t$ , where  $t = t_0 + a + 1$  (NHTSA, 2006). The equation for calculating historical vehicle survival rate at a given age is as below:

$$Survival\ rate(a, t) = \frac{Fleet\ size(a, t)}{Vehicle\ production\ volume(t_0 = t - a - 1)} \quad (C.1)$$

We approximate the vehicle survival rates of new aluminum intensive vehicles with the survival rates of corresponding steel versions in the past. To calculate the historical survival rates of the four types of vehicles, we use the vehicle registration data from IHS Markit (2019) which records the fleet age distribution by model years between 1975 – 2017 for F-150, 1966 – 2017 for Super Duty, 1998 – 2017 for Expedition and Navigator. IHS changed the registration data collection procedure in 2009 and again in 2010 (NHTSA and EPA, 2018). To avoid the inclusion of incompatible registration data from IHS after 2008, we focused on the fleet age distribution and fleet size data between 2000 and 2008. This gives the fleet size information of 1975 – 2008 model year F-150 between age 1 and age 34, 1966 – 2008 model year Super Duty between age 1 and age 43, 1999 – 2008 model year Expedition and Navigator between age 1 and age 11.

For 1966-1994 model year F-150 and F-50s, the U.S. production volume by model year is available from (Gunnell, 2003). For 1999-2008 model year Navigator and Expedition, the vehicle production volume is approximated as the vehicle fleet size at age  $a = 0$  due to lack of initial production data. This approximation assumes that all the vehicles of model year  $t_0$ , are sold by  $t_0 + 1$ . Since the first generation of Navigator and Expedition only started in 1998 and 1997 respectively,

there is a lack of information of survival rate beyond 11 years of vehicle life using registration data between 2000 and 2008. However, a similar type of vehicle, the Ford Explorer started production in 1991. Its registration data is available and is used to approximate the vehicle survival rates of Navigator and Expedition between 12 and 18 years old. To append the survival rate data of the Explorer to that of the Navigator and Expedition, we combine their survival rates using equation C2 (derived from equation C1) which calculates the survival rate of a vehicle at age  $a$  in year  $t$  with the survival rate at age  $a - 1$  in year  $t - 1$  and fleet size data in both years.

$$Survival\ rate(a, t) = Survival\ rate(a - 1, t - 1) * \frac{vehicle\ fleet\ size(a, t)}{vehicle\ fleet\ size(a - 1, t - 1)} \quad (C.2)$$

The calculated historical survival rates from registration data (1) ignores the impact of delayed vehicle sales and dual registration in states (the national level registration data is the aggregate of state level registration data and a vehicle could be registered in more than one state due to legislation requirements and interstate mitigation), and (2) are only available for a short period of vehicle ages for each model year of the four types of vehicle. To extrapolate the vehicle survival rate model that show the survival rates of a vehicle at all ages and minimizes the impact of delayed sales and dual registration, we first group the calculated vehicle survival rates by vehicle generation and then fit the NHTSA (2006) survival rate model (equation C3) to the grouped survival rates using least-squares regression with a vehicle totaling loss constraint. The optimization is conducted using Matlab's `fmincon` function with interior point algorithm. We use the NHTSA (2006) model parameter as the initial guess for the optimization. The step tolerance, constraint tolerance and optimization tolerance are 1E-10, 1E-6, 1E-6 respectively.

$$Survivalrate(a, g) = 1 - exp(-exp(c_1 + (c_2 \times a))) \quad (C.3)$$

Where  $a$  is the age of vehicles from model generation,  $g$ , and  $c_1$  and  $c_2$  are fitted constants that define the shape of the survival rate curve. The vehicle generation in this study refer to the consecutive years of types of vehicle without a major redesign. Within each vehicle generation, it is assumed that the survival rate of vehicles are relatively consistent (Bento, Roth, and Zuo, 2013; Greene and Chen, 1981; Walker, 1968).

Table C.1: Vehicle generation by model years

Generation (g)	F-150	F-Series	Expedition	Navigator
Generation 1	N/A	N/A	1997-2002	1998-2002
Generation 2	N/A	N/A	2003-2006	2003-2006
Generation 3	N/A	N/A	2007-2017	2007-2017
Generation 5	N/A	N/A	N/A	N/A
Generation 6	1973-1979	1973-1979	N/A	N/A
Generation 7	1980-1986	1980-1986	N/A	N/A
Generation 8	1987-1991	1987-1991	N/A	N/A
Generation 9	1992-1997	1992-1997	N/A	N/A

*Vehicle totaling* is a term used by insurance companies when a vehicle needs to be scrapped after a collision because it is not economically feasible to repair it. For vehicles, less than ten years old, the survival rate is largely determined by the totaling rate (Figure C1).

## Share of Overall Claim Count by Vehicle Age

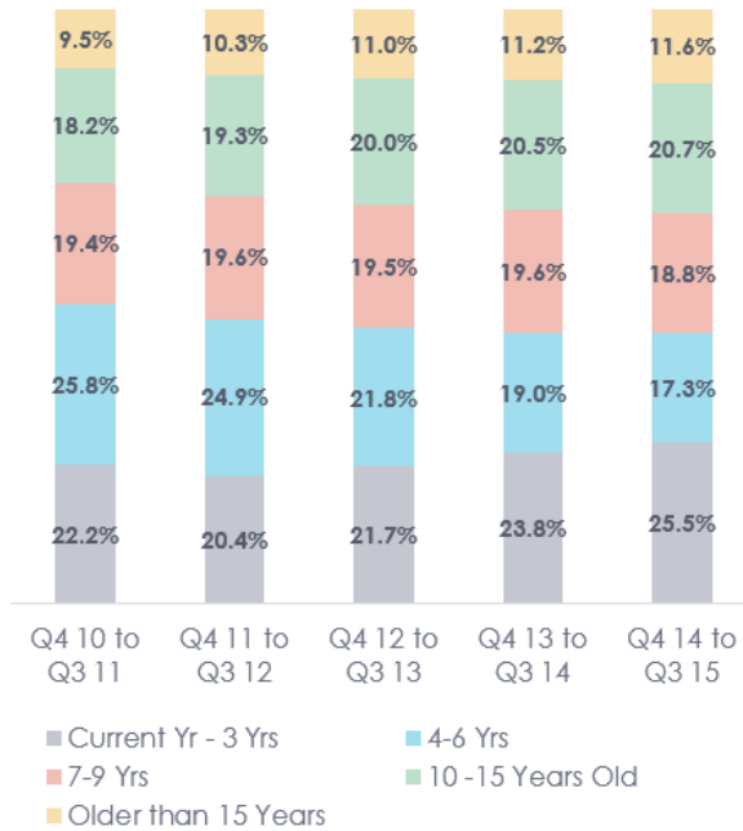


Figure C.1: Share of overall claim count by vehicle age (CCC, 2015)

Hartwig and Weisbart (2016) report the likelihood of vehicles being involved in a collision which results in an insurance claim being made. CCC (2015) report the percentage of insurance claims for vehicles of different ages that are flagged as a “total loss”. The totaling data from Hartwig and Weisbart (2016) and CCC (2015) are combined to calculate the vehicle survival rate just based on the avoidance of totaling the vehicle (Figure C2)(CCC, 2015; Hartwig and Weisbart, 2016). The mean of the calculated vehicle survival rate based on the avoidance of totaling the vehicle is used as a constraint for the nonlinear least square fitting. It ensures that during the first 9 years the survival rate is within  $\pm 5\%$  of the calculated mean vehicle survival rate based on the avoidance of totaling the vehicle.

A weakness of using vehicle total loss related survival rate as the constraint is that some of the vehicles claimed “total loss” could be rebuilt and re-registered. In the U.S., a vehicle that is declared total loss or write-offs due to severe damage (by collision, impact, fire, or flood) or theft and dismantling must be assigned a classification, which is called “branded” (Sawyer-Beaulieu

and Tam, 2006). Each state in the U.S. has different brand system that distinguish between normal vehicles and salvage/rebuilt vehicles in the vehicle title and the branding system may further split vehicles into rebuild, flooded, hail, salvage, junk and other types according to vehicle conditions (Keathley et al., 2019). According to the study of Keathley et al. (2019), the state of Kentucky issues around 84,368 (in 2014) to 110,449 (2018) salvage and rebuilt titles comparing to 1,890,079 vehicles registered in 2010. However, they also noted that the salvage titles can be retitled as rebuilt titles and it is difficult to ascertain the true number of titles issued (Keathley et al., 2019). Importantly, in order for rebuilt vehicles to be legally operated on road, they must be registered again following the same procedure as normal vehicle. Thus, the survivability of rebuilt vehicles will be captured by vehicle registration data once they are re-registered. The consideration of both vehicle totaling loss and registration data dampen the uncertainties in survival rate model due to the salvage/rebuilt route.

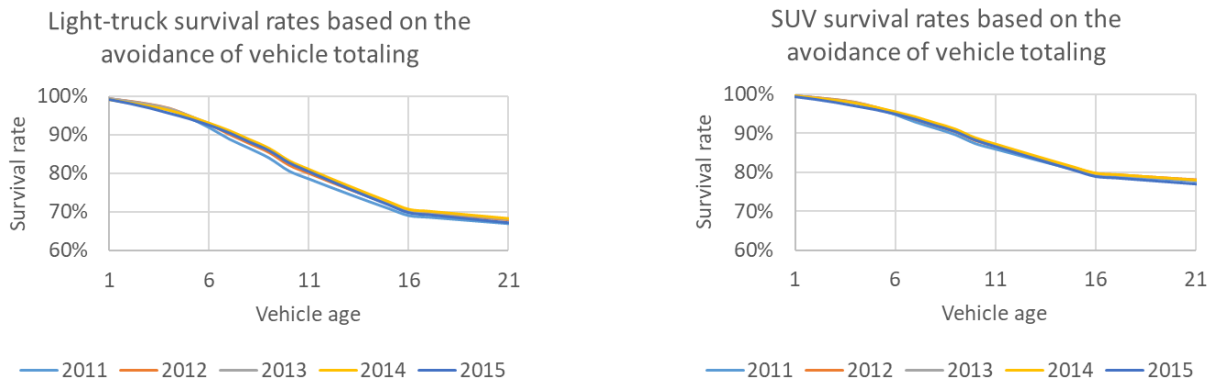


Figure C.2: Vehicle survival rates based on the avoidance of vehicle totaling loss

The calculated survival rates by generation are shown as colored dots in Figure C3 and the solid lines show the fitted survival rate models by vehicle generation.

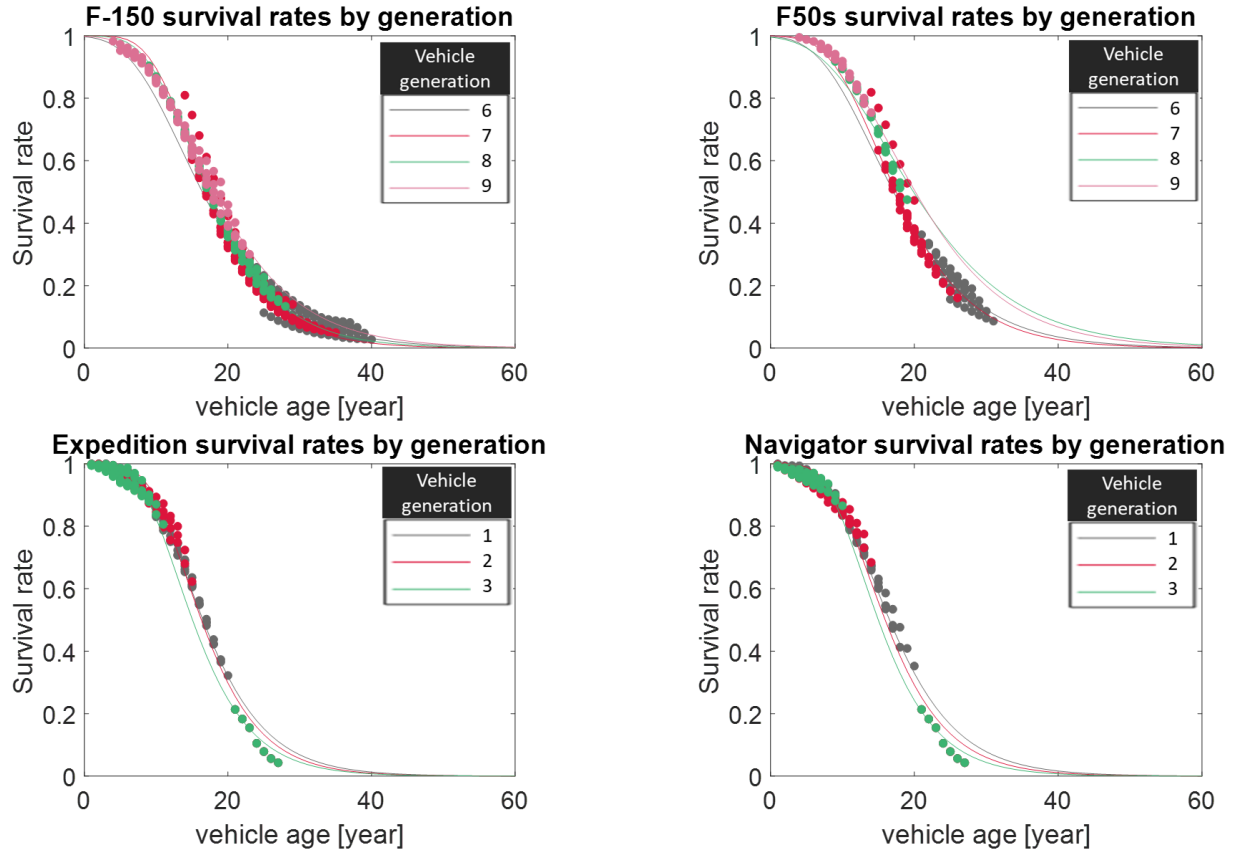


Figure C.3: Vehicle survival rates by generations (starting with 6th generation for F-150 and Super Duty and 1st generation for Expedition and Navigator)

The survival rate from NHTSA (2006) is chosen according to statistical test of registration data which showed a linear relationship between survival rate and  $1 - \text{EXP}[-\text{EXP}(A + B \times \text{Age})]$  (NHTSA, 2006). Based on the fitted model, we first calculate the corresponding vehicle lifespan distribution (the probability mass function) using equation C5 and then use the vehicle lifespan distribution to calculate the mean vehicle lifespan of each vehicle generation using equation C6.

$$pmf(a) = survivalrate(a - 1) - survivalrate(a) \quad (C.4)$$

$$meanvehiclelifespan = \sum_{a=1}^{a_{max}=40} pmf(a) * a \quad (C.5)$$

Here we assume the maximum possible vehicle life,  $a_{max}$  will be 40 years. The results of the calculated mean vehicle lifespan are shown in Table C2.

Table C.2: Mean vehicle lifespan by vehicle generation (starting with 6th generation for F-150 and Super Duty and 1st generation for Expedition and Navigator)

Generation (g)	F-150	Super Duty	Expedition	Navigator
Generation 1	N/A	N/A	17.23 (baseline)	17.32 (baseline)
Generation 2	N/A	N/A	16.94	16.64
Generation 3	N/A	N/A	15.71	15.63
Generation 5	N/A	N/A	N/A	N/A
Generation 6	17.39	18.07	N/A	N/A
Generation 7	17.92	18.33	N/A	N/A
Generation 8	18.18	20.68	N/A	N/A
Generation 9	19.02 (baseline)	21.00 (baseline)	N/A	N/A

The baseline scenario is selected such that it has the largest mean vehicle lifespan across all vehicle generations which coincident with the most recent vehicle generation for F-150 and Super Duty (F-50s). The pessimistic scenario is defined as the minimum possible survival rate across all vehicle ages which corresponds to the minimum possible mean vehicle lifespan. To obtain the survival rate parameters for the pessimistic scenario, we fit the survival rate model to the minimum possible mean vehicle lifespan data again (see Table C4 for parameter values of  $c_1$  and  $c_2$ ). Using the vehicle life constraint in Eqn. C7, we define the optimistic scenario by assuming the same amount of improvement in mean vehicle lifespan is made in the optimistic scenario comparing to baseline scenario comparing to that from the pessimistic scenario to the baseline scenario.

$$\frac{\text{mean vehicle lifespan}_{\text{optimistic}}}{\text{mean vehicle lifespan}_{\text{base}}} = \frac{\text{mean vehicle lifespan}_{\text{base}}}{\text{mean vehicle lifespan}_{\text{pessimistic}}} \quad (\text{C.6})$$

To obtain the survival rate parameters for the optimistic scenario, we run the optimization algorithm using baseline generation survival rates as input data with the vehicle totaling and mean vehicle lifespan (fourth column of Table C3) constraints.

Table C.3: Mean vehicle lifespan by scenarios

	Baseline	Pessimistic	Optimistic
F-150	19.02	16.71	21.58
Super Duty	21.00	17.73	24.77
Expedition	17.23	15.71	18.71
Navigator	17.32	15.63	19.01

Table C4 and Figure C4 shows the parameters and the corresponding derived survival rates scenarios.

Table C.4: Parameters of survival rate models by scenarios

	Navigator		Expedition		Super Duty		F-150	
	c1	c2	c1	c2	c1	c2	c1	c2
baseline	2.27	-0.16	2.43	-0.17	1.96	-0.12	1.93	-0.13
pessimistic	2.37	-0.18	2.37	-0.18	1.95	-0.14	2.01	-0.15
optimistic	2.24	-0.14	2.40	-0.15	1.96	-0.09	1.92	-0.11

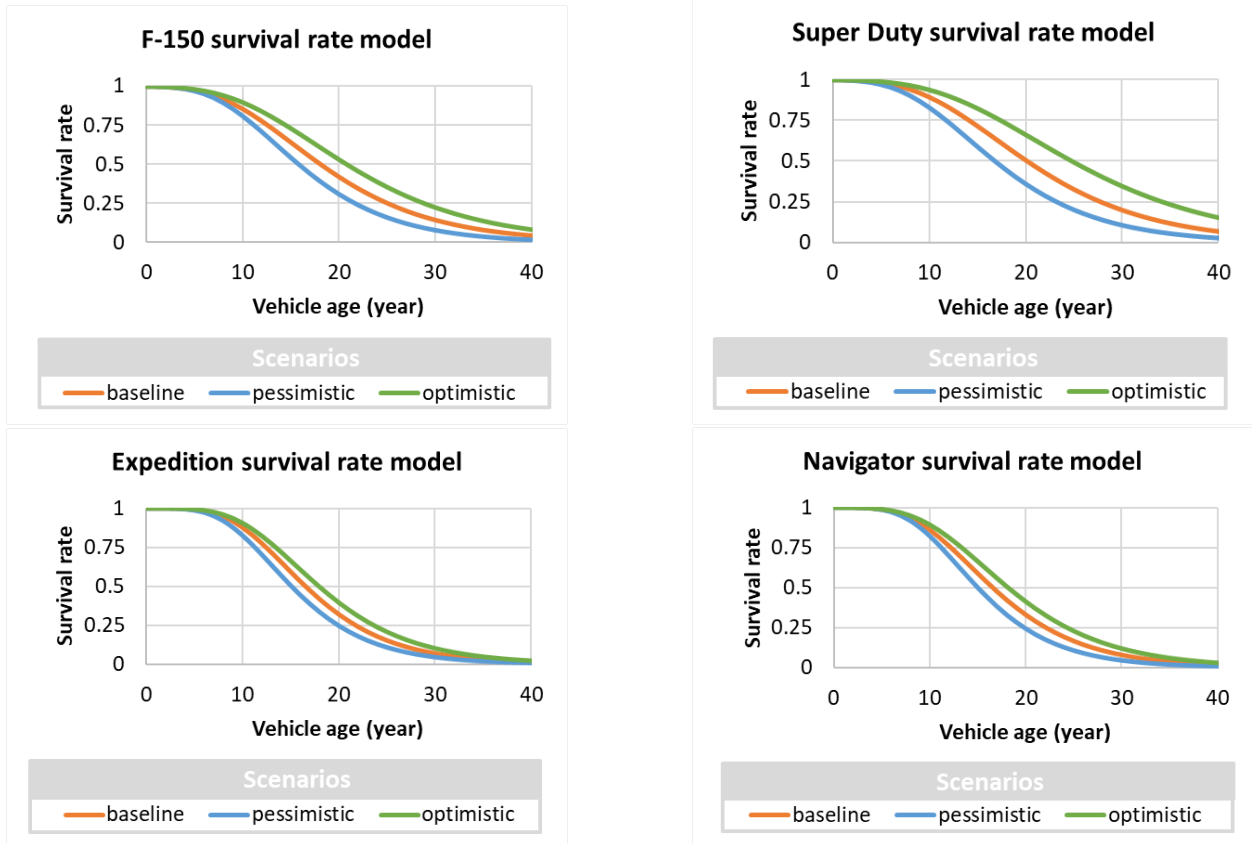


Figure C.4: Vehicle survival rates by scenarios

### C.1.2 Vehicle lifespan model

To prepare for the dynamic material flow analysis (DMFA) calculation, we calculate the lifespan probability distribution according to the survival rate in the three scenarios using equation C5 shown in section 1.1. The resulted lifespan probability distributions for the four types of vehicles are shown in Figure C5 (same as Figure 2 in the main manuscript).



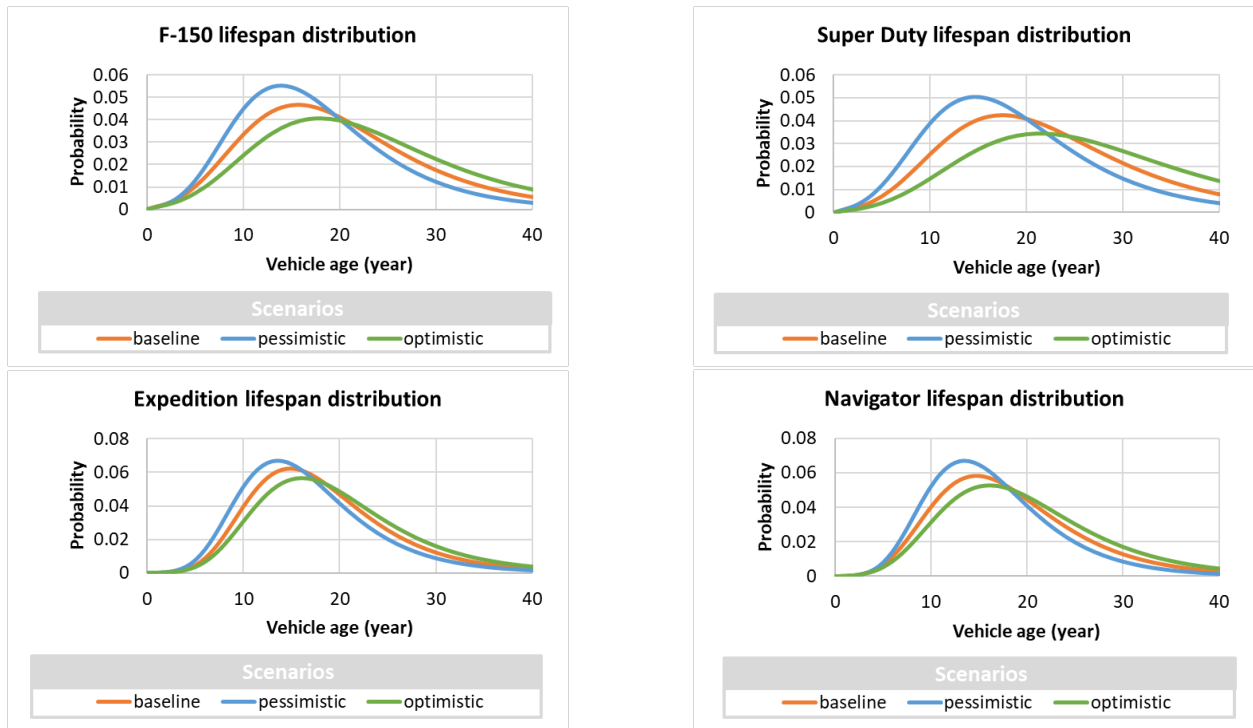


Figure C.5: Lifespan distributions for (a) F-150, (b) Super Duty trucks, (c) expedition, and (d) navigator

## C.2 Dynamic material flow analysis (DMFA)

Material flow analysis (MFA) is a method to quantify the stocks and flows of metals in a defined temporal and economic or geographic boundaries. It can be dynamic, which assesses the stocks and flows of material in a system over time, or static, which is a snapshot of the system usually for a single year (McMillan et al., 2010). A flow driven dynamic material flow analysis (DMFA) predicts future stocks and scraps using demand as exogenous data while a stock driven DMFA predicts how new demand and scrap changes to meet the required service or product level. Flow driven DMFA has been applied by various researchers to forecast future material stock and scraps. For example, Hashimoto et al. (2007, 2009) and Fishman et al., (2014) used flow driven DMFA to forecast national level construction material flows. A stock driven DMFA methods, e.g., logistic curves, are most appropriate when predicting material production or product sales as a proxy of the total service to a society. For example, predicting the total light duty vehicles sales or U.S. steel demand (Cooper et al., 2020) would be appropriate using the stock-based model. Modaresi and Muller (2012) and Lovik et a. (2014) also used the stock-based model to study global automotive aluminum flows. However, for the study of individual product, e.g., F-150., a stock driven DMFA is likely to be not appropriate because there is a lack of data for understanding the saturation stock level; in this case, we are far from the inflection point. Therefore, we decided to use the flow driven

DMFA to calculate future vehicle stock and scraps based on EIA’s predicted vehicle sales growth rates under its reference, low economic growth and high economic growth scenarios. The following section presents the data and methods for the DMFA analysis.

### C.2.1 Historical and prospective annual sales

According to the results of the Annual Energy Outlook (2019) presented by the U.S. Energy Information Administration, U.S. light duty vehicle sales are projected to grow linearly at around 0.8%, -0.1% and 1% in the expected, low, and high economic growth scenarios respectively (EIA, 2019). Figure C6 presents the historical and prospective annual sales of the sum of the four types of vehicle according to EIA’s prediction.

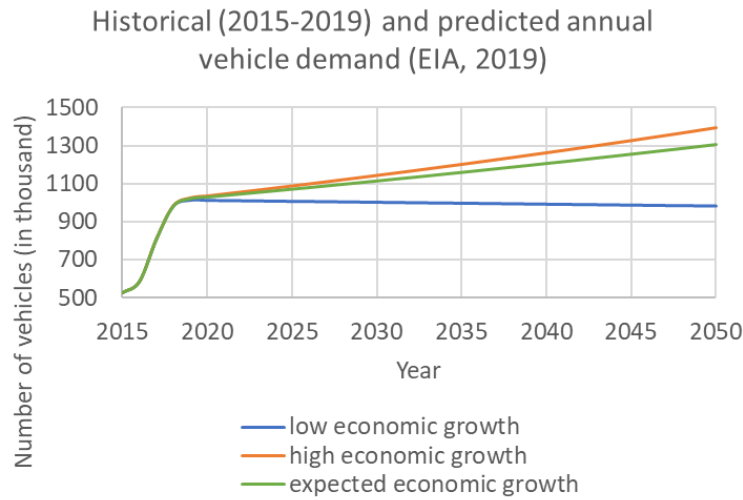


Figure C.6: Historical and predicted future annual sales of the four types of vehicle

### C.2.2 Vehicle and alloy scrap and stock

To estimate the amount of vehicle leaving registration (scrapped) each year and the amount of vehicles on-road as stock, we conducted a flow-driven DMFA. Given the historical and predicted annual vehicle sales, we can estimate the scrap and stock of vehicles in each year using equation 8 and 9 below:

$$Scrap(t) = \sum_{a=1}^{a_{max}} (Sales(t-a) * pdf(a)) \quad (C.7)$$

$$Stock(t) = Stock(t-1) + Sales(t) - Scrap(t) \quad (C.8)$$

To translate from vehicle sales, scrap and stock to the corresponding volumes, scrap and stocks

of the autobody aluminum sheet alloys in the four types of vehicles, we combine this vehicle DMFA results with the alloy weight in each vehicle model data (Table 1 in the main manuscript). Since the F-Series and the Expedition/Navigator each have various models, we use an average weight of metal per vehicle, estimated from a historical model distribution for each vehicle. For example, around 522,837 aluminum intensive Ford F-150 were sold in the U.S. in 2015 and, on average, each contained around 92.6 kg low Cu autobody sheet aluminum alloys, so that the total amount of low Cu alloy put on the road is 48,414 metric ton. Similarly, we calculate the amount of other autobody sheet alloys added to the stock (on-road) and scrapped each year between 2015 and 2050. Detail results are shown in Section C4.

### **C.3 Markov chain vehicle destination study**

This section summarizes the Markov chain study including used vehicle export and derivation of the transitional probabilities.

#### **C.3.1 Used vehicle export**

To estimate the probability for a used vehicle to be exported out of the U.S. at different ages, we collect the used vehicle export information from CarExportAmerica.com in 2019. The website listed all the used vehicles to be exported in real time. As the time of the data collection (Sep. 21<sup>st</sup>, 2019), there were 63,266 entries of vehicle data listed, of which 7,696 were Ford vehicles and 334 were Lincoln vehicles (Car Export America, 2019). Table C5 shows the share of the four types of vehicle in all used vehicles to be exported calculated as the number of types of vehicle to be exported divided by the total listed number of vehicles. This ratio is assumed to approximate the share of the four types of vehicle (F-150, Super Duty trucks, Expedition and Navigator) exported each year.

Table C.5: Number of the four types of vehicle and (column 1) share of the four types of vehicle in all used vehicles to be exported (column 2) and age distribution (column 3-5)

	Number of vehicles to be exported 2019	Share of types of vehicle in all used vehicles to be exported	Share of vehicle exported at age 1-10	Share of vehicle exported at age 11-30	Share of vehicle exported at age 30+
F-150	633	1.0%	90%	6%	3%
Super Duty	759	1.2%	48%	40%	11%
Expedition	127	0.2%	92%	8%	0%
Navigator	63	0.1%	94%	6%	0%
Other	62001	98.0%	N/A	N/A	N/A
Total	63266	100%	100%	100%	100%

For each vehicle listed on the CarExportAmerica.com, the vehicle age information is included. Therefore, in addition to the overall share of the four types of vehicle exported among all used vehicles, we also estimate the approximate age distribution of exported vehicles as shown in Table C5 (column 3-5).

The International Trade Administration publishes an annual used vehicle export statistics in the U.S. between 2014 and 2018 (U.S. International Trade Commission, 2019). Combining this data with the estimated share of the four types of vehicle to be exported among all used vehicles, we estimate the annual export of the four vehicles between 2014 and 2018 using equation 10.

$$export_{byvehicle} = export_{total} * shareofvehicleintotal \quad (C.9)$$

The results of the estimated annual export of the four types of vehicle are shown in Table C6 below.

Table C.6: Annual used vehicle export estimation between 2014 and 2018

	Annual export estimates by vehicle model				
	2014	2015	2016	2017	2018
F-150	7330	5721	5623	6453	7936
Super Duty	8590	6704	6590	7563	9301
Expedition	1494	1166	1146	1315	1617
Navigator	700	547	537	617	758

Based on vehicle registration and survival rate model, we estimated the annual used vehicle deregistered for the four types of vehicle by age groups and compare that with the vehicle export estimation in Table C6 to derive the ratio of vehicle that are exported to the all the vehicles that are deregistered from the U.S. registration system.

Table C.7: Mean vehicle deregistered by age groups and share of vehicle exported comparing to overall deregistration

	average vehicle deregistered by age groups				share of vehicle exported comparing to overall deregistration			
	F-150	Super Duty	Expedition	Navigator	F-150	Super Duty	Expedition	Navigator
age 1-10	108226	67874	4365	1686	0.04	0.03	0.29	0.24
age 11-30	648065	227909	19052	5960	0.00	0.03	0.02	0.02
age 30+	57019	12992	0	0	0.00	0.01	0.00	0.00

### C.3.2 Transitional probability estimation

Combining the results of Table C7, export vehicle age distribution in Figure C7 and the survival rate model in Figure C4, we estimated the transition probability of vehicles that ended up into the scrap, vintage and export states defined in Figure C8 below.

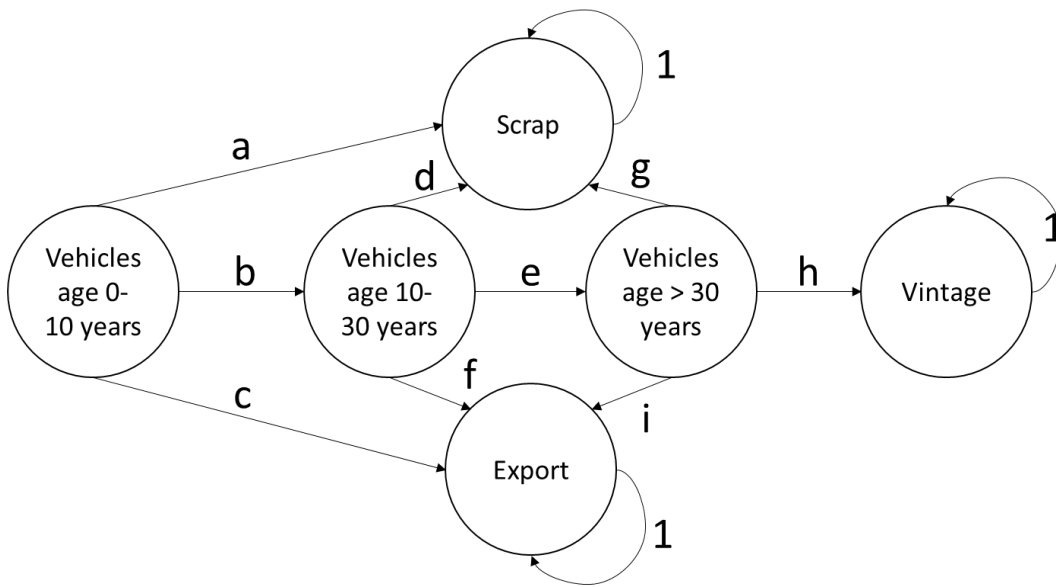


Figure C.7: Definition of the stage in the Markov chain study

The probability of a vehicle to stay in the fleet is obtained from the survival rate model estimation ( $b$  and  $e$ ). To differentiate the probability of vehicle been scrapped or exported at early ages of a vehicle, the estimated amount of vehicle exported are compared to the estimated amount of vehicle deregistered (Table C7). The derived ratio times the probability of a vehicle deregistered from the fleet gives the probability of a vehicle been exported during each life stage (probabilities  $c$ ,  $f$  and  $i$ ). The probability of vehicles scrapped in the U.S. at an early age is derived from the share of remaining deregistered vehicles ( $a$  and  $d$ ). For vehicle older than 30 years, an absolute 1% of all vehicles are assumed to enter the vintage state. Comparing it with the predicted percentage

of vehicle deregistered after 30 years, we estimated the probability of vehicles  $i$  30 years been “hibernated” as vintage vehicles ( $h$ ). The difference between 1 and  $I + h$  gives the probability of vehicles  $i$  30 years scrapped in the U.S ( $g$ ).

#### **C.4 Analysis results**

Section 4.1-4.3 summarizes the DMFA results of vehicle and alloys between 2015 and 2050 in the baseline, pessimistic and optimistic vehicle survival scenarios.

##### **C.4.1 Baseline vehicle survival scenario**

Figure C9, Figure C10 and Figure C11 show the DMFA results under baseline survival rate scenario with reference, low and high sales growth rate prediction respectively.

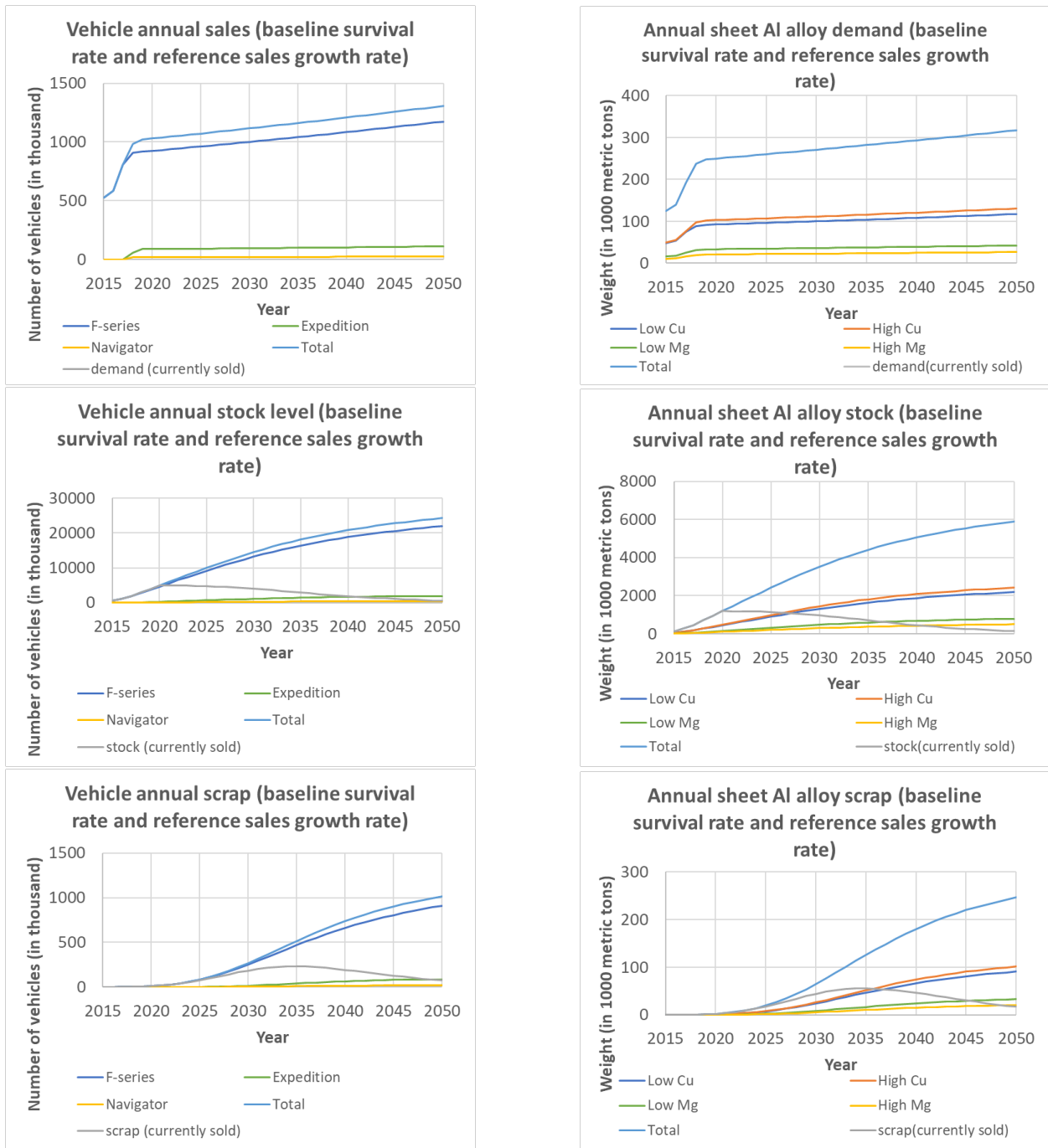


Figure C.8: Annual sales, stock level and de-registered from fleet according to types of vehicle (left) and alloy families (right) under baseline survival rate and reference sales growth rate

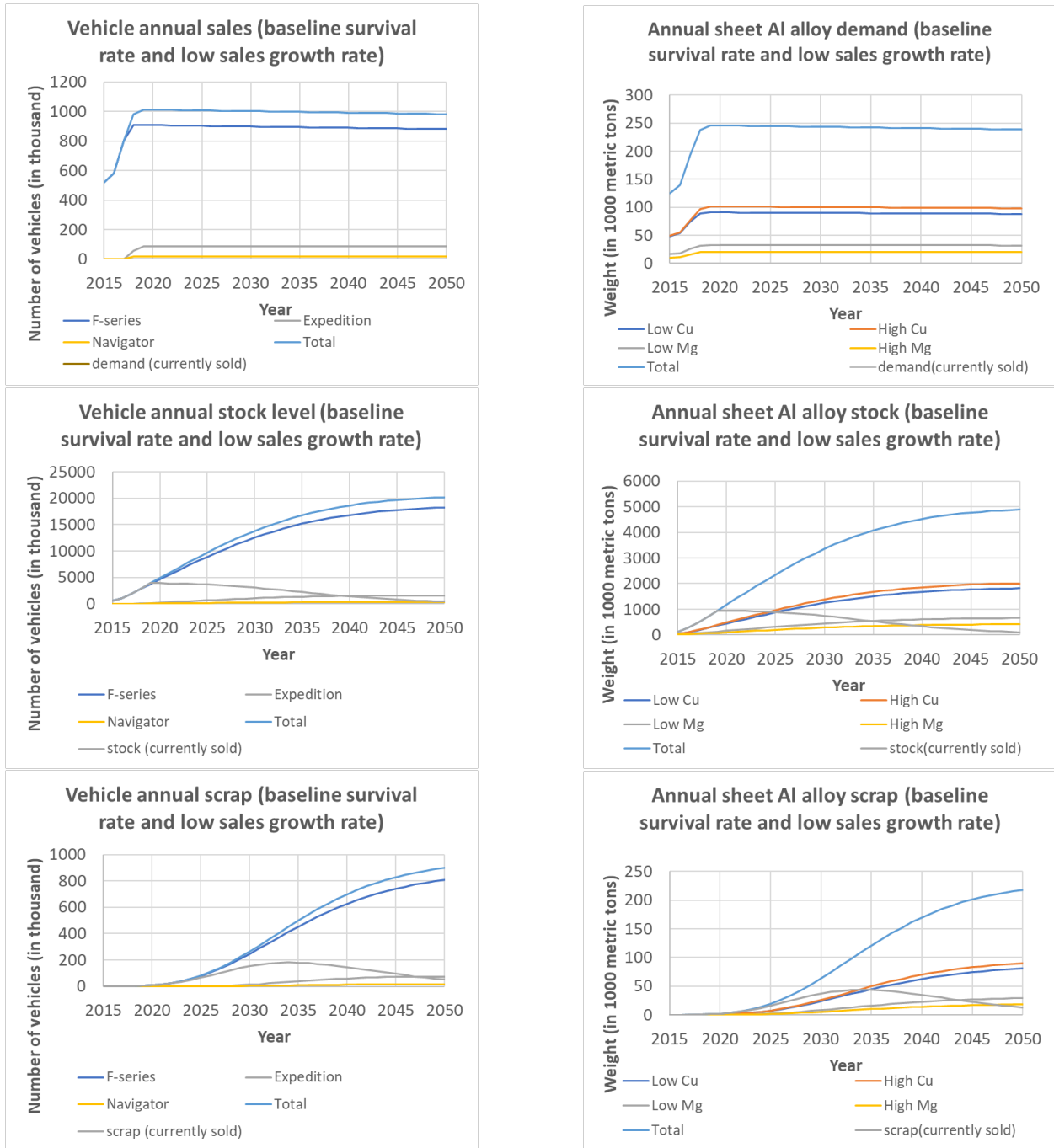


Figure C.9: Annual sales, stock level and de-registered from fleet according to types of vehicle (left) and alloy families (right) under baseline survival rate and low sales growth rate



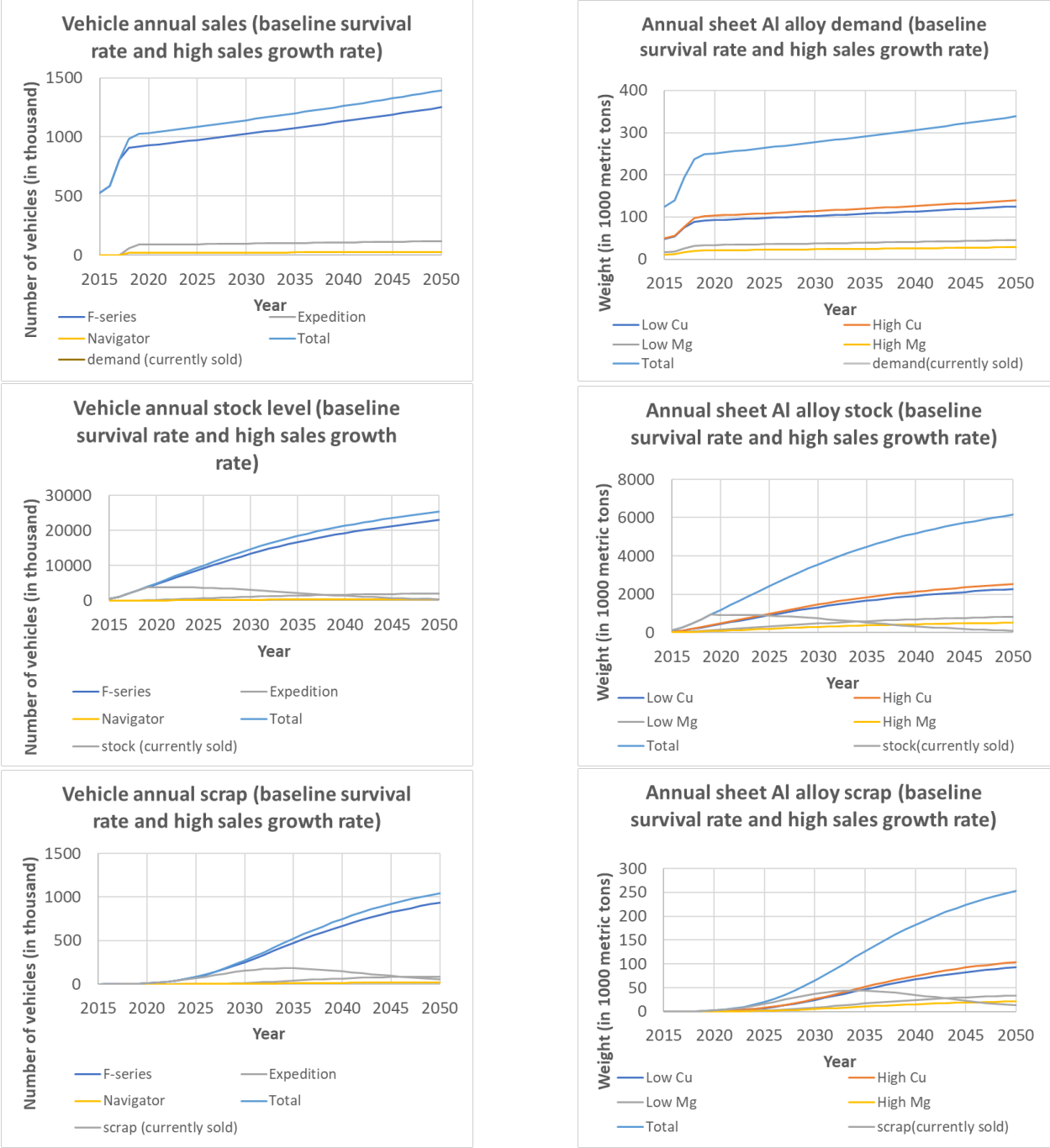


Figure C.10: Annual sales, stock level and de-registered from fleet according to types of vehicle (left) and alloy families (right) under baseline survival rate and high sales growth rate

**C.4.2 Pessimistic vehicle survival scenario**

Figure C12, Figure C13 and Figure C14 show the DMFA results under pessimistic survival rate scenario with reference, low and high sales growth rate prediction respectively.

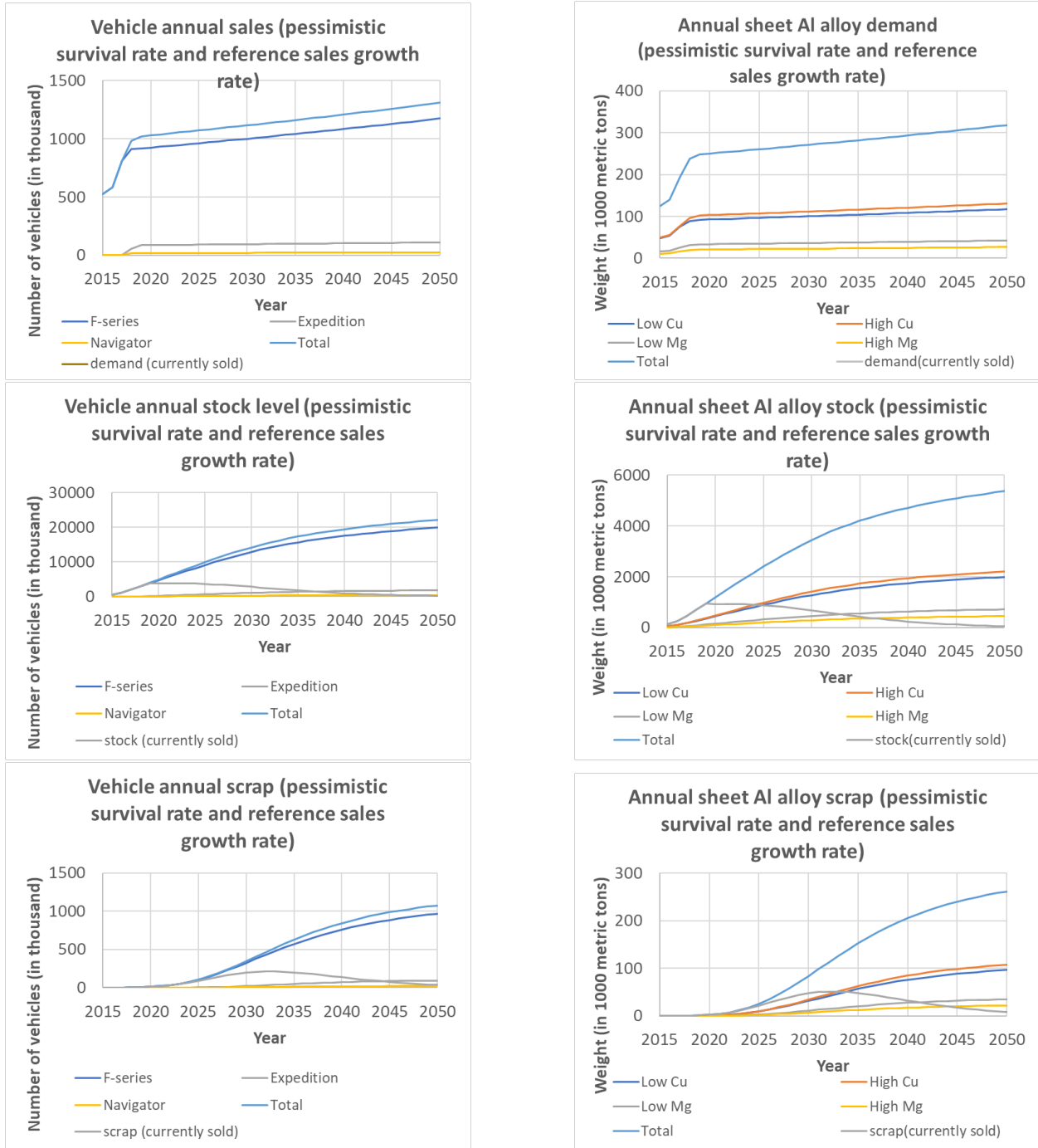


Figure C.11: Annual sales, stock level and de-registered from fleet according to types of vehicle (left) and alloy families (right) under pessimistic survival rate and reference sales growth rate

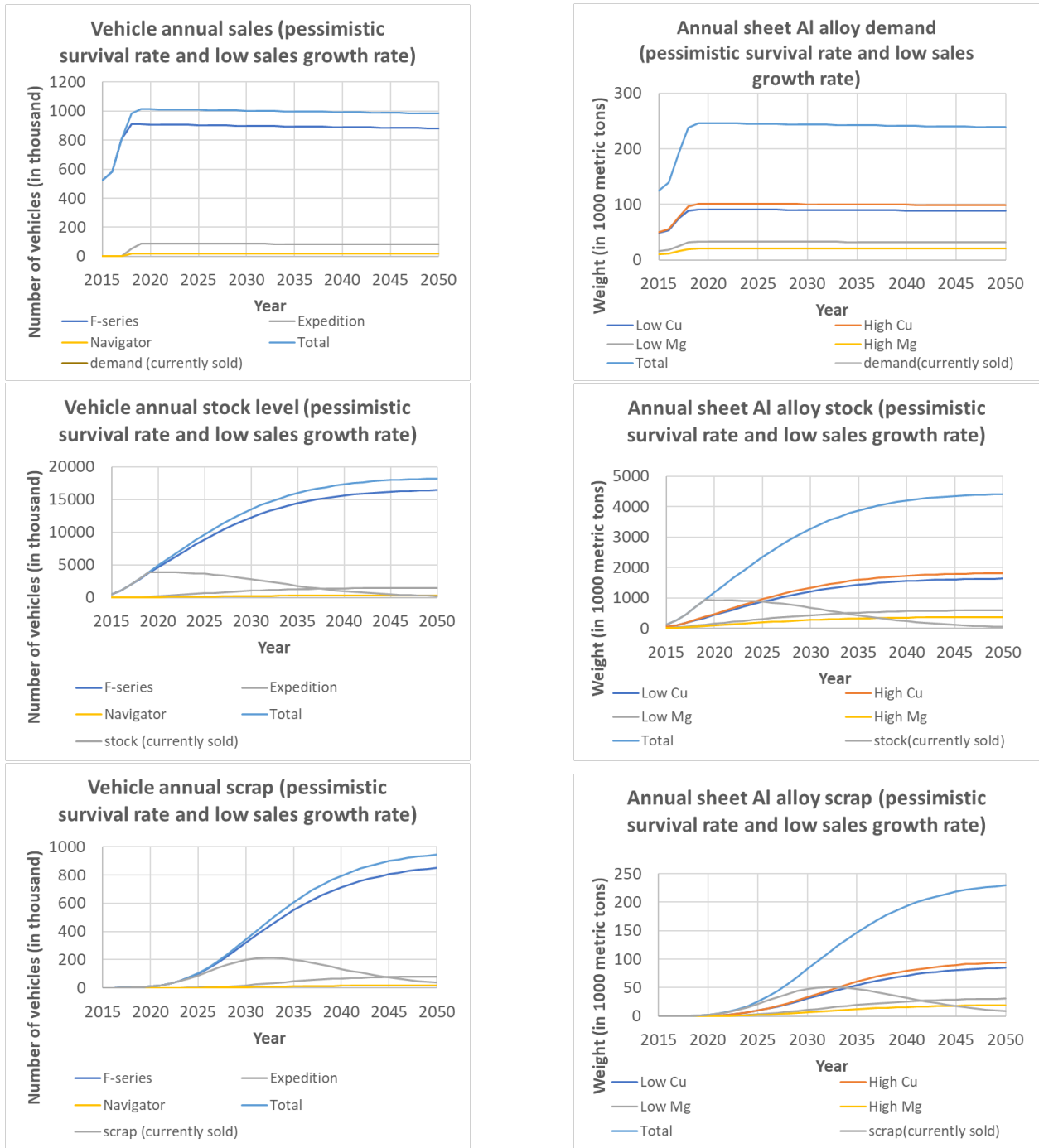


Figure C.12: Annual sales, stock level and de-registered from fleet according to types of vehicle (left) and alloy families (right) under pessimistic survival rate and low sales growth rate

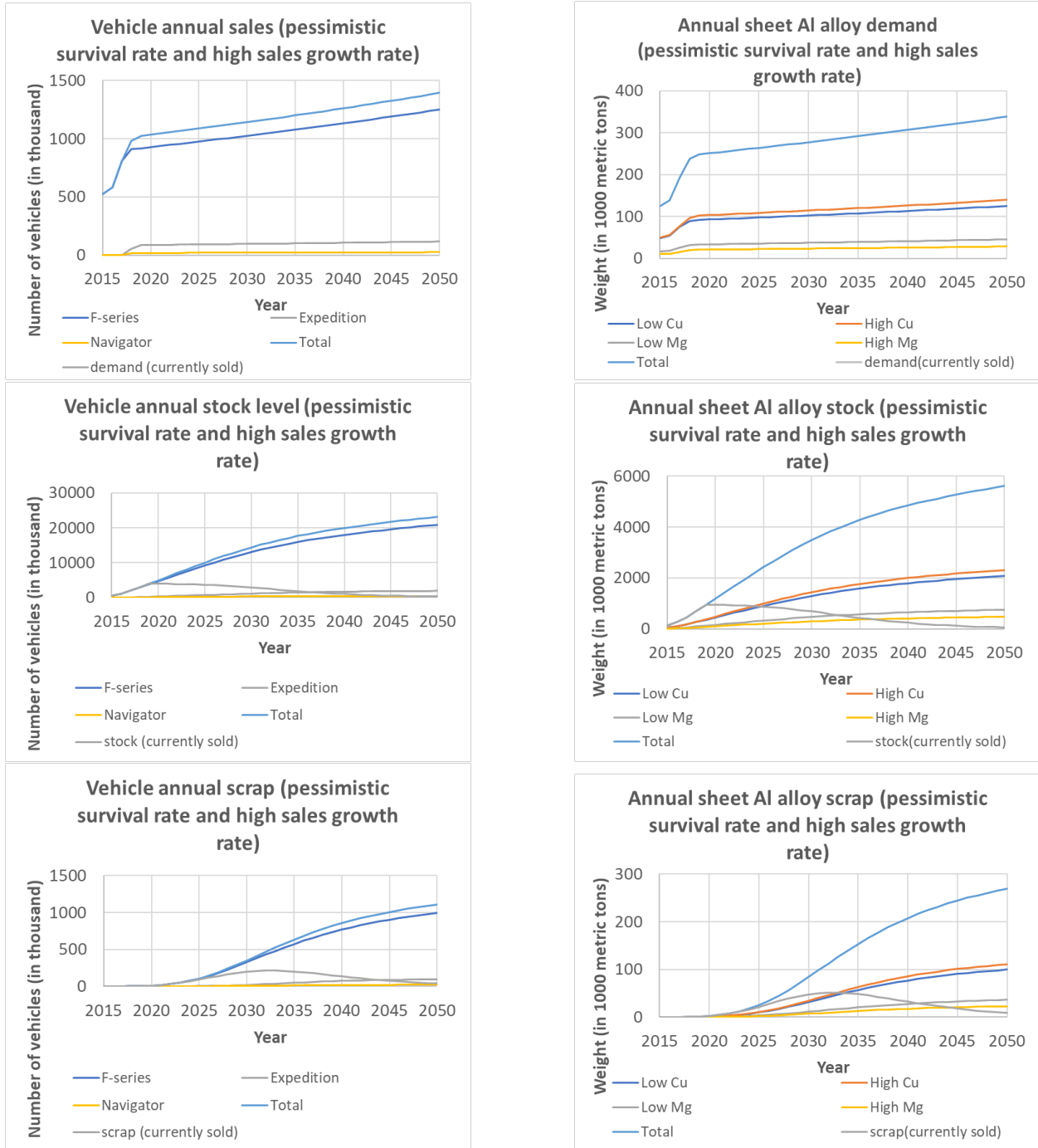


Figure C.13: Annual sales, stock level and de-registered from fleet according to types of vehicle (left) and alloy families (right) under pessimistic survival rate and high sales growth rate

### C.4.3 Optimistic vehicle survival scenario

Figure C15, Figure C16 and Figure C17 show the DMFA results under optimistic survival rate scenario with reference, low and high sales growth rate prediction respectively.

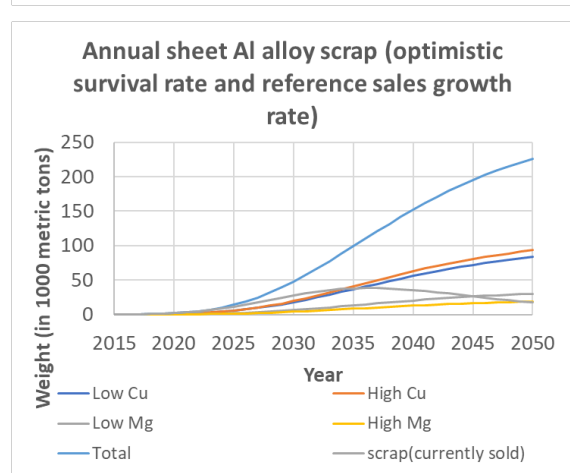
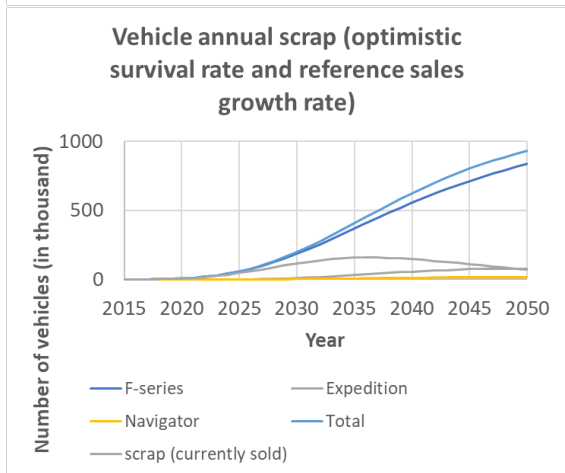
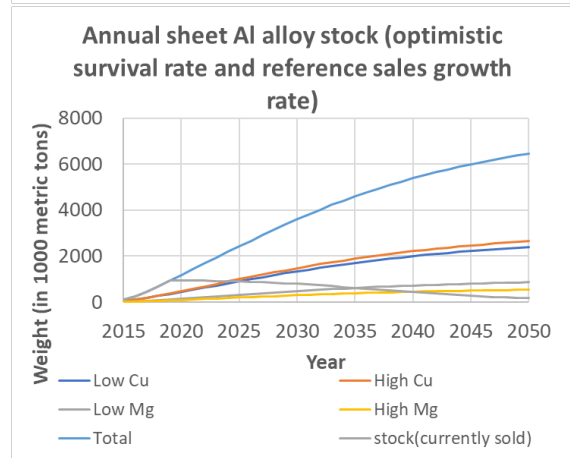
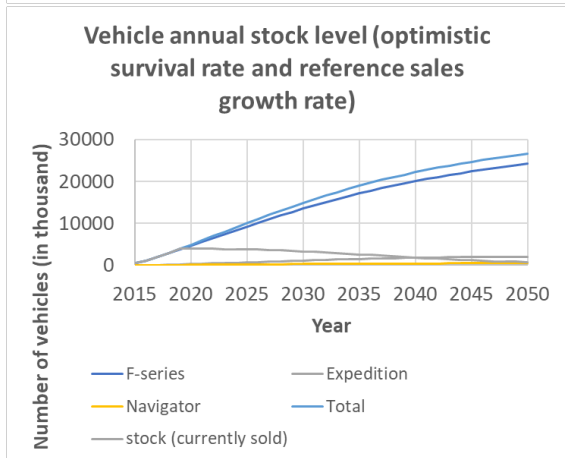
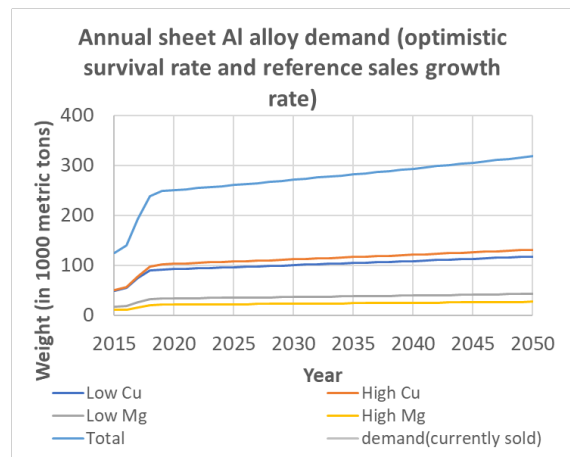
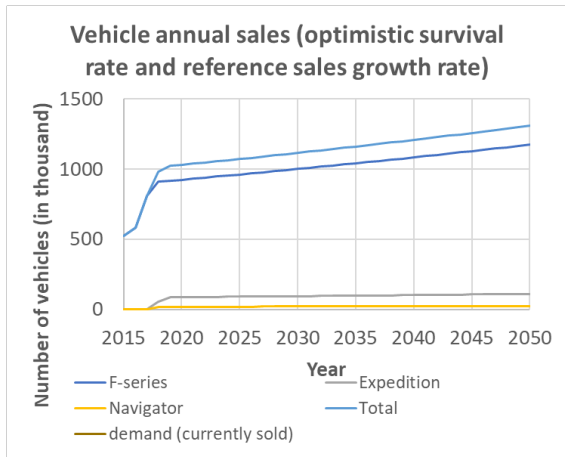


Figure C.14: Annual sales, stock level and de-registered from fleet according to types of vehicle (left) and alloy families (right) under optimistic survival rate and reference sales growth rate

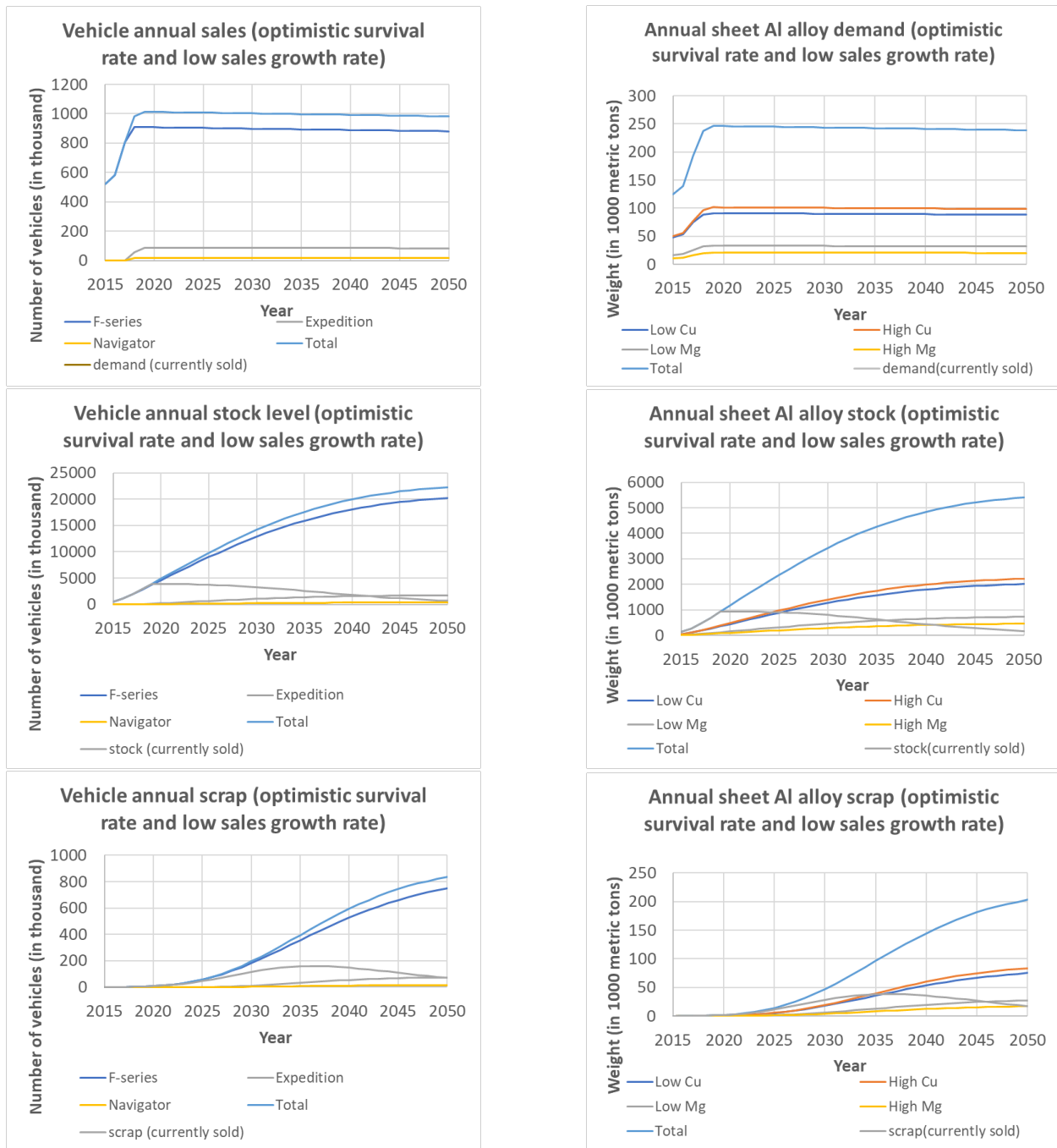


Figure C.15: Annual sales, stock level and de-registered from fleet according to types of vehicle (left) and alloy families (right) under optimistic survival rate and low sales growth rate

### C.5 Autobody sheet scrap compositional analysis

The results of the scrap composition analysis between 2020 and 2050 in the baseline, pessimistic and optimistic vehicle survival scenarios are presented in the supporting information (<https://www.sciencedirect.com/science/article/pii/S0921344920305255>).

Combining the vehicle alloy composition data (Table 2 in the main manuscript) with the scrap prediction from DMFA (Section C4), we estimate the chemical composition of scraps under three scenarios: all alloy scraps mixed, Cu alloys mixed, and Mg alloys mixed.

### C.6 Diagram for profit opportunity for recycling aluminum

Figure C18 shows the price profiles for primary aluminum versus post-consumer aluminum scrap grades, Twitch and Taint.

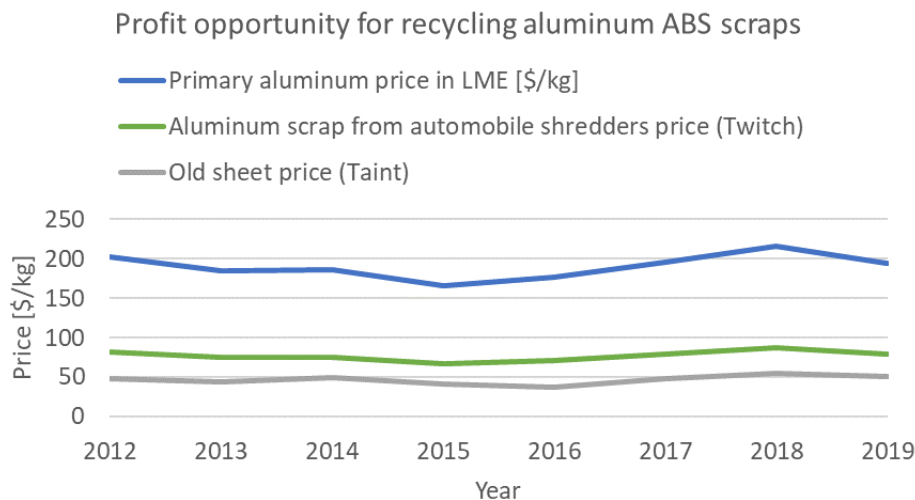


Figure C.16: Price profiles for primary aluminum versus post-consumer aluminum scrap grades. Graph constructed from London Metals Exchange data (LME, 2020), Taylor(2013), and Schlesinger (2014).

### C.7 Reference

Bento, Antonio M., Kevin D. Roth, and Yiou Zuo. 2013. "Vehicle Lifetime Trends and Scrappage Behavior in the U.S. Used Car Market." *SSRN Electronic Journal* 39(1).

"Car Export America." 2019. <https://www.carexportamerica.com/> (December 18, 2019).

CCC. 2015. "What's Driving Total Loss Frequency?" <https://www.cccis.com/2015/11/13/whats-driving-total-loss-frequency/> (October 31, 2019).

Commerce, U.S. Department of. 2015. *Trends in U.S. Vehicle Exports*.

Cooper, D.R., Ryan, N.A., Syndergaard, K. and Zhu, Y., 2020. The potential for material circularity and independence in the US steel sector. *Journal of Industrial Ecology*.

EIA. 2019. *Annual Energy Outlook 2019 with Projections to 2050*. [www.eia.gov/ao](http://www.eia.gov/ao) (June 16, 2019).

Fishman, T., Schandl, H., Tanikawa, H., Walker, P., Krausman, F., 2014. Accounting for the material stock of nations. *J. Ind. Ecol.* 18 (3), 407–420.

Greene, David L., and C. K. Eric Chen. 1981. “Scrapage and Survival Rates of Passenger Cars and Light Trucks in the U.S., 1966-1977.” *Transportation Research Part A: General* 15(5): 383–89.

Gunnell, John. 2003. *Standard Catalog of Light-Duty Ford Trucks 1905-2002*. (October 31, 2019).

Hashimoto, S., Tanikawa, H., Moriguchi, Y., 2007. Where will large amounts of material accumulated within the economy go? –A material flow analysis of construction minerals for Japan. *Waste Manage.* 27, 1725–1738.

Hashimoto, S., Tanikawa, H., Moriguchi, Y., 2009. Framework for estimating potential wastes and secondary resources accumulated within an economy –A case study of construction minerals in Japan. *Waste Manage.* 29, 2859–2866.

Hartwig, Robert P, and Steven Weisbart. 2016. *More Accidents, Larger Claims Drive Costs Higher*. [www.iii.org](http://www.iii.org) (October 31, 2019).

Keathley, Valerie, Andrew Martin, Jeeyen Koo, and Jennifer Walton. 2019. *Issues Pertaining to Rebuilt Vehicle Titles*. Lexington, KY.

NHTSA, and EPA. 2018. “The Safer Affordable Fuel-Efficient (SAFE) Vehicles Rule for Model Years 2021-2026 Passenger Cars and Light Trucks.” *Federal Register* 83(165): 42986–500.

Sawyer-Beaulieu, Susan S., and Edwin K.L. Tam. 2006. “Regulation of End-of-life Vehicle (ELV) Retirement in the US Compared to Canada.” *International Journal of Environmental Studies* 63(4): 473–86. <http://www.tandfonline.com/doi/abs/10.1080/00207230600802106> (March 9, 2020).

Taylor, Brian (2013) Mixed Signals: Features - Commodity Focus. *Recycling today*

Walker, Franklin V. 1968. “Determinants of Auto Scrapage.” *The Review of Economics and Statistics* 50(4): 503–6.

Allwood, Julian M., Jonathan M. Cullen, and Rachel L. Milford. 2010. “Options for Achieving a 50% Cut in Industrial Carbon Emissions by 2050.” *Environmental Science and Technology* 44(6): 1888–94.

Ambrose, Fred, R. D. Brown, Dominic Montagna, and H. V. Makar. 1983. “Hot-Crush Technique for Separation of Cast- and Wrought-Aluminum Alloy Scrap.” *Conservation and Recycling* 6(1–2): 63–69.

Atherton, John. 2007. “Declaration by the Metals Industry on Recycling Principles.” *International Journal of Life Cycle Assessment* 12(1): 59–60.

Bauer, Siegfried. 2012. “Sustainable Materials: With Both Eyes Open.” *Materials Today* 15(9): 410.

Bertram, M. et al. 2017. “A Regionally-Linked, Dynamic Material Flow Modelling Tool for Rolled, Extruded and Cast Aluminium Products.” *Resources, Conservation and Recycling*



125(March): 48–69.

Chen, Wei Qiang, and T. E. Graedel. 2012. “Dynamic Analysis of Aluminum Stocks and Flows in the United States: 1900–2009.” *Ecological Economics* 81: 92–102.

Cooper, Daniel R. 2018. “How Recycling More Steel and Aluminum Could Slash Imports without a Trade War.” *PBS News Hour*.

Cullen, Jonathan M., and Julian M. Allwood. 2013. “Mapping the Global Flow of Aluminum: From Liquid Aluminum to End-Use Goods.” *Environmental Science and Technology* 47(7): 3057–64.

Davis, J.R. 2001. “Aluminum and Aluminum Alloys.” *Light Metals and alloys*: 66.

Diwekar, Urmila. 2003. *Introduction to Applied Optimization*. New York: Springer Science+Business Media.

Gaustad, Gabrielle, Elsa Olivetti, and Randolph Kirchain. 2010. “Design for Recycling.” *Journal of Industrial Ecology* 14(2): 286–308.

Gaustad, Gabrielle, Elsa Olivetti, and Randolph Kirchain. 2012. “Improving Aluminum Recycling: A Survey of Sorting and Impurity Removal Technologies.” *Resources, Conservation and Recycling* 58: 79–87. <http://dx.doi.org/10.1016/j.resconrec.2011.10.010>.

Gesing, A., and R. Wolanski. 2001. “Recycling Light Metals from End-of-Life Vehicles.” *Jom* 53(11): 21–23.

Hatayama, Hiroki et al. 2006. “Dynamic Substance Flow Analysis of Aluminum and Its Alloying Elements.” *Nippon Kinzoku Gakkaishi/Journal of the Japan Institute of Metals* 70(12): 975–80.

Hatayama, Hiroki, Ichiro Daigo, Yasunari Matsuno, and Yoshihiro Adachi. 2009. “Assessment of Recycling Potential of Aluminum in Japan, the United States, Europe and China.” *Nippon Kinzoku Gakkaishi/Journal of the Japan Institute of Metals* 72(10): 813–18.

Intergovernmental Panel on Climate Change. 2007. *Climate Change 2007-Mitigation of Climate Change: Working Group III Contribution to the Fourth Assessment Report of the IPCC*. Cambridge University Press.

ISO 7376:2009. 2008. “International Standard Iso.” 2008.

Jang, Yong Chul, and Mincheol Kim. 2010. “Management of Used&End-of-Life Mobile Phones in Korea: A Review.” *Resources, Conservation and Recycling* 55(1): 11–19.

Jofre, Sergio, and Tohru Morioka. 2005. “Waste Management of Electric and Electronic Equipment: Comparative Analysis of End-of-Life Strategies.” *Journal of Material Cycles and Waste Management* 7(1): 24–32.

McMillan, Colin A., Michael R. Moore, Gregory A. Keoleian, and Jonathan W. Bulkley. 2010. “Quantifying U.S. Aluminum in-Use Stocks and Their Relationship with Economic Output.” *Ecological Economics* 69(12): 2606–13.

McMillan, Colin A., Steven J. Skerlos, and Gregory A. Keoleian. 2012. “Evaluation of the

Metals Industry's Position on Recycling and Its Implications for Environmental Emissions." *Journal of Industrial Ecology* 16(3): 324–33.

Milford, Rachel L., Julian M. Allwood, and Jonathan M. Cullen. 2011. "Assessing the Potential of Yield Improvements, through Process Scrap Reduction, for Energy and CO<sub>2</sub> Abatement in the Steel and Aluminium Sectors." *Resources, Conservation and Recycling* 55(12): 1185–95. <http://dx.doi.org/10.1016/j.resconrec.2011.05.021>.

Milford, Rachel L., Stefan Pauliuk, Julian M. Allwood, and Daniel B. Müller. 2013. "The Roles of Energy and Material Efficiency in Meeting Steel Industry CO<sub>2</sub> Targets." *Environmental Science and Technology* 47(7): 3455–62.

Modaresi, Roja, and Daniel B. Müller. 2012. "The Role of Automobiles for the Future of Aluminum Recycling." *Environmental Science and Technology* 46(16): 8587–94.

Muñiz-Lerma, Jose Alberto, Manas Paliwal, In Ho Jung, and Mathieu Brochu. 2017. "Fractional Crystallization Model of Multicomponent Aluminum Alloys: A Case Study of Aircraft Recycling." *Metallurgical and Materials Transactions B: Process Metallurgy and Materials Processing Science* 48(2): 1024–34.

Pauliuk, Stefan, Rachel L. Milford, Daniel B. Müller, and Julian M. Allwood. 2013. "The Steel Scrap Age." *Environmental Science and Technology* 47(7): 3448–54.

Schlesinger, Mark E. 2014. *Aluminum Recycling*. Second ed. CRC Press.

Steuer, Ralph E. 1984. "Sausage Blending Using Multiple Objective Linear Programming." *Management Science* 30(11): 1376–84.

The Aluminum Association Inc. 2006. "International Alloy Designations and Chemical Composition Limits for Wrought Aluminum and Wrought Aluminum Alloys." The Aluminum Association, Arlington, Virginia (April 2006): 28.

U.S. Department of Commerce. 2018. *The Effect of Imports of Aluminum on the National Security*. <http://www.bis.doc.gov> (January 30, 2020). Williams, H Paul. 2013. *Model Building in Mathematical Programming*. John Wiley&Sons.

Wyss, R. K., and P. B. Schultz. 1999. "Color Sorting Aluminum Alloy Scrap for Recycling." *Light Metals: Proceedings of Sessions, TMS Annual Meeting (Warrendale, Pennsylvania) (June)*: 1093–98.

Zhang, Yin. 1998. "Solving Large-Scale Linear Programs by Interior-Point Methods under the Matlab Environment." *Optimization Methods and Software* 10(1): 1–31.

Allwood, J. M., Cullen, J.M., Cooper, D.R., Milford, R., Patel, A., Carruth, M. and McBrien, M. (2010). *Conserving our metal energy: Avoiding melting steel and aluminum scrap to save energy and carbon*. WellMet2050.

Aluminum Association. (2009). *International alloy designations and chemical composition limits for wrought aluminum and wrought aluminum alloys*. Teal Sheets, 1-28.

Aluminium Insider. (2019). China Government Planning Strict New Standards for Imported Scrap Aluminium, Copper.

Arowosola, A., and Gaustad, G. (2019). Estimating increasing diversity and dissipative loss of critical metals in the aluminum automotive sector. *Resources, Conservation and Recycling*, 150, pp. 104382.

Bertram, M., S. Ramkumar, H. Rechberger, G. Rombach, C. Bayliss, K. J. Martchek, D. B. Müller, and G. Liu. (2017). A regionally-linked, dynamic material flow modelling tool for rolled, extruded and cast aluminium products. *Resources, Conservation and Recycling*, 125, pp. 48–69.

CCC. (2015). What's Driving Total Loss Frequency?

Chappuis, L. (2015). Aluminum Recycling and the 2015 Ford F-150. *Light Metal Age*, 73, 16–18.

Chappuis, L. (2018). Keynote presentation: The Growth of Aluminum Auto Body Sheet in the U.S. and the Challenges for Sheet-to-sheet Recycling. 16th International Conference on Aluminum Alloys (ICAA16).

Chappuis, L., and Sanders, R. (2019). Automotive aluminum - part VII aluminum intensive vehicles make headway. *Automotive Materials and Processes*, 20–25.

Cooper, D. R. & Allwood, J. M. (2012). Reusing steel and aluminum components at end of product life. *Environmental Science and Technology*. 46, 10334–40.

CSB. (2020). US Car Sales Data .

Desai, P. (2019). Graphic: An abundance of aluminum scrap to spur U.S. recyclers. Reuters.

De Moraes, H.L., de Oliveira, J.R., Espinosa, D.C.R. and Tenório, J.A.S., (2006). Removal of iron from molten recycled aluminum through intermediate phase filtration. *Materials transactions*, 47(7), pp.1731-1736.

EIA. (2019). Annual Energy Outlook 2019 with projections to 2050.

EPA, and NHTSA. (2012). Joint Technical Support Document: Final Rulemaking for 2017-2025 Light-Duty Vehicle Greenhouse Gas Emission Standards and Corporate Average Fuel Economy Standards. *Epa.Gov*, 602.

Ford. (2014). Engineering material specification. Aluminum alloy, sheet, heat treatable, enhanced hemming

Ford. (2020). Engineering material specification. Aluminum alloy, sheet, heat treatable, structural, high strength, thick gage

Ford. (2020). Ford Motor Company Financials: quarterly sales reports.

Fridstrøm, L., Østli, V., and Johansen, K. W. (2016). A stock-flow cohort model of the national car fleet. *European Transport Research Review*, 8(3), pp. 1-15.

Gaustad, G., Olivetti, E., and Kirchain, R. (2012). Improving aluminum recycling: A survey of sorting and impurity removal technologies. *Resources, Conservation and Recycling*, 58, pp. 79–87.

Goel, R., Upadhyay, M., Maulik, O., Prasad, Y.V.S.S. and Kumar, V., (2014). Effect of magnesium on strain hardening response of Al-Mg-Mn based alloys. *Procedia Materials Science*, 5, pp.1241-1247.

Greenspan, A., and Cohen, D. (1999). Motor Vehicle Stocks, Scrapage, and Sales. *Review of Economics and Statistics*, 81(3), pp. 369–383. Gunnell, J., Kowalke, R. and Lichty, R.C., 2002. *Standard Catalog of Ford, 1903-2003*. Krause.

Hartwig, R. P., and Weisbart, S. (2016). More Accidents, Larger Claims Drive Costs Higher.

Hatayama, H., Daigo, I., Matsuno, Y., and Adachi, Y. (2012). Evolution of aluminum recycling initiated by the introduction of next-generation vehicles and scrap sorting technology. *Resources, Conservation and Recycling*, 66, pp. 8–14.

IHS Markit. (2019). Vehicle registration data.

Kelly, S., and Apelian, D. (2016). Automotive aluminum recycling at end of life: a grave-to-gate analysis. Center for Resource Recovery and Recycling (CR3), Metal Processing Institute, Worcester Polytechnic Institute, pp. 1–36.

Kim, H.C. and Wallington, T.J., (2013). Life-cycle energy and greenhouse gas emission benefits of lightweighting in automobiles: review and harmonization. *Environmental science & technology*, 47(12), pp.6089-6097.

Kumar, S. P., Roy, M. R., and Sailaja, M. (2015). Finite Element Analysis of Alloy Wheel. *International Journal of Engineering and Management Research (IJEMR)*, 5(2), pp. 544-550.

Laser, S. and Stowell, A.F., (2019). Thinking like Apple's recycling robots: towards the activation of responsibility in a post environmentalist world. *Ephemera: Theory and Politics in Organization*, 20(2).

LME. (2020). London Metal Exchange: LME Aluminium.

Løvik, A. N., Modaresi, R., and Müller, D. B. (2014). Long-term strategies for increased recycling of automotive aluminum and its alloying elements. *Environmental Science and Technology*, 48(8), pp. 4257–4265.

Milford, R. L., Allwood, J. M., and Cullen, J. M. (2011). Assessing the potential of yield improvements, through process scrap reduction, for energy and CO<sub>2</sub> abatement in the steel and aluminium sectors. *Resources, Conservation and Recycling*, 55(12), 1185–1195.

Milovanoff, A., Kim, H.C., De Kleine, R., Wallington, T.J., Posen, I.D. and MacLean, H.L., (2019). A Dynamic Fleet Model of US Light-Duty Vehicle Lightweighting and Associated Greenhouse Gas Emissions from 2016 to 2050. *Environmental science & technology*, 53(4), pp.2199-2208.

Modaresi, R., and Müller, D. B. (2012). The role of automobiles for the future of aluminum recycling. *Environmental Science and Technology*, 46(16), pp.8587–8594.

Modaresi, R., Pauliuk, S., Lovik, A.N. and Muller, D.B., (2014) Global carbon benefits of material substitution in passenger cars until 2050 and the impact on the steel and aluminum

industries. *Environmental science & technology*, 48(18), pp.10776-10784.

NHTSA. (2006). Vehicle survivability and travel mileage schedules.

NHTSA, and EPA. (2018). The Safer Affordable Fuel-Efficient (SAFE) Vehicles Rule for Model Years 2021-2026 Passenger Cars and Light Trucks. *Federal Register*, 83(165), 42986–43500.

Reuters, 2019, Factbox: China to tighten restrictions on scrap metal imports from Monday.

Schlesinger, Mark E. (2014). *Aluminum Recycling* (Second edition). CRC Press.

Schlesinger, Mark E., (2018) *Recycling of Aluminum*. *Aluminum Science and Technology ASM Handbook*, pp. 96–107.

Sekulic, Z., Bartulovic, Z., Mihajlovic, S., Ignjatovic, M., Savic, L., Jovanovic, V., and Nisic, D. (2017). The choice of high gradient magnetic separation processes for removal of Fe<sub>2</sub>O<sub>3</sub> carriers from quartz raw material. *Gospodarka Surowcami Mineralnymi*, 33. Pp. 93–106.

Sherman, Don. (2014) Leave the Iron On: Ford Buries New-Age Iron in Its Aluminum-Intensive 2015 F-150. *Car and Driver*.

Simon, T.R., Cong, L., Zhai, Y., Zhu, Y. and Zhao, F., (2018). A Semi-automatic System for Efficient Recovery of Rare Earth Permanent Magnets from Hard Disk Drives. *Procedia CIRP*, 69, pp.916-920.

Southwood, Mike. (2019) The problem with zorba. *Recycling today: Features - Aluminum Market Report*

Tita, Bob. (2019) Aluminum Scrap Abounds Thanks to Tariffs. *The Wall Street Journal*.

U.S. Department of Commerce. (2018). *The Effect of Imports of Aluminum on the National Security*.

U.S. International Trade Commission. (2019). *Industry&Analysis*.

USGS. (2017). *2017 Minerals Yearbook Aluminum*.

WardsAuto. (2019). GM’s Carbon-Fiber Pickup Bed Just a Start, Automaker Says.

WAS. (2020). 2019 Chevy Silverado Reduces Weight with AHSS.

White, J., and Carey, N. (2018). New Ram pickup notches win for steel in U.S. truck market.

Zhu, Y., and Cooper, D. R. (2019). An optimal reverse material supply chain for U.S. Aluminum scrap. *Procedia CIRP*, 80, 677–682.

Zhu, Y., and Cooper, D. R. (2022). Refining technology roadmap for increasing U.S. aluminum recycling rate. To Be Submitted to *Environmental Science and Technology*.

## Appendix D

### Recycling technology catalog

This recycling technology catalogue contains descriptions of three separation technologies (e.g., color sorting and etching) and eight refining technologies (e.g., electro-refining for magnesium removal). Separation technologies help to distinguish between different aluminum types (e.g., wrought vs cast), alloy families (e.g., 1xxx vs 5xxx), and individual alloys e.g., 6061 vs 6063). During a separation process, the scrap remains in a (semi-) solid state and the output must be fed through a refining technology to produce a liquid metal. The baseline refining technology modeled in this work is an industry standard reverberatory furnace in which natural gas is burned to melt the scrap charge. The homogenized composition of the scrap charge is adjusted by adding virgin metals. In addition to the reverberatory furnace, seven nascent refining technologies are modeled. All these nascent refining technologies purify the aluminum scrap charge in the (semi-) liquid state. For each technology, the catalogue quantifies its separation or refining potential, process yield ratio, cost, emission, and current industry use. Detailed literature reviews have been conducted to produce the catalogue and semi-structured interviews with industry experts (e.g., The Aluminum Recyclers Council) are used as validation. This catalogue is needed to help understand how these technologies could be incorporated into a reverse material supply chain.

Information about the recycling technology catalog is published at: [https://docs.google.com/spreadsheets/d/e/2PACX-1vSO4e5WQCzJxxBalFrgleQa6wE2EjiD.YWP GmfGGt95DuLsO\\_RjWS\\_UWlp0Y0dJlA/pubhtml](https://docs.google.com/spreadsheets/d/e/2PACX-1vSO4e5WQCzJxxBalFrgleQa6wE2EjiD.YWP GmfGGt95DuLsO_RjWS_UWlp0Y0dJlA/pubhtml)

#### D.1 Reference

1. Pressley, P. N., Levis, J. W., Damgaard, A., Barlaz, M. A. and DeCarolis, J. F. Analysis of material recovery facilities for use in life-cycle assessment. *Waste Manag.* 35, 307–317 (2015).
2. Gaustad, G., Olivetti, E. and Kirchain, R. Improving aluminum recycling: A survey of sorting and impurity removal technologies. *Resour. Conserv. Recycl.* 58, 79–87 (2012).
3. U.S. Department of the Interior and U.S. Geological survey. Mineral commodity summaries 2018. (2018).

4. statista. Projected annual inflation rate in the United States from 2010 to 2023. (Accessed: 1st April 2019)
5. Enparantza, R., Revilla, O. and Azkarate, A. A life cycle cost calculation and management system for machine tools. 13th CIRP Int. Conf. Life Cycle Eng. 717–722 (2006).
6. Erumban, A. A. LIFETIMES OF MACHINERY AND EQUIPMENT: EVIDENCE FROM DUTCH MANUFACTURING. (2008).
7. Dahmus, J. B. and Gutowski, T. G. An Environmental Analysis of Machining. in Proceedings of IMECE2004 643–652 (2008). doi:10.1115/imece2004-62600
8. Dittrich, M. A. et al. Exergy analysis of incremental sheet forming. *Prod. Eng.* 6, 169–177 (2012).
9. Cooper, D. R., Rossie, K. E. and Gutowski, T. G. The energy requirements and environmental impacts of sheet metal forming: An analysis of five forming processes. *J. Mater. Process. Technol.* 244, 116–135 (2017).
10. Bell, S., Davis, B., Javaid, A. and Essadiqi, E. Final Report on Scrap Management, Sorting and Classification of Aluminum. (2003). doi:10.13140/RG.2.2.30171.98089
11. Wyss, R. K. and Schultz, P. B. Color sorting aluminum alloy scrap for recycling. *Light Met. Proc. Sess. TMS Annu. Meet.* (Warrendale, Pennsylvania) 1093–1098 (1999).
12. Gaustad, G., Olivetti, E. and Kirchain, R. Design for Recycling. *J. Ind. Ecol.* 14, 286–308 (2010).
13. Wesort. Metal Color Sorter.(Accessed: 4th May 2019)
14. Brown, C. Regeneration of Caustic Solutions. *Plat. Surf. Finish.* 0–3 (1982).
15. Alibaba. Caustic Soda/NaOH/Sodium Hydroxide in flakes/pearls/liquid. (Accessed: 20th April 2019)
16. Anhui Wenyao Intelligent Photoelectronic Technology Co. Ltd. Wenyao Metals color sorter/color sorting machine manufacturer. (Accessed: 11th April 2019)
17. Ambrose, F., Brown, R. D., Montagna, D. and Makar, H. V. Hot-crush technique for separation of cast- and wrought-aluminum alloy scrap. *Conserv. Recycl.* 6, 63–69 (1983).
18. Duane, R. D. R. Separation of cast and wrought aluminum alloys by thermomechanical processing / by R.D. Brown, Jr., F. Ambrose, and D. Montagna. (1985).
19. Gilstad, G. Life Cycle Assessment of Secondary Aluminium Refining. (2013).
20. Furu, J. An Experimental and Numerical Study of Heat Transfer in Aluminium Melting and Remelting Furnaces. (2013).
21. Application Note Libs-. LIBS FOR AUTOMATED ALUMINUM SCRAP SORTING. 028, 1–4
22. Javaid, A. and Essadiqi, E. Final Report on Scrap Management, Sorting and Classification of Steel. 23, 22 (2003).

23. Gesing, A. and Wolanski, R. Recycling light metals from end-of-life vehicles. *Jom* 53, 21–23 (2001).
24. Werheit, P. et al. Automated LIBS sorting system for single piece analysis in metal recycling. 1–13 (2011).
25. Steinert. STEINERT STARTS OPERATION OF THE FIRST INDUSTRIAL LIBS SYSTEM FOR SEPARATING ALUMINIUM SCRAP ALLOYS.
26. Gesing, A., Gesing, M., Erdmann, T. and GmbH, T. Advanced Industrial Technologies for Aluminium Scrap Sorting. *Alum.* Oct. 12-14 (2010).
27. Campanella, B. et al. Classification of wrought aluminum alloys by ANN evaluation of LIBS spectra from aluminum scrap samples. *Spectrochim. Acta - Part B At. Spectrosc.* 134, 52–57 (2017).
28. Fushun Ejet Magnetic Equipment Co. Ltd. Sophisticated technologies 1400KG scrap metal recycling sorter.
29. Laserglow Technologies. 1064 nm AOM Q-Switched DPSS Laser System.
30. Schlesinger, M. E. *Aluminum Recycling*. (CRC Press, 2014). doi:10.1201/9781420006247
31. Li, T., Hassan, M., Kuwana, K., Saito, K. and King, P. Performance of secondary aluminum melting: Thermodynamic analysis and plant-site experiments. *Energy* 31, 1769–1779 (2006).
32. Gangoli, B. S., Kenworthy, B., Buragino, G. and Hewertson, R. *Oxy-Fuel Technologies and Strategies for Secondary Aluminum Melting Operations*. (2017).
33. DeYoung, D. H., Wang, C. and Wiswall, J. *Alcoa Final Technical Report*. (2011).
34. Milford, R. L., Pauliuk, S., Allwood, J. M. and Müller, D. B. The roles of energy and material efficiency in meeting steel industry CO<sub>2</sub> targets. *Environ. Sci. Technol.* 47, 3455–3462 (2013).
35. Utigard, T. A., Roy, R. R. and Friesen, K. The Roles of Molten Salts in the Treatment of Aluminum. *Can. Metall. Q.* 40, 327–334 (2001).
36. Utigard, T. A. et al. The properties and uses of fluxes in molten aluminum processing. *Jom* 50, 38–43 (1998).
37. Wtlliams, E. M., Mccarthy, R. W., Levy, S. A. and Sigworth, G. K. REMOVAL OF ALKALI METALS FROM ALUMINUM. *Essent. Readings Light Met.* 71–79 (2016).
38. Tiwari, B. L. Demagging Processes for Aluminum Alloy Scrap. *JOM* 34, 54–58 (1982).
39. Fu, Q. and Evans, J. W. Chlorine fluxing for removal of magnesium from molten aluminum: Part II. Mathematical model. *Metall. Mater. Trans. B* 29, 979–986 (2007).
40. Qian, J. W. F., Dong, X. and Evans. Chlorine fluxing for removal of magnesium from molten aluminum: Part I Laboratory-scale measurements of reaction rates and bubble behavior. *Metall. Mater. Trans. B* 29, 971–978 (1998).
41. Leboeuf, S., Dupuis, C., Maltais, B., Thibault, M.-A. and Smarason, E. IN-LINE SALT FLUXING PROCESS: THE SOLUTION TO CHLORINE GAS UTILIZATION IN CASmOUSES.



Essent. Readings Light Met. 126–131 (2016). doi:10.1080/08827508.2010.542211

42. Majidi, O., Shabestari, S. G. and Aboutalebi, M. R. Study of fluxing temperature in molten aluminum refining process. *J. Mater. Process. Technol.* 182, 450–455 (2007).

43. David, E. and Kopac, J. Aluminum recovery as a product with high added value using aluminum hazardous waste. *J. Hazard. Mater.* 261, 316–324 (2013).

44. Zhang, L., Gao, J., Damoah, L. N. W. and Robertson, D. G. Removal of iron from aluminum: A review. *Miner. Process. Extr. Metall. Rev.* 33, 99–157 (2012).

45. David, E. and Kopac, J. Aluminum recovery as a product with high added value using aluminum hazardous waste. *J. Hazard. Mater.* 261, 316–324 (2013).

46. Sanders, R. E. Technology innovation in aluminum products. *Jom* 53, 21–25 (2001).

47. Lindsay, S. J. Very high purity aluminum: An historical perspective. *Jom* 66, 217–222 (2014).

48. Hammervold, J., Pettersen, J. and Moe Bjørnbet, M. Lifecycle Assessment and Lifecycle Costing of Aluminium Wrought-to-Wrought Recycling. *Mater. Sci. Forum* 794–796, 1065–1070 (2014).

49. Kamavaram, V., Mantha, D. and Reddy, R. G. Recycling of aluminum metal matrix composite using ionic liquids: Effect of process variables on current efficiency and deposit characteristics. *Electrochim. Acta* 50, 3286–3295 (2005).

50. Endo, A., Miyake, M. and Hirato, T. Electrodeposition of Aluminum from 1,3-Dimethyl-2-Imidazolidinone/ $\text{AlCl}_3$  baths. *Electrochim. Acta* 137, 470–475 (2014).

51. Pradhan, D. and Reddy, R. G. Mechanistic study of Al electrodeposition from EMIC- $\text{AlCl}_3$  and BMIC- $\text{AlCl}_3$  electrolytes at low temperature. *Mater. Chem. Phys.* 143, 564–569 (2014).

52. Drini, B., Katgerman, L. and Boom, R. Metal refining with fractional crystallisation: State-of-the-art and future prospects. 1–10 (2005).

53. Kahveci, A. I. and Unal, A. Refining of a 5XXX Series Aluminum Alloy Scrap by Alcoa Fractional Crystallization Process. *Essent. Readings Light Met. Alum. Reduct. Technol* 2, 979–991 (2000).

54. Mehmetaj, B., Bruinsma, O. S. L., Kool, W. H., Jansens, P. J. and Katgerman, L. Aluminium Scrap Recycling With Solid Layer Fractional Crystallization. *Chem. Eng. Trans.* 1, 879–884 (2002).

55. Sillekens, W. H. Refining aluminium scrap by means of fractional crystallisation: Technical feasibility. *Proc. Fourth ASM Int. Conf. Exhib. Recycl. Met. ASM Eur.* (1999).

56. Muñiz-Lerma, J. A., Paliwal, M., Jung, I. H. and Brochu, M. Fractional Crystallization Model of Multicomponent Aluminum Alloys: A Case Study of Aircraft Recycling. *Metall. Mater. Trans. B Process Metall. Mater. Process. Sci.* 48, 1024–1034 (2017).

57. Sillekens, W. H., Verdoes, D. and Boender, W. Refining aluminium scrap by means of

fractional crystallisation: Status and prospects for development. *Metall* 56, (2002).

58. Sillekens, W. H. H., Verdoes, D. and Boender, W. Refining aluminium scrap by means of fractional crystallisation: Status and prospects for development. *Metall* 56, (2002).

59. Lotfollahi, M. N. Design of optimal process flowsheet for fractional crystallization separation process. *Iran. J. Chem. Chem. Eng.* 28, 63–73 (2009).

60. Ohtaki, M., Arakawa, T. and Murata, F. A New Proposal of Continuous Agitation Vacuum Distillation Process (CAVP) to Remove Zn from Aluminum Scrap Melt. *Recycl. Met. Eng. Mater.* 993–1003 (2013). doi:10.1002/9781118788073.ch87

61. Gesing, A. J., Das, S. K. and Loutfy, R. O. Production of magnesium and aluminum-magnesium alloys from recycled secondary aluminum scrap melts. *REWAS 2016 Towar. Mater. Resour. Sustain.* 68, 253–254 (2016).

62. Gesing, A. J. and Das, S. K. Use of Thermodynamic Modeling for Selection of Electrolyte for Electrorefining of Magnesium from Aluminum Alloy Melts. *Metall. Mater. Trans. B Process Metall. Mater. Process. Sci.* 48, 132–145 (2017).

63. Alibaba. Factory Advanced Electrorefining Gold Processing Plants.

## BIBLIOGRAPHY

- Accenture (2011). *Plug-in electric vehicles Changing perceptions, hedging bets*. Accenture end-consumer survey on the electrification of private transport.
- Ahmadi, S., S. M. T. Bathaee, and A. H. Hosseinpour (2018). Improving fuel economy and performance of a fuel-cell hybrid electric vehicle (fuel-cell, battery, and ultra-capacitor) using optimized energy management strategy. *Energy Conversion and Management* 160, 74–84.
- AISI (2015). American iron and steel institute profile 2015.
- Allwood, J. M., M. F. Ashby, T. G. Gutowski, and E. M. E. A. W. P. Worrell (2010). *Resour. Conserv. Recycl* 55, 362–381.
- Allwood, J. M., J. M. Cullen, M. A. Carruth, D. R. Cooper, M. McBrien, R. L. Milford, M. C. Moynihan, and A. C. Patel (2012). *Sustainable materials: with both eyes open*. UIT Cambridge Limited Cambridge, UK.
- Allwood, J. M., J. M. Cullen, D. R. Cooper, R. Milford, A. Patel, M. Carruth, and M. McBrien (2010). Conserving our metal energy: Avoiding melting steel and aluminum scrap to save energy and carbon. *WellMet 2050*.
- Allwood, J. M., J. M. Cullen, and R. L. Milford (2010). Options for achieving a 50% cut in industrial carbon emissions by 2050. *Environmental Science & Technology*.
- Ambrose, F., R. D. Brown, D. Montagna, and H. V. Makar (1983). Hot-crush technique for separation of cast- and wrought-aluminum alloy scrap. *Conserv. Recycl.* 6, 63–69.
- Ambrose, H., A. Kendall, M. Lozano, S. Wachche, and L. Fulton (2020). Trends in life cycle greenhouse gas emissions of future light duty electric vehicles. *Transportation Research Part D: Transport and Environment* 81.
- Andersen, J. and B. Hyman (2001). Energy and material flow models for the us steel industry.
- Argonne (2020). Argonne the greenhouse gases, regulated emissions, and energy use in technologies (greet) model.
- at Argonne National Laboratory, T. R. C. (2020). Light duty electric drive vehicles monthly sales updates 2020.
- Atherton, J. (2007). Declaration by the metals industry on recycling principles. *The International Journal of Life Cycle Assessment* 12(1), 59.

- Bastani, P., J. B. Heywood, and C. Hope (2012). The effect of uncertainty on us transport-related ghg emissions and fuel consumption out to 2050. *Transportation Research Part A: Policy and Practice* 46(3), 517–548.
- Bauer, C., J. Hofer, H.-J. Althaus, A. Del Duce, and A. Simons (2015). The environmental performance of current and future passenger vehicles: Life cycle assessment based on a novel scenario analysis framework. *Applied energy* 157, 871–883.
- Bauer, S. (2012). Sustainable materials: With both eyes open. *Materials Today* 15, 9.
- Baumert, K. A., T. Herzog, and J. Pershing (2005). Navigating the numbers: Greenhouse gas data and international climate policy.
- Bertram, M., S. Ramkumar, H. Rechberger, G. Rombach, C. Bayliss, K. J. Martchek, D. B. Muller, and G. Liu (2017). A regionally-linked, dynamic material flow modelling tool for rolled, extruded and cast aluminium products. *Resources, Conservation and Recycling* 125, 48–69.
- Biden, J. (2021). The Biden plan for a clean energy revolution and environmental justice.
- Black, F. M., L. E. High, and J. M. Lang (1980). Composition of automobile evaporative and tailpipe hydrocarbon emissions. *Journal of the Air Pollution Control Association* 30(11), 1216–1220.
- BloombergNEF (2020). Electric vehicle outlook 2020.
- Board, C. A. R. (2020). Advanced clean cars program.
- Brooker, A., J. Gonder, L. Wang, E. Wood, S. Lopp, and L. Ramroth (2015). *FASTSim: A model to estimate vehicle efficiency, cost and performance (No. 2015-01-0973)*. SAE Technical Paper.
- Brunner, P. H. and H. Rechberger (2017). *Handbook of Material Flow Analysis: For Environmental, Resource, and Waste Engineers*. CRC Press: Boca Raton.
- Buehler, R. (2011). Determinants of transport mode choice: a comparison of Germany and the USA. *Journal of transport geography* 19(4), 644–657.
- Byrd, R. H., M. E. Hribar, and J. Nocedal (1999). An interior point algorithm for large-scale nonlinear programming. *SIAM J. Optim* 9, 877–900.
- Carruth, M. A. and J. M. A. Allwood (2013). Novel process for transforming sheet metal blanks: Ridged die forming. *CIRP Ann* 62, 267–270.
- Cencic, O. (2016). Nonlinear data reconciliation in material flow analysis with software stan. *Sustain. Environ* 26, 291–298.
- Chan, S., L. F. Miranda-Moreno, A. Alam, and M. Hatzopoulou (2013). Assessing the impact of bus technology on greenhouse gas emissions along a major corridor: A lifecycle analysis. *Transportation Research Part D: Transport and Environment* 20, 7–11.
- Chen, W.-Q. and T. E. Graedel (2012). Dynamic analysis of aluminum stocks and flows in the United States: 1900–2009. *Ecological Economics* 81, 92–102.

- Chester, M. V. and A. Cano (2016). Time-based life-cycle assessment for environmental policy-making: Greenhouse gas reduction goals and public transit. *Transportation Research Part D: Transport and Environment* 43, 49–58.
- Ciez, R. E. and J. F. Whitacre (2019). Examining different recycling processes for lithium-ion batteries. *Nature Sustainability* 2(2), 148–156.
- Cochran, J., P. Denholm, B. Speer, and M. Miller (2015). Grid integration and the carrying capacity of the us grid to incorporate variable renewable energy (no. *NREL/TP- 6, A20–62607*).
- Company, T. D. J. (2018). *Primary Iron and U. S. Scrap Chemical Compositions*;
- Connolly, D., H. Lund, B. V. Mathiesen, and M. Leahy (2011). The first step towards a 100% renewable energy-system for ireland. *Applied Energy* 88(2), 502–507.
- Cooper, D. (2014). Reuse of steel and aluminium without melting.
- Cooper, D. R., K. E. Rossie, and T. G. Gutowski (2017). The energy requirements and environmental impacts of sheet metal forming: An analysis of five forming processes. *Journal of Materials Processing Technology* 244, 116–135.
- Craglia, M. and J. Cullen (2020). Do vehicle efficiency improvements lead to energy savings? *The rebound effect in Great Britain* 88.
- Cullen, J. M. and J. M. Allwood (2013). Mapping the global flow of aluminum: From liquid aluminum to end-use goods. *Environmental science & technology* 47(7), 3057–3064.
- Cullen, J. M., J. M. Allwood, and M. D. Bambach (2012). Mapping the global flow of steel: from steelmaking to end-use goods. *Environmental science & technology* 46(24), 13048–13055.
- Daehn, K. E., C. Serrenho, A. Allwood, and J. M. (2017). How will copper contamination constrain future global steel recycling. *Environ. Sci* 51, 6599–6606.
- Dai, Q., J. C. Kelly, L. Gaines, and M. Wang (2019). Life cycle analysis of lithium-ion batteries for automotive applications. *Batteries* 5, 2.
- Damassa, T. (2014). *Climate Analysis Indicators Tool (CAIT)*. Dordrecht: Springer Netherlands.
- DeYoung, D. H., C. Wang, and J. Wiswall (2011). Alcoa final report on membrane purification of aluminum scrap.
- Ding, Y., Z. P. Cano, A. Yu, J. Lu, and Z. Chen (2019). Automotive li-ion batteries: current status and future perspectives. *Electrochemical Energy Reviews* 2(1), 1–28.
- Duffin, E. (2020). *Work situation of adults in the United States during the COVID-19 outbreak as of April 2020*. Retrieved from.
- Economics, M. (2018). The circular economy, a powerful force for climate mitigation.
- Edwards, M. R. and J. E. Trancik (2014). Climate impacts of energy technologies depend on emissions timing. *Nature Climate Change* 4(5), 347–352.

- Egan, S. (2021, July). Us industry (naics) report 33131: Aluminum manufacturing in the us.
- Elgowainy, A., J. Han, J. Ward, F. Joseck, D. Gohlke, A. Lindauer, T. Ramsden, M. Bidy, M. Alexander, S. Barnhart, et al. (2018). Current and future united states light-duty vehicle pathways: Cradle-to-grave lifecycle greenhouse gas emissions and economic assessment. *Environmental science & technology* 52(4), 2392–2399.
- Elgowainy, A., J. Han, J. Ward, F. Joseck, D. Gohlke, A. Lindauer, T. Ramsden, M. Bidy, M. Alexander, S. Barnhart, and I. Sutherland (2018). Current and future united states light-duty vehicle pathways: Cradle-to-grave lifecycle greenhouse gas emissions and economic assessment. *Environmental science & technology* 52(4), 2392–2399.
- Ellingsen, L. A.-W., B. Singh, and A. H. Strømman (2016). The size and range effect: lifecycle greenhouse gas emissions of electric vehicles. *Environmental Research Letters* 11(5), 054010.
- Ercan, T., N. C. Onat, and O. Tatari (2016). Investigating carbon footprint reduction potential of public transportation in united states: A system dynamics approach.
- F., C. B. G. E. L. S. L. G. P. S. S. and P. V. (2017). Classification of wrought aluminum alloys by an evaluation of libs spectra from aluminum scrap samples. *Spectrochimica Acta Part B: Atomic Spectroscopy* 134, 52–57.
- Fagnant, D. J. and K. M. Kockelman (2014). The travel and environmental implications of shared autonomous vehicles, using agent-based model scenarios. *Transportation Research Part C: Emerging Technologies* 40, 1–13.
- Farrington, R. and J. Rugh (2000). Impact of vehicle air-conditioning on fuel economy, tailpipe emissions, and electric vehicle range (no. NREL/CP-, 540–28960).
- FHWA (2020). Federal highway administration (fhwa) forecasts of vehicle miles traveled.
- (FHWA)., F. H. A. (2021, March). 1969-2019. traffic volume trends.
- Field, F., R. Kirchain, and J. Clark (2000). Life-cycle assessment and temporal distributions of emissions: Developing a fleet-based analysis. *Journal of Industrial Ecology* 4(2), 71–91.
- Fmincon Nonlinear (2013). Fmincon nonlinear optimization documentation, matlab.
- Fridstrøm, L., V. Østli, and K. W. Johansen (2016). A stock-flow cohort model of the national car fleet. *European Transport Research Review* 8(3), 1–15.
- Fuel Flex kit (2021). Fuel flex kit. retrieved on january 15th, 2021.
- Garside, M. (2020, March). The U.S. distribution of ethanol production by feedstock type.
- Gaustad, G., E. Olivetti, and R. Kirchain (2012). Improving aluminum recycling: A survey of sorting and impurity removal technologies. *Resources, Conservation and Recycling* 58, 79–87.
- Gesing, A., M. Gesing, T. Erdmann, and T. GmbH (2010). Advanced industrial technologies for aluminium scrap sorting. *Alum. Oct*, 12–14.

- Gesing, A. and R. Wolanski (2001). Recycling light metals from end-of-life vehicles. *Jom* 53(11), 21–23.
- Greenblatt, J. B. and S. Saxena (2015). Autonomous taxis could greatly reduce greenhouse-gas emissions of us light-duty vehicles. *Nature Climate Change* 5(9), 860–863.
- Greene, D. L., H. H. Baker Jr, and S. E. Plotkin (2010). Reducing greenhouse gas emissions from us transportation.
- Greene, D. L. and J. DeCicco (2000). Engineering-economic analyses of automotive fuel economy potential in the united states. *Annual Review of Energy and the Environment* 25(1), 477–535.
- Greene, D. L., S. Park, and C. Liu (2014). Public policy and the transition to electric drive vehicles in the us: The role of the zero emission vehicles mandates. *Energy Strategy Reviews* 5, 66–77.
- Grunditz, E. (2016). *Design and assessment of battery electric vehicle powertrain, with respect to performance, energy consumption and electric motor thermal capability*. Chalmers University of Technology.
- Gutowksi, T. G., S. Sahni, J. M. Allwood, M. F. Ashby, and E. Worrell (2013). The energy required to produce materials: constraints on energy-intensity improvements, parameters of demand. *Philosophical Transactions of the Royal Society A: Mathematical, Physical and Engineering Sciences* 371(1986), 20120003.
- Gütschow, J., A. Günther, M. L. Jeffery, and R. Gieseke (2021, February). The PRIMAP-hist national historical emissions time series (1850-2018) v2.2.
- Haas, W., F. Krausmann, D. Wiedenhofer, and M. Heinz (2015). How circular is the global economy?: An assessment of material flows, waste production, and recycling in the european union and the world in 2005. *J. Ind. Ecol* 19, 765–777.
- Harper, C. D., C. T. Hendrickson, S. Mangones, and C. Samaras (2016). Estimating potential increases in travel with autonomous vehicles for the non-driving, elderly and people with travel-restrictive medical conditions. *Transportation research part C: emerging technologies* 72, 1–9.
- Harper, G., R. Sommerville, E. Kendrick, L. Driscoll, P. Slater, R. Stolkin, A. Walton, P. Christensen, O. Heidrich, S. Lambert, and A. Abbott (2019). Recycling lithium-ion batteries from electric vehicles. *Nature* 575(7781), 75–86.
- Hatayama, H., I. Daigo, Y. Matsuno, and Y. Adachi (2007). Dynamic substance flow analysis of aluminum and its alloying elements. *Materials transactions* 70(12), 975–80.
- Hatayama, H., I. Daigo, Y. Matsuno, and Y. Adachi (2009). Assessment of recycling potential of aluminum in japan, the united states, europe and china. *Nippon Kinzoku Gakkaishi/Journal of the Japan Institute of Metals* 72(10), 813–18.
- Hatayama, H., I. Daigo, Y. Matsuno, and Y. Adachi (2010). Outlook of the world steel cycle based on the stock and flow dynamics.

- Hatayama, H., I. Daigo, Y. Matsuno, and Y. Adachi (2012). Evolution of aluminum recycling initiated by the introduction of next-generation vehicles and scrap sorting technology. *Resources, Conservation and Recycling* 66, 8–14.
- Hawkins, T. R., B. Singh, G. Majeau-Bettez, and A. H. Strømman (2013). Comparative environmental life cycle assessment of conventional and electric vehicles. *Journal of industrial ecology* 17(1), 53–64.
- Heard, B. P., B. W. Brook, T. M. Wigley, and C. J. Bradshaw (2017).
- Hernandez, A. G., L. Paoli, and J. M. Cullen (2018). How resource-efficient is the global steel industry.
- Heywood, J., D. MacKenzie, I. B. Akerlind, P. Bastani, I. Berry, K. Bhatt, A. Chao, E. Chow, V. Karplus, D. Keith, and M. Khusid (2015). *On the road toward 2050: Potential for substantial reductions in light-duty vehicle energy use and greenhouse gas emissions*. Engineering System Division: Massachusetts Institute of Technology Sloan Automotive Laboratory.
- Holcomb, G. (2021, July). Us industry (naics) report 33111: Iron & steel manufacturing in the us.
- Horton, P. M. and J. M. Allwood (2017). Yield improvement opportunities for manufacturing automotive sheet metal components. *J. Mater* 249, 78–88.
- Igarashi, Y., E. Kakiuchi, I. Daigo, Y. Matsuno, and Y. Adachi (2007). Estimation of steel consumption and obsolete scrap generation in japan and asian countries in the future.
- International Energy Agency (2008). Energy technology perspective scenario and strategies to 2050.
- IPCC (2014). Climate change 2014: synthesis report. contribution of working groups i, ii and iii to the fifth assessment report of the intergovernmental panel on climate change.
- Jang, Y. C. and M. Kim (2010). Management of used & end-of-life mobile phones in korea: A review. *Resources, Conservation and Recycling* 55(1), 11–19.
- Javid, R. J. and A. Nejat (2017). A comprehensive model of regional electric vehicle adoption and penetration. *Transport Policy* 54, 30–42.
- Jofre, S. and T. Morioka (2005). Waste management of electric and electronic equipment: Comparative analysis of end-of-life strategies. *Journal of Material Cycles and Waste Management* 7(1), 24–32.
- Karabasoglu, O. and J. Michalek (2013). Influence of driving patterns on life cycle cost and emissions of hybrid and plug-in electric vehicle powertrains. *Energy policy* 60, 445–461.
- Ke, W., S. Zhang, X. He, Y. Wu, and J. Hao (2017). Well-to-wheels energy consumption and emissions of electric vehicles: Mid-term implications from real-world features and air pollution control progress. *Applied Energy* 188, 367–377.



- Kelly, J. C., J. L. Sullivan, A. Burnham, and A. Elgowainy (2015). Impacts of vehicle weight reduction via material substitution on life-cycle greenhouse gas emissions. *Environmental science & technology* 49(20), 12535–12542.
- Kim, H. J., G. A. Keoleian, and S. J. Skerlos (2011). Economic assessment of greenhouse gas emissions reduction by vehicle lightweighting using aluminum and high-strength steel. *Journal of Industrial Ecology* 15(1), 64–80.
- Kim, H.-J., C. McMillan, G. A. Keoleian, and S. J. Skerlos (2010). Greenhouse gas emissions payback for lightweighted vehicles using aluminum and high-strength steel. *Journal of Industrial Ecology* 14(6), 929–946.
- Kopec, G. M., J. M. Allwood, J. M. Cullen, and D. Ralph (2016). A general nonlinear least squares data reconciliation and estimation method for material flow analysis. *Journal of Industrial Ecology* 20(5), 1038–1049.
- Kopelias, P., E. Demiridi, K. Vogiatzis, A. Skabardonis, and V. Zafiropoulou (2020). Connected & autonomous vehicles—environmental impacts—a review. *Science of the total environment* 712.
- Levasseur, A., O. Cavalett, J. S. Fuglestvedt, T. Gasser, D. J. Johansson, S. V. Jørgensen, M. Rauegi, A. Reisinger, G. Schivley, A. Strømman, and K. Tanaka (2016). Enhancing life cycle impact assessment from climate science: Review of recent findings and recommendations for application to lca. *Ecological Indicators* 71, 163–174.
- Lewis, A. M., J. C. Kelly, and G. A. Keoleian (2014). Vehicle lightweighting vs. electrification: life cycle energy and ghg emissions results for diverse powertrain vehicles. *Applied Energy* 126, 13–20.
- Liao, J., Y. Zhu, and R. D. Cooper (2021). Reducing emissions by using products more intensively.
- Logan, K. G., J. D. Nelson, and A. Hastings (2020). Electric and hydrogen buses: Shifting from conventionally fuelled cars in the uk. *Transportation Research Part D: Transport and Environment* 85.
- Luk, J. M., H. C. Kim, R. De Kleine, T. J. Wallington, and H. L. MacLean (2017). Review of the fuel saving, life cycle ghg emission, and ownership cost impacts of lightweighting vehicles with different powertrains. *Environmental science & technology* 51(15), 8215–8228.
- Lupton, R. C. and J. M. Allwood (2018). Incremental material flow analysis with bayesian inference. *J. Ind. Ecol* 22, 1352–1364.
- Ma, H., F. Balthasar, N. Tait, X. Riera-Palou, and A. Harrison (2012). A new comparison between the life cycle greenhouse gas emissions of battery electric vehicles and internal combustion vehicles. *Energy policy* 44, 160–173.
- Majeau-Bettez, G., T. R. Hawkins, and A. H. Strømman (2011). Life cycle environmental assessment of lithium-ion and nickel metal hydride batteries for plug-in hybrid and battery electric vehicles. *Environmental science & technology* 45(10), 4548–4554.

- Masson-Delmotte, V., P. Zhai, H.-O. Pörtner, D. Roberts, J. Skea, P. R. Shukla, A. Pirani, W. Moufouma-Okia, C. Péan, R. Pidcock, et al. (2018). Global warming of 1.5 c. *An IPCC Special Report on the impacts of global warming of 1*, 1–9.
- Material Economics (2018). The circular economy, a powerful force for climate mitigation.
- Mayyas, A., M. Omar, M. Hayajneh, and A. R. Mayyas (2017). Vehicle's lightweight design vs. electrification from life cycle assessment perspective. *Journal of Cleaner Production* 167, 687–701.
- McCollum, D. and C. Yang (2009). Achieving deep reductions in us transport greenhouse gas emissions: Scenario analysis and policy implications. *Energy Policy* 37(12), 5580–5596.
- McMillan, C. A., M. R. Moore, G. A. Keoleian, and J. W. Bulkley (2010). Quantifying us aluminum in-use stocks and their relationship with economic output. *Ecological Economics* 69(12), 2606–2613.
- McMillan, C. A., S. J. Skerlos, and G. A. Keoleian (2012). Evaluation of the metals industry's position on recycling and its implications for environmental emissions. *Journal of Industrial Ecology* 16(3), 324–33.
- Messagie, M., F. S. Boureima, T. Coosemans, C. Macharis, and J. V. Mierlo (2014). A range-based vehicle life cycle assessment incorporating variability in the environmental assessment of different vehicle technologies and fuels. *Energies* 7(3), 1467–1482.
- Mian, A. and A. Sufi (2012). The effects of fiscal stimulus: Evidence from the 2009 cash for clunkers program. *The Quarterly journal of economics* 127(3), 1107–1142.
- Michaelis, P. and T. Jackson (2000a). Material and energy flow through the uk iron and steel sector. part 1: 1954–1994. *Resources, Conservation and Recycling* 29(1-2), 131–156.
- Michaelis, P. and T. Jackson (2000b). Material and energy flow through the uk iron and steel sector: Part 2: 1994–2019. *Resources, Conservation and recycling* 29(3), 209–230.
- Midrex Technologies, Inc. (2014). World direct reduction statistics.
- Milford, R. L., J. M. Allwood, and J. M. Cullen (2011). Assessing the potential of yield improvements, through process scrap reduction, for energy and co2 abatement in the steel and aluminium sectors. *Resources, Conservation and Recycling* 55(12), 1185–1195.
- Milford, R. L., S. Pauliuk, J. M. Allwood, and D. B. Muller (2013). The roles of energy and material efficiency in meeting steel industry co2 targets. *Environmental Science and Technology* 47(7), 3455–62.
- Miller, S. A. and B. R. Heard (2016). The environmental impact of autonomous vehicles depends on adoption patterns.
- Milovanoff, A., H. C. Kim, R. De Kleine, T. J. Wallington, I. D. Posen, and H. L. MacLean (2019). A dynamic fleet model of us light-duty vehicle lightweighting and associated greenhouse gas emissions from 2016 to 2050. *Environmental science & technology* 53(4), 2199–2208.

- Milovanoff, A., I. D. Posen, and H. L. MacLean (2020). Electrification of light-duty vehicle fleet alone will not meet mitigation targets. *Nature Climate Change* 10(12), 1102–1107.
- Miotti, M., G. J. Supran, E. J. Kim, and J. E. Trancik (2016). Personal vehicles evaluated against climate change mitigation targets. *Environmental science & technology* 50(20), 10795–10804.
- Moawad, A., N. Kim, N. Shidore, and A. Rousseau (2016). *Assessment of Vehicle Sizing, Energy Consumption and Cost Through Large Scale Simulation of Advanced Vehicle Technologies*. United States.
- Modaresi, R. and D. B. Muller (2012, May). The role of automobiles for the future of aluminum recycling. *Environmental Science and Technology* 46(16), 8587–94.
- Modaresi, R., S. Pauliuk, A. N. Lovik, and D. B. Muller (2014). Global carbon benefits of material substitution in passenger cars until 2050 and the impact on the steel and aluminum industries. *Environmental science & technology* 48(18), 10776–10784.
- Morgan, J. and J. Liker (2018). *Designing the Future*. McGraw-Hill: New York.
- Morrison, G. M., A. Allan, and R. Carpenter (2010). Abating greenhouse gas emissions through cash-for-clunker programs.
- Moynihan, M. C. and J. M. Allwood (2012). The flow of steel into the construction sector. *Resour. Conserv. Recycl* 68, 88–95.
- Muller, D. B., T. Wang, and B. Duval (2011). Patterns of iron use in societal evolution.
- Muller, D. B., T. Wang, B. Duval, and T. E. Graedel (2006). Exploring the engine of anthropogenic iron cycles.
- Nakajima, K., W. Tamaki, D. Fujimaki, and I. Daigo (2005). Flow analysis in japan.
- Nemec, R. U. S. (2018). Steel pipe makers win trade dumping case.
- NHTSA (2017). Summary of travel trends 2017 national household travel survey.
- Norwegian E.V. policy. (2021). Norway is leading the way for a transition to zero emission in transport. last accessed: March, 15th, 2021.
- Oberhausen, G., Y. Zhu, and D. R. Cooper (2021). Reducing the environmental impacts of aluminum extrusion.
- Office of Governor Gavin Newsom (2020). Governor newsom announces california will phase out gasoline-powered cars & drastically reduce demand for fossil fuel in california’s fight against climate change.
- OICA (2016). Cars; world motor vehicle production by country and type.
- Omar, M. (2011). *The Automotive Body Manufacturing Systems and Processes*. John Wiley & sons: New York.

- Onat, N. C., M. Kucukvar, O. Tatari, and G. Egilmez (2016). Integration of system dynamics approach toward deepening and broadening the life cycle sustainability assessment framework: a case for electric vehicles. *The International Journal of Life Cycle Assessment* 21(7), 1009–1034.
- Pacific Gas and Electric (2017). Pg&e renewable energy deliveries grow; ghg-free portfolio is nearly 70 percent.
- Pauliuk, S., R. L. Milford, D. B. Muller, and J. M. Allwood (2013). The steel scrap age. *Environmental Science and Technology* 47(7), 3448–54.
- Pauliuk, S., T. Wang, and D. Muller (2012). Moving toward the circular economy: The role of stocks in the chinese steel cycle. *Environ. Sci and Technol*, 148–154.
- Pauliuk, S., T. Wang, and D. B. Muller (2013). Steel all over the world: Estimating in-use stocks of iron for 200 countries.
- Phlips, P. and T. Megli (2017). Powertrain efficiency in the us fleet on regulatory drive cycles and with advanced technologies. *SAE International Journal of Fuels and Lubricants* 10(2), 537–555.
- Pleißmann, G., M. Erdmann, M. Hlusiak, and C. Breyer (2014). *Global energy storage demand for a 100*.
- Ploeg, F. V. D. (1988). Balancing large systems of national accounts. *Comput. Sci* 1, 31–39.
- Preckel, R. and P. Vivian (2018). Horizontal shale drilling fuels strong consumption.
- Pretorius, E. (2018). Personal communication with the authors.
- Raykar, S. S. S. (2015). Analysis of energy use and carbon emissions from automobile manufacturing (doctoral dissertation, massachusetts institute of technology).
- Reck, B. and S. Althaf (2021). Mapping the materials base for remade.
- Replogle, M. A. and L. M. Fulton (2014). A global high shift scenario: impacts and potential for more public transport, walking, and cycling with lower car use.
- Rod, O., C. Becker, and M. Nylén (2006). Opportunities and and dangers of using residual elements in steels. *Lit Study* 819.
- RU., A. (1999). The second law, the fourth law, recycling and limits to growth. *Ecological Economics* 29, 473–483.
- Ryan, N. A., S. A. Miller, S. J. Skerlos, and D. R. Cooper (2020). Reducing co2 emissions from us steel consumption by 70% by 2050. *Environmental Science & Technology* 54(22), 14598–14608.
- Sager, J., J. S. Apte, D. M. Lemoine, and D. M. Kammen (2011). Reduce growth rate of light-duty vehicle travel to meet 2050 global climate goals. *Environmental Research Letters* 6, 2.
- Schmidt, M. (2008a). The sankey diagram in energy and material flow management - part i: History. *J. Ind. Ecol* 12, 82–94.

- Schmidt, M. (2008b). The sankey diagram in energy and material flow management - part ii: Methodology and current applications. *J. Ind. Ecol* 12, 173–185.
- Schmuck, R., R. Wagner, G. H'orpel, T. Placke, and M. Winter (2018). Performance and cost of materials for lithium-based rechargeable automotive batteries. *Nature Energy* 3(4), 267–278.
- Schnatterly, J. (2010). *Steel Content of American Auto. Autosteel[Online]*. Watching Our Weight.
- Serrenho, A. C., J. B. Norman, and J. M. Allwood (2017). The impact of reducing car weight on global emissions: the future fleet in great britain. *Philosophical Transactions of the Royal Society A: Mathematical, Physical and Engineering Sciences* 375(2095), 20160364.
- Shabbir, W. and S. A. Evangelou (2014). Real-time control strategy to maximize hybrid electric vehicle powertrain efficiency. *Applied energy* 135, 512–522.
- Shinnar, R. (2003). The hydrogen economy, fuel cells, and electric cars. *Technology in society* 25(4), 455–476.
- Sorrell, S. and J. Dimitropoulos (2008). The rebound effect: Microeconomic definitions, limitations and extensions. *Ecological Economics* 65(3), 636–649.
- Statista (2021). What percentage of your workforce will remain permanently remote post-covid who were not remote before covid? retrieved from: Last accessed: March 15th, 2021.
- Sterner, E. O. and D. J. Johansson (2017). The effect of climate–carbon cycle feedbacks on emission metrics. *Environmental Research Letters* 12, 3.
- Supekar, S. D. and S. J. Skerlos (2017). Analysis of costs and time frame for reducing co2 emissions by 70% in the us auto and energy sectors by 2050. *Environmental science & technology* 51(19), 10932–10942.
- Sutherland, J. W., S. J. Skerlos, K. R. Haapala, D. Cooper, F. Zhao, and A. Huang (2020). Industrial sustainability: Reviewing the past and envisioning the future. *Journal of Manufacturing Science and Engineering* 142, 11.
- Taiebat, M., A. L. Brown, H. R. Safford, S. Qu, and M. Xu (2018). A review on energy, environmental, and sustainability implications of connected and automated vehicles. *Environmental science & technology* 52(20), 11449–11465.
- Tanaka, K. (2011). Review of policies and measures for energy efficiency in industry sector. *Energy policy* 39(10), 6532–6550.
- Thomas, J. (2014). Drive cycle powertrain efficiencies and trends derived from epa vehicle dynamometer results. *SAE International Journal of Passenger Cars-Mechanical Systems* 7(2014), 1374–1384.
- Twidale, S. (2020). Britain to ban new petrol cars by 2030 on road to net zero emissions.
- U. S. EPA (2018). Light-duty automotive technology, carbon dioxide emissions , and fuel economy trends: 1975 through 2012.

UCUSA (2019). Each country's share of co2 emissions.

UN (2020). United Nations Comtrade Database[Online] .

United States Geological Survey (2016a). 2015 minerals yearbook: Iron and steel scrap.

United States Geological Survey (2016b). Iron and steel.

United States Geological Survey (2016c). Iron and steel scrap.

United States Geological Survey (2016d). Iron ore.

U.S. Census Bureau (2015). U.s. imports for consumption of steel products.

U.S. Department of Commerce (2018). The effect of imports of aluminum on the national security. (january 30.

U.S. Department of Energy (2016). 2016 billion-ton report advancing domestic resources for a thriving bioeconomy.

U.S. Department of Energy (DOE) (2015). Quadrennial technology review 2015.

U.S. EIA (2020). Annual energy outlook. table 8: Electricity supply, disposition, prices, and emissions.

U.S. EPA (2007). Energy independence and security act of 2007.

U.S. EPA (2019). Final rulemaking for modifications to fuel regulations to provide flexibility for e15 and to elements of the renewable identification number compliance system.

U.S. EPA (2020). Lifecycle greenhouse gas results.

U.S. EPA (2020). Automotive trends report. supplemental table e: Detailed real-world fuel economy, co2 emissions, and vehicle attribute and technology data.

U.S. EPA (2021). Inventory of U.S. greenhouse gas emissions and sinks: 1990-2019.

U.S. EPA and NHTSA (2016). Interim joint technical assessment report: Light-duty vehicle greenhouse gas emission standards and corporate average fuel economy standards for model years 2017-2025. table e1.5-1.

U.S. International Trade Commission (2018). Minerals and metals.

USABC (2020). Development of advanced high-performance batteries for electric vehicle (ev) applications request for proposal information (rfpi).

USGS (2021a, Jan). U.s. geological survey (usgs) mineral commodity summaries aluminum.

USGS (2021b, Jan). U.s. geological survey (usgs) mineral commodity summaries: Iron and steel.

USGS (2021c, Jan). Usgs mineral commodity summaries iron and steel scraps.

- Van Haaren, R. (2011). Assessment of electric cars' range requirements and usage patterns based on driving behavior recorded in the national household travel survey of 2009. *Earth and Environmental Engineering Department, Columbia University, Fu Foundation School of Engineering and Applied Science, New York 51*, 2011.
- Wang, T., D. B. Muller, and T. E. Graedel (2007). Forging the anthropogenic iron cycle.
- Ward, J. W., J. J. Michalek, I. L. Azevedo, C. Samaras, and P. Ferreira (2019). Effects of on-demand ridesourcing on vehicle ownership, fuel consumption, vehicle miles traveled, and emissions per capita in us states. *Transportation Research Part C: Emerging Technologies 108*, 289–301.
- Wolfram, P., Q. Tu, N. Heeren, S. Pauliuk, and E. G. Hertwich (2021). Material efficiency and climate change mitigation of passenger vehicles. *Journal of Industrial Ecology 25*(2), 494–510.
- WorldSteel (2017). Steel statistical yearbook.
- Worrell, E., L. Bernstein, J. Roy, L. Price, and J. Harnisch (2009). Industrial energy efficiency and climate change mitigation. *Energy efficiency 2*(2), 109.
- Worrell, E., L. Price, M. Neelis, C. Galitsky, and N. Zhou (2007). World best practice energy intensity values for selected industrial sectors.
- Xu, J., F. Lin, M. M. Doeff, and W. Tong (2017). A review of ni-based layered oxides for rechargeable li-ion batteries. *Journal of Materials Chemistry A 5*(3), 874–901.
- Yang, C., D. McCollum, R. McCarthy, and W. Leighty (2009). Meeting an 80% reduction in greenhouse gas emissions from transportation by 2050: A case study in california. *Transportation Research Part D: Transport and Environment 14*(3), 147–156.
- Yang, Y., S. Qu, B. Cai, S. Liang, Z. Wang, J. Wang, and M. Xu (2020). Mapping global carbon footprint in china. *Nature communications 11*(1), 1–8.
- Yellishetty, M., P. G. Ranjith, A. I. O. Tharumarajah, and S. Production (2010). Trends and material flows in the world: Is this really sustainable.
- Zhu, Y., L. B. Chappuis, R. De Kleine, H. C. Kim, T. J. Wallington, G. Luckey, and D. R. Cooper (2020). The coming wave of aluminum sheet scrap from vehicle recycling in the united states. *Resources, Conservation and Recycling 164*.
- Zhu, Y. and D. R. Cooper (2019). An optimal reverse material supply chain for us aluminum scrap. *Procedia CIRP 80*, 677–682.
- Zhu, Y., S. Skerlos, M. Xu, and D. R. Cooper (2020). System level impediments to achieving absolute sustainability using lca. *Procedia CIRP 90*, 399–404.
- Zhu, Y., K. Syndergaard, and D. R. Cooper (2019). Mapping the annual flow of steel in the united states. *Environmental science & technology 53*(19), 11260–11268.